HYDROPEROXIDE MEASUREMENTS IN OUTDOOR ENVIRONMENTS

Dissertation

zur Erlangung des Grades
„Doktor der Naturwissenschaften – Dr. rer. nat.“
im Promotionsfach Chemie
am Fachbereich Chemie, Pharmazie, Geographie und Geowissenschaften
der Johannes-Gutenberg-Universität Mainz

Zaneta Teresa Hamryszczak
geb. in Przemysl (Polen)

Mainz 2023

1. Gutachter

2. Gutachter

Tag der mündlichen Prüfung: 24.10.2023

Meiner Familie.

Formal declaration

I hereby declare that I have written the dissertation thesis independently and without any unauthorized external assistance. I have used exclusively the acknowledged literature and other sources marked and listed separately in the supplement.

Mainz, August 2023

_____

Abstract

Hydroperoxides are well-acknowledged trace species in the oxidative chemistry of the atmosphere. On the one side, hydroperoxides and especially hydrogen peroxide (H_2O_2), serve as a reservoir of the main atmospheric oxidant, the hydroperoxyl radical (OH), and of the peroxy radicals (HO_2), which are often collectively defined as HO_x ($HO_x = OH + HO_2$). On the other side, hydroperoxides are known to convert sulfur dioxide (SO_2) and to a minor extent nitrogen dioxide (NO_2) into sulfuric acid (H_2SO_4) and nitric acid (HNO_3) in the atmospheric aqueous phase (cloud, fog, and rain) leading to their acidification. Therefore, hydroperoxide in situ observations add to an improved understanding of self-cleansing processes in the atmosphere. This work is focused on airborne hydroperoxide measurements using a tool specifically designed to meet the requirements of dynamic, high-altitude, and long-range measurements on board the research aircraft, High-Altitude and Long-range Observatory (HALO). The Hydrogen Peroxide and Higher Organic Peroxides (HYPHOP) monitor is based on a dual-enzyme fluorescence spectroscopy technique, which enables tracking hydrogen peroxide and total organic hydroperoxides mixing ratios at a 1-Hz measurement frequency. The instrument was deployed in several airborne research projects, among which the most recent three aircraft campaigns, Chemistry of the Atmosphere: Field Experiment in Africa (CAFE-Africa), BLUESKY, and CAFE-Brazil are presented in detail regarding the hydroperoxide observations.

The first section focuses on the theoretical background of the atmosphere and its main gaseous- and aqueous-phase chemistry. In the second section, the measurement technique and the corresponding analytical methods are discussed. The section characterizes the measurement method and data acquisition with special emphasis on potential measurement inconsistencies induced by dynamic flight patterns. The instrument's precision based on the measurement results from the most recent airborne campaign, CAFE-Brazil for H_2O_2 and the sum of organic hydroperoxides (ROOH) were determined to be 6.4% (at 5.7 ppb_v) and 3.6% (at 5.8 ppb_v), respectively. The instrument's limit of detection at a 1-Hz data acquisition frequency were 20 ppt_v and 19 ppt_v for H_2O_2 and ROOH, respectively. Based on the performed analyses, technical and physical challenges do not critically impact the measurement performance of the HYPHOP monitor.

In situ observations of hydroperoxides based on airborne campaigns are presented in the following sections (Sect. 3. – Sect. 5.). During the BLUESKY campaign, performed in May – June 2020 mainly over central and southern Europe (35° N – 60° N; 15° W – 15° E), average mixing ratios of 0.23 (±0.18) ppb_v, 0.42 (±0.25) ppb_v, and 0.48 (±0.17) ppb_v for H_2O_2 and 0.37 (±0.23) ppb_v, 0.57 (±0.30) ppb_v, and 0.62 (±0.36) ppb_v for ROOH in the upper troposphere, the middle troposphere, and the boundary layer, respectively, were measured (Sect. 3.). In contrast to previous measurements during the HOOVER campaign (HO_x Over EuRope; 2006 – 2007) and UTOPIHAN-ACT II/IIII campaign (Upper Tropospheric Ozone: Processes Involving HO_x and NO_x: The Impact of Aviation and Convectively Transported Pollutants in the Tropopause Region; 2002 – 2004), vertical profiles of measured H_2O_2 display diminished mixing ratios particularly above the boundary layer, which is most likely caused by cloud scavenging and subsequent rainout of the highly soluble trace species. The expected inverted C-shaped vertical distribution with maximum H_2O_2 mixing ratios at 3 – 7 km was not observed during the BLUESKY campaign. The observations are partly reproduced by the global circulation ECHAM/MESSy Atmospheric Chemistry (EMAC) model. The strong impact of the H_2O_2 cloud and precipitation scavenging is confirmed by a sensitivity study performed using the EMAC model. The differences arising between the H_2O_2 observations and simulations are most likely due to difficulties in wet scavenging simulations caused by the limited resolution of the model.

Analyses of the hydroperoxide distribution during the CAFE-Africa aircraft campaign performed in August – September 2018 over the tropical Atlantic and the western coast of Africa (10° S – 50° N; 50° W – 15° E) reveal average mixing ratios of 0.18 (±0.13) ppb_v, 2.19 (±1.86) ppb_v and 2.25 (±1.30) ppb_v for H_2O_2 and 0.15 (±0.07) ppb_v, 0.55 (±0.25) ppb_v, and 0.70 (±0.18) ppb_v for ROOH in the upper troposphere, the middle troposphere, and in the boundary layer, respectively (Sect. 4.). In opposition to the expected latitudinal dependency in the distribution of hydroperoxides, H_2O_2 observations do not

display any clear trend from the tropics towards the subtropics. Locally increased H_2O_2 mixing ratios of up to 1 ppb_v were detected in the Intertropical Convergence Zone (ITCZ), in proximity to the tropical storm Florence over the Atlantic Ocean, and over the west African coast. Observation-based photostationary steady-state (PSS) calculations produce up to a factor of 2 lower H_2O_2 mixing ratios in the ITCZ and in the north of the sampled region relative to in situ observations. In contrast, in the south of the sampled area, PSS calculations tend to overestimate the H_2O_2 levels by up to a factor of 3. Analogously, simulations performed by the EMAC model tend to overestimate the H_2O_2 mixing ratios in the southern part of the sampled region. Based on PSS calculations and EMAC simulations a latitudinal trend towards the subtropics with maximum H_2O_2 mixing ratios in the tropics was expected. However, according to in situ observations, the spatial distribution of H_2O_2 displays nearly no latitudinal dependency originating from photochemical processes in the tropical upper troposphere. The observations suggest an influence of convective transport processes in tropical and subtropical regions. Convective processes in the ITCZ and the enhanced presence of clouds in the south of the ITCZ are most likely the main causes for the deviations between the observations and both, PSS calculations and EMAC simulations.

The most recent airborne hydroperoxide measurements were performed during the CAFE-Brazil campaign in December 2022 – January 2023 mainly over the Amazon Basin (12 °S–4 °N; 70–38 °W; Sect. 5.). Average H_2O_2 mixing ratios of 0.74 (±0.25) ppb_v, 0.45 (±0.26) ppb_v, and 0.12 (±0.09) ppb_v were measured in the boundary layer, the middle and upper troposphere. Accordingly, average ROOH mixing ratios of 0.89 (±0.31) ppb_v, 0.62 (±0.34) ppb_v, and 0.22 (±0.12) ppb_v were detected in the sampled region. The highest average hydroperoxide mixing ratios were detected at altitudes of approximately 2 km, according to expectations. In the boundary layer, decreasing hydroperoxide mixing ratios reflect the effect of deposition processes on the trace species. The levels decrease towards the upper troposphere due to diminished availability of the hydroperoxide precursor, HO_2. However, at 10 – 13 km in the upper troposphere, the hydroperoxide levels rise to approximately 20% of the measured maxima above the boundary layer, most likely due to convective transport. Generally, ROOH mixing ratios are approximately by a factor of 1.3 – 1.5 higher relative to the H_2O_2 observations throughout the entire tropospheric column. Specifically, in the upper troposphere (above 8 km) ROOH mixing ratios seem to be up to a factor of 5 higher than H_2O_2 levels. The increased ROOH mixing ratios are most likely due to sufficient availability of the hydroperoxide precursor, HO_2, and vegetation emission-based production. Hydrogen peroxide is expected to be removed by deposition via precipitation and vegetation uptake in the lower troposphere. In the upper troposphere, H_2O_2 is assumed to be removed via temporal or permanent processes in the lower part of the convective clouds. The ROOH mixing ratios seem not to be affected by wet deposition removal. In the perspective of previous measurements in the South-American region, i. e. GABRIEL campaign (Guyanas Atmosphere-Biosphere exchange and Radicals Intensive Experiment with the Learjet; 2005), the measured hydroperoxide levels are significantly lower (up to a factor of 5). The high deviations between the campaign results are most likely due to contrasting meteorological conditions and the resulting significantly higher cloud scavenging and precipitation during CAFE-Brazil. EMAC simulations of the trace species tend to overestimate the mixing ratios of hydroperoxides, especially in the boundary layer and in the tropospheric regions affected by clouds. Most likely, the differences between the simulations and in situ observations are caused by difficulties in deposition simulations due to the limitations in the model's resolution.

Zusammenfassung

Hydroperoxide gelten als bedeutende Spurenspezies in der oxidativen Chemie der Atmosphäre. Einerseits dienen Hydroperoxide und insbesondere Wasserstoffperoxid (H_2O_2) als Reservoir des wichtigsten atmosphärischen Oxidationsmittels, des Hydroperoxylradikals (OH) und des Peroxyradikals (HO_2), die oft zusammenfassend als HO_x definiert werden (HO_x= OH + HO_2). Andererseits ist bekannt, dass Hydroperoxide in der atmosphärischen wässrigen Phase (Wolken, Nebel und Regen) Schwefeldioxid (SO_2) und in geringem Maße Stickstoffdioxid (NO_2) in Schwefelsäure (H_2SO_4) bzw. Salpetersäure (HNO_3) umwandeln, was zu Bildung des sog. Sauren Regens führt. Daher tragen In-situ-Beobachtungen von Hydroperoxiden zu einem besseren Verständnis von Selbstreinigungsprozessen in der Atmosphäre bei. Diese Arbeit konzentriert sich auf luftgestützte Hydroperoxid-Messungen mit einem Instrument, das speziell für die Anforderungen dynamischer Messungen in großer Höhe und über große Entfernungen an Bord des Forschungsflugzeugs High-Altitude and Long-Range Observatory (HALO) entwickelt wurde. Der Hydrogen Peroxide and Higher Organic Peroxides Monitor (HYPHOP) beruht auf einer Dual-Enzym-Fluoreszenzspektroskopie-Technik, die es ermöglicht, die Mischungsverhältnisse von Wasserstoffperoxid und gesamten organischen Hydroperoxiden bei einer Messfrequenz von 1 Hz zu detektieren. Das Instrument wurde in mehreren luftgestützten Forschungsprojekten eingesetzt, darunter die jüngsten drei Messkampagnen Chemistry of the Atmosphere: Field Experiment in Africa (CAFE-Africa), BLUESKY und CAFE-Brazil. Die Ergebnisse dieser Messkampagnen werden nachfolgend im Hinblick auf die Hydroperoxid-Beobachtungen ausführlich vorgestellt.

Das erste Kapitel der Arbeit fokussiert sich auf die theoretischen Hintergründe der Atmosphäre und ihre wichtigste Gas- und Wasserphasenchemie. Im zweiten Abschnitt werden die Messtechnik und die Analysemethoden besprochen. Das Kapitel behandelt die Messmethode und Datenerfassung mit besonderem Schwerpunkt auf möglichen Messinkonsistenzen, die durch dynamische Flugmuster verursacht werden. Die Präzision des Instruments wurde auf der Grundlage der Messergebnisse der letzten Messkampagne, CAFE-Brazil für H_2O_2 und die Summe organischer Hydroperoxide (ROOH) mit 6,4 % (bei 5,7 ppb_v) bzw. 3,6 % (bei 5,8 ppb_v) ermittelt. Die Nachweisgrenze des Geräts bei einer Datenerfassungsfrequenz von 1 Hz betrug 20 ppt_v und 19 ppt_v für H_2O_2 bzw. ROOH. Basierend auf den durchgeführten Analysen haben technische und physikalische Herausforderungen keinen wesentlichen Einfluss auf die Messleistung des HYPHOP-Monitors.

In den folgenden Kapiteln werden Ergebnisse der In-situ-Beobachtungen von Hydroperoxiden basierend auf flugzeuggetragenen Messkampagnen vorgestellt (Kapitel 3. – 5.).Während der BLUESKY-Kampagne, die im Mai – Juni 2020 hauptsächlich über Mittel- und Südeuropa (10° S – 50° N; 50° W – 15° E) durchgeführt wurde, wurden mittlere Mischungsverhältnisse von 0,23 (±0,18) ppb_v, 0,42 (±0,25) ppb_v und 0,48 (±0,17) ppb_v für H_2O_2 sowie 0,37 (±0,23) ppb_v, 0,57 (±0,30) ppb_v, und 0,62 (±0,36) ppb_v für ROOH in den oberen und mittleren Troposphäre bzw. in der Grenzschicht ermittelt (Kapitel 3.). Im Gegensatz zu früheren Messungen während der HOOVER-Kampagne (HO_x Over EuRope; 2006 – 2007) und UTOPIHAN-ACT II/IIII- Kampagne (Upper Tropospheric Ozone: Processes Involving HO_x and NO_x: The Impact of Aviation and Convectively Transported Pollutants in the Tropopause Region; 2002 – 2004), weisen Vertikalprofile des gemessenen H_2O_2 verringerte Mischungsverhältnisse auf, insbesondere oberhalb der Grenzschicht, was höchstwahrscheinlich durch Aufnahme in Wolken und anschließenden Niederschlag der hochlöslichen Spurenspezies verursacht wird. Die erwartete invertierte c-förmige vertikale Verteilung mit maximalen H_2O_2-Mischungsverhältnissen bei 3 – 7 km wurde während der BLUESKY-Kampagne nicht beobachtet. Die Messergebnisse werden teilweise durch das globale numerische Zirkulationsmodell ECHAM/MESSy Atmospheric Chemistry (EMAC) reproduziert. Der starke Einfluss der Abtragung von H_2O_2 durch Wolken und Niederschlag wird durch eine Sensitivitätsstudie, die mit dem EMAC-

Modell durchgeführt wurde, bestätigt. Die Unterschiede zwischen den H_2O_2-Beobachtungen und den Simulationen sind höchstwahrscheinlich auf Schwierigkeiten bei Simulation der nassen Deposition zurückzuführen, die durch die begrenzte Auflösung des Modells verursacht wird.

Analysen der Hydroperoxid-Verteilung während der CAFE-Africa-Flugzeugkampagne, die im August – September 2018 über dem tropischen Atlantik und der Westküste Afrikas durchgeführt wurde (10° S – 50° N; 50° W – 15° E), zeigen durchschnittliche Mischungsverhältnisse von 0,18 (±0,13) ppb_v, 2,19 (±1,86) ppb_v und 2,25 (±1,30) ppb_v für H_2O_2 bzw. 0,15 (±0,07) ppb_v, 0,55 (±0,25) ppb_v, und 0,70 (±0,18) ppb_v für ROOH in der oberen und mittleren Troposphäre bzw. in der planetaren Grenzschicht (Kapitel 4.). Im Gegensatz zur erwarteten Breitengradabhängigkeit der Hydroperoxid-Verteilung zeigen die Wasserstoffperoxid-Beobachtungen keinen klaren Trend von den Tropen bis hin zu den Subtropen. Lokal erhöhte H_2O_2-Mischungsverhältnisse von bis zu 1 ppb_v wurden in der Intertropischen Konvergenzzone (ITCZ), in der Nähe des Tropensturms Florence über dem Atlantischen Ozean und über der westafrikanischen Küste festgestellt. Messungsbasierte Photostationäre Steady-State-Berechnungen (PSS) deuten auf bis zu einem Faktor 2 niedrigeren H_2O_2-Mischungsverhältnisse im ITCZ und im Norden der beprobten Region im Vergleich zu den In-situ-Beobachtungen. Im Gegensatz dazu neigen PSS-Berechnungen im Süden des untersuchten Gebiets dazu, die H_2O_2-Werte um bis zu den Faktor 3 zu überschätzen. Analog dazu ergeben Simulationen, die mit dem EMAC-Modell durchgeführt wurden, überhöhte H_2O_2-Werte im südlichen Teil der untersuchten Region. Basierend auf PSS-Berechnungen und EMAC-Simulationen wird ein Breitengradtrend in Richtung der Subtropen mit maximalen H_2O_2-Mischungsverhältnissen in den Tropen erwartet. In-situ-Beobachtungen zufolge gibt es jedoch keinen ausgeprägten Breitengradienten in der oberen Troposphäre. Die räumliche Verteilung von H_2O_2 weist nahezu keine Breitenabhängigkeit, die auf photochemische Prozesse in der tropischen oberen Troposphäre zurückzuführen ist, auf. Die Beobachtungen deuten auf einen Einfluss konvektiver Transportprozesse in den beprobten Regionen hin. Konvektive Prozesse in der ITCZ und zunehmende Präsenz von Wolken im Süden der ITCZ sind höchstwahrscheinlich die Hauptursachen für die Abweichungen zwischen den Beobachtungen und den PSS-Berechnungen als auch den EMAC-Simulationen.

Die jüngsten flugzeuggetragenen Hydroperoxid-Messungen wurden während der CAFE-Brazil-Kampagne im Dezember 2022 – Januar 2023 hauptsächlich über dem Amazonasbecken (12 °S – 4 °N; 70 – 38 °W) durchgeführt (Kapitel 5.). Die durchschnittlichen H_2O_2-Mischungsverhältnisse von 0,74 (±0,25) ppb_v, 0,45 (±0,26) ppb_v und 0,12 (±0,09) ppb_v wurden in der Grenzschicht, der mittleren und oberen Troposphäre gemessen. Analog wurden in der beprobten Region durchschnittliche ROOH-Mischungsverhältnisse von 0,89 (±0,31) ppb_v, 0,62 (±0,34) ppb_v und 0,22 (±0,12) ppb_v festgestellt. Die höchsten durchschnittlichen Hydroperoxid-Mischungsverhältnisse wurden erwartungsgemäß in Höhen von etwa 2 km festgestellt. In der Grenzschicht spiegeln abnehmende Hydroperoxid-Mischungsverhältnisse den Einfluss von Ablagerungsprozessen auf die Spurenspezies wider. Aufgrund der geringeren Verfügbarkeit des Hydroperoxid-Vorläufers, HO_2 nehmen die Werte in Richtung der oberen Troposphäre ab. Entgegen der Erwartungen, steigen die Hydroperoxid-Werte in 10 – 13 km Höhe in der oberen Troposphäre auf etwa 20% der gemessenen Maxima oberhalb der Grenzschicht an, was höchstwahrscheinlich auf konvektiven Transport zurückzuführen ist. Im Allgemeinen sind die ROOH-Mischungsverhältnisse etwa um den Faktor 1,3 – 1,5 höher im Vergleich zu den H_2O_2-Beobachtungen entlang der gesamten troposphärischen Säule. Insbesondere in der oberen Troposphäre (oberhalb von 8 km) scheinen die ROOH-Mischungsverhältnisse bis zu einem Faktor 5 höher zu sein als die H_2O_2-Werte. Die erhöhten ROOH-Mischungsverhältnisse sind höchstwahrscheinlich auf die ausreichende Verfügbarkeit des Hydroperoxid-Vorläufers, HO_2 und die auf Vegetationsemissionen basierende Produktion zurückzuführen. Es wird erwartet, dass Wasserstoffperoxid durch Deposition über Niederschlag und Vegetationsaufnahme in der unteren Troposphäre entfernt wird. In der oberen Troposphäre wird angenommen, dass H_2O_2 über temporäre oder permanente Prozesse im unteren Teil der konvektiven Wolken entfernt wird. Die ROOH-Mischungsverhältnisse scheinen hierdurch zu deutlich geringerem Anteil beeinflusst zu werden. Im Hinblick auf frühere Messungen im

südamerikanischen Raum, während der GABRIEL-Kampagne (Guyanas Atmosphere-Biosphere exchange and Radicals Intensive Experiment with the Learjet; 2005), sind die gemessenen Hydroperoxid-Werte deutlich niedriger (bis zu einem Faktor 5). Die hohen Abweichungen zwischen den Kampagnenergebnissen sind höchst-wahrscheinlich auf unterschiedliche meteorologische Bedingungen und die daraus resultierende deutlich höhere Wolkenbedeckung und Niederschlagsmenge während der CAFE-Brazil-Kampagne zurückzuführen. EMAC-basierte Simulationen der Spurenspezies neigen dazu, die Hydroperoxid-Werte zu überschätzen, insbesondere in der Grenzschicht und in den von Wolken betroffenen troposphärischen Regionen. Höchstwahrscheinlich sind die Unterschiede zwischen den Simulationen und In-situ-Beobachtungen auf Schwierigkeiten bei Simulationen der Depositionsprozesse aufgrund der begrenzten Auflösung des Modells zurückzuführen.

Table of Contents

1. Introduction

The following section is dedicated to the theoretical background of the atmosphere and its main processes. The chemistry of the atmosphere and in specific of the troposphere, is controlled by a variety of chemical homogeneous and heterogeneous reactions, for example, oxidations, reductions, photolysations, and additions. In the following, an overview of the atmosphere's composition and the corresponding characteristics will be discussed (Sect. 1.1.). Section 1.2. gives a brief outline of the troposphere, its meteorology, and chemistry. Finally, Sections 1.3. and 1.4. review the hydroperoxide chemistry and their literature known trends in the troposphere based on previous research results.

1.1. The Earth‘s atmosphere

The atmosphere, a multiphase and multicomponent thermodynamic system surrounding the Earth, has formed from volatile compounds emitted by the planet. It is a suspension consisting primarily of a variety of gases and aerosol particles, which remains in a constant exchange with the space on the one side, and the Earth's surface including the anthroposphere (human-modified environment) and the biogeosphere (soil, water, flora, and fauna), on the other. In the atmosphere, the chemically inert and non-soluble nitrogen (N_2) is its most abundant constituent (78%) followed by oxygen (O_2) as the second most abundant gas (21%), which was initially produced by cyanobacteria approximately 2300 million years ago (Seinfeld and Pandis, 2006). The third gas adding to today's atmospheric composition is argon (Ar) with a constant mixing ratio of approximately 1%. The next prominent constituent of today's atmosphere with concentrations up to 3% on a regional scale, is water vapor, which can be found mainly in the lower part of the atmosphere (Seinfeld and Pandis, 2006). The abundance of water vapor is controlled mainly by the interactions between the atmosphere and the cryo- and hydrosphere via evaporation and precipitation. The remaining constituents with a total atmospheric concentration of up to 1% are the so-called trace gases and aerosols. The atmospheric trace species formed via emissions from the earth's surface are predominantly controlled by uptake and release from the biosphere, the hydrosphere, and the lithosphere. They play a major role in the atmospheric radiative balance and chemistry.

The Earth's atmosphere is generally subdivided into upper and lower regions, which consist of a course of sublayers defined by their altitude-dependent temperature and pressure trends. The vertical profile of the temperature throughout the atmosphere is linked to solar radiative processes in the atmosphere such as absorption, emission, transmission as well as vertical mixing of the air masses. As a result, the observed temperature profile reflects the characteristic processes of the individual atmospheric layers

and, thus, is important for their naming. The following figure illustrates a simplified structure of the atmosphere subdivided into the single layers based on the vertical profile of the temperature (Fig. 1).

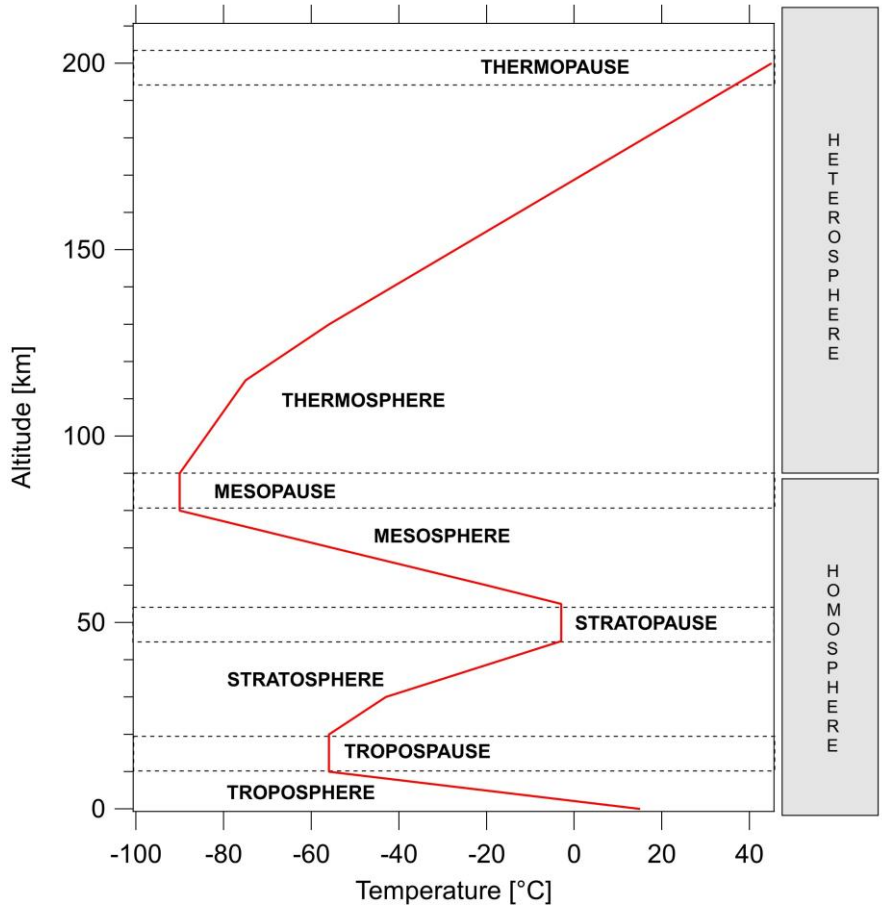

Figure 1: Atmospheric layers (figure adapted from Seinfeld and Pandis, 2006).

Mesosphere, thermosphere, and exosphere are separated from each other by mesopause, and the thermopause and form the upper atmosphere. The highest layers of the atmosphere are often defined as the heterosphere due to their lack of homogeneous gaseous composition. The exosphere is the most distant layer of the atmosphere reaching up to 1000 km (Seinfeld and Pandis, 2006). The so-called magnetopause limits its extension toward space. Exospheric gas molecules bear high kinetic energy enabling them to withstand gravity and leave the atmospheric gaseous shell into space (Harteck, 1951). The adjacent thermosphere separated from the exosphere by the thermopause at approximately 200 km is characterized by a highly variable temperature and rapid vertical mixing due to the restricted impact of gravity and diffusion. The high temperature of the thermosphere is a result of short-wave, X-ray, and corpuscular radiation absorption. In combination with the low particle density in the thermosphere, this gives rise to high-temperature fluctuations of many hundreds of K within the layer (Kraus, 2004). The layer below, the mesosphere is separated from the heterosphere by the mesopause, the coldest region of the atmosphere (-90°C; Kraus, 2004). The mesopause at about 80 – 90 km defines the region of consistent and well-mixed atmospheric gas composition throughout the entire extension of the air layers

below. The mesosphere is characterized by decreasing pressure, and temperature with increasing distance from the earth's surface and strong convective activities of the airmasses.

The lower atmosphere is defined as the region up to 50 km of altitude and consists of the troposphere and stratosphere, which are separated by the tropopause (Seinfeld and Pandis, 2006). The stratosphere is often linked to the so-called ozone layer containing approximately 90% of the atmospheric ozone and protecting the earth's surface from the harmful effect of solar irradiation, i. e. extensive UV light exposition. In the stratosphere, the temperature increases with increasing distance to the earth as a result of slow vertical mixing of the air masses and heat emission due to short-wave UV radiation absorption (240 – 320 nm) and conversion by the stratospheric ozone. Consequently, the temperature profile of the stratosphere reflects the intensity of the absorption of solar radiation and correlates with the amount of available stratospheric ozone. Below the stratosphere, the tropopause serves as a distinction between the stratosphere and the troposphere. As defined by the World Meteorological Organization (WMO), the tropopause is a region with temperature variation of less than 2 K per 1 km depicting the layer with nearly constant temperature dissipation in the atmosphere (on average approximately -56 °C; Holton et al., 1995). The temperature inversion from the troposphere to the stratosphere at the tropopause causes restrictions in the interexchange between these two layers. Due to the low temperature at the tropopause, the water vapor condenses almost completely at the tropopause resulting in dry stratospheric air with no weather phenomena with the exception of stratospheric clouds at 22 – 29 km forming at temperatures below -78 °C from HNO_3 and H_2SO_4 embedded in ice particles. The distance of the tropopause relative to the earth's surface varies with temperature reflecting season, latitude-dependent gas expansion processes linked to solar irradiation, and vertical mixing. While at the poles the lowest altitudes of the tropopause are reported, the maximal distance to the earth's surface in close proximity to the equator is assumed to be at approximately 16 km altitude. The characteristics of the lowest atmospheric layer, the troposphere, are discussed in the following section (Sect. 1.2.).

1.2. The troposphere

The troposphere at up to 15 km above the surface is the atmospheric region impacted by dynamic processes and high vertical mixing constituting the meteorology of the atmosphere. Due to decreasing solar irradiation absorption and emission, the temperature within the troposphere decreases with increasing distance to the earth's surface, which is representing the warmest point of the tropospheric column. The solar irradiation on the earth's surface causes warming of the air directly above the surface, which is followed by air mixing in terms of convection (vertical mixing), convergence, and divergence of horizontal air flows. The troposphere accounts for approximately 80% of the total atmospheric mass, which results in its high atmospheric pressure relative to the layers above (Seinfeld and Pandis, 2006).

The troposphere contains the majority of the water vapor. Due to the temperature dependence of the water vapor pressure, vertically rising humidity leads to an oversaturation of more than 100%, which results in cloud formation. Higher up in the troposphere, due to condensation processes of the rising air parcels beforehand, a significantly reduced water vapor amount is established. Furthermore, the high water vapor content in the troposphere influences a large number of processes, including the release of latent heat through condensation, which also leads to vertical air mass movement. The troposphere is generally subdivided into the planetary/marine boundary layer (PBL/MBL) with a variable thickness of 500 – 2,000 m above the oceans and the continents, respectively, and the free troposphere. Especially the PBL is key to understanding the exchange between the earth's surface and the atmosphere (Möller, 2017). It is described as the tropospheric region highly influenced by the earth's surface forcing, i. e. warming, cooling, and water vapor fortification on the surface.

The chemical composition of the atmosphere, i. e. troposphere, is dependent on natural (biogenic and geogenic), and anthropogenic (human-related) sources and their emission fluxes. The chemistry of the troposphere is significantly influenced by the physical and chemical conditions of the emitted atmospheric constituents, which impact their transport, transformation, and removal in the atmosphere. The emissions in the atmospheric trace gas cycles contain a large variety of sources, for instance, biological activities, vulcanism, soil-related processes, lightning, and biomass burning, but also human industrial activities, aviation, seafaring, and combustion emissions. Emission fluxes from the anthroposphere and biogeosphere form prominent sources of trace gases and aerosol particles. The fluxes are not only dependent on regional emission sources and their distribution, but also on seasonal, and diurnal variabilities due to biogenic and anthropogenic processes linked with light, temperature, and water availability. Deposition processes, and uptake serving as the ultimate trace species sinks in the atmosphere display accordingly regional, temporal, and seasonal variations. Chemical transformations produce, on the one side, secondary tropospheric substances such as carbon monoxide (CO), ozone (O_3), and hydroperoxides. On the other side, chemical reactions also remove trace species. As a result, the variety of the atmospheric sources and sinks and their complex coupling on different temporal and spatial scales establish a budget for each trace species and its atmospheric lifetime. Per definition, the lifetime describes the average dwell time of a trace constituent in the atmosphere from its emission to its ultimate removal (Seinfeld and Pandis, 2006). Fig. 2 gives an overview of the main tropospheric trace gases and their lifetime in the atmosphere.

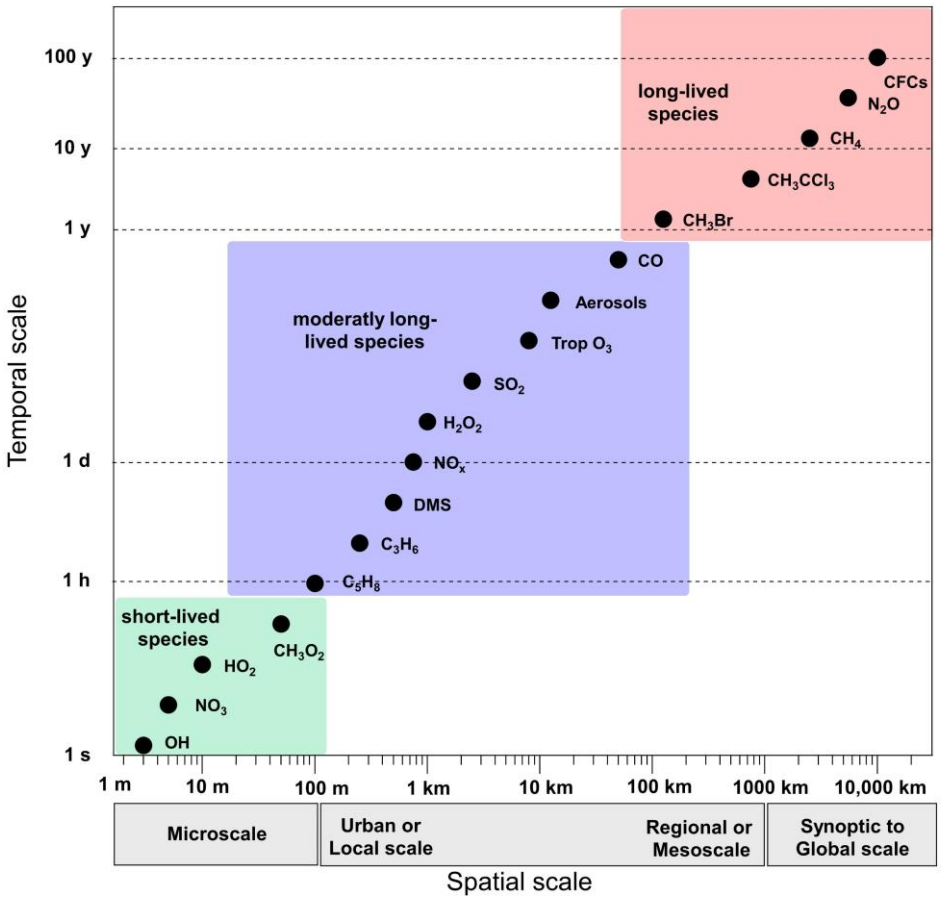

Figure 2: Spatial and temporal variability of atmospheric trace species (figure adapted from Seinfeld and Pandis, 2006).

In dependence of their atmospheric lifetime, trace species are displaying both, spatial and temporal variabilities in the atmosphere. Established by the temperature inversion at the tropopause separating the troposphere from the stratosphere, mixing between the airmasses of these regions is mostly negligible. However, trace gases with a longevity of more than 1 year, such as methane (CH_4), chlorofluorocarbons (CFCs), or nitrous oxide (N_2O) are not removed from the atmosphere entirely. They accumulate in the atmosphere up to their global distribution and enter the lower stratosphere. Substances with lifetimes of up to 1 year do not accumulate in the atmosphere and display constant temporal average mixing ratios with spatial distribution trends in dependence of the heterogeneous distribution of their sources and sinks. Many of these moderately long-lived compounds emitted into the atmosphere are converted into soluble species by oxidation and can be removed from the atmosphere by both, wet and dry deposition. Thus, they are only of local and regional importance for the tropospheric composition.

The abundance of atmospheric trace species has several important effects on the atmosphere and its climate. For instance, greenhouse gases (GFGs) impact solar irradiation absorption and emission altering the temperature in the atmosphere causing so-called global warming. CFCs and other ozone-depleting substances have a tremendous effect on the O_3 budget in the stratosphere causing an increasing

amount of harmful UV radiation in the troposphere (Molina and Rowland, 1974). Formation of the so-called cloud condensation nuclei (CCN) from aerosol particles abundant in the troposphere and the subsequent cloud formation not only alters the solar irradiation cycle but also affects the hydrosphere and impacts the wet deposition of trace species in the atmosphere. And finally, the abundance and diversity of atmospheric oxidative species determines the lifetime and chemical composition of the atmospheric pollutants (CH_4, CO, nonmethane hydrocarbons – NMHC; Reeves and Penkett, 2003). Nonetheless, these pollutants can in turn affect the oxidative species causing changes in the atmospheric composition. Molecular oxygen forms the main part of the atmospheric oxidative substances. However, because of their increased reactivity, trace gases such as the hydroxyl radical (OH) and the hydroperoxyl radical (HO_2) often summed as the HO_x (HO_x = OH + HO_2), O_3, and nitrate (NO_3) also strongly influence the oxidizing and self-regenerating capacity of the atmosphere. The hydroxyl radical is formed from O_3 during the day and is thus, responsible for the daytime oxidizing processes in the atmosphere. The tropospheric chemistry is highly dependent on the abundance of the hydroxyl radical, which is reacting with nearly all atmospheric trace gases, making it the primary oxidizing agent of the atmosphere (Levy, 1971). The importance of OH for the self-cleansing capacity of the atmosphere derives from its high reactivity and relatively high mixing ratios. When reacting with atmospheric trace species, OH is generated in catalytic cycles, which lead to lasting mixing ratios in the long term. OH radicals are regenerated by conversions involving HO_2, hydroperoxides, and formaldehyde (HCHO; Lee et al., 2000). Starting with OH, a myriad of reactions in the troposphere occurs. Among these, hydroperoxide formation and destruction are of importance for the chemistry of the troposphere, as will be discussed in the following section (Sec. 1.3.). Processes involving NO_3 occur in the dark and thus, dominate the oxidizing power of the atmosphere at night. The influence of O_3 is of key importance for the processes mentioned, both during the day and at night. Tropospheric O_3 originates partly from the stratosphere (15 – 40%). However, it is also formed through photochemical processes within the troposphere.

The basic composition of the tropospheric air is assumed to be temporally constant, thus it is not affecting the diverse weather phenomena in the troposphere. The weather is far more impacted by the presence or absence of trace species, water vapor, and ozone. The impact of the single constituents varies based on the constituent, its amount, and its atmospheric lifetime. Meteorology is by definition the science of atmospheric motion and its phenomena (Möller, 2017). It describes phenomena such as winds, clouds, precipitation, temperature, and relative humidity. Weather results from vertical, and horizontal atmospheric heat transfer from regions absorbing high density of solar irradiation to regions with lower absorption. The differences occur mainly due to sun angle variations with latitude and the tilt in Earth's axis relative to its orbital plane. The decreasing air temperature from the tropics towards the poles caused by the decreasing irradiation angle gives rise to large-scale circulation (Hadley cell, Ferrel, and polar cells) and jet streams in the atmosphere. Further, the tilt in the Earth's axis causes

differences in solar irradiation angles, which in effect is responsible for the seasons. Variating surface temperature followed by air pressure differences paired with the Coriolis force creates a deflecting horizontal pressure gradient moving air between regions with higher and lower pressure, the wind.

Clouds are dual-phase systems consisting of gaseous and aqueous phases, which are formed via condensation of water vapor on atmospheric aerosol particles (CCN) due to air oversaturation caused by adiabatic processes transporting the air from high-temperature regions to regions with lower temperatures via convection (uplifting from warm air from the earth's surface), forcing by the topographical characteristics such as mountains or via cold air passing over rough surfaces and the subsequent exchange with the warm air at the surface (turbulence). In clouds, trace gases and aerosols are exchanged between the two phases, whilst diverse reactions take place in each phase separately (Warneck, 1991). The chemical composition of CCN determines the aqueous-phase chemistry of the cloud droplet and its ability to absorb trace gases from the gaseous phase of the cloud. In marine environments, sea salt aerosol (SSA) is the main constituent of cloud aerosol. A considerable amount of excess sulfate and nitrate ions originating from the conversion of dimethyl sulfide (DMS), SO_2, and NO_2 accompany sea salt particles in marine clouds (Warneck, 1988). In continental clouds, the variety of aerosols sufficient as CCN extends over a large spectrum of anthropogenic and natural sources (Warneck, 1988). The distribution of trace gases in the two-phase system of clouds depends on their Henry's law coefficient. Soluble species such as hydroperoxides or formaldehyde (HCHO) are likely to transfer into cloud droplets, while less soluble trace gases as, for instance, CO_2, NO_2, O_3, hydrocarbons, or SO_2 remain mostly in the gaseous phase of the cloud. A variety of trace gases (CO_2, HNO_3, NH_3, and SO_2) form additional ions in the aqueous phase, influencing further the distribution of trace gases between both phases. Thus, clouds are considered impactful chemical reactors. Based on the large suite of reactions within the cloud phases and the corresponding interactions between them, a complex system of processes affecting trace gas chemistry arises. Apart from their role in homogeneous and heterogeneous chemical reactions, clouds serve as a transport medium and play an important role in the permanent and temporal removal via wet deposition, and redistribution in the atmosphere after evaporation. Subsequent evaporation and condensation until a final dissipation of the cloud into atmospheric water vapor (cloud processing) alters significantly the local and regional composition of the atmosphere. Additionally, cloud droplets and ice particles act as solar irradiation modifiers by scattering and reflecting the visible and infrared irradiation and, thus, altering not only the atmospheric temperature but also a myriad of photochemical processes. In the stratosphere, ice particles in stratospheric clouds are known to significantly affect the atmospheric chemistry and Earth's climate by processes depleting O_3 from the stratosphere (Seinfeld and Pandis, 2006 and references therein). In clouds, numerous microphysical processes take place in dependence on the cloud's vertical resolution, dynamics, and temperature. They result in cloud droplet growth as well as various precipitation forms. The cloud particle growth proceeds via coalescence (collision of liquid particles), accretion (collision

between a solid and liquid particle), and aggregation (collision of two ice particles). In warm clouds, the coalescence, according to Langmuir, is the most favorable rain drop formation process resulting mostly in light rain (drizzle) at middle and high latitudes and large droplet rain in the tropics. Aggregation, on the other hand, takes place predominantly in clouds at temperatures below -39 °C, where spontaneous freezing of supercooled cloud droplets occurs (Möller, 2017). In mixed clouds, the Bergeron-Findeisen process takes place, where ice particles grow due to the supersaturation of the ice particle according to its low saturation vapor pressure by consuming the supercooled water vapor from its surrounding followed by accretion of liquid particles in lower parts of the cloud while falling. Deep convection refers to precipitating clouds extending from the earth's surface to the tropopause up to 200 hPa pressure altitude (cumulonimbus clouds). Especially within the tropics (but not only) deep convective cells occur due to the increased earth's surface temperatures caused by strong solar irradiation and a high content of water vapor in the air. A bandlike area in close proximity to the equator is characteristic for highly dynamic convective weather phenomena reaching up to the upper troposphere (Intertropical Convergence Zone; ITCZ; Hastenrath and Lamb, 1977; Waliser and Gautier, 1993). The ITCZ is a low-pressure area defining the region of the convergence of air masses originating from both hemispheres and, thus, the ascending branch of the Hadley circulation (Waliser and Gautier, 1993). In this area, deep convective processes are key to the rapid vertical transport of a variety of trace species from the BL towards the upper troposphere (Prather and Jacob, 1997; Wennberg et al., 1998). Since the 1980s numerous research groups studied deep convective processes in the scope of an efficient mechanism for the vertical distribution of tropospheric trace species (Bozem et al., 2017 and references therein). A large number of studies showed that rapid upward transport of VOCs related to convective cells locally leads to a very effective increase in HO_x concentrations in the upper troposphere (Lelieveld and Crutzen, 1994; Prather and Jacob, 1997; Cohan et al., 1999; Mari et al., 2003). This effect is additionally intensified by the NO produced by lightning in thunderstorms. Convective transport increases further mixing ratios of highly soluble trace species such as hydroperoxides in the upper troposphere (Jaeglé et al., 1997; Prather and Jacob, 1997; Jaeglé et al., 2000; Klippel et al., 2011; Bozem et al., 2017; Nussbaumer et al., 2021). The first reports were published by Chatfield and Crutzen (1984) suggesting that convective transport of H_2O_2 might be a valuable source of HO_x in the upper troposphere (UT). The highly soluble species are assumed to reach the UT due to incomplete removal by precipitation (Crutzen and Lawrence, 2000; Barth et al., 2001; Bela et al., 2016; Bozem et al., 2017).

1.3. Chemistry and the role of hydroperoxides in the atmosphere

In general, hydroperoxides play a key role in tropospheric photochemistry in many respects. Hydroperoxides have a direct influence on the formation and decomposition of radicals such as hydroxyl radicals (OH), hydroperoxyl, and alkyl peroxy radicals (HO_2 and RO_2) reflecting the radical

levels in the troposphere. Hydroperoxides display further a strong connection to O_3 and NO_x chemistry (NO_x= NO + NO_2), displaying the diversity of reactions involving hydroperoxides in the atmosphere. Thus, they are directly related to the oxidation capacity of the atmosphere. Furthermore, due to their high solubility, hydroperoxides have a distinctive chemistry in the aqueous phase of the atmosphere making them important oxidants on their own as for instance sulfur dioxide (SO_2), and to a minor extent nitrogen dioxide (NO_2) conversions into sulfuric acid (H_2SO_4), and nitric acid (HNO_3; Penkett et al., 1979; Robbin Martin and Damschen, 1981; Damschen and Martin, 1983; Calvert et al., 1985; Zhou and Lee, 1992). This section is dedicated to the complex processes affecting the budget of hydroperoxides and the role of trace species in the troposphere. The discussion of the chemical hydroperoxide production and destruction presented in this work is based on the work of Seinfeld and Pandis (2006), Möller (2017), and the data derived from the IUPAC Task group on the Atmospheric Chemical Kinetic Data Evaluation (Ether, 2017). Fig. 3 illustrates simplified processes involving photochemical production and destruction of hydroperoxides.

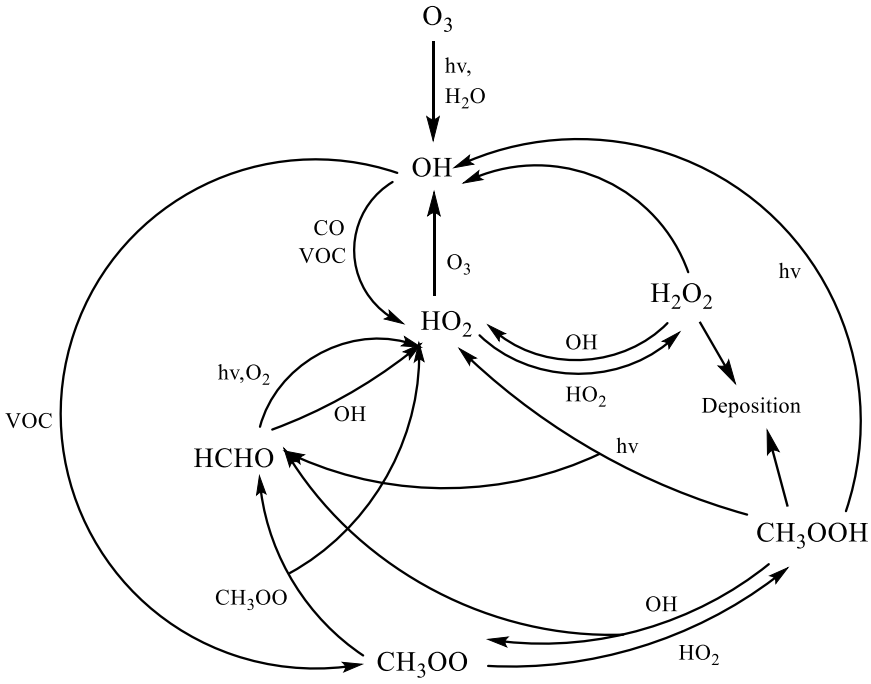

Figure 3: Photochemical production and destruction of hydroperoxides in the atmosphere (figure adapted from Reeves, C. E. and Penkett, S. A.: Measurements of peroxides and what they tell us, Chemical reviews, 103, 5199–5218, https://doi.org/10.1021/cr0205053, 2003. Copyright 2003 American Chemical Society.).

The production mechanism of hydroperoxides was first proposed by Levy in 1971. Destruction and formation of ozone are of central importance for the formation of hydroperoxides in the troposphere. 15 – 40% of tropospheric O_3 comes from the stratosphere, where it is formed by the photodissociation of O_2. From the stratosphere, O_3 enters the troposphere through dynamic processes. In addition, O_3 is also produced to a certain extent in intratropospheric formations, especially within anthropogenically forced processes. Ozone photolysis in the troposphere (at $\lambda < 319$ nm) and the subsequent hydrolysis to

OH form the starting point of the hydroperoxide production (R1 – R2). The processes include photolytic degradation of ozone induced by irradiation absorption, the subsequent production of the ground-state oxygen atom (O), and the excited singlet oxygen species, $O(^1D)$ and its consequent hydrolysis to the OH radical. Further, reactions with long-lived species such as methane alter the yield of OH (R3). The hydrolysis and the conversion of the excited singlet oxygen species by CH_4 are competing with collisions with highly abundant N_2 and O_2 (defined in the following as quenchers, Q). Q are quenching the odd oxygen species by absorbing its kinetic energy and its impulse without altering it chemically (R4). The collisions form in consequence an inactive triplet oxygen $O(^3P)$. Despite the fact that the reaction rate of R4 is by an order of magnitude lower than that of R2, the production of OH radicals is highly dependent on the available amount of water vapor in the air (Crutzen, 1973; Reeves and Penkett, 2003).

$$O_3 \xrightarrow{h\nu\ (\lambda<319\ nm)} O_2 + O(^1D) \quad \text{(R1)}$$

$$O(^1D) + H_2O \rightarrow 2\ OH \quad \text{(R2)}$$

$$O(^1D) + CH_4 \rightarrow OH + CH_3 \quad \text{(R3)}$$

$$O(^1D) + Q \rightarrow O(^3P) + Q \quad \text{(R4)}$$

Analogous processes occur in the stratosphere, with ozone photodissociation as the starting point of the transformation. In the stratosphere, additionally, N_2O forms a source of odd oxygen via photolysis. However, N_2O might also impact negatively the amount of $O(^1D)$ via conversion reaction to NO, which occurs predominantly in the tropical region of the stratosphere. Another additional source of OH radicals is the photolysis of nitrous acid (HONO; R5) being a valuable source of OH in polar regions and during the early morning hours in urban regions (Villena et al., 2011; Czader et al., 2012).

$$HONO \xrightarrow{h\nu\ (\lambda<400\ nm)} OH + NO \quad \text{(R5)}$$

The highly reactive OH radicals are involved in a myriad of chemical transformations in the atmosphere excluding its main constituents, N_2, O_2, H_2O, and CO_2. Among these conversions, reactions with carbon monoxide, CH_4, and volatile organic compounds (VOCs) lead to the formation of the hydroperoxide precursors, HO_2 and RO_2 (R6 – R8). The formation of HO_2 and RO_2 consists of the production of highly reactive hydrogen and alkyl radicals (H and R) in the first step followed instantaneously by the addition of oxygen molecules or quenching by collision partners Q. Additionally, HO_2 is produced directly by photolysis of formaldehyde (HCHO; R9).

$$OH + CO + O_2 \rightarrow HO_2 + CO_2 \quad \text{(R6)}$$

$$CH_4 + OH + O_2 \rightarrow CH_3OO + H_2O \quad \text{(R7)}$$

$$RH + OH + O_2 \rightarrow RO_2 + H_2O \quad \text{(R8)}$$

$$HCHO + O_2 \xrightarrow{h\nu\ (\lambda<319\ nm)} H + HO_2 + CO \quad (R9)$$

In NO-poor regions, HO_2 and RO_2 are subsequently converted into hydrogen peroxide (H_2O_2), and higher organic hydroperoxides (ROOH; R10 – R12). Based on the inverse dependency of H_2O_2 production rates on temperature and pressure, it is assumed that the H_2O_2 formation proceeds most likely via a cyclic hydrogen bond intermediate (Möller, 2017). The recombination to hydroperoxides competes with other possible reactions, such as O_3 removal by HO_2 typically at 20 ppb_v of O_3 in the MBL (R13; Lee et al., 2000). This reaction belongs to an O_3 removal cycle by HO_x linked with R14. ROOH contains a large variety of organic hydroperoxides such as methyl hydroperoxide (CH_3OOH; MHP), ethyl hydroperoxide (CH_3CH_2OOH; EHP), hydroxyl methyl hydroperoxide ($CH_2(OH)OOH$; HMHP), peroxy acetic acid ($CH_3C(O)OOH$; PAA), and isoprene hydroperoxide (ISOPOOH). The mechanisms leading to the formation of higher organic hydroperoxides based on alkanes are assumed to be analogous to the formation mechanisms of MHP (Calvert and Madronich, 1987). The composition of ROOH depends on the environmental characteristics and the tropospheric region (Hellpointner and Gäb, 1989; Hewitt and Kok, 1991; Fels and Junkermann, 1994). However, within the large variety of ROOH MHP is the most prominent trace species (Lee et al., 1998; O'Sullivan et al., 1999)

$$2\,HO_2 \rightarrow H_2O_2 + O_2 \quad (R10)$$

$$CH_3OO + HO_2 \rightarrow CH_3OOH + O_2 \quad (R11)$$

$$RO_2 + HO_2 \rightarrow ROOH + O_2 \quad (R12)$$

$$O_3 + HO_2 \rightarrow OH + 2O_2 \quad (R13)$$

$$O_3 + OH \rightarrow O_2 + HO_2 \quad (R14)$$

Apart from the presented reactions, a vast diversity of alternative production paths, especially regarding higher organic peroxides has to be considered. EHP originates from the conversion of acetaldehyde (CH_3CHO) with ethyl peroxyl radical (R15), which forms also via the reaction from ethene with chlorine radicals followed by the addition of oxygen (R16). The formation of EHP is diminished in urban regions by recombination to ethoxy radicals (R17), which react consequently to acetaldehyde and HO_2 via the abstraction of a hydrogen radical (R18) or the addition of an oxygen molecule (R19). The formed acetaldehyde can subsequently serve as an additional source of hydroperoxide precursors (R9). Analogous production paths are expected based on higher RO_2. However, the abstraction of hydrogen radicals from the corresponding peroxy radical becomes more prominent with the increasing branching of the alkane source due to the pronounced stability of the peroxy radical.

$$CH_3CH_2OO + CH_3CHO \rightarrow CH_3CH_2OOH + CH_3CO \quad (R15)$$

$$C_2H_6 + Cl + O_2 \rightarrow CH_3CH_2OO + HCl \quad (R16)$$

$$CH_3CH_2OO + CH_3CH_2OO \rightarrow 2\,CH_3CH_2O + O_2 \quad \text{(R17)}$$

$$CH_3CH_2O \rightarrow CH_3CHO + H \quad \text{(R18)}$$

$$CH_3CH_2O + O_2 \rightarrow CH_3CHO + HO_2 \quad \text{(R19)}$$

Further, alkenes are sources of hydroperoxides, as shown below on the exemplary conversion of ethene (Fig. 4). The ozonolysis of ethene via a Crigee-intermediate at high relative humidity leads to the formation of HMHP (Gäb et al., 1985). The conversion via Crigee-intermediates is assumed to be a nighttime source of ROOH (Lee et al., 2000).

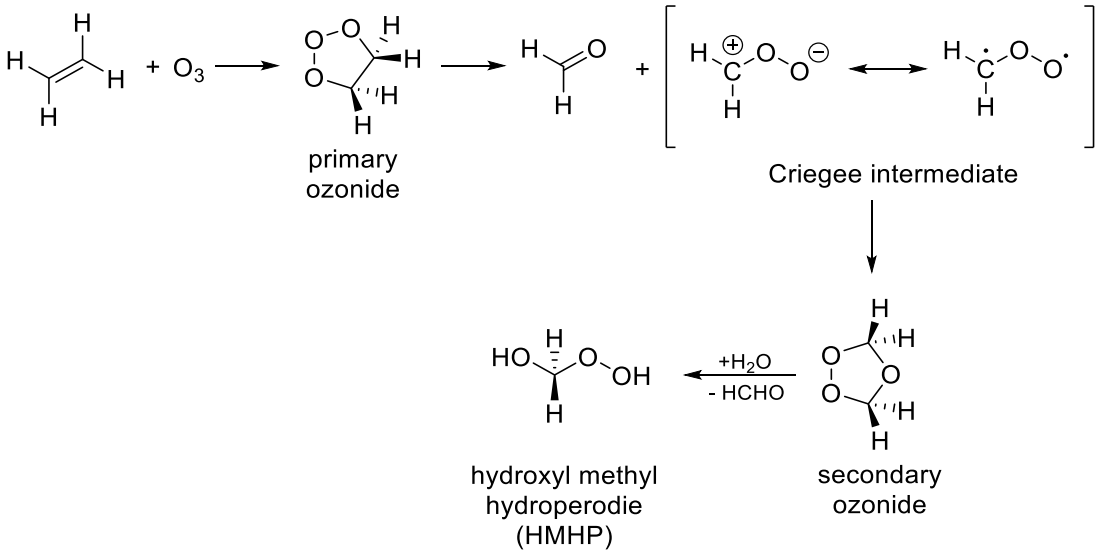

Figure 4: Exemplary conversion of ethene to hydroxyl methyl hydroperoxide (HMHP).

In NO-rich regions, the ozonolysis of alkenes competes with OH reaction followed by NO reaction to form aldehydes and HO_2 as presented exemplary (R20 – R24).

$$C_2H_4 + OH \rightarrow HOCH_2CH_2 \quad \text{(R20)}$$

$$HOCH_2CH_2 + O_2 \rightarrow HOCH_2CH_2O_2 \quad \text{(R21)}$$

$$HOCH_2CH_2O_2 + NO \rightarrow HOCH_2CH_2O + NO_2 \quad \text{(R22)}$$

$$HOCH_2CH_2O \rightarrow HOCH_2 + HCHO \quad \text{(R23)}$$

$$HOCH_2 + O_2 \rightarrow HO_2 + HCHO \quad \text{(R24)}$$

Isoprene, as a representative of conjugated alkenes reacts with OH to form a variety of ISOPOOH species, as illustrated in the reaction scheme below (Wennberg et al., 2018; Fig. 5). The OH radical adds to isoprene at C1 or C4 and forms β-hydroxy isoprene radicals, which react instantaneously with oxygen to form hydroxy isoprene peroxyl radical. The reaction is followed by the formation of isomers via the conversion of HO_2 in a NO-poor environment. Additionally, in a NO-poor environment,

ISOPOOH is formed directly via photooxidation of isoprene (Becker et al., 1990, 1993; Wennberg et al., 2018; Fig. 6). In a NO-rich environment the formation of ISOPOOH competes with the conversion to formaldehyde and methyl vinyl ketone (MVK).

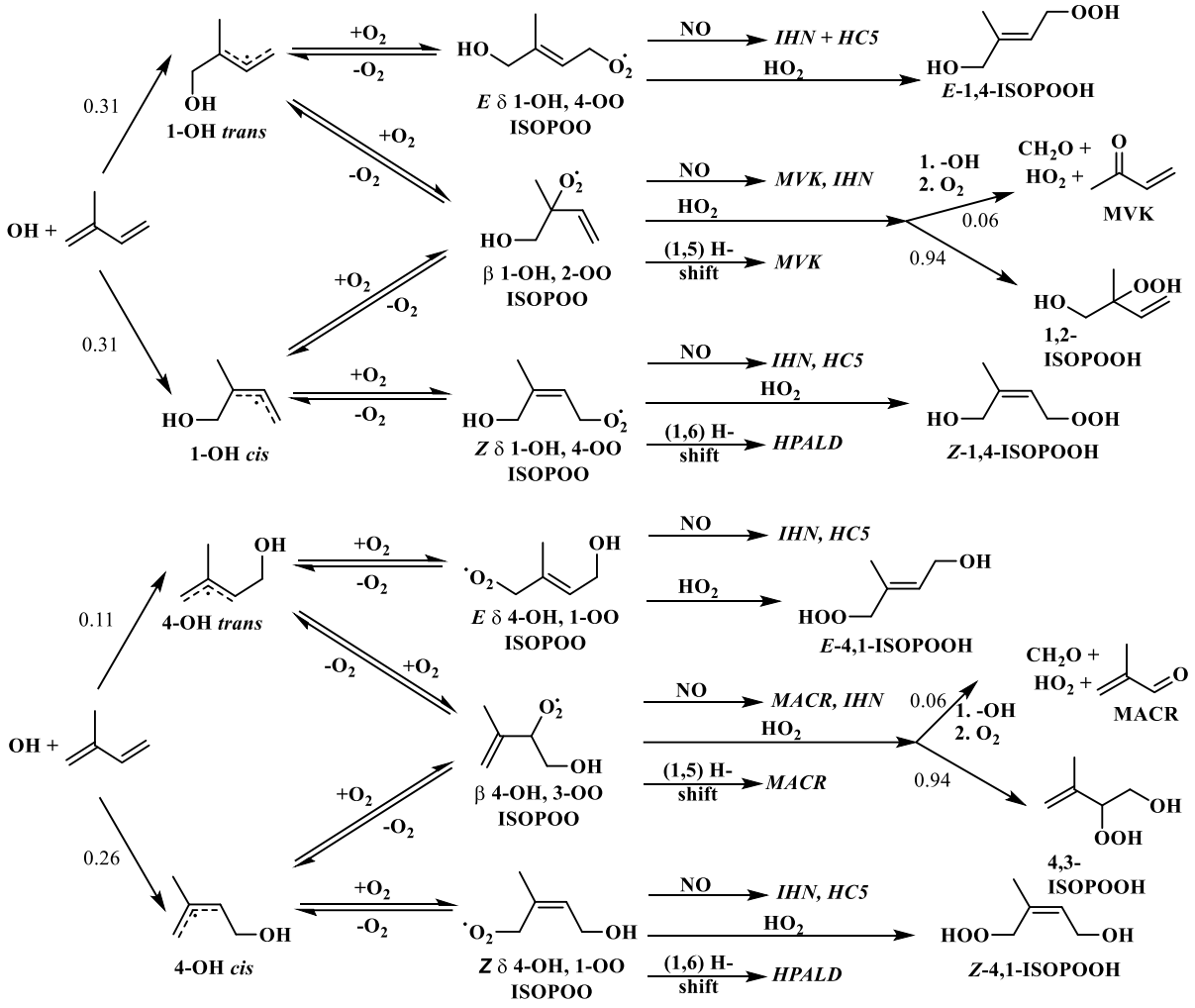

Figure 5: Dynamics of the isoprene + OH system (figure adapted with permission from Wennberg, P. O., Bates, K. H., Crounse, J. D., Dodson, L. G., McVay, R. C., Mertens, L. A., Nguyen, T. B., Praske, E., Schwantes, R. H., Smarte, M. D., St Clair, J. M., Teng, A. P., Zhang, X., and Seinfeld, J. H.: Gas-Phase Reactions of Isoprene and Its Major Oxidation Products, Chemical reviews, 118, 3337–3390, https://doi.org/10.1021/acs.chemrev.7b00439, 2018. Copyright 2018 American Chemical Society.).

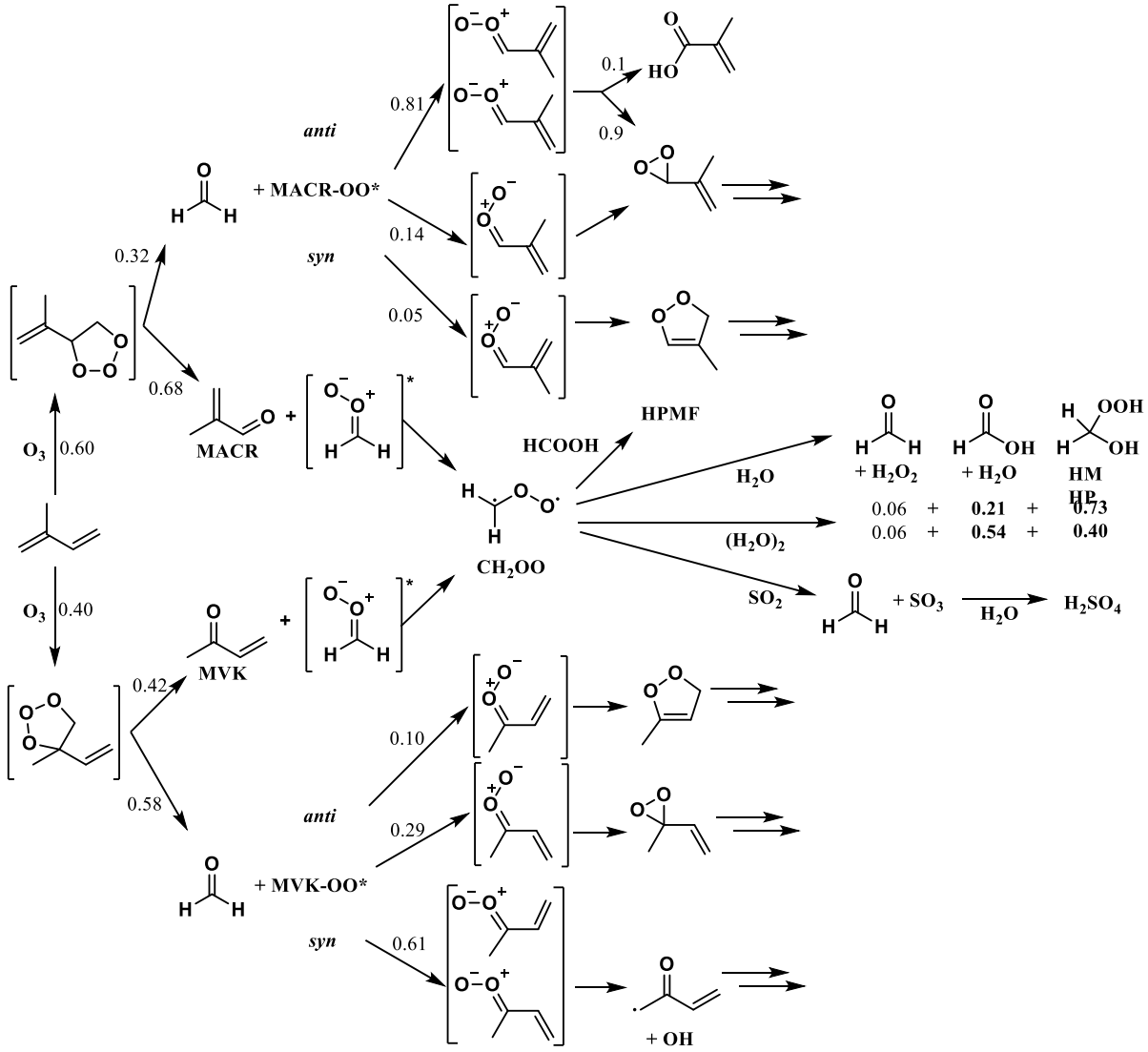

Figure 6: Dynamics of the isoprene + ozone system (figure adapted with permission from Wennberg, P. O., Bates, K. H., Crounse, J. D., Dodson, L. G., McVay, R. C., Mertens, L. A., Nguyen, T. B., Praske, E., Schwantes, R. H., Smarte, M. D., St Clair, J. M., Teng, A. P., Zhang, X., and Seinfeld, J. H.: Gas-Phase Reactions of Isoprene and Its Major Oxidation Products, Chemical reviews, 118, 3337–3390, https://doi.org/10.1021/acs.chemrev.7b00439, 2018. Copyright 2018 American Chemical Society.).

Peroxy acetic acid is formed via photooxidation of acetone (R25) and via acetaldehyde reaction with OH followed by conversion of the formed acetyl peroxyl radical with HO_2 (R26 – R27). The methyl peroxyl radical formed in R25 constitutes an additional source of MHP. Also, acetyl peroxyl radical itself forms an additional methyl peroxyl radical source via a competing conversion with NO and the subsequent reaction with oxygen (R28 – R29). Another source of PAA is the thermal decomposition of peroxyacetyl nitrate (PAN).

$$CH_3C(O)CH_3 + 2\,O_2 \xrightarrow{h\nu\ (\lambda<360\ nm)} CH_3C(O)OO + CH_3\,OO \quad \text{(R25)}$$

$$CH_3CHO + OH + O_2 \rightarrow CH_3C(O)OO + H_2O \quad \text{(R26)}$$

$$CH_3C(O)OO + HO_2 \rightarrow CH_3C(O)OOH + O_2 \quad \text{(R27)}$$

$$CH_3C(O)OO + NO \rightarrow CH_3C(O)O + NO_2 \quad \text{(R28)}$$

$$CH_3C(O)O + O_2 \rightarrow CH_3OO + CO_2 \quad \text{(R29)}$$

Further, airborne measurements gave evidence of secondary as well as direct production of hydroperoxides due to enhanced photochemistry during biomass burning episodes (Lee et al., 2000 and references therein).

The most prominent photochemical sinks of hydroperoxides are photodissociation and hydroxyl radical addition (R30 – R34). H_2O_2 photodissociation was first reported by Urey et al. (1929) and is considered to be the most prominent HO_x feedback in the free troposphere until the present day (R30; Crutzen et al., 1999). While hydroperoxide photolysis returns the highly reactive species, OH, the addition of hydroxyl radicals to hydroperoxides is assumed to be a photochemical hydroperoxide sink producing the corresponding radicals, where one HO_x is lost to H_2O (R33 – R34). The reaction rates increase with increasing altitude due to the declining availability of hydroperoxide precursors in the upper troposphere linked to the decreasing amount of water vapor suppressing the odd oxygen species conversion (R2; Lee et al., 2000). Due to their photolytic conversion capability, hydroperoxides are considered a valuable HO_x reservoir in the troposphere (Fischer et al., 2015; Fischer et al., 2018).

$$H_2O_2 \xrightarrow{h\nu\ (\lambda<360\ nm)} 2\ OH \quad \text{(R30)}$$

$$CH_3OOH\ (+O_2) \xrightarrow{h\nu\ (\lambda<360\ nm)} CH_3O + OH + HO_2 \quad \text{(R31)}$$

$$CH_3O + O_2 \rightarrow HCHO + HO_2 \quad \text{(R32)}$$

$$H_2O_2 + OH \rightarrow HO_2 + H_2O \quad \text{(R33)}$$

$$CH_3OOH + OH \rightarrow CH_3OO + H_2O \quad \text{(R34)}$$

Hydroperoxide mixing ratios are highly sensitive to the amount of nitrogen oxide (NO) and nitrogen dioxide (NO_2), CO, CH_4 as well as higher carbohydrates in the atmosphere (Logan et al., 1981; Lee et al., 2000 and references therein). In dependence on the environment (urban vs. pristine region) a large suite of competing hydroperoxide precursor conversions diminishes the amount of hydroperoxides in the troposphere (Fig. 7). By definition, hydroperoxide production is NO_x-limited (Campbell et al., 1979; Jaeglé et al., 1999). Above NO_x mixing ratios of 50 ppt_v, hydroperoxide production is inhibited, due to the faster conversion of HO_x with NO_x.

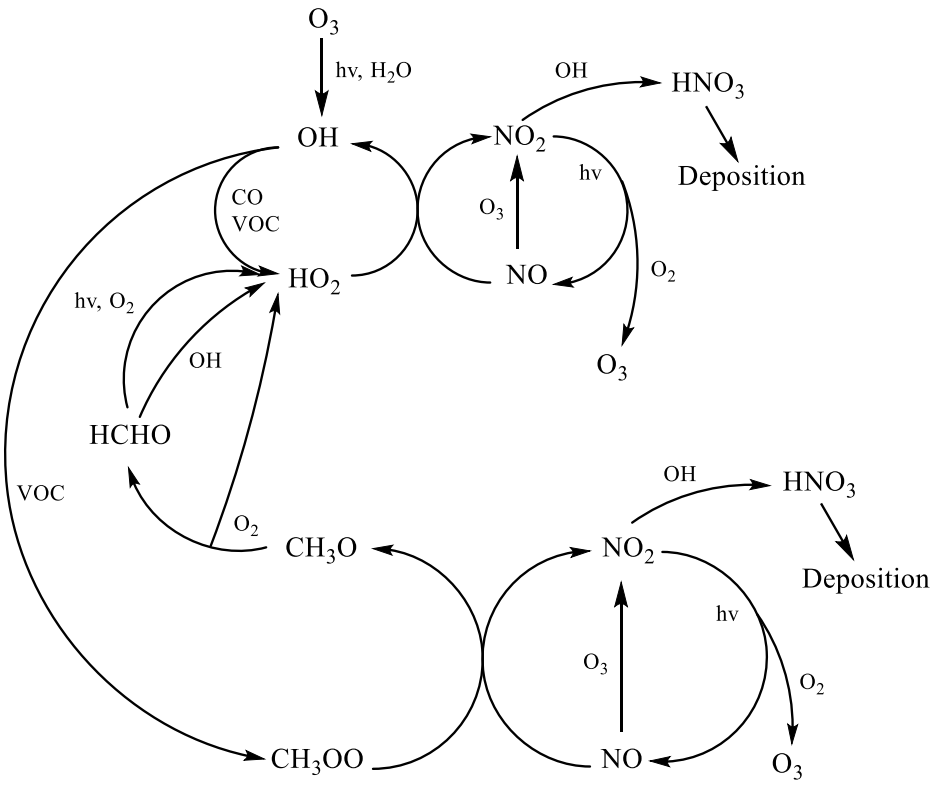

Figure 7: Hydroperoxide cycle in NOx-rich environments (figure adapted from Reeves, C. E. and Penkett, S. A.: Measurements of peroxides and what they tell us, Chemical reviews, 103, 5199–5218, https://doi.org/10.1021/cr0205053, 2003. Copyright 2003 American Chemical Society.).

In a NO_x-rich environment, hydroperoxyl and alkyl peroxyl radicals oxidize NO to NO_2 and corresponding HO_x radicals (R35 – R36). Conversion of hydroperoxyl radicals with NO to OH is considered the most prominent source involved in the OH-recycling reforming readily O_3 (Reeves and Penkett, 2003; Fischer et al., 2015). In NO_x-rich regions, methyl peroxyl radicals form hydroperoxyl radicals and formaldehyde, which constitute an HO_2 radical and CO (R36 – R37). The effectiveness of the conversion increases with decreasing humidity, leading to an additional HO_x source in a dry environment (Lee et al., 2000 and references therein).

$$HO_2 + NO \rightarrow OH + NO_2 \quad \text{(R35)}$$

$$CH_3OO + NO + O_2 \rightarrow HCHO + NO_2 + HO_2 \quad \text{(R36)}$$

$$HCHO + OH + O_2 \rightarrow HO_2 + CO + H_2O \quad \text{(R37)}$$

However, hydroperoxides can still be formed in polluted air, since it might contain a significant amount of NMHCs being a valuable source of hydroperoxides as well as H_2O_2 via the NMHC breakdown process (Reeves and Penkett, 2003).

For hydroperoxides, the majority of the homogeneous reaction processes in the gas and liquid cloud phase are analogous to the conversions discussed above. In the aqueous phase of the clouds,

hydroperoxide production takes place analogously to the gas phase via HO_2 radicals, which is the dominant production path in the liquid phase. Already in 1982, Heikes et al. reported about potential H_2O_2 production in cloud droplets. However, despite the fast aqueous-phase conversion, the impact of the cloud-droplet H_2O_2 formation is assumed to be of minor importance due to the lower accessibility of the liquid water in clouds relative to the water vapor amount in the gaseous phase. At pH values above 4.5 and at low SO_2 mixing ratios, a reaction of HO_2 with O_2 adds to the aqueous-phase H_2O_2 production (R38 – R40).

$$HO_2 + H_2O \rightarrow H_3O^+ + O_2^- \quad \text{(R38)}$$

$$O_2^- + HO_2 \rightarrow HO_2^- + O_2 \quad \text{(R39)}$$

$$HO_2^- + H_3O^+ \rightarrow H_2O_2 + H_2O \quad \text{(R40)}$$

Additionally, photochemical reactions of organic substances and transition metal complexes in continental clouds can be considered hydroperoxide sources (Kormann et al., 1988; Zuo and Hoigne, 1992; Zuo and Deng, 1997). In continental clouds, the hydroperoxide chemistry is significantly dependent on the presence of different trace gases and aerosol particles originating from natural and anthropogenic emissions, often bearing metal particles and metal ions with catalytic impact on the aqueous phase. The most compelling difference in the chemistry of continental clouds to marine clouds is the impact of SO_2 oxidation by hydroperoxides in the liquid phase leading to an important decrease in the hydroperoxide mixing ratios in the atmosphere (R41 – R44; Hoffmann and Edwards, 1975; Penkett et al., 1979; Robbin Martin and Damschen, 1981). The reaction of hydroperoxide with sulfur dioxide in clouds produces sulfuric acid and the subsequent precipitation is a well-known phenomenon of the so-called acidic rain. The reaction rate increases with decreasing amounts of available H_2O_2 in cloud or fog droplets (McArdle and Hoffmann, 1983; Lind et al., 1987) and an increasingly acidic environment. As was postulated in the 1980s by Kelly et al., the conversion of SO_2 with H_2O_2 to H_2SO_4 has its peak rates at pH < 4.5. Analogous aqueous-phase reactions are also known for ROOH, for instance, MHP, PAA or ISOPOOH (R45 – R46), however, only when H_2O_2 is limited (Lind and Kok, 1986; Zhou and Lee, 1992).

$$SO_2 + H_2O \rightleftharpoons SO_2 \cdot H_2O \quad \text{(R41)}$$

$$SO_2 \cdot H_2O \rightleftharpoons HSO_3^- + H^+ \quad \text{(R42)}$$

$$HSO_3^- + H_2O_2 \rightleftharpoons HSO_4^- + H_2O \quad \text{(R43)}$$

$$HSO_4^- + H^+ \rightarrow H_2SO_4 \quad \text{(R44)}$$

$$2HSO_3^- + 2CH_3OOH \rightarrow SO_4^{2-} + CH_3SO_4^- + H_2O + CH_3OH + H^+ \quad \text{(R45)}$$

$$HSO_3^- + CH_3C(O)OOH \rightarrow SO_4^{2-} + CH_3C(O)OH + H^+ \quad \text{(R46)}$$

Equivalent reactions with NO_x were reported in the past (R47 – R50; Damschen and Martin, 1983; Calvert et al., 1985).

$$NO + OH \rightarrow HNO_2 \quad \text{(R47)}$$

$$NO + NO_2 + H_2O \rightarrow 2HNO_2 \quad \text{(R48)}$$

$$HNO_2 + H_2O_2 \rightarrow HOONO + H_2O \quad \text{(R49)}$$

$$HOONO \rightarrow H^+ + NO_3^- \quad \text{(R50)}$$

Another important aqueous-phase sink of hydroperoxides is their reaction with metal particles and metal ions (R51 – R54; Kelly et al., 1985; Zuo and Hoigné, 1993). The reaction of transition metal ions proceeds analogously to the Fenton reaction leading to the formation of HO_2, OH, and alkoxy (RO) radicals reducing the amount of hydroperoxides in the ambient air (Graedel et al., 1986; Weinstein-Lloyd and Schwartz, 1991; Zepp et al., 1992).

$$Fe^{2+} + H_2O_2 \rightarrow Fe^{3+} + OH + OH^- \quad \text{(R51)}$$

$$OH + H_2O_2 \rightarrow H_2O + HO_2 \quad \text{(R52)}$$

$$HO_2 + H_2O_2 \rightarrow OH + H_2O + O_2 \quad \text{(R53)}$$

$$Fe^{2+} + ROOH \rightarrow Fe^{3+} + RO + OH^- \quad \text{(R54)}$$

Until present, extensive scientific research was dedicated to the topic of distribution in the dual-phase system of clouds and concentrations of hydrogen peroxide in their aqueous phase (Kelly et al., 1985; Olszyna et al., 1988; Sakugawa et al., 1990; Sakugawa et al., 1993). In the cloud gas phase, the average hydrogen peroxide mixing ratio was reported to be between 0.1 ppb_v and 0.2 ppb_v, while the concentration of H_2O_2 in the liquid phase was determined to be between 10^{-7} M and 10^{-4} M (Zuo and Hoigné, 1993). Additionally, in the gaseous phase, hydroperoxide mixing ratios increase with increasing intensity of solar irradiation, temperature, VOCs concentration, and water vapor amount in the clouds. However, higher mixing ratios for NO_x and SO_2 reduce the formation of hydrogen peroxide in clouds (Kelly et al., 1985; Jacob et al., 1990; Sakugawa et al., 1990).

1.4. Spatial and temporal trends of the hydroperoxide distribution in the troposphere

Atmospheric H_2O_2 was first detected by Buffani in 1972. The highest H_2O_2 levels until present were recorded during the California smog episode in 1978 (Kok et al., 1978). Hydroperoxides have an average atmospheric lifetime of a few days, thus they are subject to both spatial and seasonal variations (Heikes et al., 1996; Reeves and Penkett, 2003). The formation of hydroperoxides from HO_x occurs

only during the day since the photochemical decomposition of O_3 serves as the main source of HO_x. Hydroperoxide fluctuations are thus, reflected in diurnal cycles with maximum mixing ratios in temporal proximity to the time of the sun's highest point and minima during the night. The resulting maximum values stem from the hydroperoxide formation via ozone photolysis with maximum mixing ratios for the warm seasons (Ayers et al., 1996; Lee et al., 2000 and references therein). Due to the high reactivity of the HO_x species, the hydroperoxide levels decrease to their minimum until nighttime.

Humidity, temperature, and pressure as well as solar irradiation have a major impact on the chemical processes of hydroperoxides (Logan et al., 1981; Kleinman, 1986, 1991; Lee et al., 2000 and references therein). Dry and wet deposition affect levels of hydroperoxides in the atmosphere representing their most impactful sinks in the troposphere (Fischer et al., 2015; Dienhart et al., 2023). Generally, the global distribution of hydroperoxides is determined by transport and deposition processes as well as photochemical processes in the troposphere. With increasing solar irradiation and temperature, the formation of hydroperoxides increases due to enhanced photochemical activity (Lee et al., 2000 and references therein). With increasing altitude and thus, distance from the earth's surface linked with decreasing humidity, the amount of hydroperoxide precursors decreases leading to an increased contribution of hydroperoxide photolysis to the HO_x budget (Heikes et al., 1996; Jaeglé et al., 2000). The trend is most prominent in NO_x-poor environments. In the marine boundary layer, further reduction in the mixing ratios from the tropics to the poles was reported with maximum hydroperoxide mixing ratios of up to 500 ppt_v in tropical regions (Heikes et al., 1996; Fischer et al., 2015). In NO_x-rich regions, hydroperoxide vertical, and latitudinal distribution are reported to be more complex (Nunnermacker et al., 2008). In the planetary boundary layer, due to the increased deposition paired with the increased mixing of the air masses, low hydroperoxide levels are expected (Heikes et al., 1996; Lee et al., 1998). Maximum hydroperoxide mixing ratios directly above the tropospheric boundary layer at altitudes of 2 – 5 km, especially in the northern hemisphere, were reported (Heikes et al., 1987; Daum et al., 1990; Snow et al., 2007; Stickler et al., 2007; Klippel et al., 2011). In effect, the vertical distribution of hydroperoxides follows an inverted C-shaped trend throughout the tropospheric column (Weinstein-Lloyd et al., 1998; Klippel et al., 2011). However, numerous research groups reported peak hydroperoxide levels in the upper troposphere due to convection (Weinstein-Lloyd et al., 1998; Crutzen and Lawrence, 2000; Snow et al., 2007; Klippel et al., 2011; Bela et al., 2016; Bozem et al., 2017). The comparably low sensitivity of ROOH relative to H_2O_2 regarding wet and dry deposition, linked to the two orders of magnitude lower Henry's law coefficient, results in a significantly diminished vertically inverted C-shaped trend (Klippel et al., 2011). Furthermore, a latitudinal dependence of the mixing ratios was observed reflecting the enhanced photochemical activity and high availability of water vapor (Jacob and Klockow, 1992; O'Sullivan et al., 1996; Allen et al., 2022). The maximum hydroperoxide levels were reported directly above the tropical boundary layer in close proximity to the equator (Hafermann, 2016). Lower values were recorded with increasing distance from the equator (O'Sullivan et al., 1996). However, the hydroperoxide levels seem to be approximately by a factor of up to 2 higher

in the northern versus southern hemisphere (Lee et al., 2000 and references therein). These results were also obtained in the upper troposphere (Jacob and Klockow, 1992; Lee et al., 2000). Nonetheless, the hydroperoxide distribution trends, especially for H_2O_2, might be severely perturbed due to its dependence on the meteorological environment, as will be discussed in the scope of this work based on three research projects, Chemistry of the Atmosphere: Field Experiment in Africa (CAFE-Africa), BLUESKY and Chemistry of the Atmosphere: Field Experiment in Brazil (CAFE-Brazil).

2. Methods

Measurements of trace gases in the troposphere provide information on the resilience and oxidation capacity of the atmosphere. In this chapter, methods required for hydroperoxide analyses derived from in situ measurements are presented. Sect. 2.1. describes the measurement setup used for airborne hydroperoxide measurements, the peroxide monitor HYPHOP (HYdrogen Peroxide and Higher Organic Peroxides monitor). Here, a detailed measurement method characterization and the required data analyses are discussed in the scope of a research article with the title: "HYPHOP: a tool for high-altitude, long-range monitoring of hydrogen peroxide and higher organic peroxides in the atmosphere" submitted to the journal *Atmospheric Measurement Techniques* (AMT) in June 2023. The following sections give an overview of further supporting methods used for hydroperoxide data analysis, as hydroperoxide simulations with the global numerical 3-D ECHAM5/MESSy Atmospheric Chemistry model (EMAC; Sect. 2.2.), meteorology reanalysis data by Copernicus, ERA5 (Sect. 2.3.), and hydrogen peroxide mixing ratio calculations based on quasi-photostationary steady-state assumption (PSS; Sect. 2.4.).

2.1. Hydrogen Peroxide and Higher Organic Peroxides monitor – HYPHOP

The section discusses in detail the hydroperoxide measurement technique applied during the airborne measurements on board the research aircraft, High-Altitude and Long-range Observatory (HALO), and the corresponding data acquisition, and processing. The description of the measurement method, data processing, and the evaluation of the potential interference sources affecting airborne hydroperoxide measurements were submitted as a research article with the title: "HYPHOP: a tool for high-altitude, long-range monitoring of hydrogen peroxide and higher organic peroxides in the atmosphere" to the journal *Atmospheric Measurement Techniques* (AMT) and were recently published as a preprint in the scope of the *Atmospheric Measurement Techniques Discussions* (AMTD). The manuscript draft is presented in this work in its preprint state. As the first author of the manuscript, together with H. Fischer I planned the study and performed the corresponding measurements during the first phase of the measurements, whilst D. Dienhart and A. Hartmann covered the hydroperoxide measurements during the second phase of the airborne campaign. Supported by D. Dienhart and A. Hartmann, I processed and analyzed the data. The manuscript was written with the contribution of all co-authors.

In the manuscript, an instrumental setup designed specifically for airborne hydroperoxide measurements deployed on the HALO aircraft, HYPHOP monitor based on dual-enzyme fluorescence spectroscopy is introduced. The measuring principle is based on a 2-channel technique by Lazrus

(Lazrus et al., 1985; Lazrus et al., 1986), with which not only H_2O_2 can be measured, but also an estimate of ROOH in the atmosphere. The main goal of the work presented below was the characterization of the measurement method and data acquisition with special emphasis on potential interferences impacting instrumental uncertainty. Physically driven interferences were examined based on a test flight to investigate potential measurement inconsistencies arising from the dynamic movement patterns of the aircraft. Technical and physical challenges during flight maneuvers do not impact the instrumental performance and thus, the absolute measurements of hydroperoxide levels. The monitor resolves sufficiently dynamic processes such as convective transport in the South Atlantic Convergence Zone (SACZ) as shown in the overview of the measurement campaign, Chemistry of the Atmosphere: Field Experiment in Brazil performed in December 2022 – January 2023 (CAFE-Brazil).

https://doi.org/10.5194/amt-2023-114
Preprint. Discussion started: 12 June 2023

Atmospheric Measurement Techniques Discussions

HYPHOP: a tool for high-altitude, long-range monitoring of hydrogen peroxide and higher organic peroxides in the atmosphere

Zaneta Hamryszczak[1], Antonia Hartmann[1], Dirk Dienhart[1], Sascha Hafermann[1], Bettina Brendel[1], Rainer Königstedt[1], Uwe Parchatka[1], Jos Lelieveld[1,2] and Horst Fischer[1]

[1]Atmospheric Chemistry Department, Max Planck Institute for Chemistry, Mainz, 55128, Germany
[2]Climate and Atmosphere Research Center, The Cyprus Institute, Nicosia, 1645, Cyprus

Correspondence to: Zaneta Hamryszczak (z.hamryszczak@mpic.de) and Horst Fischer (horst.fischer@mpic.de)

Abstract.

Measurements of hydroperoxides help improve our understanding of atmospheric oxidation processes. Here, we introduce an instrument setup designed for airborne hydroperoxide measurements. The HYdrogen Peroxide and Higher Organic Peroxides (HYPHOP) monitor has been deployed on the German High-Altitude and Long-range Observatory (HALO) aircraft and is based on dual-enzyme fluorescence spectroscopy, enabling measurements up to ambient pressure of approximately 150 hPa pressure altitude (13.5–14 km). We characterized the measurement method and data acquisition of HYPHOP with special emphasis on potential sources of interference impacting instrument uncertainty. Physically derived interference was examined based on a dedicated test flight to investigate potential measurement inconsistencies arising from the dynamic movement patterns of the aircraft. During the test flight, the hydroperoxide monitor was operated in the background air sampling mode with purified air by scrubbing atmospheric trace gases, to investigate the instrument stability and potential parameters that might affect the measurements. We show that technical and physical challenges during flight maneuvers do not critically impact the instrument performance and the absolute measurements of hydroperoxide levels. Dynamic processes such as convective transport in the South Atlantic Convergence Zone (SACZ) are well-resolved as shown in the overview of a recent measurement campaign, Chemistry of the Atmosphere: Field Experiment in Brazil, in December 2022–January 2023 (CAFE-Brazil). The instrument precision based on the measurement results during CAFE-Brazil for hydrogen peroxide and the sum of organic hydroperoxides is estimated to be 6.4% (at 5.7 ppbv) and 3.6% (at 5.8 ppbv), respectively, and the corresponding detection limits 20 pptv and 19 pptv for a data acquisition frequency of 1 Hz, subsequently integrated over 120 second time intervals.

1 Introduction

Hydroperoxides are key contributors to the self-cleaning capacity of the troposphere due to their dual role as sinks and sources of the main atmospheric oxidant, the hydroperoxyl radical (OH) and of peroxy radicals (HO_2), often collectively described as HO_x (HO_x= HO_2+OH; Gunz and Hoffmann, 1990; Lee et al., 2000; Reeves and Penkett, 2003 and the references therein). Due to their relatively high solubility and reactivity, hydroperoxides, especially H_2O_2, play an important role in the chemistry of

https://doi.org/10.5194/amt-2023-114
Preprint. Discussion started: 12 June 2023

Atmospheric Measurement Techniques Discussions

the liquid phase of clouds, rain, and fog (Kelly et al., 1985; Madronich, 1987; Olszyna et al., 1988; Sakugawa et al., 1990; Lelieveld and Crutzen, 1991, 1994; Edy et al., 1996).

Schöne et al. reported the first findings on the abundance of hydrogen peroxide (H_2O_2) in the atmospheric aqueous phase in the 19th century (1874, 1893, 1894), but it was only in the 1970s that hydroperoxides became the focus of significant scientific attention (Gunz and Hoffmann, 1990 and references therein). The 1980s saw extensive work on the role of hydroperoxides in the generation of sulfuric acid and nitric acid in clouds, rain, and fog leading to characterization of the phenomena of so-called acidic fog and rain (Hoffmann and Edwards, 1975; Penkett et al., 1979; Robbin Martin and Damschen, 1981; Damschen and Martin, 1983; Kunen et al., 1983; Calvert et al., 1985; Lee and Lind, 1986). More recent studies on the hydroperoxides have provided insights into their tropospheric abundance and their importance in atmospheric oxidative processes (Gunz and Hoffmann, 1990; Sakugawa et al., 1990; Reeves and Penkett, 2003; Klippel et al., 2011; Fischer et al., 2019; Hottmann et al., 2020; Allen et al., 2022a; Allen et al., 2022b; Hamryszczak et al., 2022; Dienhart et al., 2023; Hamryszczak et al., 2023). Thus, it is not surprising that over the past decades, numerous hydroperoxide measurement methods have been established to investigate the species in both the gaseous and aqueous phases of the atmosphere.

The first highly sensitive H_2O_2 measurements were performed using luminol and peroxy oxalate-based chemiluminescent techniques (Kok et al., 1978; Bufalini et al., 1979; Kelly et al., 1979; Kok, 1980; Heikes et al., 1982; Römer et al., 1985; Heikes et al., 1987; Jacob and Klockow, 1992). Guilbault et al. (1968) proposed an enzyme fluorescence technique using peroxidase to detect hydrogen peroxide Later, Lee et al. (1990; 1994) presented an alternative non-enzymatic measurement technique based on the H_2O_2 Fenton reaction. Alternative methods, such as high-performance liquid chromatography (HPLC) paired with post-column derivatization (Hellpointner and Gäb, 1989; Hewitt and Kok, 1991; Fels and Junkermann, 1994; Kok et al., 1995; Lee, 1995) and tunable diode laser absorption spectroscopy (TDLAS; Slemr et al., 1986; Mackay et al., 1990) have likewise been widely adopted for measuring H_2O_2 in ambient air. Further, gas chromatography techniques were used to sample hydrogen peroxide and ROOH organic hydroperoxides (Kok et al., 1995 and the references therein). The most recently developed and optimized technique described by Crounse et al. (2006) and St.Clair et al. (2010) uses measurements based on soft chemical ionization and compact time-of-flight mass spectroscopy complimented by triple quadrupole mass spectrometry. The method was used to detect hydroperoxides in the troposphere with high sensitivity (California Institute of Technology Chemical Ionization Mass Spectrometers, CIT-CIMS).

The measurement technique presented in this work is based on the wet chemical dual-enzyme measurement system of Lazrus et al. (1985; 1986), which has been successfully employed in numerous research groups (Gunz and Hoffmann, 1990 and references therein). With this method, hydroperoxides are detected using p-hydroxyphenyl acetic acid (POPHA) and horseradish peroxidase (HRP). The stoichiometric reaction of these compounds yields a hydroperoxide-specific chemiluminescent molecule (Guilbault et al., 1968), which is detected by fluorescence spectroscopy. The distinction between H_2O_2 and ROOH is achieved by selective destruction of the former with catalase in a dual-reactor system.

To meet the requirements of long measurement flights under highly dynamic airborne conditions, the Hydrogen Peroxide and Higher Organic Peroxides (HYPHOP) instrument was developed based on the commercially available AL2001CA

https://doi.org/10.5194/amt-2023-114
Preprint. Discussion started: 12 June 2023


Atmospheric Measurement Techniques Discussions

hydroperoxide monitor (Aero-Laser, Garmisch-Partenkirchen, Germany). HYPHOP was designed as a lightweight and compact monitor, where the measurement process and the complementary data acquisition are controlled by a compact V25 control unit (Max Planck Institute for Chemistry, Mainz, Germany). The instrument was further equipped with a constant pressure inlet unit (CPI), making it suitable for *in situ* measurements under varying ambient air pressures. HYPHOP was designed in 2014 and was first installed onboard of the High Altitude and Long-range research aircraft (HALO) in January 2015 during the Oxidation Mechanism Observation (OMO) project. Since that time, it has been deployed successfully in 53 measurement flights with more than 330 flight hours of tropospheric and lower stratospheric hydroperoxide measurements during aircraft campaigns (Hottmann et al., 2020; Hamryszczak et al., 2022; Hamryszczak et al., 2023). The instrument is deployed together with the Tracer In-Situ TDLAS (Tunable Diode Laser Absorption Spectroscopy) for Atmospheric Research (TRISTAR) in a 19'' measurement rack and uses two measurement channels for continuous measurements (Tomsche et al., 2019). HYPHOP tracks total levels of ambient hydroperoxides and the sum of organic peroxides separately. By subtracting the organic hydroperoxide mixing ratios from the total measured hydroperoxides, hydrogen peroxide mixing ratios are determined.

Based on studies of hydroperoxide reactions with other tropospheric trace gases, different chemical sources of interference affecting the measurement method have been identified (Heikes et al., 1982; Graedel and Goldberg, 1983; Graedel et al., 1986; Weschler et al., 1986; Jackson and Hewitt, 1999). On the one hand, reactions with sulfur dioxide, (SO_2), metal ions and nitrogen oxide (NO) in the atmospheric aqueous phase lead to a significant loss of the ambient H_2O_2 in liquid samples. On the other hand, H_2O_2 production via adsorption of ozone (O_3) on wet surfaces leads to positive interference in the measurement system. Additionally, due to the specific measurement setup, instrument precision may suffer from various physical noise sources, such as cabin temperature altering the solubility, mainly of organic hydroperoxides, in the analytic solution and incomplete transmission of the trace gases due to wall loses in the inlet of the system. Detection instabilities might also be triggered by rapid aircraft movements and turbulence affecting both the liquid and gaseous mass transport during the operation.

This work describes the measurement method and characteristics and addresses potential sources of inconsistencies caused by chemical and physical interference during measurement flights. To examine the effect of physical interference on *in situ* hydroperoxide measurements, an individual test flight to examine the impact of aircraft movement patterns on the measurement outcome was designed and performed during the preliminary phase of the Chemistry of the Atmosphere – Field Experiment in Brazil (CAFE-Brazil; October–November 2022) campaign based out of the German Aerospace Center (DLR) in Oberpfaffenhofen (Germany). A detailed introduction to the instrument setup on board of the research aircraft, the measurement method, data acquisition, and signal correction are given in the following sections (Sect. 2.1 and Sect. 2.2). Additionally, we address potential chemically and physically derived inconsistencies, analyze their impact on airborne hydroperoxide measurements, and characterize the instrument in detail (Sect. 2.3 and 2.4). In Sect. 3, an overview of the instrument performance is given based on the measurement results during the CAFE-Brazil aircraft campaign. Finally, we present an overview of the characteristics of the hydroperoxide monitor (Sect. 4).

https://doi.org/10.5194/amt-2023-114
Preprint. Discussion started: 12 June 2023

Atmospheric Measurement Techniques Discussions

2 HYPHOP: HYdrogen Peroxide and Higher Organic Peroxide monitor

2.1 Measurement method and instrument setup on board of the HALO research aircraft

During airborne measurements performed with the research aircraft HALO, the HYPHOP monitor is deployed into a single 19" measurement frame rack together with the TRISTAR instrument. The rack is further equipped with a manually cooled liquid container department and a constant pressure inlet (CPI) pump. Both HYPHOP and TRISTAR are simultaneously connected to a bypass that channels the sampled ambient air from the Teflon-coated trace gas inlet (TGI) embedded in a stainless-steel compartment. Fig. S1a provides a picture of the instrumental setup on board of HALO. Since the commercially available peroxide monitor was designed to perform measurements under standard conditions, the airflow system of HYPHOP was extended by the CPI system, ensuring constant pressure of the sampled air during airborne measurements at highly variable ambient pressure conditions. The technical circuit of the system is presented as a diagram below (Fig. 1).

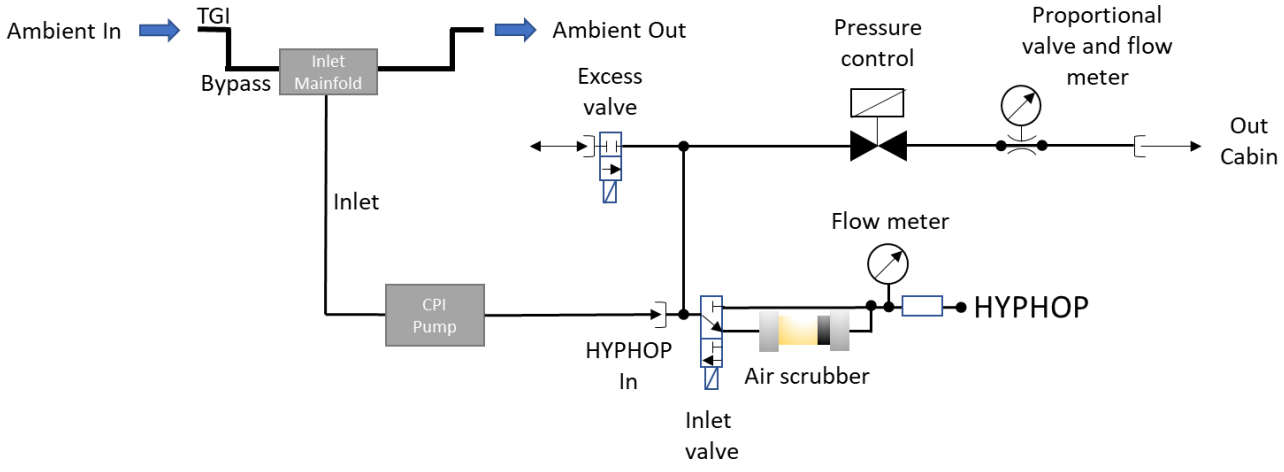

Figure 1: Technical circuit diagram of the airflow system.

During airborne measurements, ambient air is sampled from the top of the aircraft fuselage through a Teflon-coated tubing installed in a forward-facing stainless-steel TGI connected to a bypass consisting of a 1.45 m-long ½ in. PFA (perfluoro alkoxy alkane) tube inside the aircraft and to an exit through a second TGI. The gas inlet system consisting of connection tubing from the bypass via a Teflon inlet manifold (length: 0.27 m) to the CPI pump (length: 2.65 m) and further to the monitor (length: 1.15 m) is made of a ¼ in. PFA tubing to reduce potential surface effects and wall losses. The CPI system contains an internal CPI control unit and a Teflon-coated membrane pump (type MD 1C; Vacuubrand, Wertheim, Germany), generating an excess airflow of up to approximately 10 standard liters per minute (slm) to the sampling inlet of the monitor. The CPI is connected via the inlet manifold to an external pressure sensor tracking the ambient pressure (inlet pressure). The internal CPI control unit consists of a proportionality valve with an airflow sensor, an excess valve, and a pressure control unit in front of the sampling coil to ensure nearly constant pressure during the measurement flights. The highly sensitive proportionality valve

https://doi.org/10.5194/amt-2023-114
Preprint. Discussion started: 12 June 2023

Atmospheric Measurement Techniques Discussions

controls the airflow through the instrument based on variations of the measured ambient pressure detected by the sensor in the inlet, so that a stable airflow of approximately 2 slm is achieved. Excess air is ejected into the cabin. The additional excess valve is activated when the measured air pressure of the sampling line exceeds 1100 hPa, thus preventing damage to the instrument due to overpressure. With higher altitudes, the pump output increases, and, thus, the line pressure and the airflow are stabilized to approximately ambient pressure and 2 slm.

After traversing the inlet system, the ambient air is passed through a reaction coil (glass) with a simultaneous injection of a precooled buffered sampling solution (4–6 °C; pH = 5.8–6.0) consisting of potassium hydrogen phthalate (KHP) and sodium hydroxide (NaOH; 1 M) in purified water. From the reaction coil, the hydroperoxide-enriched sampling solution is subdivided into two reactors (channels A and B), where an analogously precooled fluorescence solution consisting of p-hydroxyphenyl acetic acid (POPHA) and horseradish peroxidase (HRP) and a precooled sodium hydroxide solution (NaOH; 1 M) are added. Fig. 2 gives an overview of the liquid flow circuit of HYPHOP. The front view of the instrument is displayed in Fig. S1b in the Supplement of this work.

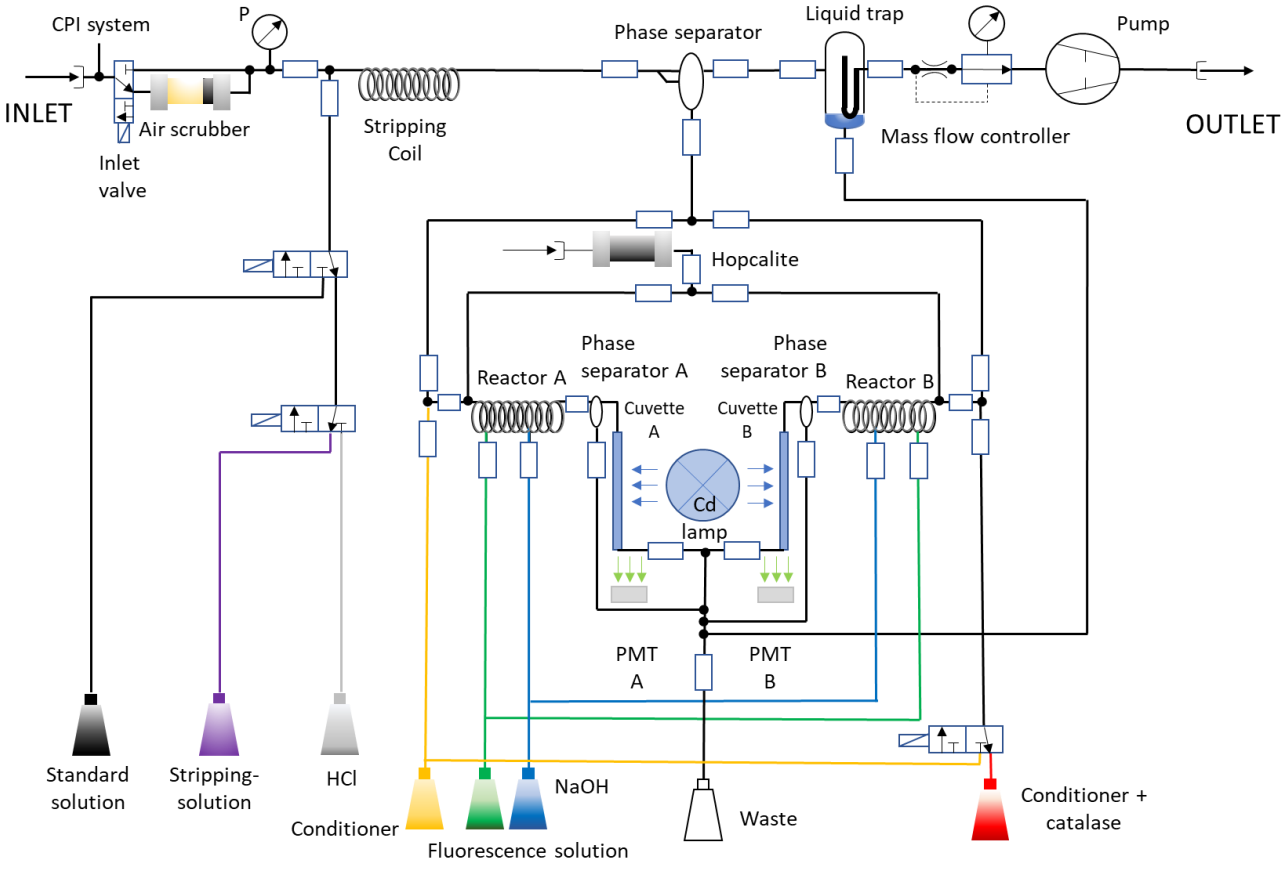

Figure 2: Liquid flow diagram of HYPHOP.

https://doi.org/10.5194/amt-2023-114
Preprint. Discussion started: 12 June 2023


Atmospheric Measurement Techniques Discussions

The hydroperoxides are detected based on stoichiometric reaction with POPHA, which yields a chemiluminescent POPHA-dimer (6,6'-dihydroxy-3,3'-biphenyl diacetic acid). The catalytic center of HRP enables a species-specific binding of the hydroperoxides, which subsequently react with POPHA to form chemiluminescent-active dimers. This chemiluminescent compound is then measured with a Cd pen ray lamp (UVP, Inc., Upland, United States) at 326 nm by means of fluorescent spectroscopy. The species-specific fluorescence is detected at 400–420 nm using two parallel photomultiplier tubes (PMT; Type: H957-29, Hamamatsu, Japan) at both channels separately as electrical signals, which are translated into mixing ratios using a four-point calibration described in Sect. 2.2. The concentration of H_2O_2 in the sample is determined as the difference between the total concentration of hydroperoxides (channel A) and the sum of the organic peroxides (ROOH; channel B), where the added catalase selectively destroys hydrogen peroxide in the sampling solution. The corresponding chemical reactions (SR1–SR4) are presented in the Supplement of this work. The catalase destruction efficiency of hydrogen peroxide is determined via liquid calibration of the instrument at 0.95–0.99 using an H_2O_2 liquid standard (0.99 µmol L^{-1}) produced in a serial dilution from a constantly cooled H_2O_2 stock solution.

2.2 Data acquisition and signal correction

HYPHOP operates in three modes: liquid calibration, background and ambient mode. The monitor is controlled by a V25 control unit (Max Planck Institute for Chemistry, Mainz, Germany). The control unit is a multitasking, multiprocessing real-time operating system, which consists of a command interpreter and a configuration compiler for mode application, data storage, and PC communication. The valves switch between the supply tubing of the solutions required for each mode and between ambient and purified air, respectively, depending on the operating mode which is managed by the V25 unit (Fig. 2). During the ambient (measure) mode, the sampling process is performed as described above. In the background mode, hydroperoxide-free air samples are produced and measured frequently in order to investigate any temperature-related altering of the hydroperoxide signals during the flights. The background air is generated by transmitting ambient air through a scrubber, the zero-gas cartridge, containing silica gel (type IAC-502; Infiltec, Speyer, Germany), which adsorbs the moisture from the air sample and hopcalite (type IAC-330; Infiltec, Speyer, Germany). The latter destroys atmospheric hydroperoxides and other trace gases, enabling estimation of the instrument background, and is used during the calibration.

The calibration mode is performed on the ground prior to each measurement flight, during which a liquid H_2O_2 standard is measured in order to determine the hydroperoxide detection sensitivity and to estimate a signal reference required to transfer the detected electric signal into hydroperoxide mixing ratios. During this process, the instrument generates constantly purified hydroperoxide-free air analogous to the background measurement procedure. Prior to the calibration, both channels are flushed with hydrochloric acid (HCl; 1 M) in order to remove remaining catalase and any potential residuals from previous ambient measurements. The calibration process is subdivided into four phases (four-point calibration) using a freshly prepared liquid standard (2–4 °C) obtained from a serial dilution of a constantly cooled hydrogen peroxide stock solution. In the first step of the liquid calibration, the standard is injected into the sampling coil. In the second and third steps, purified air is sampled and

https://doi.org/10.5194/amt-2023-114
Preprint. Discussion started: 12 June 2023

Atmospheric Measurement Techniques Discussions

channel B is operated with and without the addition of catalase. In the last step, the liquid H_2O_2 standard is injected again with the addition of catalase in channel B.

The concentration of hydrogen peroxide ($[H_2O_2]$) in the liquid standard is determined by means of a redox titration with potassium permanganate ($KMnO_4$) under acidic conditions (H_2SO_4) as presented in the Supplement of this work (SR5–SR7 and Eq. S1). The corresponding mixing ratios can be calculated using the measured air and liquid flows of the instrument. Based on the four-point calibration process, the sensitivities of the channels (s_A, s_B) are determined (Eq. 1–2).

$$s_A = \frac{U_{A,S} - U_{A,0}}{\mu_S} \quad (1)$$

$$s_B = \frac{U_{B,S} - U_{B,0}}{\mu_S} \quad (2)$$

Here, $U_{A,S}$ and $U_{B,S}$ are the measured voltages during the first phase of the liquid calibration in the respective channels, and $U_{A,0}$ and $U_{B,0}$ are the corresponding signals measured in the second phase of the calibration. μ_S is the mixing ratio of the standard solution under consideration of the molar air volume (V_m) and the measured standardized mass flows ($Q_{Stripping}$, Q_{Air}; Eq. S2 – S3):

$$\mu_S = \frac{[H_2O_2]}{10^4} \cdot 10^9 \cdot V_m \cdot \frac{Q_{Stripping}}{Q_{Air}} \quad (3)$$

The corresponding catalase destruction efficiency of hydrogen peroxide in channel B, ε, is derived from the following equation:

$$\varepsilon = 1 - \left(\frac{U_{BK,S} - U_{BK,0}}{U_{B,S} - U_{B,0}} \cdot \frac{U_{A,S} - U_{A,0}}{U_{AK,S} - U_{AK,0}} \right) \quad (4)$$

with the voltages (U) in both channels during the consecutive phases of the liquid calibration (liquid standard injection: S; background measurement: 0; background measurement with catalase: K,0; liquid standard injection with catalase: K, S).

Based on the specific sensitivities, and the destruction efficiency, the absolute peroxide mixing ratios $\mu_{H_2O_2}$ and μ_{ROOH} in the sample are determined using the following equations:

$$\mu_{H_2O_2} = \frac{U_A - U_{AK,0}}{s_A} - \frac{(U_B - U_{BK,0})}{s_B} \cdot \varepsilon \quad (5)$$

$$\mu_{ROOH} = \frac{U_B - U_{BK,0}}{s_B} - (1 - \varepsilon) \cdot \mu_{H_2O_2} \quad (6)$$

Due to the characteristics of the wet chemical measurement method, signal corrections have to be initially performed in order to obtain absolute hydroperoxide mixing ratios. In order to account for potential measurement divergencies and background signal alterations initiated by pressure and temperature instabilities during the measurement flights, the frequently measured background signal is interpolated. Further, the tracked and interpolated background signal is subtracted from the measurements to give the actual hydroperoxide signals in the ambient air.

The time delay caused by the liquid transport process of the monitor is accounted for by shifting the obtained signals by the time difference between the valve switches and the corresponding signal response during the background measurements. The

https://doi.org/10.5194/amt-2023-114
Preprint. Discussion started: 12 June 2023


Atmospheric Measurement Techniques Discussions

time modification is calculated as the mean time delay based on all performed background measurements during the respective flight.

To account for wall loses at the inner surface of the bypass, the inlet, and the Teflon-coated CPI pump, the inlet transmission efficiency has to be determined. Due to the high flow rates through the installed bypass and attached inlet (30 slm and 10 slm, respectively), potential wall losses in the tubing are assumed to have a minor impact on the hydroperoxide measurements. The Teflon coating of the membrane pump is expected to absorb hydroperoxides, and, thus, decrease the species inlet transmission from the TGI to the monitor. The subsequent wall loss at the inner surface of the CPI pump is measured using hydrogen peroxide and peroxy acetic acid (PAA) gas standards produced by permeation sources. The sources are operated at 28 °C and 40 °C based on a H_2O_2 (30%) or PAA solution (37%), respectively, which is filled into a 1/8" LDPE tubing with an approximate length between 8–20 cm, depending on the desired mixing ratio. The permeation device is flushed with purified air at approximately 60 standard cubic centimeters per minute (sccm) and subsequently diluted with approximately 10 slm of purified air. The purified air is generated by the removal of trace gases from ambient air using zero gas cartridges containing silica gel and hopcalite as described above. The generated gas standard is injected into the inlet with and without the CPI pump in the air sampling system. The inlet transmission efficiency is then determined based on the detected hydroperoxide mixing ratios with the addition of the CPI pump relative to the detected mixing ratios without the CPI pump in the inlet system separately for H_2O_2 and ROOH. The permeation rate of the corresponding species is determined based on the work by Pilz and Johann (1974) by transmitting the permeation gas through three impinger flasks. Two of these are installed in series and a third flask serves to determine the chemical background. Spectrophotometrical determination of H_2O_2 in the collection samples is achieved by the addition of acidified (HCl) titanium chloride solution and subsequent measurement of the absorption at 415 nm.

Due to the temperature-dependent solubility of hydroperoxides determined by Henry's law, the measurement results must be additionally modified relative to the efficiency of the sampling solution used to scrub the trace gases from the ambient air. The sampling efficiency gives the relative amount of the hydroperoxides transferred into the sampling solution and has been investigated by numerous research groups in the past years (Lee et al., 2000 and references therein). Based on the precooled sampling solution (4–6 °C), we assume sampling efficiencies of 1 and 0.6 for H_2O_2 and the ROOH. Please note that the organic hydroperoxide sampling efficiency is based on the approximation that in the free troposphere methyl hydroperoxide (MHP) is the most prominent ROOH (Lee et al., 2000). However, the composition of the organic hydroperoxides is expected to vary in the boundary layer, i.e., in pristine regions with extended amounts of vegetation-related emissions or due to specific primary emissions such as biomass burning events (Fels and Junkermann, 1994; Lee et al., 1997; Valverde-Canossa et al., 2005; Hua et al., 2008). MHP is known to be less soluble than, e.g., PAA and hydroxymethyl hydroperoxide (HMHP) in aqueous solutions, while ethyl hydroperoxide (EHP) is expected to be similarly soluble (O'Sullivan et al., 1996). Thus, the sampling efficiency of 0.6 is an estimate for the lower limit of the ROOH sampling efficiency. The transmission efficiency during the most recent field campaign was calculated to be 82% (± 1.6%) for H_2O_2 and 95% (±1.1%) for ROOH.

https://doi.org/10.5194/amt-2023-114
Preprint. Discussion started: 12 June 2023

Atmospheric Measurement Techniques Discussions

2.3 Potential sources of error: chemical and physical interferences

Based on numerous studies on the reactions of hydrogen peroxide with other tropospheric trace gases, the monitor's precision is negatively impacted by chemical interference induced by reactions with sulfur dioxide (SO_2), nitrogen oxide (NO), and metal ions in the liquid phase. Studies on acid rain have shown that the oxidation of SO_2 by H_2O_2 in cloud droplets might lead to a significant loss of the ambient hydrogen peroxide in the generated samples. Graedel and Goldberg (1983) described the reaction of hydrogen peroxide with iron ions (Fe^{2+}) analogous to the Fenton reaction. Comparable results were later found for organic hydroperoxides (Weschler et al., 1986). In 1982, Staehelin and Hoigne investigated the production of H_2O_2 by passing ozone through an impinger flask containing purified water. Heikes (1982; 1984) described production of H_2O_2 via adsorption of ozone on wet surfaces. The corresponding reactions are included in the Supplement of this work (SR8–SR16).

In order to account for the negative impact of reactions with metal ions and SO_2 on measurements, sufficient amounts of ethylene diamine tetra acetic acid (EDTA; 100 mg per 5 L), and of formaldehyde (HCHO; 1 mL per 5 L) are added to the buffered sampling solution. The corresponding reactions are presented in the Supplement (SR17–SR18). Further, the obtained data is corrected for the positive ozone interference by subtracting the determined amount of hydrogen peroxide per 100 ppbv of ozone. The correction factor is determined by plotting the measured H_2O_2 mixing ratios versus the O_3 mixing ratios measured under laboratory conditions or during measurement flights in the lower stratosphere under the assumption that ambient levels of hydrogen peroxide are close to zero above the tropopause due to the reduced availability of the H_2O_2 precursor HO_2. Based on the most recent measurements, the correction factor comes to 0.01 ppbv H_2O_2/100 ppbv O_3. The commercially available Aero-Laser instrument estimates a potential negative interference with NO in ambient air of 0.012 ppbv H_2O_2/100 ppbv NO, which is only relevant under highly polluted conditions.

Furthermore, physical errors might arise from interference between aircraft movement and the individual components of the monitor. Large ambient pressure variations might affect the airflow during the measurements. Dynamic pitch angle alterations, high descent or ascent rates of the aircraft, as well as instrument valves switching at maximum altitudes, are all factors that can lead to temporal sampling line pressure inconsistencies. Also, liquid transport might be affected by changes in the aircraft movement pattern, especially by pitch and roll angle changes during spiraling maneuvers. Furthermore, cabin temperature but also cabin pressure may have a significant effect on the signal detection in both channels.

The instrument performance and the impact of physical noise sources were examined during an individual test flight as part of the most recent CAFE-Brazil campaign performed on November 22, 2022 from the German Aerospace Center (Deutsches Zentrum für Luft- und Raumfahrt, DLR) base of operation in Oberpfaffenhofen (Germany; 48° 4' N, 11° 16' E). The four-hour flight consisted of numerous maneuvers including rapid flight direction changes and flight altitude variations at alternating ascent and descent rates (1,500–3,000 ft/min). The vertical maneuvers covered an altitude range of a few tens of meters up to 15,000 m above the earth's surface. The average aircraft speed was determined to be approximately 193 ± 48.5 m $\cdot$ s^{-1}. Fig. S2 shows the three-dimensional flight pattern of the aircraft during the test flight. During the flight, HYPHOP was operated in a

https://doi.org/10.5194/amt-2023-114
Preprint. Discussion started: 12 June 2023

Atmospheric Measurement Techniques Discussions

continuous background mode, sampling dried and peroxide-free air at approximately 2.3 slm and 4–6°C liquid solution temperature.

Fluctuations of the temperature reported during the flights (flight log book) might affect the measured temperature at the stripping coil. However, due to the precooled measurement solutions transported via the sampling coil, we assume the impact of any low-range temperature variability to be of minor importance for the solubility of hydroperoxides. Nonetheless, fluctuations in the cabin temperature might influence both the excitation and the detection process. Fig. 3 displays the temporal series of the tracked sampling coil temperature, the lamp voltage, and the PMT temperature with respect to the altitude.

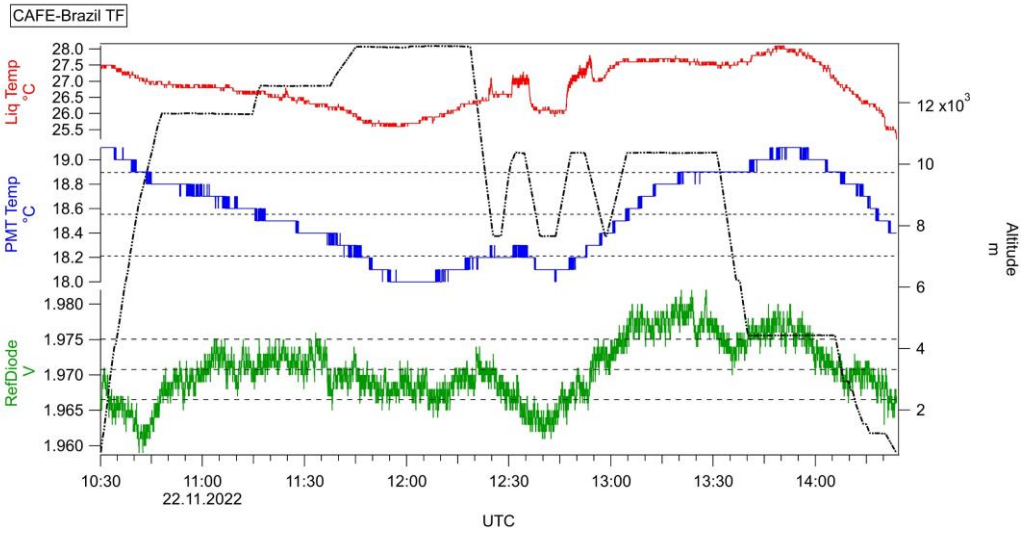

Figure 3: Temporal series of the Cd lamp (reference diode; green) with the respective average and 1σ standard deviation range (dashed lines) during the test flight performed on November 22, 2022 complimented by the GPS flight altitude (right plot; black), observed temperature at the sampling coil (Liq Temp; red) and PMT temperature (blue). The data is displayed with 1-Hz measurement frequency.

Temperature modifications within the cabin indicated by LiqTemp (red data) are clearly followed by inconsistencies in the Cd lamp and the PMT signals. The calculated average of the lamp signal and the PMT temperature are 1.971 ± 0.004 V and 18.55 ± 0.341 °C, respectively. Nonetheless, as displayed in Fig. 3 (bottom left and middle left plots), the reference diode signal and PMT temperature fluctuations remain essentially within the range of 1-sigma, giving a relative variation of 0.2% and 1.8% in the lamp voltage and the PMT temperature, respectively. Translated onto the relative deviation of the measurements in both channels based on an average hydroperoxide signal of the liquid standard (5 ppbv), the average uncertainty arising from the temperature-dependent noise is assumed to be maximally 1.6%. In order to account for potentially higher temperature-dependent signal drifts, frequent background measurements are performed during the measurement flights.

Since the dual-enzyme system is based on a wet-chemical measurement setup, we checked whether there is an impact of the dynamic flight patterns on the liquid transport during various maneuvers. In order to analyze the impact of aircraft movement in detail, a temporal series of the measured background signals in both channels was converted to hydroperoxide mixing ratios under consideration of the aircraft's roll angle and body pitch rate (Fig. 4). Tracked latitude and longitude were plotted in order

https://doi.org/10.5194/amt-2023-114
Preprint. Discussion started: 12 June 2023

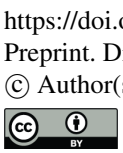

Atmospheric Measurement Techniques Discussions

to distinguish between actual flight maneuvers and stabilization processes of the aircraft due to turbulence, ascent, and descent maneuvers.

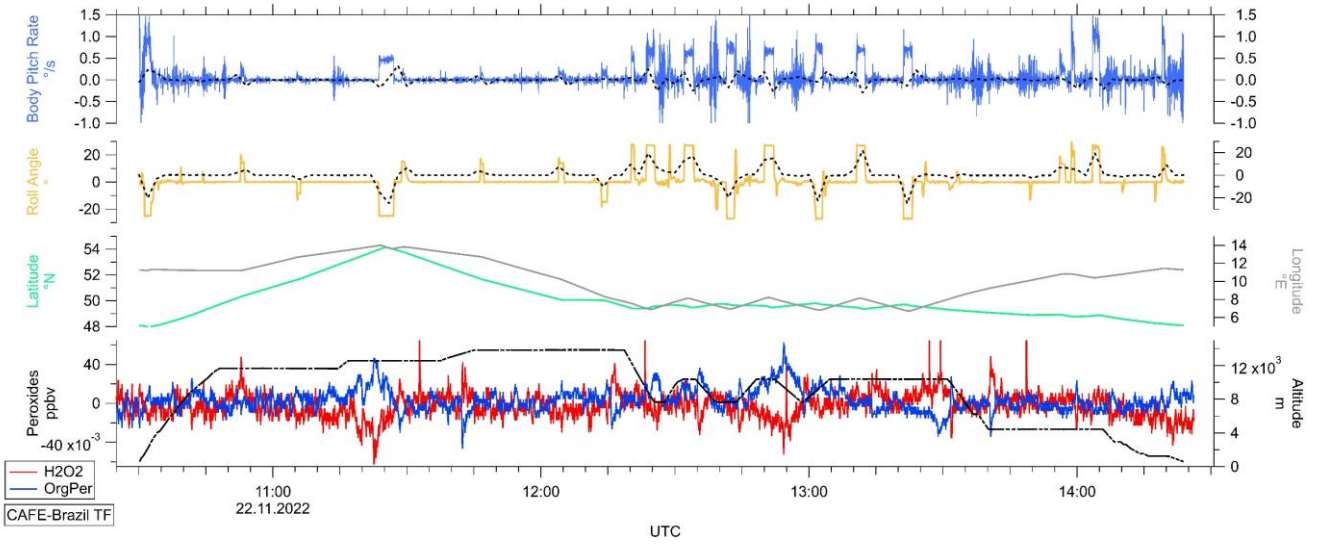

Figure 4: Temporal series of the measured signals in channel A (H_2O_2 + ROOH; red) and B (ROOH; dark blue; bottom plot) relative to the GPS flight altitude (black), latitude (green), longitude (grey), roll angle (yellow) and body pitch rate (blue; top plot) of the aircraft during the test flight of the CAFE-Brazil campaign performed on November 22, 2022 with 1-Hz measurement frequency. Dashed lines (black) represent the temporal trends of the roll angle and the body pitch rate based on 2-min bins.

The signals of the measured background correlate with changes in the roll angle of the aircraft (yellow plot). Further, the signals harbor additional irregular noise of up to ± 20 pptv, which is most likely initiated by body pitch rate changes of the aircraft during flight level alterations and turbulence. A comparable, but far more distinct periodic fluctuation of the background mixing ratios was observed during the test flights during the OMO-EU campaign in January 2015 (Fig. S3 in the Supplement). During frequent turns, the roll angle of the aircraft changes, which might result in motion of the measurement solutions in the liquid containers. In effect, air might be transported into the liquid system and accumulate in the flow-through cuvettes, where the motion might then be translated into characteristic periodic signal fluctuations due to variation in the density-dependent extinction coefficient. Fig. S4 in the Supplement displays the flight pattern of the performed test flight with respect to the measured background signals and the pitch and roll angles of the aircraft. While the pitch angle modifications during descent and ascent maneuvers do not seem to correlate with the variations of the measured hydroperoxide mixing ratios, there is a clear connection between the extremes in the measured mixing ratios and the most significant changes in the aircraft roll angle. Consequently, the most impactful factors seem to be the roll angle changes and body pitch rate adjustments due to turbulence, ascent, and descent of the aircraft. As shown in Fig. 4 and Fig. S3, the corresponding noise is assumed to be minor (up to 40 pptv for a few seconds during extended constant spiraling maneuvers) and does not seem to significantly affect the hydroperoxide data in the final temporal resolution of about 120 sec (Fig. S5).

Apart from the liquid transport within the instrument, also the ambient air transport might be significantly affected by the flight maneuvers. Fig. 5 gives an overview of the instrumental line and inlet pressures measured in the sampling line by the CPI

https://doi.org/10.5194/amt-2023-114
Preprint. Discussion started: 12 June 2023

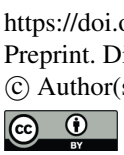

Atmospheric Measurement Techniques Discussions

control unit and at the inlet manifold, respectively, the air mass flow tracked by the CPI internal unit, and the aircraft body pitch rate, which gives an overview on the performed descent and ascent maneuvers.

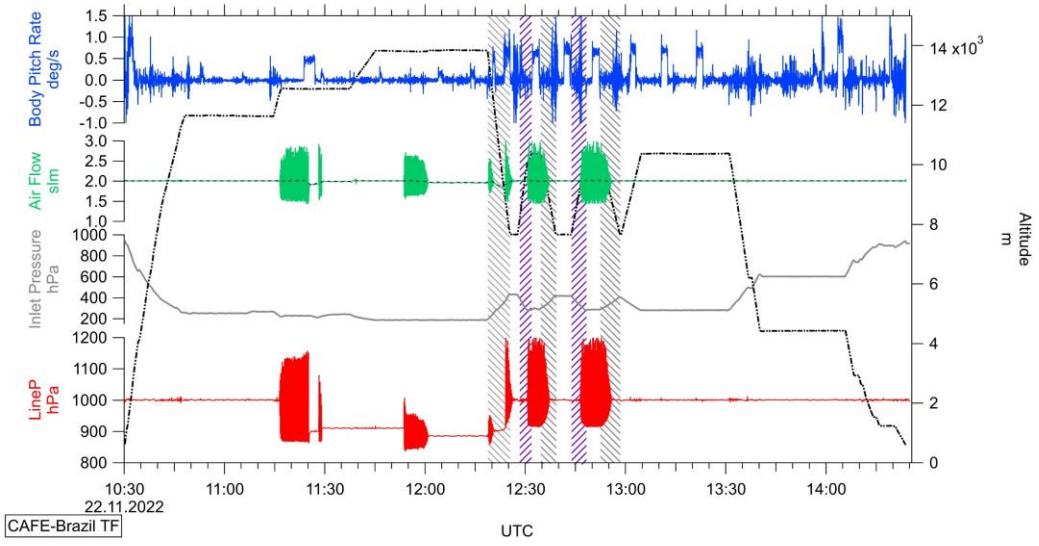

Figure 5: Temporal series of the tracked line pressure (red) complimented by the GPS flight altitude (black), measured inlet pressure (grey), the air mass flow (green), and body pitch rate (blue) of the aircraft during the test flight of the CAFE-Brazil campaign performed on November 22, 2022 with 1-Hz measurement frequency. Rapid descent and ascent rates of the aircraft (2,000–3,000 ft/min) are highlighted in grey and purple, respectively.

The sampling line pressure variations occur on one side during high-altitude flight legs as well as during rapid aircraft descent and ascent with rates of 2,000 ft/min or higher (maneuvers highlighted in grey and purple during the descent and ascent maneuvers, respectively). Additionally, atmospheric turbulence in close proximity to the jet stream reported during the lower flight legs (12.15–13.00 UTC) seem to affect the stability of the line pressure. Furthermore, from previous airborne measurements, we know that especially at high altitudes valve switches might induce line pressure fluctuations as well.

The CPI system seems to be triggered by the high airflow variability at the valves and adjustments of the pump speed, which results in an oscillating sampling line pressure. Most likely, during turbulence and rapid aircraft descent and ascent, the valve needles shift and alter the airflow in and/or out of the sampling line, leading to peaks in the detected line pressure and the described airflow regulation problems in the CPI system. However, the comparison of the background signals measured in both channels during the line pressure fluctuations does not correlate with short-term airflow fluctuations. Furthermore, no considerable measurement disturbances were observed during measurement flights where the line pressure fluctuations occurred, as exemplified in the Supplement of this work (Fig. S6). The high fluctuation frequency paired with the instrument's temporal resolution means that the average line pressure and air mass flow (975 ± 43.5 hPa and 2.00 ± 0.02 slm, respectively based on a 120 sec time sample) and, thus, the sample volume, do not seem to vary enough to affect the measured hydroperoxide mixing ratios significantly.

https://doi.org/10.5194/amt-2023-114
Preprint. Discussion started: 12 June 2023

Atmospheric Measurement Techniques Discussions

2.4 Instrument characterization: precision, limit of detection, temporal resolution, and total measurement uncertainty

According to the International Union of Pure and Applied Chemistry (IUPAC), the instrument detection limit (IDL) is defined as the smallest amount of an analyte, which produces a statistically significantly higher signal than the blank signal (Gold, 2019). Applied to our measurement method, the limit of detection is defined as the hydroperoxide mixing ratio, which can be distinguished from the background with a certainty of at least 95%. Analysis of the IDL is performed based on the 2-sigma uncertainty of the background measurements frequently performed during the measurement flights. The 2-sigma standard deviations ($2\sigma_{A,0}$, $2\sigma_{B,0}$) are calculated for both channels separately by determining the values for a background sample of approximately 200 points (at a resolution of 1 Hz). The limit of detection is consequently calculated by applying the subsequent inlet transmission efficiencies ($ITE_{H_2O_2}$, ITE_{ROOH}) and the catalase destruction efficiency (ε) on the determined values:

$$IDL_{H_2O_2} = \sqrt{\left(\frac{2\sigma_{A,0}}{ITE_{H_2O_2}}\right)^2 + \left(\frac{2\sigma_{B,0}\cdot\varepsilon}{ITE_{ROOH}}\right)^2} \quad (7)$$

A corresponding calculation is performed for the limit of detection of ROOH. Here, due to the lack of detailed information on organic hydroperoxide composition in the sampled ambient air, an additional correction factor based on the sampling efficiency of MHP (0.6) is incorporated:

$$IDL_{ROOH} = \frac{2\sigma_{B,0}}{0{,}6\cdot ITE_{ROOH}} \quad (8)$$

The detection limit of the instrument based on the 2σ uncertainty of 101 background measurements during the most recent measurement campaign, CAFE-Brazil, was determined to be 0.020 ppbv and 0.019 ppbv for H_2O_2 and ROOH, respectively.

The instrument precision characterizes random errors and thus illustrates the proximity of the performed airborne measurements relative to each other. The instrument precision is determined from the reproducibility of 15 liquid calibrations during CAFE-Brazil. Thus, it accounts for instrument noise, sensitivity drifts, and errors in the preparation of the liquid standards. Applied to hydroperoxide measurements, the precision is based on the 1-sigma uncertainty of the respective signals in the first phase of the calibration procedure. The hydrogen peroxide precision of the instrument is then determined using the resulting 1sigma standard deviations of both channels ($\sigma_{S,A}$, $\sigma_{S,B}$), corrected by the corresponding inlet transmission efficiencies ($ITE_{H_2O_2}$, ITE_{ROOH}) and the catalase destruction efficiency (ε). The organic hydroperoxide precision is based on the signal standard deviation in channel B during the first calibration phase ($\sigma_{S,B}$) and the corresponding channel sensitivity (ITE_{ROOH}) and is extended by the sampling efficiency of 0.6.

$$P_{H_2O_2} = \sqrt{\left(\frac{\sigma_{S,A}}{ITE_{H_2O_2}}\right)^2 + \left(\frac{\sigma_{S,B}\cdot\varepsilon}{ITE_{ROOH}}\right)^2} \quad (9)$$

$$P_{Org.HP} = \frac{\sigma_{S,B}}{0{,}6\cdot ITE_{ROOH}} \quad (10)$$

During the most recent measurement campaign over the Amazon region, i.e., CAFE-Brazil, the precision of the instrument was determined to be 6.4% at 5.7 ppbv and 3.6% at 5.8 ppbv for H_2O_2 and ROOH, respectively.

https://doi.org/10.5194/amt-2023-114
Preprint. Discussion started: 12 June 2023


Atmospheric Measurement Techniques Discussions

Despite HYPHOP's ability to detect trace gas species with a 1-Hz frequency, due to the wet chemical measurement approach, the instrument's time resolution is heavily dependent on the liquid transport velocity during operation. The temporal resolution is defined as the time required to track a significant increase of the measured hydroperoxide mixing ratios. The determination of HYPHOP's maximal temporal resolution is based on analysis of the time needed to flush the flow through cuvettes with fresh solutions defined as three times the volume of the cuvette at a given liquid flow velocity. The determination of the minimal temporal resolution of the instrument is based on the time tracked between 10% and 90% of the signal rise and fall in both channels based on liquid calibrations and background measurements. For the purposes of a detailed study on the instrument time resolution, the 10/90-method was further applied to liquid calibration measurements at varying H_2O_2 standard concentrations as well as peak mixing ratio events during flight legs in the upper troposphere associated with convective transport. Tab. S1. in the Supplement lists the means (±1σ) of the determined values. Based on the performed analysis, the time resolution based on the 10/90 method is determined to be 114 (± 15.2) sec. The highest temporal resolution based on the flow-through cuvette flushing is determined to be 52.5 (±2.32) sec. Considering the maximum and minimum values of the instrumental time resolution the spatial resolution at the average cruise speed of the aircraft (192 ± 46.5 $m \cdot s^{-1}$) is approximately 11.5–23 km during the most recent field experiment (CAFE-Brazil).

The monitor's total measurement uncertainty (TMU) is defined based on Gauss's law for the propagation of uncertainties. The expression incorporates both the systematic and statistically driven deviations occurring during the measurement process and distinguishes between the measured species, i.e., hydrogen peroxide and the sum of organic hydroperoxides separately. The calculation of the hydrogen peroxide TMU is based on the standard deviations arising from the inlet transmission efficiency ($\sigma(\mathrm{ITE}_{H_2O_2})$), ozone interference ($\sigma(IO_3)$), standard solution ($\sigma(\mathrm{LqStd})$), and the determined instrument precision ($P_{H_2O_2}$). The corresponding total measurement uncertainty of ROOH is calculated based on the estimated instrument precision (P_{ROOH}) and the errors of the inlet and solution transmission efficiencies ($\sigma(\mathrm{ITE}_{H_2O_2})$, $\sigma(\mathrm{STE}_{ROOH})$).

$$\mathrm{TMU}_{H_2O_2} = \sqrt{{P_{H_2O_2}}^2 + \sigma(\mathrm{LqStd})^2 + \sigma(\mathrm{ITE}_{H_2O_2})^2 + \sigma(IO_3)^2} \quad (11)$$

$$\mathrm{TMU}_{ROOH} = \sqrt{{P_{ROOH}}^2 + \sigma(\mathrm{STE}_{ROOH})^2 + \sigma(\mathrm{ITE}_{H_2O_2})^2} \quad (12)$$

The instrument precision (P) based on the 1σ standard deviation of the respective signals in the first phase of the calibration procedure contributes further to the uncertainty of the standard (LqStd). The uncertainty of the inlet efficiency (ITE) is based on the 1σ standard deviation from the inlet sampling efficiencies for hydrogen peroxide and the sum of organic peroxides. The uncertainty of the ozone interference (IO_3) is derived from the 1σ standard deviation of the linear regression of H_2O_2 versus O_3. The inlet efficiency uncertainty was determined to be 1.6% for H_2O_2 and 1.1% for ROOH. The uncertainty of O_3 interference was determined under laboratory conditions as 10.2%. During the CAFE-Brazil campaign, the total measurement uncertainties of H_2O_2 and ROOH were determined to be 12% and 40%, respectively. The determined parameters are comparable with those of previous campaigns, i.e., OMO (Hottmann et al., 2020), CAFE-Africa (Hamryszczak et al., 2023), and BLUESKY (Hamryszczak et al., 2022), as presented in Tab. S2. Considering the entirety of performed airborne

https://doi.org/10.5194/amt-2023-114
Preprint. Discussion started: 12 June 2023


Atmospheric Measurement Techniques Discussions

measurements between 2015 and 2023, the TMU varied between 9–28% and 40–41%, with precision of up to 1.3% (at 5.9 ppbv) and 6.4% (at 5.7 ppbv) for H_2O_2 and ROOH, respectively. The instrument limit of detection varied within the range of 8–53 pptv for H_2O_2 and 6–52 pptv for ROOH, respectively. Further, based on the all the datasets from the previous measurement campaigns, the temporal resolution was determined to be 120 sec. Further potential optimization of the temporal resolution can be performed by reducing the dead volume of the liquid supply through reduction of the tubing length or by optimization of the peristaltic pump speed at the potential cost of an increased LOD.

3 Performance of HYPHOP during CAFE-Brazil

During the CAFE-Brazil aircraft campaign in December 2022 and January 2023, 20 measurement flights were conducted, mostly over the Amazon Basin in Brazil (12 °S–4 °N; 70–38 °W). The main objective of the field experiment was to investigate the distribution of trace gases, aerosols, and radicals under pristine conditions in contrast to environments affected by anthropogenic emissions. The campaign also focused on convective transport and the interactions between the tropospheric layers under different meteorological conditions, the interaction between the biosphere and the atmosphere from the perspective of atmospheric chemical exchange processes, and cloud formation over the tropical rainforest. The flights were performed from the base of operation in Manaus (3° 6′ S, 60° 1′ W) and covered the altitudinal range between a few tens of meters above the surface and an altitude of approximately 15 km. Fig. S7 gives an overview of the performed flights during the campaign and the regions covered. The observed mixing ratios of hydroperoxides during CAFE-Brazil are presented in a latitude vs. longitude plot with mean mixing ratio values binned into a subset of 1° x 1° bins along the flight tracks for the three tropospheric layers (0 < 2 km: top panel; 2 < 8 km: middle panel; ≥ 8 km: bottom panel; Fig. 4). The color scale represents the measured mixing ratios of H_2O_2 (left panel) and ROOH (OrgPer; right panel). Please note that for resolution purposes the color scaling varies between the panels.

https://doi.org/10.5194/amt-2023-114
Preprint. Discussion started: 12 June 2023

Atmospheric Measurement Techniques Discussions

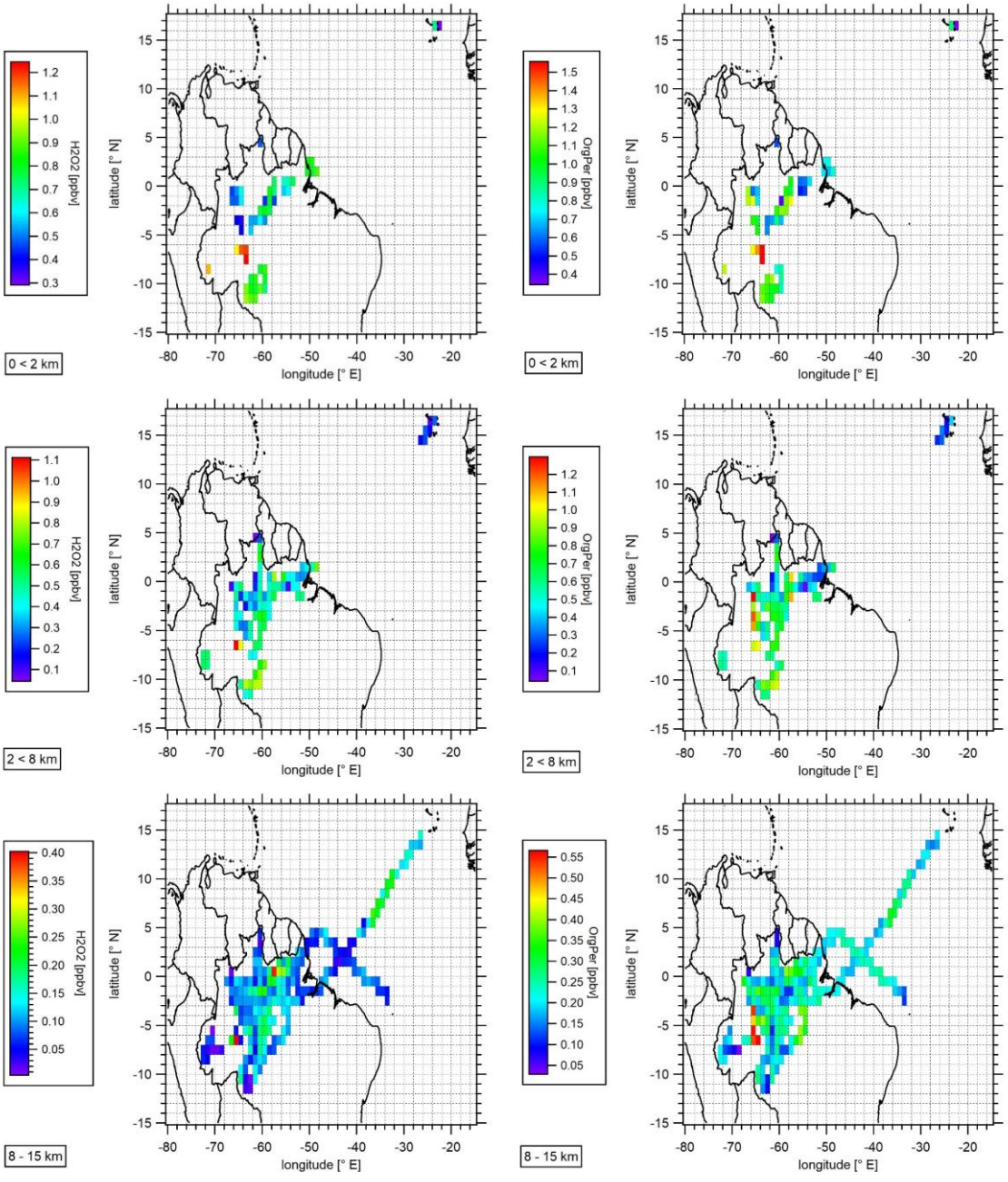

Figure 6: Spatial distribution of measured hydrogen peroxide (left panel) and the sum of organic hydroperoxides (right panel) in the boundary layer (top panel), middle troposphere (middle panel), and the upper troposphere (≥ 8 km; bottom panel) during the CAFE-Brazil campaign. Data were binned into a 1° x 1° subset over the flight tracks based on a 1-Hz measurement frequency. Please note that for resolution purposes the color scaling differs between plots. Global coastline and global country boundaries are based on data set available from WaveMetrics. [1]

[1] WaveMetrics, Inc. 10200 SW Nimbus, G-7 Portland , OR 97223;

https://doi.org/10.5194/amt-2023-114
Preprint. Discussion started: 12 June 2023

Atmospheric Measurement Techniques Discussions

The mean (± 1σ) and median mixing ratios based on all measured H_2O_2 and ROOH species during the campaign were 0.30 (± 0.30) ppbv, 0.17 ppbv and 0.43 (± 0.36) ppbv, 0.28 ppbv, respectively, with maximum mixing ratios reaching 1.94 ppbv and 1.73 ppbv for hydrogen peroxide and the total organic hydroperoxides, respectively. Please note that the mean and median hydroperoxide mixing ratios were calculated based on measurement results with the instrumental measurement frequency of 1 Hz. Table S3 in the Supplement gives an overview of H_2O_2 and ROOH mean (±1σ) and median mixing ratios with the corresponding maximum peroxide levels for each tropospheric layer.

The highest mean (±1σ) and median mixing ratios were detected between altitudes of 0 and 2 km. The mean and median hydroperoxide levels decrease progressively with increasing altitude, with the lowest mixing ratios measured in the upper troposphere (UT; above 8 km). Especially above 2 km, a trend of increasing hydroperoxide levels from the coastal area towards the central Amazon Forest was observed. This may be expected due to the influence of vegetation-derived VOC emissions. Generally, ROOH levels appear to be approximately a factor of 1.5 higher relative to H_2O_2 throughout the entire troposphere. The high ROOH mixing ratios are most likely due to an efficient production based on vegetation emissions and the sufficient availability of HO_2 radicals derived from the photolysis of carbonyls and the photooxidation of VOCs and CO by OH radicals. Additionally, hydrogen peroxide is expected to be affected to a larger extent by deposition processes due to its higher solubility and uptake by vegetation.

Slightly higher hydroperoxide levels were observed in the upper troposphere as a result of air masses originating from the South Atlantic Convergence Zone (SACZ), where average mixing ratios of 0.15–0.25 ppbv and 0.25–0.40 ppbv for H_2O_2 and ROOH, respectively, over a 1° x 1° bin of merged data were observed. These maxima are most likely due to the atmospheric transport of hydroperoxides or precursors to the upper troposphere. Locally, peaking hydroperoxide levels in the UT were further observed in the northeastern and southwestern parts of the sampled region. Here, the mean mixing ratios were between 0.35 ppbv and 0.55 ppbv with maxima of up to 0.40 ppbv and 0.56 ppbv for H_2O_2 and ROOH, respectively. Based on the flight log book, strong convective activity during the respective measurement flights was reported in the sampled regions. The overall mean vertical hydroperoxide distribution over the sampled region is displayed in Fig. 7.

Data access under: https://www.wavemetrics.net/Downloads/IgorGIS/GISData/; <last access: 09.06.2023>

https://doi.org/10.5194/amt-2023-114
Preprint. Discussion started: 12 June 2023

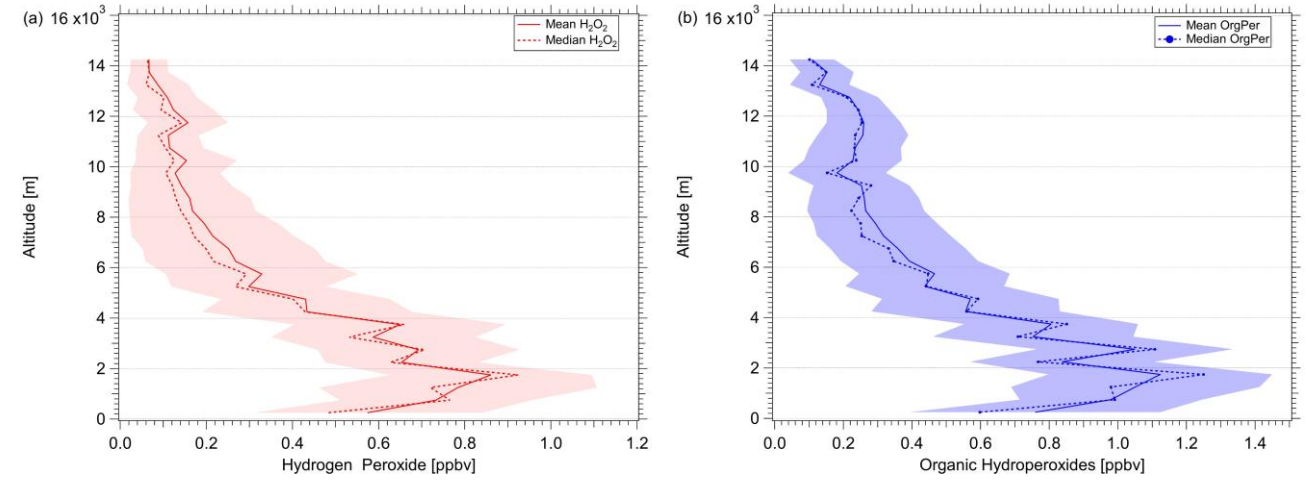

Figure 7: Vertical profiles of H_2O_2 (red; a) and ROOH (blue; b). Vertical profiles were calculated as means and medians over 500-m layers over the atmospheric column based on data with 1-Hz measurement frequency obtained in the sampled region.

In general, the observed vertical hydroperoxide distributions follow the expected trends throughout the troposphere (Fig. 7). The lowest hydroperoxide mixing ratios (± 1σ) of 0.07 (± 0.04) ppbv for H_2O_2 and 0.11 (± 0.06) ppbv for ROOH were measured in the upper troposphere. The highest mean values (± 1σ) of 0.86 (± 0.23) ppbv and 1.12 (± 0.33) ppbv for H_2O_2 and ROOH, respectively, were measured directly above the boundary layer (~ 2 km) in the lower free troposphere. Below 1 km, hydroperoxide levels decrease to 0.57 (± 0.26) ppbv and 0.75 (± 0.36) ppbv for H_2O_2 and the organic hydroperoxides, respectively, reflecting the impact of deposition processes involving vegetation in the boundary layer.

The hydroperoxide vertical profiles show increased levels in the UT (10–13 km), which might indicate convective outflow. Here, the mixing ratios increase to approximately 0.16 (± 0.09) ppbv and 0.26 (± 0.11) ppbv for H_2O_2 and ROOH, which is approximately 19% and 23%, respectively, corresponding to the measured maximum hydroperoxide mixing ratios directly above the boundary layer. The comparison of H_2O_2 and ROOH vertical profiles shows a high abundance of ROOH throughout the entire tropospheric column relative to H_2O_2. Especially in the UT, the ROOH mixing ratios seem to increase significantly in comparison to H_2O_2 (up to a factor of 5). H_2O_2 is temporarily or permanently removed by wet deposition in the lower part of convective clouds; the influence of wet deposition on the transport of the less soluble ROOH is expected to be smaller. Additional processes responsible for the high levels of measured organic peroxides might be of significant importance to the local budget of ROOH, which in turn can contribute to the local HO_x budget. Over the pristine Amazon forest, a large suite of VOCs, including highly oxygenated organic molecules (HOMs), which are an additional source of organic hydroperoxides in the UT, might be transported via convection from the lower troposphere. Further analysis of these data, incorporating results with additional trace gases, will be the subject of future work.

https://doi.org/10.5194/amt-2023-114
Preprint. Discussion started: 12 June 2023

Atmospheric Measurement Techniques Discussions

4. Conclusions

In this work, we introduced a hydroperoxide measurement setup designed for operation on board of the research aircraft HALO. The presented wet chemical, dual-enzyme measurement method enables us to perform *in situ* measurements up to the tropopause and lower stratosphere (1000–150 hPa). Potential chemical interference affecting the airborne hydroperoxide measurements can be easily eliminated or corrected by simply adding reactants (EDTA; HCHO) or in the data acquisition process. Based on a test flight specifically dedicated to investigating measurement inconsistencies arising from the dynamic flight patterns of the aircraft, we analyzed potential noise sources affecting the background signal. Despite technical challenges during the dynamic flight maneuvers, the majority of these issues do not have a significant impact on the determination of the absolute hydroperoxide mixing ratios during background measurements. The instrument shows some periodic fluctuations, which are most likely induced by the roll angle changes during the flight maneuvers. The periodically increased noise during the performed experiment flight was estimated to be in the approximate range of the IDL. The observed periodic variation of the signal is assumed to only have a minor impact on the hydroperoxide measurements due to significantly higher levels of this species in the troposphere. Changes in cabin temperature exerted an impact on noise at the lowest mixing ratios, which is likewise not considered to affect the measurements. Rapid line pressure variations due to temporal pressure instabilities, most likely caused by valve needle operation inconsistencies, were also observed during the high flight legs as well as during rapid descent and ascent maneuvers. No significant impact on the signals in either of the channels and thus on the measurements was observed. Due to the determined instrument temporal resolution of approximately 120 sec, the high-frequency airflow fluctuations are assumed not to affect the sampling volume significantly and thus likely have no impact on the measured mixing ratios of hydroperoxides. However, instrument performance can be further optimized by minimizing the technical disturbances during the measurement flights. Potential higher temperature-dependent signal drifts are corrected by frequent background examination on the consecutive flight legs during the measurements. Furthermore, the instrument time resolution can be increased by reducing the length of the liquid supply tubing. Analysis of potential noise sources impacting the *in situ* measurements shows that the hydroperoxide data is of sufficient quality for atmospheric studies. Based on the most recent airborne measurements during the CAFE-Brazil aircraft campaign, HYPHOP faithfully captures the temporal and spatial variability of hydroperoxides in the troposphere. Dynamic processes such as convection, cloud scavenging, and subsequent rainout or horizontal transport of the hydroperoxides are sufficiently well captured by the instrument through the entire tropospheric column and along the long-range measurement flight tracks.

Data availability. All data measured during the CAFE-Brazil campaign are available upon request.

Author contributions. HF and ZH designed the study; JL and HF planned the campaign; ZH, DD, and AH performed the measurements; ZH, DD, and AH processed and analyzed the data; RK, SH, and HF designed the instrument; RK, UP, SH, BB, DD, and ZH optimized the instrument; ZH wrote the manuscript draft with contributions of all co-authors.

Competing interests. The authors declare that they have no conflicts of interest.

Acknowledgments. The authors are very grateful to the CAFE-Brazil team, Forschungszentrum Jülich, Karlsruhe Institute of Technology and Deutsches Zentrum für Luft- und Raumfahrt (DLR) in Oberpfaffenhofen, whose support was essential for the project.

References

Allen, H. M., Crounse, J. D., Kim, M. J., Teng, A. P., Ray, E. A., McKain, K., Sweeney, C., and Wennberg, P. O.: H 2 O 2 and CH 3 OOH (MHP) in the Remote Atmosphere: 1. Global Distribution and Regional Influences, Journal of Geophysical Research: Atmospheres, 127, https://doi.org/10.1029/2021JD035701, 2022a.

Allen, H. M., Bates, K. H., Crounse, J. D., Kim, M. J., Teng, A. P., Ray, E. A., and Wennberg, P. O.: H 2 O 2 and CH 3 OOH (MHP) in the Remote Atmosphere: 2. Physical and Chemical Controls, Journal of Geophysical Research: Atmospheres, 127, https://doi.org/10.1029/2021JD035702, 2022b.

Bufalini, J. J., Lancaster, H. T., Namie, G. R., and Gay, B. W.: Hydrogen peroxide formation from the photooxidation of formaldehyde and its presence in rainwater, Journal of Environmental Science and Health Part A: Environmental Science and Engineering, 14, 135–141, https://doi.org/10.1080/10934527909374867, 1979.

Calvert, J. G., Lazrus, A., Kok, G. L., Heikes, B. G., Walega, J. G., Lind, J., and Cantrell, C. A.: Chemical mechanisms of acid generation in the troposphere, Nature, 317, 27–35, https://doi.org/10.1038/317027a0, 1985.

Crounse, J. D., McKinney, K. A., Kwan, A. J., and Wennberg, P. O.: Measurement of gas-phase hydroperoxides by chemical ionization mass spectrometry, Anal. Chem., 78, 6726–6732, https://doi.org/10.1021/ac0604235, 2006.

Damschen, D. E. and Martin, L.R.: Aqueous aerosol oxidation of nitrous acid by O2, O3 AND H2O2, Atmospheric Environment (1967), 17, 2005–2011, https://doi.org/10.1016/0004-6981(83)90357-8, available at: https://www.sciencedirect.com/science/article/pii/0004698183903578, 1983.

Dienhart, D., Brendel, B., Crowley, J. N., Eger, P. G., Harder, H., Martinez, M., Pozzer, A., Rohloff, R., Schuladen, J., Tauer, S., Walter, D., Lelieveld, J., and Fischer, H.: Formaldehyde and hydroperoxide distribution around the Arabian Peninsula – evaluation of EMAC model results with ship-based measurements, Atmos. Chem. Phys., 23, 119–142, https://doi.org/10.5194/acp-23-119-2023, 2023.

Edy, J., Cautenet, S., and Brémaud, P.: Modeling ozone and carbon monoxide redistribution by shallow convection over the Amazonian rain forest, J. Geophys. Res., 101, 28671–28681, https://doi.org/10.1029/96JD01867, 1996.

Fels, M. and Junkermann, W.: The occurrence of organic peroxides in air at a mountain site, Geophys. Res. Lett., 21, 341–344, https://doi.org/10.1029/93GL01892, 1994.

530 Fischer, H., Axinte, R., Bozem, H., Crowley, J. N., Ernest, C., Gilge, S., Hafermann, S., Harder, H., Hens, K., Janssen, R. H. H., Königstedt, R., Kubistin, D., Mallik, C., Martinez, M., Novelli, A., Parchatka, U., Plass-Dülmer, C., Pozzer, A., Regelin, E., Reiffs, A., Schmidt, T., Schuladen, J., and Lelieveld, J.: Diurnal variability, photochemical production and loss processes of hydrogen peroxide in the boundary layer over Europe, Atmos. Chem. Phys., 19, 11953–11968, https://doi.org/10.5194/acp-19-11953-2019, 2019.

535 Gold, V.: The IUPAC Compendium of Chemical Terminology, International Union of Pure and Applied Chemistry (IUPAC), Research Triangle Park, NC, 2019.

Graedel, T. E. and Goldberg, K. I.: Kinetic studies of raindrop chemistry: 1. Inorganic and organic processes, J. Geophys. Res., 88, 10865, https://doi.org/10.1029/JC088iC15p10865, 1983.

Graedel, T. E., Mandich, M. L., and Weschler, C. J.: Kinetic model studies of atmospheric droplet chemistry: 2.

540 Homogeneous transition metal chemistry in raindrops, J. Geophys. Res., 91, 5205, https://doi.org/10.1029/JD091iD04p05205, 1986.

Guilbault, G. G., Brignac, P. J., and Juneau, M.: New substrates for the fluorometric determination of oxidative enzymes, Anal. Chem., 40, 1256–1263, https://doi.org/10.1021/ac60264a027, 1968.

Gunz, D. W. and Hoffmann, M. R.: Atmospheric chemistry of peroxides: a review, Atmospheric Environment. Part A.

545 General Topics, 24, 1601–1633, https://doi.org/10.1016/0960-1686(90)90496-A, 1990.

Hamryszczak, Z. T., Pozzer, A., Obersteiner, F., Bohn, B., Steil, B., Lelieveld, J., and Fischer, H.: Distribution of hydrogen peroxide over Europe during the BLUESKY aircraft campaign, Atmos. Chem. Phys., 22, 9483–9497, https://doi.org/10.5194/acp-22-9483-2022, 2022.

Hamryszczak, Z., Dienhart, D., Brendel, B., Rohloff, R., Marno, D., Martinez, M., Harder, H., Pozzer, A., Bohn, B., Zöger,

550 M., Lelieveld, J., and Fischer, H.: Measurement report: Hydrogen peroxide in the upper tropical troposphere over the Atlantic Ocean and western Africa during the CAFE-Africa aircraft campaign, Atmos. Chem. Phys., 23, 5929–5943, https://doi.org/10.5194/acp-23-5929-2023, 2023.

HEIKES, B. G., LAZRUS, A. L., KOK, G. L., Kunen, S. M., Gandrud, B. W., Gitlin, S. N., and Sperry, P. D.: Evidence for aqueous phase hydrogen peroxide synthesis in the troposphere, J. Geophys. Res., 87, 3045,

555 https://doi.org/10.1029/JC087iC04p03045, 1982.

Heikes, B. G.: Aqueous h2o2 production from o3 in glass impingers, Atmospheric Environment (1967), 18, 1433–1445, https://doi.org/10.1016/0004-6981(84)90050-7, 1984.

Heikes, B. G., Kok, G. L., Walega, J. G., and Lazrus, A. L.: H 2 O 2 O 3 and SO 2 measurements in the lower troposphere over the eastern United States during fall, J. Geophys. Res., 92, 915, https://doi.org/10.1029/JD092iD01p00915, 1987.

560 Hellpointner, E. and Gäb, S.: Detection of methyl, hydroxymethyl and hydroxyethyl hydroperoxides in air and precipitation, Nature, 337, 631–634, https://doi.org/10.1038/337631a0, available at: https://www.nature.com/articles/337631a0.pdf, 1989.

Hewitt, C. N. and Kok, G. L.: Formation and occurrence of organic hydroperoxides in the troposphere: Laboratory and field observations, J Atmos Chem, 12, 181–194, https://doi.org/10.1007/BF00115779, available at: https://link.springer.com/content/pdf/10.1007/BF00115779.pdf, 1991.

Hoffmann, M. R. and Edwards, J. O.: Kinetics of the oxidation of sulfite by hydrogen peroxide in acidic solution, J. Phys. Chem., 79, 2096–2098, https://doi.org/10.1021/j100587a005, 1975.

Hottmann, B., Hafermann, S., Tomsche, L., Marno, D., Martinez, M., Harder, H., Pozzer, A., Neumaier, M., Zahn, A., Bohn, B., Stratmann, G., Ziereis, H., Lelieveld, J., and Fischer, H.: Impact of the South Asian monsoon outflow on atmospheric hydroperoxides in the upper troposphere, Atmos. Chem. Phys., 20, 12655–12673, https://doi.org/10.5194/acp-20-12655-2020, 2020.

Hua, W., Chen, Z. M., Jie, C. Y., Kondo, Y., Hofzumahaus, A., Takegawa, N., Chang, C. C., Lu, K. D., Miyazaki, Y., Kita, K., Wang, H. L., Zhang, Y. H., and Hu, M.: Atmospheric hydrogen peroxide and organic hydroperoxides during PRIDE-PRD'06, China: their concentration, formation mechanism and contribution to secondary aerosols, Atmos. Chem. Phys., 8, 6755–6773, https://doi.org/10.5194/acp-8-6755-2008, 2008.

Jackson, A. V. and Hewitt, C. N.: Atmosphere Hydrogen Peroxide and Organic Hydroperoxides: A Review, Critical Reviews in Environmental Science and Technology, 29, 175–228, https://doi.org/10.1080/10643389991259209, 1999.

Jacob, P. and Klockow, D.: Hydrogen peroxide measurements in the marine atmosphere, J Atmos Chem, 15, 353–360, https://doi.org/10.1007/BF00115404, 1992.

Kelly, T. J., Daum, P. H., and Schwartz, S. E.: Measurements of peroxides in cloudwater and rain, J. Geophys. Res., 90, 7861–7871, https://doi.org/10.1029/JD090iD05p07861, 1985.

Kelly, T. J., Stedman, D. H., and Kok, G. L.: Measurements of H 2 O 2 and HNO 3 in rural air, Geophys. Res. Lett., 6, 375–378, https://doi.org/10.1029/GL006i005p00375, 1979.

Klippel, T., Fischer, H., Bozem, H., Lawrence, M. G., Butler, T., Jöckel, P., Tost, H., Martinez, M., Harder, H., Regelin, E., Sander, R., Schiller, C. L., Stickler, A., and Lelieveld, J.: Distribution of hydrogen peroxide and formaldehyde over Central Europe during the HOOVER project, Atmos. Chem. Phys., 11, 4391–4410, https://doi.org/10.5194/acp-11-4391-2011, 2011.

Kok, G. L.: Measurements of hydrogen peroxide in rainwater, Atmospheric Environment (1967), 14, 653–656, https://doi.org/10.1016/0004-6981(80)90048-7, 1980.

Kok, G. L., McLaren, S. E., and Staffbach, T. A.: HPLC Determination of Atmospheric Organic Hydroperoxides, Journal of Atmospheric and Oceanic Technology, 12, 282–289, https://doi.org/10.1175/1520-0426(1995)012<0282:HDOAOH>2.0.CO;2, available at: https://journals.ametsoc.org/downloadpdf/journals/atot/12/2/1520-0426_1995_012_0282_hdoaoh_2_0_co_2.pdf, 1995.

Kok, G. L., Holler, T. P., Lopez, M. B., Nachtrieb, H. A., and Yuan, M.: Chemiluminescent method for determination of hydrogen peroxide in the ambient atmosphere, Environ. Sci. Technol., 12, 1072–1076, https://doi.org/10.1021/es60145a010, 1978.

Kunen, S. M., LAZRUS, A. L., KOK, G. L., and HEIKES, B. G.: Aqueous oxidation of SO 2 by hydrogen peroxide, J. Geophys. Res., 88, 3671, https://doi.org/10.1029/JC088iC06p03671, 1983.

LAZRUS, A. L., G. L. Kok, J. A. Lind, S. N. Gitlin, B. G. Heikes, and R. E. Shelter: Automated Fluorometric Method for Hydrogen Peroxide in Air, Anal. Chem., 58, 594–597, 1986.

Lazrus, A. L., Kok, G. L., Gitlin, S. N., Lind, J. A., and McLaren, S. E.: Automated fluorimetric method for hydrogen peroxide in atmospheric precipitation, Anal. Chem., 57, 917–922, https://doi.org/10.1021/ac00281a031, 1985.

Lee, J. H., Tang, I. N., Weinstein-Lloyd, J. B., and Halper, E. B.: Improved nonenzymatic method for the determination of gas-phase peroxides, Environmental Science and Technology; (United States), 28:6, https://doi.org/10.1021/es00055a032, 1994.

Lee, J. H., Tang, I. N., and Weinstein-Lloyd, J. B.: A non-enzymatic method for the determination of hydrogen peroxide in atmospheric samples, Anal. Chem., 62, 2381–2384, https://doi.org/10.1021/ac00220a022, 1990.

Lee, M.: Hydrogen Peroxide, Methyl Hydroperoxide, and Formaldehyde in Air Impacted by Biomass Burning, Ph.D. Thesis, 1995.

Lee, M., Heikes, B. G., and O'Sullivan, D. W.: Hydrogen peroxide and organic hydroperoxide in the troposphere: a review, Atmospheric Environment, 34, 3475–3494, https://doi.org/10.1016/S1352-2310(99)00432-X, available at: https://www.sciencedirect.com/science/article/pii/S135223109900432X, 2000.

Lee, Y.-N. and Lind, J. A.: Kinetics of aqueous-phase oxidation of nitrogen(III) by hydrogen peroxide, J. Geophys. Res., 91, 2793, https://doi.org/10.1029/JD091iD02p02793, 1986.

Lelieveld, J. and Crutzen, P. J.: Role of deep cloud convection in the ozone budget of the troposphere, Science (New York, N.Y.), 264, 1759–1761, https://doi.org/10.1126/science.264.5166.1759, 1994.

Lelieveld, J. and Crutzen, P. J.: The role of clouds in tropospheric photochemistry, J Atmos Chem, 12, 229–267, https://doi.org/10.1007/BF00048075, 1991.

Mackay, G. I., Mayne, L. K., and Schiff, H. I.: Measurements of H 2 O 2 and HCHO by Tunable Diode Laser Absorption Spectroscopy During the 1986 Carbonaceous Species Methods Comparison Study in Glendora, California, Aerosol Science and Technology, 12, 56–63, https://doi.org/10.1080/02786829008959325, 1990.

Madronich, S.: Photodissociation in the atmosphere: 1. Actinic flux and the effects of ground reflections and clouds, J. Geophys. Res., 92, 9740, https://doi.org/10.1029/JD092iD08p09740, 1987.

Olszyna, K. J., Meagher, J. F., and Bailey, E. M.: Gas-phase, cloud and rain-water measurements of hydrogen peroxide at a high-elevation site, Atmospheric Environment (1967), 22, 1699–1706, https://doi.org/10.1016/0004-6981(88)90398-8, 1988.

O'Sullivan, D. W., Lee, M., Noone, B. C., and Heikes, B. G.: Henry's Law Constant Determinations for Hydrogen Peroxide, Methyl Hydroperoxide, Hydroxymethyl Hydroperoxide, Ethyl Hydroperoxide, and Peroxyacetic Acid, J. Phys. Chem., 100, 3241–3247, https://doi.org/10.1021/jp951168n, 1996.

630 Penkett, S. A., Jones, B.M.R., Brich, K. A., and Eggleton, A.E.J.: The importance of atmospheric ozone and hydrogen peroxide in oxidising sulphur dioxide in cloud and rainwater, Atmospheric Environment (1967), 13, 123–137, https://doi.org/10.1016/0004-6981(79)90251-8, available at: https://www.sciencedirect.com/science/article/pii/0004698179902518, 1979.

Pilz, W. and Johann, I.: Die Bestimmung Kleinster Mengen von Wasserstoffperoxyd in Luft, International journal of
635 environmental analytical chemistry, 3, 257–270, https://doi.org/10.1080/03067317408071087, 1974.

Reeves, C. E. and Penkett, S. A.: Measurements of peroxides and what they tell us, Chemical reviews, 103, 5199–5218, https://doi.org/10.1021/cr0205053, 2003.

Robbin Martin, L. and Damschen, D. E.: Aqueous oxidation of sulfur dioxide by hydrogen peroxide at low pH, Atmospheric Environment (1967), 15, 1615–1621, https://doi.org/10.1016/0004-6981(81)90146-3, available at:
640 https://www.sciencedirect.com/science/article/pii/0004698181901463, 1981.

Römer, F. G., Viljeer, J. W., van den Beld, L., Slangewal, H. J., Veldkamp, A. A., Kema, N. V., and Reunders, H.F.R.: The chemical composition of cloud and rainwater. Results of preliminary measurements from an aircraft, Atmospheric Environment (1967), 19, 1847–1858, https://doi.org/10.1016/0004-6981(85)90010-1, 1985.

Sakugawa, H., Kaplan, I. R., Tsai, W., and Cohen, Y.: Atmospheric hydrogen peroxide, Environ. Sci. Technol., 24, 1452–
645 1462, https://doi.org/10.1021/es00080a002, 1990.

Schöne, E.: Ueber den Nachweis des Wasserstoffhyperoxyds in der atmosphärischen Luft und den atmosphärischen Niederschlägen, Fresenius, Zeitschrift f. anal. Chemie, 33, 137–184, https://doi.org/10.1007/BF01335790, 1894.

Schöne, E.: Zur Frage über das Vorkommen des Wasserstoffhyperoxyds in der atmosphärischen Luft und den atmosphärischen Niederschlägen, Ber. Dtsch. Chem. Ges., 26, 3011–3027, https://doi.org/10.1002/cber.189302603136,
650 1893.

Schöne, E.: Ueber das atmosphärische Wasserstoffhyperoxyd, Ber. Dtsch. Chem. Ges., 7, 1693–1708, https://doi.org/10.1002/cber.187400702232, 1874.

Slemr, F., Harris, G. W., Hastie, D. R., Mackay, G. I., and Schiff, H. I.: Measurement of gas phase hydrogen peroxide in air by tunable diode laser absorption spectroscopy, Journal of Geophysical Research: Atmospheres, 91, 5371–5378,
655 https://doi.org/10.1029/JD091iD05p05371, available at: https://onlinelibrary.wiley.com/doi/pdf/10.1029/JD091iD05p05371, 1986.

St Clair, J. M., McCabe, D. C., Crounse, J. D., Steiner, U., and Wennberg, P. O.: Chemical ionization tandem mass spectrometer for the in situ measurement of methyl hydrogen peroxide, The Review of scientific instruments, 81, 94102, https://doi.org/10.1063/1.3480552, 2010.

660 Staehelin, J. and Hoigne, J.: Decomposition of ozone in water: rate of initiation by hydroxide ions and hydrogen peroxide, Environ. Sci. Technol., 16, 676–681, https://doi.org/10.1021/es00104a009, 1982.

https://doi.org/10.5194/amt-2023-114
Preprint. Discussion started: 12 June 2023

Tomsche, L., Pozzer, A., Ojha, N., Parchatka, U., Lelieveld, J., and Fischer, H.: Upper tropospheric CH_4 and CO affected by the South Asian summer monsoon during the Oxidation Mechanism Observations mission, Atmos. Chem. Phys., 19, 1915–1939, https://doi.org/10.5194/acp-19-1915-2019, 2019.

Valverde-Canossa, J., Wieprecht, W., Acker, K., and Moortgat, G. K.: H2O2 and organic peroxide measurements in an orographic cloud: The FEBUKO experiment, Atmospheric Environment, 39, 4279–4290, https://doi.org/10.1016/j.atmosenv.2005.02.040, 2005.

Weschler, C. J., Mandich, M. L., and Graedel, T. E.: Speciation, photosensitivity, and reactions of transition metal ions in atmospheric droplets, J. Geophys. Res., 91, 5189, https://doi.org/10.1029/JD091iD04p05189, 1986.

Supplement of:
HYPHOP: a tool for high-altitude, long-range monitoring of hydrogen peroxide and higher organic peroxides in the atmosphere

Zaneta Hamryszczak[1], Antonia Hartmann[1], Dirk Dienhart[1],Sascha Hafermann[1], Bettina Brendel[1], Rainer Königstedt[1], Uwe Parchatka[1], Jos Lelieveld[1,2] and Horst Fischer[1]

[1]Atmospheric Chemistry Department, Max Planck Institute for Chemistry, Mainz, 55128, Germany
[2]Climate and Atmosphere Research Center, The Cyprus Institute, Nicosia, 1645, Cyprus

Correspondence to: Zaneta Hamryszczak (z.hamryszczak@mpic.de) and Horst Fischer (horst.fischer@mpic.de)

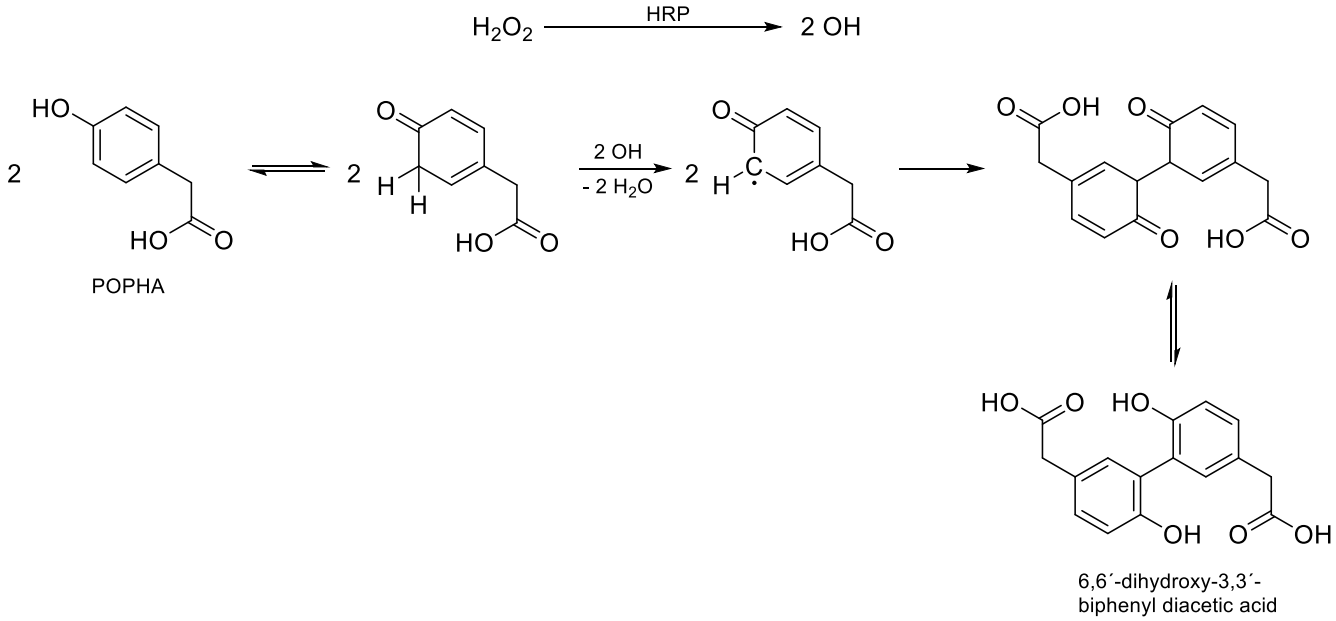

(SR1)

$$H_2O_2 + \text{catalase}_{red} \rightarrow H_2O + \text{catalase}_{ox} \quad \text{(SR2)}$$

$$H_2O_2 + \text{catalase}_{ox} \rightarrow H_2O + O_2 + \text{catalase}_{red} \quad \text{(SR3)}$$

$$2\,H_2O_2 \rightarrow 2\,H_2O + O_2 \quad \text{(SR4)}$$

$$H_2O_2 + 2\,H_2O \rightarrow O_2 + 2\,H_3O^+ + 2\,e^- \quad \text{(SR5)}$$

$$MnO_4^- + 8\,H_3O^+ + 5\,e^- \rightarrow Mn^{2+} + 12\,H_2O \quad \text{(SR6)}$$

$$2\,MnO_4^- + 5\,H_2O_2 + 6\,H_3O^+ \rightarrow 2\,Mn^{2+} + 5\,O_2 + 14\,H_2O \quad \text{(SR7)}$$

$$c(H_2O) = 5 \cdot \left(\frac{c(KMnO_4) \cdot V(KMnO_4)}{2 \cdot V(H_2O_2)_{STM}} \right) \quad \text{(S1)}$$

$$Q_{Air} = Q_{real} \cdot \frac{T_{std} \cdot p_{real}}{T_{real} \cdot p_{std}} \quad \text{(S2)}$$

$$Q_{Stripping} = \frac{V_{Stripping}}{t} \quad \text{(S3)}$$

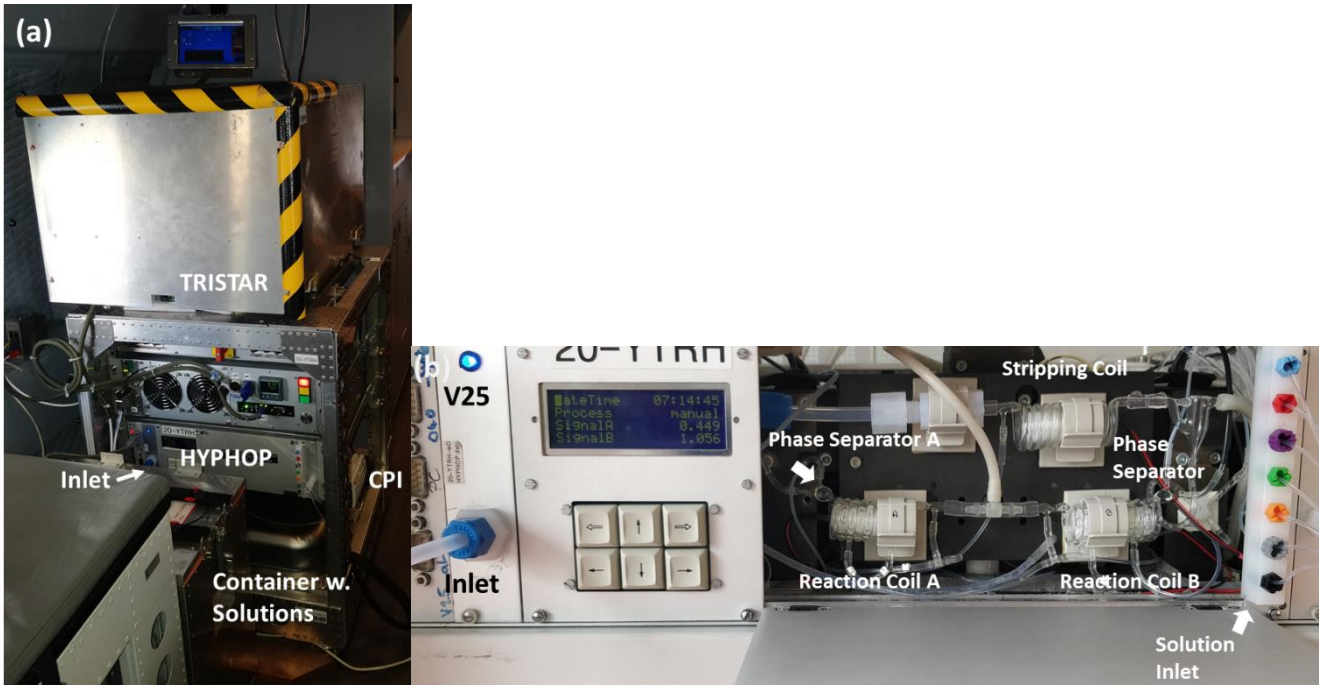

Figure S1: Front view of the measurement rack (a) and the HYPHOP monitor (b).

$$SO_2 + 2\,H_2O \rightleftharpoons HSO_3^- + H_3O^+ \quad \text{(SR8)}$$

$$HSO_3^- + H_2O_2 \rightarrow HSO_4^- + H_2O \quad \text{(SR9)}$$

$$HSO_4^- + H_3O^+ \rightarrow H_2SO_4 + H_2O \quad \text{(SR10)}$$

$$HSO_3^- + CH_3OOH \rightarrow SO_4^{2-} + CH_3SO_4^- + H_2O + CH_3OH + H^+ \quad \text{(SR11)}$$

$$HSO_3^- + CH_3C(O)OOH \rightarrow SO_4^{2-} + CH_3C(O)OH + H^+ \quad \text{(SR12)}$$

$$Fe^{2+} + H_2O_2 \rightarrow Fe^{3+} + OH + OH^- \quad \text{(SR13)}$$

$$OH + H_2O_2 \rightarrow H_2O + HO_2 \quad \text{(SR14)}$$

$$HO_2 + H_2O_2 \rightarrow OH + H_2O + O_2 \quad \text{(SR15)}$$

$$Fe^{2+} + ROOH \rightarrow Fe^{3+} + RO + OH^- \quad \text{(SR16)}$$

$$SO_2 + 2H_2O \rightarrow HSO_3^- + H_3O^+ \quad \text{(SR17)}$$

$$HSO_3^- + HCHO \rightarrow HOCH_2SO_3^- \quad \text{(SR18)}$$

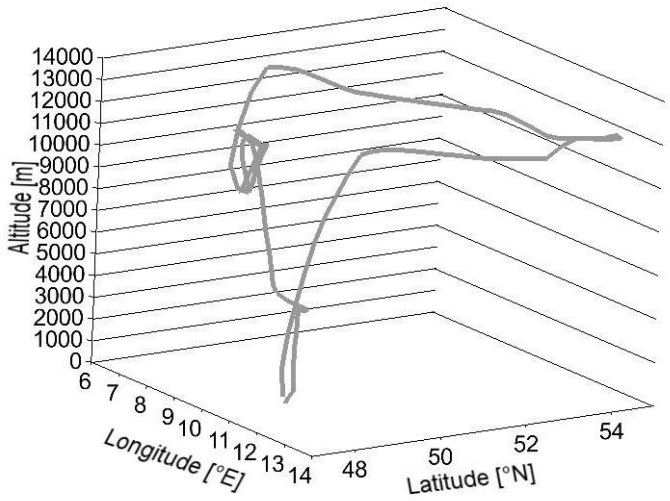

Figure S2: Flight pattern of the research aircraft HALO during the test flight on 22nd November 2022.

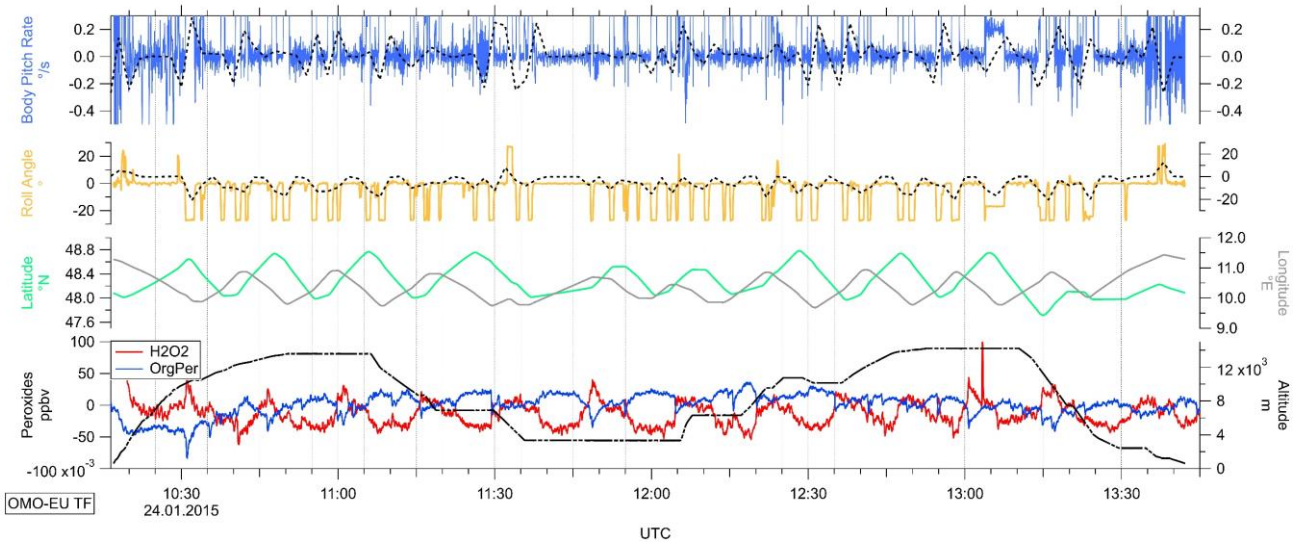

Figure S3: Temporal series of the measured signals in channel A (H_2O_2 + ROOH; red) and B (ROOH; dark blue; bottom plot) in correspondence with the altitude (black), latitude (green), longitude (grey), roll angle (yellow) and body pitch rate (blue; top plot) of the aircraft during an exemplary test flight of the OMO-EU campaign performed on 24th January 2015. Dashed lines (black) represent the temporal trends of the roll angle and the body pitch rate based on 2 min bins.

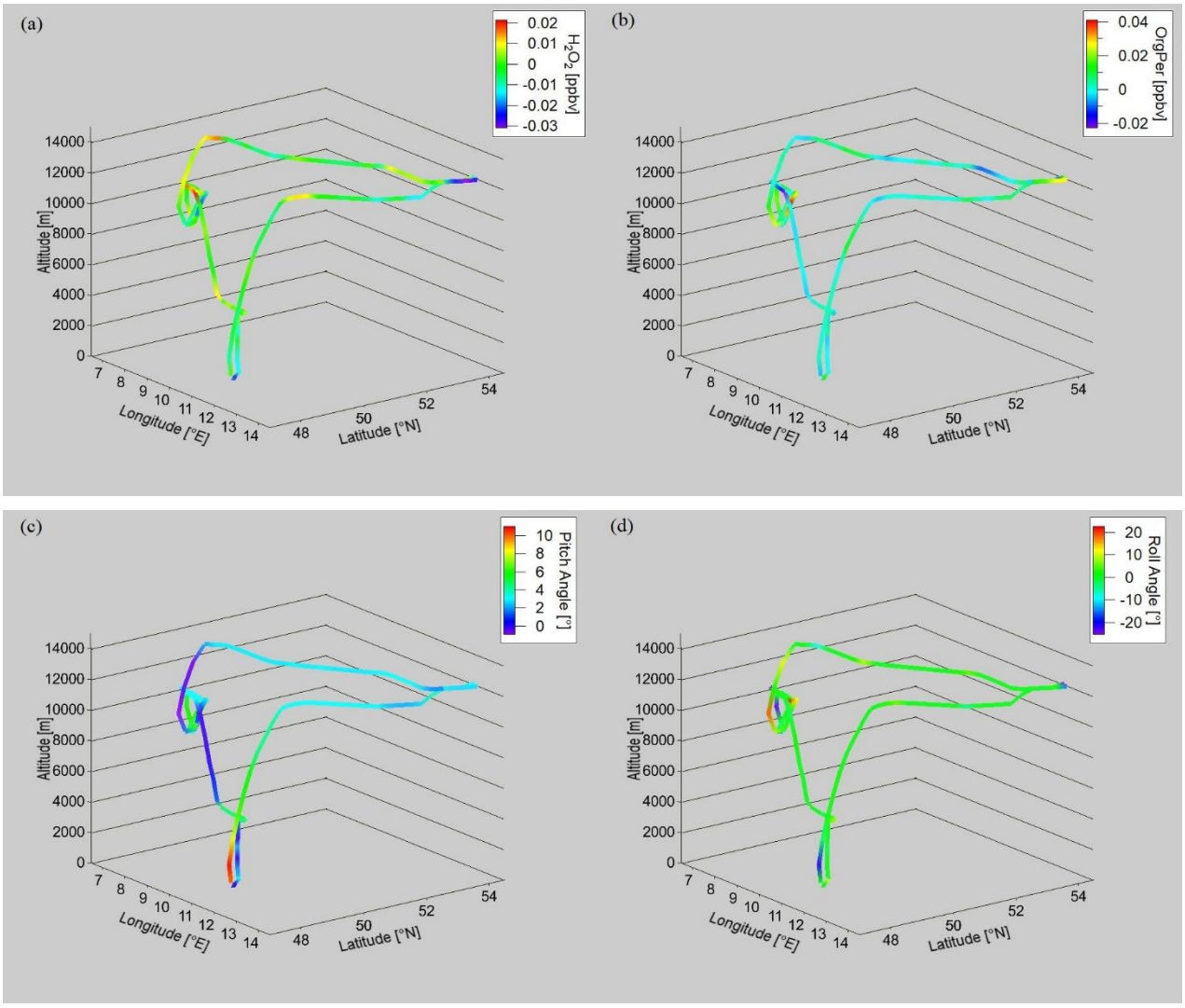

Figure S4: GPS flight pattern of the research aircraft HALO during the test flight on 22nd November 2022 with respect to the observed background signals (channel A: H_2O_2 + ROOH; (a); channel B: ROOH; (b)), pitch angle (c) and roll angle (d) of the aircraft based on the instrumental time resolution of 2 min.

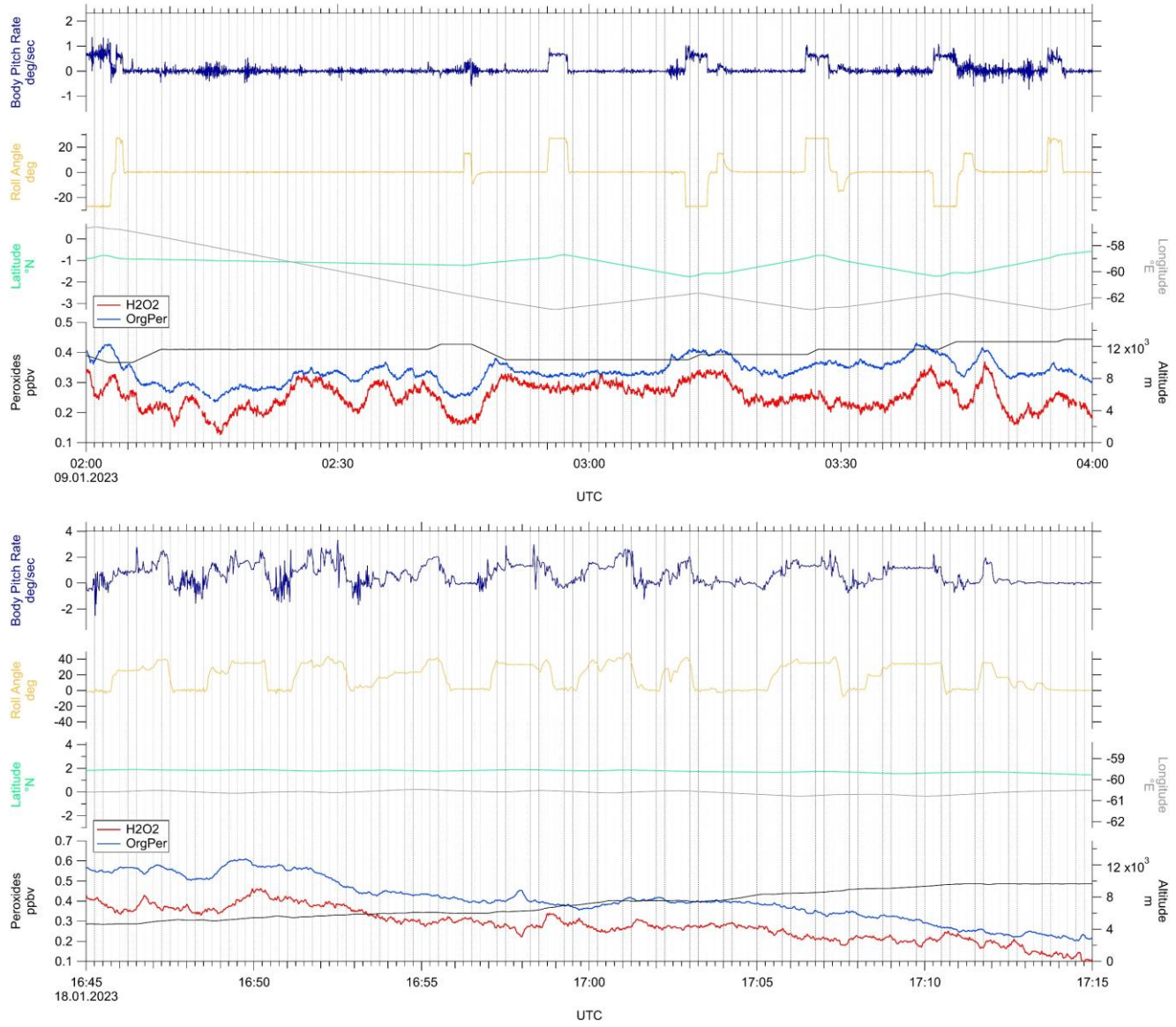

Figure S5: Temporal series of the measured hydrogen peroxide (red) and the sum of organic hydroperoxides (dark blue) in correspondence with the altitude (black), latitude (green), longitude (grey), roll angle (yellow) and body pitch rate (blue) of the aircraft during two exemplary measurement flights RF#13 (top panel) and RF#17 (bottom panel) performed on 9th and 18th January 2023 as a part of the CAFE-Brazil campaign.

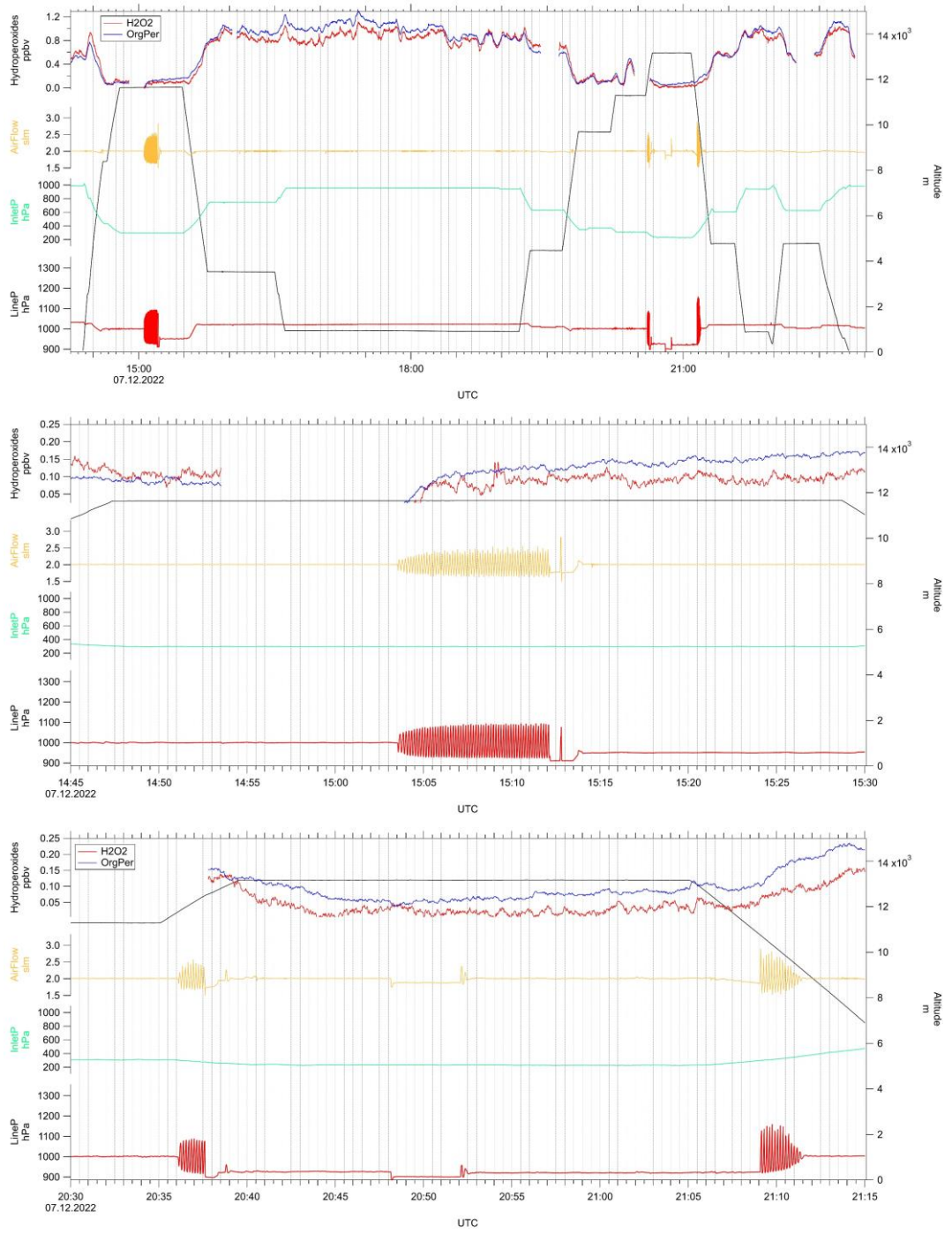

Figure S6: Temporal series of the tracked line pressure (red) complimented by the GPS flight altitude (black), measured inlet pressure (green), the air mass flow (yellow), and hydroperoxide levels (H2O2:red and ROOH: blue) of the aircraft during an exemplary measurement flight of the CAFE-Brazil campaign performed on 12th December 2022 with 1 sec temporal resolution (overview: top panel; detailed insight during high legs: middle and bottom panels).

Table S1: Mean (±1σ) of the estimated time resolution in sec based on the signal rise and fall from 10% to 90% and vice versa assumed to be the lowest temporal limit and the pump time of the flow-through cuvettes assumed as the highest temporal limit of the monitor.

Mean (±1σ) /sec	Calibrations		Background		Convection peaks		Varying LqStd		Cuvettes
Channels	**A**	**B**	**A**	**B**	**A**	**B**	**A**	**B**	
Signal rise	120 (±7.12)	135 (±10.8)	86.3 (±14.4)	88.8 (±16.3)	120 (±61.6)	124 (±59.6)	111 (±23.9)	134 (±21.2)	-
Signal fall	114 (±7.17)	107 (±30.9)	98.3 (±16.2)	99.7 (±16.1)	129 (±56.8)	132 (±53.1)	110 (±7.25)	114 (±8.58)	-
Pump-through	-	-	-	-	-	-	-	-	52.5 (±2.32)
Measurement density	15		70		22		14		4

Table S2: Instrumental precision, limit of detection, temporal resolution and total measurement uncertainty (TMU) of HYPHOP during the airborne campaigns OMO 2015 (Hottmann et al. 2020), CAFE-Africa (Hamryszczak et al. 2022a), BLUESKY 2020 (Hamryszczak et al. 2022b) and CAFE-Brazil 2022/23.

	OMO 2015	CAFE-Africa 2018	BLUESKY 2020	CAFE-Brazil 2022/23
Precision H_2O_2	0.2% (5.2 ppbv) – 1.3% (5.9 ppbv)	1.3% (5.5 ppbv)	0.3 % (5.1 ppbv)	6.4% (5.7 ppbv)
Precision ROOH	0.3% (5.0 ppbv) – 2.1% (6.0 ppbv)	0.8% (5.6 ppbv)	0.2 % (5.4 ppbv)	3.6% (5.8 ppbv)
LOD H_2O_2	8 – 53 pptv	15 pptv	35 pptv	20 pptv
LOD ROOH	9 – 52 pptv	6 pptv	13 pptv	19 pptv
Time resolution	120 sec	122 sec	120 sec	52.5 – 114 sec
TMU H_2O_2	**25%**	**9%**	**28%**	**12%**
TMU ROOH	**40%**	**41%**	**40%**	**40%**

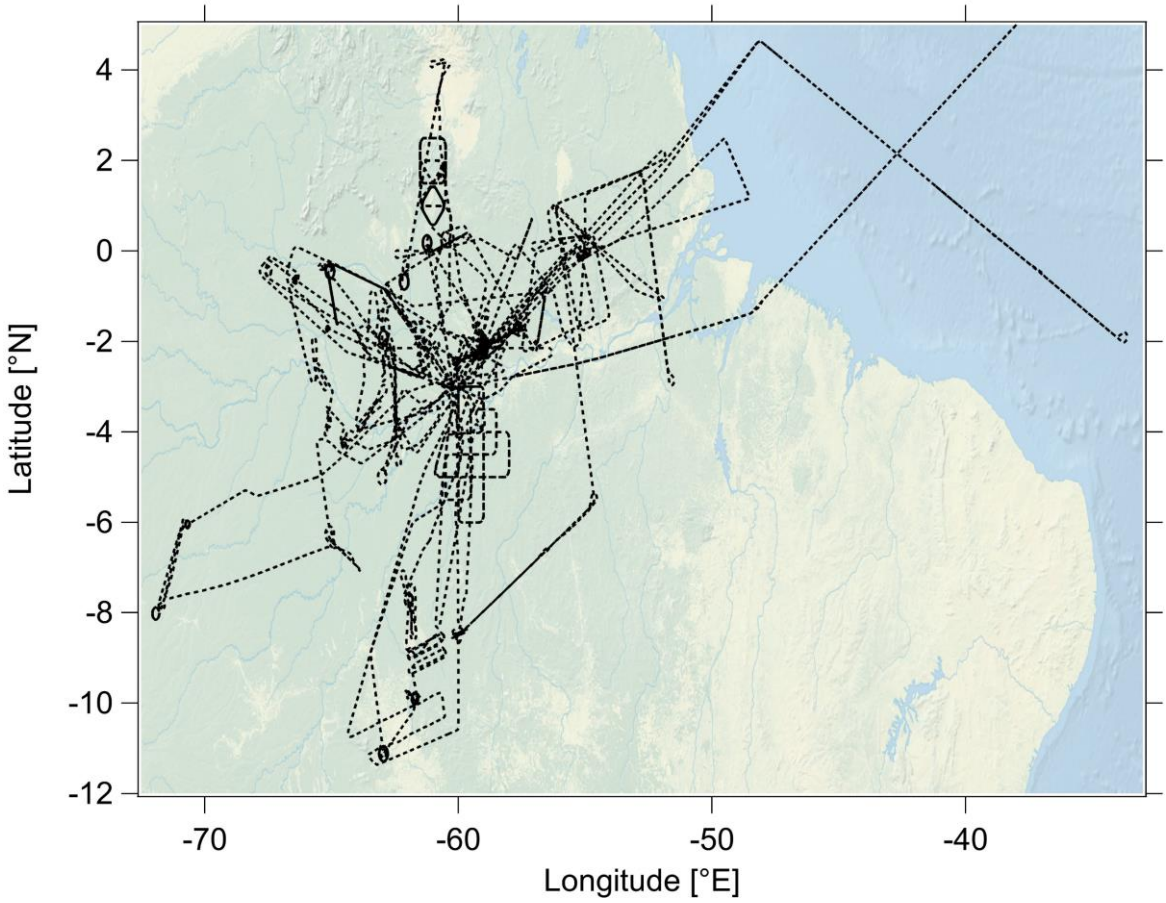

Figure S7: Spatial resolution of the flight tracks during CAFE-Brazil campaign performed in December 2022 and January 2023. Global topography relief raster is based on data set available from WaveMetrics. [1]

Table S3: Mean (±1σ), median and maximum hydroperoxide mixing ratios (ppbv) over the entire tropospheric column (left column) and subdivided into the approximate main tropospheric regions (right).

	Total		**0 < 2 km**		**2 < 8 km**		**≥ 8 km**	
	H_2O_2	**ROOH**	**H_2O_2**	**ROOH**	**H_2O_2**	**ROOH**	**H_2O_2**	**ROOH**
Mean	**0.30**	**0.43**	0.74	0.99	0.45	0.62	0.12	0.22
(±1σ)	**(±0.30)**	**(±0.36)**	(±0.25)	(±0.31)	(±0.26)	(±0.34)	(±0.09)	(±0.12)
Median	**0.17**	**0.28**	0.76	1.00	0.43	0.59	0.10	0.22
Maximum	**1.94**	**1.73**	1.76	1.73	1.94	1.51	0.85	0.85

[1] WaveMetrics, Inc. 10200 SW Nimbus, G-7 Portland , OR 97223.
https://www.wavemetrics.net/Downloads/IgorGIS/GISData/ <last access: 09.06.23023>

2.2. ECHAM5/MESSy Atmospheric Chemistry model – EMAC

Airborne hydroperoxide observations were compared to numerical simulations from the global chemistry and climate 3-D model EMAC (ECHAM/MESSy for Atmospheric Chemistry, Jöckel et al., 2010). The model numerically simulates the chemistry and dynamics of the troposphere and middle atmosphere, i. e. stratosphere, incorporating a large variety of submodels addressing chemical and meteorological processes and corresponding interactions with natural and anthropogenic emissions originating from continental and marine environments (Jöckel et al., 2006). It is based on the 5th generation of the European Centre HAMburg general circulation model developed by the Max Planck Institute for Meteorology (EMCWF HAMburg = ECHAM5; Roeckner et al., 2003; Roeckner et al., 2006). The base model, Modular Earth Submodel System (MESSy) enables data communication between the submodels and the base model (Jöckel et al., 2005; Jöckel et al., 2010; Jöckel et al., 2016). The Module for Efficiency Calculating the Chemistry of the Atmosphere (MECCA; Sander et al., 2005; Sander et al., 2011; Sander et al., 2019) simulates the tropospheric and stratospheric gaseous-phase and heterogeneous chemistry based on the Mainz Organic Mechanism (MOM), which bares approximately 600 species and their corresponding reactions, and photolysis rate calculations from a radiation transfer model (Sander et al., 2014; Sander et al., 2019). The submodel JVAL calculates the photolysis rate coefficients (Sander et al., 2014). Aqueous-phase chemistry in clouds and wet scavenging processes are based on the SCAVenging of Tracers submodel (SCAV; Tost et al., 2006). The submodels MEGAN, ONLEM, OFFLEM, TNUDGE, and DRYDEP simulate biogenic, and anthropogenic emissions and dry deposition of atmospheric gases and aerosols in the atmosphere (Kerkweg et al., 2006a; Kerkweg et al., 2006b). The CAMS-GLOB-ANTv4.2 (Granier et al., 2019) is based on EDGARv4.3.2, and EDGARv4.3.3. inventories (European Joint Center; JRC; Crippa et al., 2018) and CEDS emissions (Hoesly et al., 2018) were used to simulate anthropogenic emissions distributed vertically (Pozzer et al., 2009). Potential emission reductions during the BLUESKY campaign performed during the first European COVID-19-related lockdown in 2020 were adapted based on the studies of Guevara et al. (2021) as described in detail by Reifenberg et al. (2021). Emissions originating from biomass burning processes during the CAFE-Africa campaign were based on the Global Fire Assimilation System simulations (GFAS; Kaiser et al., 2012). A model set-up evaluation regarding different trace gases and aerosols was performed by Pozzer et al. (2022). The simulations were carried out with a vertical resolution of 47 vertical levels up to 0.01 hPa at a horizontal resolution of T63 (i. e., roughly 1.8° x 1.8°). The model results have a temporal resolution of 5 min during the BLUESKY campaign, 6 min during CAFE-Africa, and 10 min during CAFE-Brazil airborne measurements, respectively. For comparison purposes relative to the observations the simulation results were further interpolated along the GPS flight tracks using the S4D submodel (Jöckel et al., 2010). For detailed information and a

listing of the individual submodels incorporated into the EMAC model, the reader is referred to https://messy-interface.org/ [1].

2.3. H_2O_2 simulations based on the quasi-photostationary steady-state assumption

The sampled air masses were analyzed regarding their photostationary steady-state (PSS) by the comparison of the measured hydrogen peroxide mixing ratios relative to H_2O_2 simulations assuming PSS conditions based on measured precursors and H_2O_2 photochemical loss processes (HO_2, OH, $j(H_2O_2)$) and rate coefficient data from Atkinson et al. (2004). Based on the comparison, atmospheric regions with missing sinks or additional non-photochemical sources were identified and analyzed.

Generally, a species X mixing ratios change over time, d(X)/dt can be determined using the production and loss rates (P(X) and L(X)) under consideration of the species transport (T(X)) and deposition (D(X)), as presented below (Eq. 1).

$$\frac{d(X)}{dt} = P(X) - L(X) - D(X) \pm T(X) \quad (1)$$

Based on the reaction pathways presented in Sect. 1. (R10), the hydrogen peroxide production rate is derived from the recombination of HO_2 ($P(H_2O_2)$; Eq. 2). The corresponding loss rate is determined as a sum of H_2O_2 photolysis and the reaction of H_2O_2 with OH ($L(H_2O_2)$; R30 and R33; Eq. 3).

$$P(H_2O_2) = k_{HO_2+HO_2} \cdot [HO_2]^2 \quad (2)$$

$$L(H_2O_2) = \left(k_{H_2O_2+OH} \cdot [OH] + j(H_2O_2)\right) \cdot [H_2O_2] \quad (3)$$

Assuming PSS conditions, the variability over time in the species mixing ratio is negligible. Neglecting further H_2O_2 deposition and transport processes, the quasi-photostationary steady-state H_2O_2 mixing ratios are given as:

$$[H_2O_2]^{PSS} = \frac{[HO_2]^2 \cdot k_{HO_2+HO_2}}{[OH] \cdot k_{H_2O_2+OH} + j(H_2O_2)} \quad (4)$$

The rate coefficient calculations were based on the IUPAC recommendation (Atkinson et al., 2004) extended by parameters measured along the GPS flight tracks (Eq. 5 – 6). The production rate coefficient was further extended by the factor $1 + 1.4 \cdot 10^{-21}$ cm^3 $[H_2O]$ exp(2200/T) in both expressions reflecting the water dependency of H_2O_2 levels in the atmosphere.

[1] Last access: 19.06.2023, 12:38 CET

$$k_{HO_2+HO_2} = 2.2 \cdot 10^{-13} \cdot \exp^{\frac{600}{T}} cm^3 s^{-1} + 1.9 \cdot 10^{-33}[N_2] \cdot \exp^{\frac{980}{T}} cm^6 s^{-1} \quad (5)$$

$$k_{H_2O_2+OH} = 2.9 \cdot 10^{-12} \cdot \exp^{\frac{-160}{T}} cm^3 s^{-1} \quad (6)$$

2.4. ERA5 reanalysis model – meteorological information

Observation-based hydroperoxide analyses were further supported by hourly and monthly averaged meteorological data provided by the 5th generation ECMWF reanalysis for the global climate and weather, ERA5 (Copernicus Climate Change Service (C3S) Climate Data Store (CDS; Hersbach et al. 2019)). The reanalyses combine globally derived climate and weather observations with model data based on data assimilation, where forecasts are combined with available observations at a frequency of 12 h to produce an estimate of the atmospheric state from 1940 to the present time. ERA5 provides hourly and monthly estimates for a large variety of atmospheric, continental, and marine surface parameters, such as wind speed, dewpoint temperature, temperature, air density, boundary layer height and dissipation, cloud base height and cloud coverage, convective and large-scale precipitation, evaporation, vegetation cover, etc. The reanalysis model output is a re-gridded subset of 0.25° x 0.25° for the reanalysis and 0.5° x 0.5° for the corresponding uncertainty estimates on pressure levels (upper air) and single levels (atmospheric and land-surface) of the full ERA5 data set on native resolution. For detailed information and a listing of the individual parameter provided by ERA5 reanalysis, the reader is referred to https://cds.climate.copernicus.eu/cdsapp#!/home[2].

[2] Last access: 26.06.2023, 18:01 CET

3. The BLUESKY airborne campaign in 2020

The section is dedicated to airborne hydroperoxide analyses based on the measurement results during the BLUESKY aircraft campaign performed in May – June 2020. The objective and the scientific focus of the research project, an overview of the instrumentation on board the research aircraft HALO, and a summary of the meteorological conditions during the airborne campaign is presented in the following section (Sect. 3.1.). Sect. 3.2. gives an overview of the measured hydroperoxide mixing ratios as mean and median values for the performed measurement flights. The focus of the evaluation is on tropospheric hydrogen peroxide measurements emphasizing their tropospheric vertical and latitudinal distribution with regard to clouds relative to previous measurements over Europe, HOOVER II (HO_x Over EuRope, 2006 – 2007) and UTOPIHAN II/III (Upper Tropospheric Ozone: Processes Involving HO_x and NO_x: The Impact of Aviation and Convectively Transported Pollutants in the Tropopause Region; 2002 -2004), and EMAC simulations. The discussion of the analysis results is based on a published research article with the title: “Distribution of hydrogen peroxide over Europe during the BLUESKY aircraft campaign” (Sect. 3.3.).

3.1. The campaign – Objectives, instrumentation, and meteorological conditions

Reduced air pollution and aircraft emissions during the COVID-19-related lockdown in 2020 gave rise to intensely blue skies providing an adequate name for the campaign performed in May and June 2020 over Europe, BLUESKY (Voigt et al., 2022). The airborne BLUESKY campaign had the purpose to investigate the impact of lockdown-related reduced emissions from anthropogenic sources on the atmospheric chemistry and physics over Europe. The measurement flights sampled the atmosphere in the region from the Mediterranean to the North Atlantic flight corridor (35° N – 60 °N; 15° W – 15° E). The following figure presents the entirety of the performed flights during the measurement period (Fig. 8).

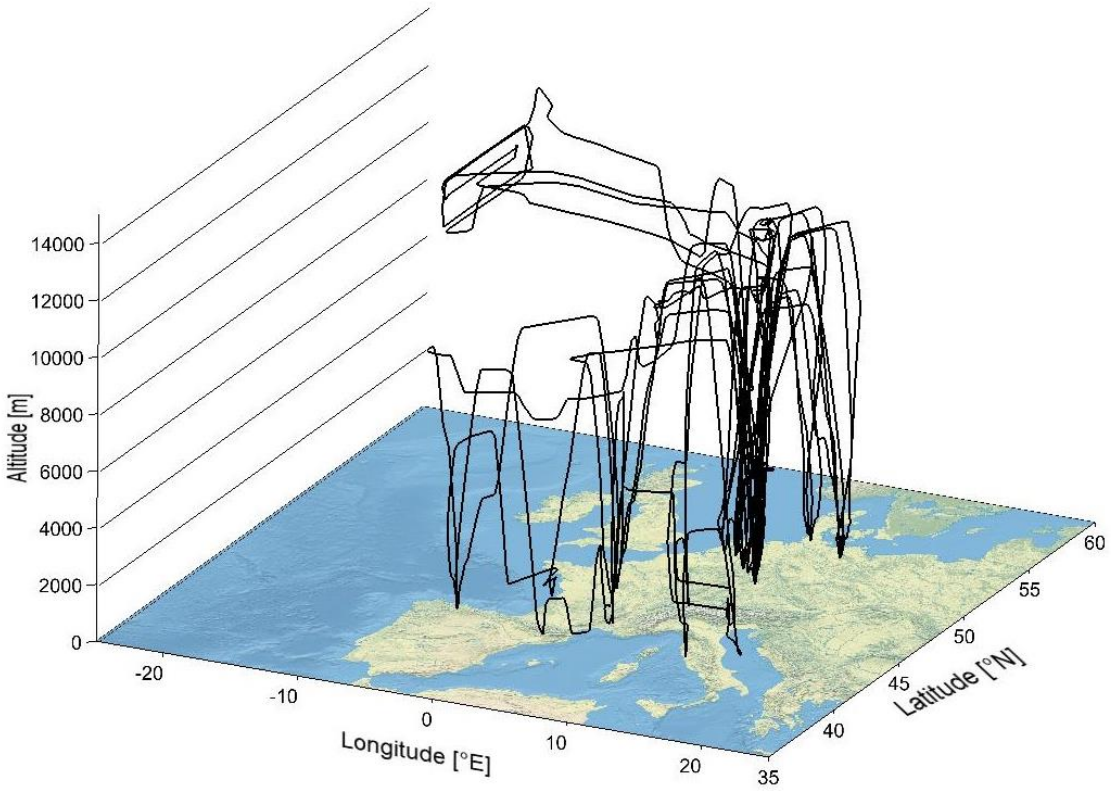

Figure 8: General overview of performed measurement flights during the BLUESKY campaign (05/06 2020) based on GPS flight tracks output by BAHAMAS instrument with 2 min temporal resolution.

During the BLUESKY campaign, eight measurement flights were performed with the German High Altitude and LOng-range research aircraft (HALO) from the base of operation of the German Aerospace Center (Deutsche Zentrum für Luft- und Raumfahrt, DLR) in Oberpfaffenhofen (Germany). Please note that flights passing the North Atlantic flight corridor were excluded from the following discussion since they were performed entirely in the lower stratosphere, where the measured levels of hydroperoxides were at the instrumental detection limit and do not add significantly to the analysis. As illustrated in Fig. 8, the majority of the flights took place over Central Europe, where vertical profile measurements were carried out with a special emphasis on urban areas and German airports. Additionally, measurement flights were conducted over Western Europe (France and Spain) and the Mediterranean region (Spanish, French, and Italian coastal areas as well as the urban regions of Rome and Milan).

During the airborne campaign, a large suite of atmospheric trace species was sampled covering a vertical range from a few tens of meters above the earth's surface up to 15 km of altitude. An overview of the research aircraft instrumentation significant to the analyses performed in the scope of this work during the measurement period, the corresponding instrumental parameters, and literature references are presented in the table below (Tab. 1).

Table 1: Instrumentation on board the research aircraft HALO relevant to the presented hydroperoxide analyses.

Measurement	Method	TMU	References
H_2O_2 **ROOH**	Chemiluminescence	H_2O_2: 9 % - 28 % ROOH: 40 % - 41 %	Hamryszczak et al. (2022)
HO_x	Laser-induced fluorescence (LIF; additional chem. conversion for HO_2)	50%[3]	Marno et al. (2020)
Actinic flux	Spectroradiometer	7 % – 8 % (15 % for $j(H_2O_2)$)	Bohn and Lohse (2017)
H_2O	TDL	5 %	Krautstrunk and Giez (2012)

Figure S1 of the Supplement in Sect. 3.3. gives an overview of the average monthly 2 m temperature, total cloud cover fraction, and total precipitation during May and June 2020 derived from ERA5 reanalysis generated using Copernicus Climate Change Service information (Hersbach et al. 2019). GPS flight tracks of measurement flights with the exception of the North Atlantic flight corridor measurements are indicated in black. The average temperature during the measurement period based on the defined region (48.75° W – 15° E; 26.5 – 72° N) was 284.66 (±9.21) K with a maximum of 308.22 K in the southern part of the region and a minimum of 250.10 K towards the north-east in May 2020. Comparably, 287.40 (±8.60) K, 311.60 K, and 259.06 K, respectively were reported in June 2020. Average total cloud coverage was 0.62 (±0.16) in May and 0.64 (±0.23) in June, respectively with a total coverage of up to unity towards the north and nearly none in the South. The distinct difference was even more pronounced in June. Total precipitation varied between 1.82 (±1.18) $\cdot$ 10^{-3} m in May and 1.77 (±1.39) $\cdot$ 10^{-3} m in June, respectively with peak values of 9.61 $\cdot$ 10^{-3} m over the Atlantic Ocean and Central Europe. In June maxima of up to 15.86 $\cdot$ 10^{-3} m were reported over North, and Central Europe as well as at the coast of Greenland. Additional information regarding meteorological conditions during single measurement flight is presented accordingly in the Supplement of the published manuscript (Fig. S2, S5, and S7) in Sect. 3.3.

[3] Please note that finalized HO_x data was available exclusively for the CAFE-Africa campaign, performed in 2018.

3.2. Overview of hydroperoxide levels during BLUESKY 2020

The measured mean hydroperoxide mixing ratios during the BLUESKY campaign are presented as latitude vs. longitude plots aggregated into a subset of 1° x 1° bins along the GPS flight tracks subdivided into the main tropospheric layers (0 < 2 km: top panel; 2 < 6 km: middle panel; ≥ 6 km: bottom panel; Fig. 9). The color scale represents the measured levels of H_2O_2 (left column) and ROOH (assumed to be mainly MHP as the upper limit of ROOH; right column). Please note that for resolution purposes the color scales vary for each plot.

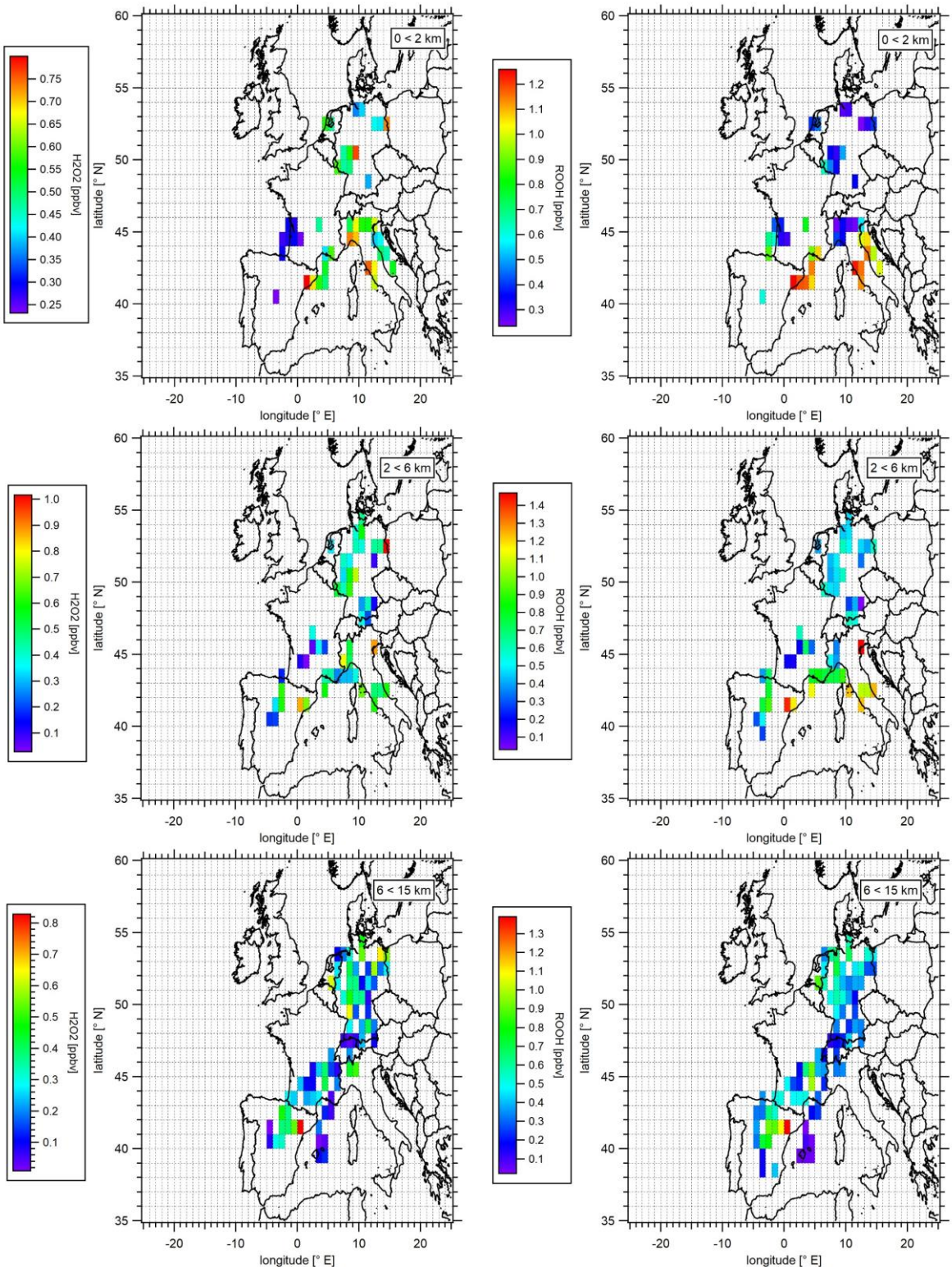

Figure 9: Spatial distribution of measured H_2O_2 (left column) and ROOH (right column) in the boundary layer (0 < 2 km; upper panel), the middle free troposphere (2 < 6 km; middle panel), and in the upper troposphere (6 < 15 km; bottom panel) during the BLUESKY campaign in May – June 2020. Data were binned into a 1° x 1° subset along the GPS flight tracks.

The mean (±1σ) and median mixing ratios based on all measured H_2O_2 and ROOH during the campaign were 0.40 (±0.23) ppb_v, 0.38 ppb_v, and 0.53 (±0.32) ppb_v, 0.41 ppb_v, respectively. The maximum mixing

ratios reached 1.45 ppb_v, and 1.46 ppb_v for H_2O_2 and the total ROOH, respectively. A table presenting an overview of the mean (±1σ), median, and the corresponding maximum H_2O_2 and ROOH mixing ratios determined under the specification of the tropospheric layer is presented below as well as partly incorporated into the Supplement of the published manuscript in the following section (Sect. 3.3.).

Table 2: Overview of the hydroperoxide mean, median, and maximum mixing ratios (ppb_v) in the boundary layer (BL), the middle troposphere (MT), and the upper troposphere (UT) during the BLUESKY aircraft campaign.

	BL (0 < 2 km)	**MT (2 < 6 km)**	**UT (6 < 15 km)**
H_2O_2			
Mean (±1σ) /ppb_v	0.48 (±0.17)	0.42 (±0.25)	0.28 (±0.22)
Median /ppb_v	0.48	0.37	0.24
Maximum /ppb_v	1.14	1.45	1.31
ROOH			
Mean (±1σ) /ppb_v	0.62 (±0.36)	0.57 (±0.31)	0.43 (±0.26)
Median /ppb_v	0.41	0.47	0.37
Maximum /ppb_v	1.44	1.46	1.39

The maximum mean (±1σ) and median H_2O_2 mixing ratios were detected within the altitudinal range of 0 > 2 km with 0.48 (±0.17) ppb_v and 0.48 ppb_v with mixing ratios reaching up to 1.14 ppb_v. For ROOH, the maximum mean (±1σ) mixing ratios were found accordingly in the boundary layer with 0.62 (±0.36) ppb_v and maximum mixing ratios of up to 1.44 ppb_v. In contrast to H_2O_2 results, the highest median and maximum ROOH mixing ratios were detected at 2 < 6 km with 0.47 ppb_v and 1.46 ppb_v. The hydroperoxide levels decrease with increasing altitude to 0.28 (±0.22) ppb_v and 0.43 (±0.26) ppb_v for H_2O_2 and ROOH, respectively, in the upper troposphere (> 6 km). Whilst H_2O_2 mixing ratios do not show any significant dependency with latitude in the corresponding tropospheric layers, ROOH levels seem to display an increasing trend with decreasing latitude in the BL and MT. However, the trend is reversed in the UT with increasing mixing ratios of ROOH towards the north-east of the sampled region. Generally, the levels of ROOH appear to be on average by a factor of 1.3 – 1.6 higher than H_2O_2 mixing ratios. With increasing altitude, the ROOH-to-H_2O_2-ratio increases locally up to a factor of 3, reflecting the impact of cloud scavenging and a subsequent rainout of the highly soluble H_2O_2 in the sampled region. Additionally, inspecting the H_2O_2 mixing ratios in the boundary layer and middle troposphere, hydrogen peroxide does not show any significant vertical trend, as has been assumed based on previous measurements in the region. H_2O_2 seems to be severely affected by clouds at altitudes between 2 – 6 km relative to the by approximately two orders of magnitude less soluble ROOH. A detailed analysis of the impact of wet deposition processes in the context of clouds is presented in the following section in the scope of a published research article with the title: “Distribution of hydrogen peroxide over Europe during the BLUESKY aircraft campaign” (Sect. 3.3.).

3.3. Analysis results in the scope of the research article: „Distribution of hydrogen peroxide over Europe during the BLUESKY campaign “

The subsection presents research study results regarding hydrogen peroxide vertical and latitudinal distribution over Europe impacted by cloud scavenging and rainout. I am the first author of the manuscript published in the journal *Atmospheric Chemistry and Physics* (ACP) on 22.07.2022 as a research article. I performed the hydroperoxide measurements and analyzed the corresponding data. Supported by H. Fischer, I designed the study and wrote the manuscript draft with the contribution of all co-authors.

Due to the high solubility of hydrogen peroxide postulated by the high Henry's law coefficient, deposition processes have a significant impact on the distribution of H_2O_2 in regions affected by high cloud coverage and precipitation episodes. Measured H_2O_2 displays a decrease in the tropospheric vertical distribution, especially above the boundary layer, in contrast to previous observations during HOOVER II and UTOPIHAN II/III. The expected inverted C-shaped vertical trend with maximum hydrogen peroxide mixing ratios at 3 – 7 km was missing during BLUESKY. The deviations are most likely due to cloud and precipitation scavenging of the highly soluble species, such as H_2O_2. A comparison with EMAC model simulations shows that the simulations partly reproduce the impact of rainout loss on the H_2O_2 vertical profile. A performed sensitivity study excluding cloud scavenging and thus, H_2O_2 deposition in cloud droplets using the EMAC model confirms the strong impact of clouds and precipitation scavenging on the local H_2O_2 budget in the troposphere. Deviations between model simulations and the observations arise most likely due to difficulties in the simulation of wet scavenging processes caused by limitations in the model's resolution.

Atmos. Chem. Phys., 22, 9483–9497, 2022
https://doi.org/10.5194/acp-22-9483-2022

Atmospheric Chemistry and Physics
Open Access
EGU

Distribution of hydrogen peroxide over Europe during the BLUESKY aircraft campaign

Zaneta T. Hamryszczak[1], Andrea Pozzer[1], Florian Obersteiner[2], Birger Bohn[3], Benedikt Steil[1], Jos Lelieveld[1,4], and Horst Fischer[1]

[1]Atmospheric Chemistry Department, Max Planck Institute for Chemistry, 55128 Mainz, Germany
[2]Karlsruhe Institute of Technology, 76131 Karlsruhe, Germany
[3]Institute of Energy and Climate Research, IEK-8: Troposphere, Forschungszentrum Jülich GmbH, 52428 Jülich, Germany
[4]Climate and Atmosphere Research Center, The Cyprus Institute, Nicosia, 1645, Cyprus

Correspondence: Zaneta T. Hamryszczak (z.hamryszczak@mpic.de) and Horst Fischer (horst.fischer@mpic.de)

Received: 2 February 2022 – Discussion started: 7 March 2022
Revised: 6 July 2022 – Accepted: 6 July 2022 – Published: 22 July 2022

Abstract. In this work we present airborne in situ trace gas observations of hydrogen peroxide (H_2O_2) and the sum of organic hydroperoxides over Europe during the Chemistry of the Atmosphere – Field Experiments in Europe (CAFE-EU, also known as BLUESKY) aircraft campaign using a wet chemical monitoring system, the HYdrogen Peroxide and Higher Organic Peroxide (HYPHOP) monitor. The campaign took place in May–June 2020 over central and southern Europe with two additional flights dedicated to the North Atlantic flight corridor. Airborne measurements were performed on the High Altitude and LOng-range (HALO) research operating out of Oberpfaffenhofen (southern Germany). We report average mixing ratios for H_2O_2 of 0.32 ± 0.25, 0.39 ± 0.23 and 0.38 ± 0.21 ppb_v in the upper and middle troposphere and the boundary layer over Europe, respectively. Vertical profiles of measured H_2O_2 reveal a significant decrease, in particular above the boundary layer, contrary to previous observations, most likely due to cloud scavenging and subsequent rainout of soluble species. In general, the expected inverted C-shaped vertical trend with maximum hydrogen peroxide mixing ratios at 3–7 km was not found during BLUESKY. This deviates from observations during previous airborne studies over Europe, i.e., 1.64 ± 0.83 ppb_v during the HOOVER campaign and 1.67 ± 0.97 ppb_v during UTOPIHAN-ACT II/III. Simulations with the global chemistry–transport model EMAC partly reproduce the strong effect of rainout loss on the vertical profile of H_2O_2. A sensitivity study without H_2O_2 scavenging performed using EMAC confirms the strong influence of clouds and precipitation scavenging on hydrogen peroxide concentrations. Differences between model simulations and observations are most likely due to difficulties in the simulation of wet scavenging processes due to the limited model resolution.

1 Introduction

Hydrogen peroxide (H_2O_2) and related organic hydroperoxide (ROOH) species have been investigated as atmospheric trace gases for many decades, and in the 1970s hydrogen peroxide was identified as a key agent in the acidification of clouds and rain through its oxidation of sulfur dioxide into sulfuric acid (Hoffmann and Edwards, 1975; Penkett et al., 1979; Robbin Martin and Damschen, 1981; Kunen et al., 1983; McArdle and Hoffmann, 1983; Calvert et al., 1985). Related studies confirmed the role of H_2O_2 as an oxidizing agent in clouds where it accelerates the conversion of NO_2 to HNO_3 (Damschen and Martin, 1983; Lee and Lind, 1986). Efforts have also been made to characterize and analyze the amount and the chemical pathways of hydrogen peroxide in clouds (Kelly et al., 1985; Olszyna et al., 1988; Sakugawa et

Published by Copernicus Publications on behalf of the European Geosciences Union.

al., 1990, 1993). Furthermore, gas-phase hydroperoxides are a reservoir of hydrogen oxide and hydrogen peroxide radicals (HO_x), which are well known for their contribution to the self-cleaning properties of the atmosphere (Levy, 1971; Lelieveld and Crutzen, 1990; Crutzen et al., 1999).

The main source of gaseous hydrogen peroxide is the self-reaction of HO_2 radicals derived from the oxidation of carbon monoxide (CO) and other trace gases by OH radicals, which are formed during photolysis of ozone and the subsequent reaction of the formed O^1D with water vapor (Crutzen, 1973; Logan et al., 1981; Kleinman, 1986; Lightfoot et al., 1992; Reeves and Penkett, 2003). The formation of the most prominent organic hydroperoxide, methyl hydroperoxide (MHP), results from the reaction of HO_2 with the methyl peroxy radical (CH_3OO) derived from methane oxidation by OH (Levy, 1971).

The formation of gaseous hydroperoxides strongly depends on the chemical composition of the troposphere as well as on meteorological conditions. Thus, mixing ratios of H_2O_2 and CH_3OOH are primarily controlled by the mixing ratios of O_3, H_2O, CO, CH_4 and NO_x ($NO + NO_2 = NO_x$) as well as by UV radiation. Hydroperoxide levels depend to a large extent on available peroxy radicals and therefore on O_3 and NO_x species as the key promoters and suppressors of hydroperoxide synthesis, since peroxy radicals generally react faster with NO than they recombine. Consequently, the budget of available peroxides is influenced by the levels of ambient NO_x (Campbell et al., 1979; Jaeglé et al., 1999; Lee et al., 2000). The amount of available H_2O_2 in the troposphere further depends on the presence of water vapor.

With increasing altitudes and latitudes, the concentration of water vapor becomes the most prominent limiting factor for precursor production. With increasing altitude, the concentration of water vapor decreases, while photolytic activity simultaneously increases, and the role of hydroperoxides as a source of HO_x becomes more prominent, leading to a decrease in hydrogen peroxide (Heikes et al., 1996b; Jaeglé et al., 1997; Faloona et al., 2000; Jaeglé et al., 2000). With increasing latitude, the zenith angle decreases, resulting in reduced UV radiation, while the amount of water is also reduced. Therefore, the availability of hydroperoxide precursors and consequently of hydroperoxides decreases towards the poles (Jacob and Klockow, 1992; Perros, 1993; Slemr and Tremmel, 1994; Snow, 2003; Snow et al., 2007).

Due to the strong sensitivity of hydrogen peroxide to deposition processes, its high solubility and pronounced mixing within the boundary layer, levels of H_2O_2 are limited at low altitudes where dry deposition and rainout remove the species from the troposphere. Consequently, the maximum mixing ratio can be expected above the boundary layer at 2–5 km, resulting in a characteristic inverted C-shaped vertical profile with increasing altitude (Hall and Claiborn, 1997; Hall et al., 1999).

An analogous but less pronounced vertical profile, due to lower sensitivity towards deposition processes, is expected for organic hydroperoxides (Palenik et al., 1987; Weinstein-Lloyd et al., 1998; Snow, 2003; Snow et al., 2007).

Clouds play a significant role in the budget of hydroperoxides in the atmosphere. Cloud uptake and subsequent rainout of hydroperoxides in the aqueous phase have a considerable impact on the distribution of hydrogen peroxide. H_2O_2 is taken up by water droplets, dissociated and partially consumed by aqueous-phase reactions within clouds (Sakugawa et al., 1990). Previous studies have reported that despite the low volume fraction of clouds in the troposphere, levels of hydroperoxides and their precursors are decreased by clouds, leading to reduced oxidation processes and therefore diminished self-cleaning efficiency of the atmosphere. Moreover, cloud-mediated upward transport processes as well as precipitation-induced downward transport of soluble trace gases and particulate matter play key roles in the vertical distribution of many species (Lelieveld and Crutzen, 1994). Additionally, scattering, reflection and diffusion of solar radiation, which take place within, above and below clouds, lead to modification of photolysis rates. Therefore, changes in soluble species as well as influences on the chemical processes and the tropospheric redistribution caused by clouds have to be considered (Madronich, 1987; Edy et al., 1996). Finally, the effective separation of soluble and insoluble gases and the consecutive perturbation of the gas-phase chemistry balance have a great impact on the budget of the species (Lelieveld and Crutzen, 1991).

The amount and fate of H_2O_2 in the dynamic multi-phase cloud system are determined by the distribution of its precursors as well as by the partitioning of H_2O_2 between gas and liquid phases. Here, the balance between H_2O_2 and HO_x ($OH + HO_2 = HO_x$) in both cloud phases is determined by the Henry coefficient and the presence of other interacting species (Brimblecombe and Dawson, 1984; Warneck, 1991, 1994). Generally, gas-phase production of OH is suppressed within clouds due to a significant pH-dependent uptake of HO_2 into the aqueous cloud phase. Further, due to its high Henry's law constant, a critical amount of hydrogen peroxide itself is transferred into the aqueous phase as well. On the other hand, the aqueous phase of clouds can be an efficient source of these species as a result of cloud evaporation, droplet elevation and freezing. Earlier studies report mixing ratios of hydrogen peroxide in the gaseous cloud phase between 0.1 and 0.2 ppb_v and concentrations of 10^{-7}–10^{-4} mol L^{-1} in the aqueous phase (Zuo and Hoigné, 1993). The budget of hydrogen peroxide within clouds further depends on conditions such as solar radiation, temperature, concentrations of volatile organic compounds (VOC) and the liquid water content that impact the mixing ratio of the trace gas. Enhanced levels of NO_x and SO_2 have a negative effect on the total hydrogen peroxide concentration (Kelly et al., 1985; Sakugawa et al., 1990). The cloud scavenging effect on MHP has to be considered as well. Despite the relatively low uptake of the species and its direct precursor CH_3OO by cloud droplets, the production of MHP is reduced as a result

of the reduced availability of OH. Thus, overall clouds lead to a loss of MHP, but to a far lesser extent than for hydrogen peroxide. Numerous reactions within the aqueous phase of clouds have to be distinguished from comparable processes in the gas phase. Here, a variety of reaction paths depending on cloud water pH and the presence of transition metals as well as related ionic species (especially in continental clouds) derived from anthropogenic and mineral sources have to be considered (Kormann et al., 1988; Zuo and Hoigne, 1992; Anastasio et al., 1994; Zuo and Deng, 1997).

The following sections (Sects. 2 and 3) introduce the BLUESKY project and give a brief description of the experimental and modeling techniques as well as the measurement framework. In Sect. 4 we present the results and discuss the measurements in comparison with simulated data and with former campaigns and examine hydrogen peroxide uptake and release processes in clouds based on a case study over Frankfurt airport. Here we will show that although the BLUESKY campaign was performed under lockdown conditions, we find that reduced H_2O_2 mixing ratios in comparison to the HOOVER and UTOPIHAN-ACT campaigns as well as the EMAC simulations are not explained by chemical but rather by meteorological conditions. This study gives a general overview of the distribution of the species in mostly clouded environments. Hence, the presented work highlights the impact of cloud scavenging and rainout processes on the budget of the species in the troposphere.

2 BLUESKY campaign description

The purpose of the airborne BLUESKY campaign was to investigate how reduced emissions from anthropogenic sources due to the COVID-19 pandemic and the related shutdown impacted the chemistry and physics of the atmosphere over Europe. To this end, the campaign obtained an overview of the distribution of a large suite of trace gases and aerosols. The decrease in air pollution and aircraft emissions provided a unique opportunity for analysis of the resulting changes in the atmosphere. The reduced pollution levels gave rise to anomalous blue skies, hence the name "BLUESKY" (Voigt et al., 2022). The project was carried out in May and June 2020 covering an area from the Mediterranean region in southern Europe (approximately 35° N) up to the North Atlantic flight corridor (approximately 60° N). During the measurement period, eight measurement flights were carried out with the German High Altitude and LOng-range research aircraft (HALO). The entirety of the flight tracks of HALO during the campaign color-coded by flight altitude is presented in Fig. 1. Flights over the North Atlantic flight corridor were not included in this study, since they were performed entirely in the lower stratosphere.

The measurement flights ranged in altitude from a few tens of meters above the earth's surface to approximately 14 km, i.e., reaching beyond the tropopause into the lower stratosphere. Individual flights were performed between 07:00 and 17:00 UTC on eight different days, with at least one maintenance day between flights. Vertical profiles were generally obtained during flybys near main European airports and urban areas in order to sample air from emission sources from the earth's surface up to the tropopause region. The flights were performed from the flight base of the German Aerospace Center (Deutsches Zentrum für Luft- und Raumfahrt), DLR, in Oberpfaffenhofen, Germany.

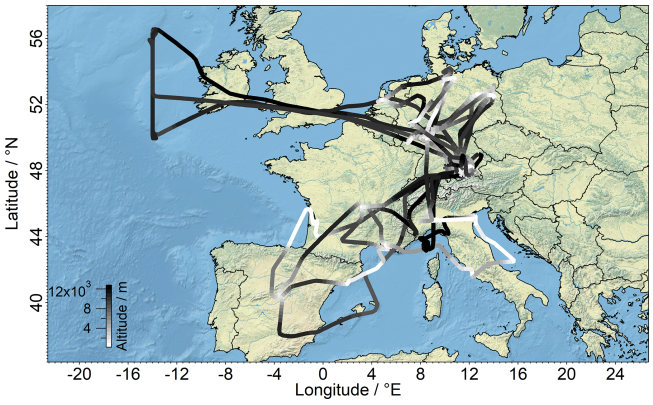

Figure 1. Flight tracks of the BLUESKY measurement campaign over Europe color-coded by GPS altitude. All flights were performed from the flight base in Oberpfaffenhofen, Germany (48° N, 11° E).

The Monthly Bulletin on the Climate in WMO Region IV (Europe and the Middle East) for the months of May and June 2020 published by DWD (Deutscher Wetterdienst) indicates a regional monthly averaged cloud coverage span of 37.5 %–75 %. The total precipitation in May and June varied locally between 100–200 mm per month and 100–150 mm per month, respectively, which amounts to 80 %–125 % of the values relative to the reference period from 1981 until 2010. The average air temperature at 2 m above the surface was approximately 2 °C higher than during the reference period of 1981–2010. An overview of the average meteorological conditions based on ERA5 reanalysis data generated by the Copernicus Climate Change Service (Hersbach et al., 2019) is presented in the Supplement (Fig. S1). Additionally, meteorological conditions for single flight days, which show cloud cover fractions of approximately 60 % and higher, with many rain events along the flight tracks at altitudes of 2–7 km, are also presented in the Supplement (Fig. S2).

3 Methods

3.1 Hydrogen peroxide measurement

Hydrogen peroxide and the sum of organic hydroperoxides were measured using a wet chemical monitoring system, the HYdrogen Peroxide and Higher Organic Peroxide monitor (HYPHOP; Stickler et al., 2006; Klippel et al., 2011;

Bozem et al., 2017; Hottmann et al., 2020), based on the work of Lazrus et al. (1985, 1986). Ambient air was probed via 1/4 in. PFA tubing installed in a stainless-steel inlet setup (TGI; trace gas inlet). From the inlet, the peroxide species were sampled via a bypass. In order to avoid any pressure and therefore airflow inconsistencies a constant pressure inlet (CPI) setup was used, which consists of a Teflon-coated membrane pump (type MD 1C; Vacuubrand, Wertheim, Germany) and a pressure control unit that adjusts the pump speed to a line pressure of 1000 hPa. The sampling efficiency of the inlet for H_2O_2 was determined to be 0.52. After passing through the CPI, ambient air enters the instrument and passes through a sampling coil with a buffered sampling solution (potassium hydrogen phthalate–NaOH; pH 6) with a stripping efficiency of 1 for hydrogen peroxide and 0.6 for MHP (Lee et al., 2000). The resulting peroxide solution was separated into two channels, to which *p*-hydroxyphenyl acetic acid (POPHA) and horseradish peroxidase (HRP) were added. The stoichiometric reaction yields the chemiluminescent compound 6,6′-dihydroxy-3,3′-biphenyldiacetic acid, which is measured by means of fluorescence spectroscopy with a Cd pen ray lamp at 326 nm. The resulting hydroperoxide-specific fluorescence (Guilbault et al., 1968) at 400–420 nm was detected using a photomultiplier tube for each channel. In order to specifically measure hydrogen peroxide, this species was selectively destroyed by catalase in one channel (channel B). H_2O_2 can then be calculated as the difference between the sum of all hydroperoxides (channel A) and the entirety of the remaining organic hydroperoxides (channel B). This measurement technique does not provide mixing ratios for individual organic hydroperoxides. Previous studies indicate that methyl hydroperoxide is the most prominent free-tropospheric component of organic hydroperoxides (90 %–100 %; Heikes et al., 1996a; Jackson and Hewitt, 1996; Walker et al., 2006; Hua et al., 2008). For this study we assumed that MHP is the sole component of organic hydroperoxides that passes the inlet and is unaffected by any further losses, and we scaled the signal of channel B with the sampling efficiency for MHP based on the stripping efficiency by a precooled buffered sampling solution at a flow rate of 0.000508 L min^{-1} in accordance with previously reported sampling efficiencies. Thus, ROOH used in this paper is an upper limit for the actual MHP in the free troposphere. In particular, in the boundary layer other organic hydroperoxide species are expected to contribute to the signal in channel B. Based on previous studies, HMHP (hydroxymethyl hydroperoxide) and extent PAA (peroxyacetic acid) and EHP (ethyl hydroperoxide) significantly contribute to the total organic hydroperoxide mixing ratios at low altitudes (Fels and Junkermann, 1994; Slemr and Tremmel, 1994; Valverde-Canossa et al., 2005; Hua et al., 2008).

The catalase efficiency for the destruction of H_2O_2 in channel B was determined via liquid calibration of the instrument at 0.95–0.98. For the simultaneous liquid calibration of both channels, an H_2O_2 standard (0.98 µmol L^{-1}) produced in a serial dilution from a stock solution was used. In order to estimate the sampling efficiency, a calibration gas was analyzed every second day during the field campaign. The calibration gas was created by an LDPE (low-density polyethylene) permeation source filled with 30 % hydrogen peroxide embedded in a temperature-controlled oven at 35 ° C and flushed with synthetic air at a rate of 60 standard cubic centimeters per minute (sccm). The defined amount of hydrogen peroxide gas was diluted with approximately 2300 sccm purified ambient air. The sampling efficiency was calculated based on the difference between the measured hydrogen peroxide levels with and without the CPI implemented into the calibration gas flow. The permeation gas can be calibrated by bubbling the gas through a water-filled flask followed by photometric examination via UV spectroscopy using the $TiCl_4$ method described by Pilz and Johann (1974). The in-flight background measurements were performed using peroxide-free air generated by a cartridge filled with hopcalite (type IAC-330) and silica gel (type IAC-502; Infiltec, Speyer, Germany).

To account for the sensitivity of hydrogen peroxide to metal ions in the Fenton reaction (Graedel et al., 1986; Zepp et al., 1992; Weinstein-Lloyd et al., 1998) as well as to sulfur dioxide (SO_2), ethylene diamine tetra acetic acid (EDTA) and formaldehyde (HCHO) were added to the stripping solution. Further, the data were corrected for existing positive ozone interference by subtraction of 0.016 ppb_v H_2O_2 / 100 ppb_v O_3. The interference was derived by plotting hydrogen peroxide mixing ratios vs. ozone mixing ratios in the lower stratosphere, assuming that ambient H_2O_2 is close to zero above the tropopause based on the decreased availability of water vapor for the H_2O_2 precursor production and simultaneously increased photolytic activity of H_2O_2. Due to instrumental issues caused by hopcalite contamination during the campaign, the uncertainty of the ozone interference was further extended by the hopcalite interference and estimated as 27 % at 0.16 ppb_v hydrogen peroxide.

The total measurement uncertainty (TMU) of the instrument was calculated as

$$\mathrm{TMU} = \sqrt{\left((P)^2 + (\mathrm{US})^2 + (\mathrm{UIE})^2 + (\mathrm{UOI})^2\right)} \quad (1)$$

and was derived by considering the instrument's precision (P), uncertainty of the standard and of the inlet efficiency (US; UIE), and uncertainty of the ozone interference (UOI). The precision was determined as 0.3 % at 5.1 ppb_v for hydrogen peroxide and 0.2 % at 5.4 ppb_v for organic peroxides. The uncertainty of the standard was included in instrument precision calculations. The uncertainty of the inlet efficiency was calculated to be 5 %. The calculated total measurement uncertainty was therefore determined at 28 % for hydrogen peroxide and 40 % for the sum of organic peroxides. Moreover, the time resolution of the instrument was determined to be 2 min based on the signal rise time from 10 % to 90 %. Based on the average cruise speed of the research aircraft of

$179 \pm 51\ \mathrm{m\ s^{-1}}$ the spatial resolution of the 2 min sample was estimated as 21.5 km. The detection limit, derived from 2σ uncertainty of 37 background measurements, was 0.035 $\mathrm{ppb_v}$ for hydrogen peroxide and 0.013 $\mathrm{ppb_v}$ for organic peroxides. For the purposes of this study, the obtained peroxide data were limited to measurements within the troposphere by removing all data points with ozone mixing ratios higher than 100 $\mathrm{ppb_v}$.

3.2 Measurement of other species

The measurements of ozone were carried out with a chemiluminescence detector calibrated by a UV photometer of the Fast AIrborne Ozone instrument, FAIRO (Zahn et al., 2012). Upward and downward spectral actinic flux density was recorded with two spectroradiometers (Bohn and Lohse, 2017). Water vapor mixing ratios and humidity measurements were obtained with the Sophisticated Hygrometer for Atmospheric ResearCh (SHARC) based on a tunable diode laser (TDL) setup (Krautstrunk and Giez, 2012). GPS data as well as temperature, pressure, wind speed and true air speed were obtained using the BAsic HALO Measurement And Sensor System, BAHAMAS. The list of campaign instrumentation as well as the complementary measurement method, TMU, and references regarding the use of each technique are given in Table 1.

3.3 ECHAM/MESSy Atmospheric Chemistry (EMAC) model

In this study, we used the global numerical 3-D model EMAC (ECHAM/MESSy for Atmospheric Chemistry, Jöckel et al., 2010), which numerically simulates the chemistry and dynamics of the troposphere and the stratosphere. EMAC incorporates a variety of submodels addressing chemical and metrological processes and their interactions with marine, continental and anthropogenic environments (Jöckel et al., 2006). The basis atmospheric model is the 5th generation of the European Centre HAMburg general circulation model (ECHAM5; Roeckner et al., 2003, 2006). For standardized data exchange between submodels and the base model, the Modular Earth Submodel System (MESSy; Jöckel et al., 2005, 2006, 2016) was used. The Module for Efficiently Calculating the Chemistry of the Atmosphere (MECCA) submodel was used to simulate stratospheric and tropospheric gaseous and heterogeneous chemistry (Sander et al., 2005, 2011, 2019). For the simulation of aqueous-phase chemistry in clouds and wet scavenging processes the Scavenging of Tracers (SCAV; Tost et al., 2006) submodel was applied. Primary emissions as well as dry deposition of atmospheric trace gases and aerosols were simulated by submodels ONLEM, OFFLEM, TNUDGE and DRYDEP (Kerkweg et al., 2006a, b). The simulations of anthropogenic emissions were based on CAMS-GLOB-ANTv4.2 (Granier et al., 2019), which uses emission data provided by the EDGARv4.3.3 inventory developed by the European Joint Research Centre (JRC; Crippa et al., 2018) and CEDS emissions (Hoesly et al., 2018). Emission reduction coefficients were additionally adapted to lockdown conditions in Europe based on the work of Guevara et al. (2021). A detailed description of the emission submodels as well as their modifications are presented in the work of Reifenberg et al. (2022). The horizontal resolution of the model in this study is T63 (i.e., roughly $1.8° \times 1.8°$) and the vertical resolution consists of 47 levels up to 0.01 hPa. The simulated data has a time resolution of 5 min. Importantly, for the purpose of comparison with the observations, the model results were interpolated along the GPS flight tracks with the S4D submodel (Jöckel et al., 2010).

4 Results

4.1 Distribution of hydrogen peroxide and comparison with previous observations over Europe

During the previous field campaigns UTOPIHAN-ACT (Upper Tropospheric Ozone: Processes Involving HO_x And NO_x: The Impact of Aviation and Convectively Transported Pollutants in the Tropopause Region) and HOOVER (HO_x OVer EuRope), numerous measurement flights were performed in 2002–2004 and 2006–2007 over Europe (Colomb et al., 2006; Stickler et al., 2006; Klippel et al., 2011). The flight tracks during the two campaigns covered a similar latitudinal and altitudinal range. Thus, parts of both campaigns performed during spring and summer seasons within the latitudinal range 40–55° N can be compared with the outcomes of our measurements. The comparison described below is restricted to HOOVER II (July 2007) and UTOPIHAN-ACT II (March 2003) and III (July 2003) to ensure overlap with the late spring and early summer measurements presented here. The latitudinal distribution of hydrogen peroxide during the three campaigns is presented in Fig. 2 as a function of latitude for three altitude ranges within the troposphere (boundary layer – BL – from $0 < 2$ km, middle troposphere – MT – from $2 < 6$ km and upper troposphere – UT – from 6–14 km). The presented mean values of the datasets with 2 min resolution are binned into subsets of 2.5° of latitude for the entirety of each tropospheric layer. The datasets can be further studied by comparing the vertical profiles of all campaigns, as displayed in Fig. 3a. The mean values of the data are binned into subsets of 0.5 km of altitude. The medians and means ($\pm 1\sigma$) of hydrogen peroxide mixing ratios calculated with 2 min resolution within the range 37.5–52.5° N for each campaign are listed in Table S1 (Supplement).

The observed distribution within the UT and the latitudinal range 37.5–52.5° N amount to a mean (median) mixing ratio of 0.28 ± 0.22 (0.24) $\mathrm{ppb_v}$ for BLUESKY, which is lower in comparison to the previously measured 0.67 ± 0.43 (0.56) $\mathrm{ppb_v}$ during HOOVER II and 0.47 ± 0.36 (0.47) $\mathrm{ppb_v}$ during UTOPIHAN-ACT. In both lower tropospheric lay-

Table 1. Overview of other observed species with corresponding measurement method, total measurement uncertainty (TMU) and references regarding the supplementary instrumentation.

Measurement	Method	TMU	References
O_3	Chemiluminescence + UV absorption	2.5 %	Zahn et al. (2012)
Actinic flux density	Spectroradiometer	7 %–8 % (15 % for $j(H_2O_2)$)	Bohn and Lohse (2017)
H_2O	TDLAS	5 %	Krautstrunk and Giez (2012)

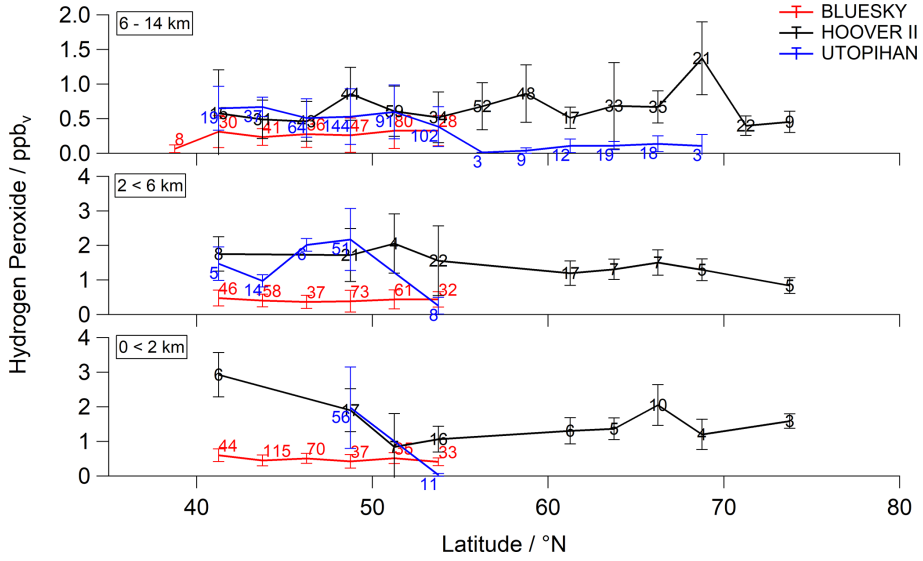

Figure 2. Latitudinal dependence of hydrogen peroxide concentrations (mean ± 1σ) compared to former campaigns (red: BLUESKY; black: HOOVER II; blue: UTOPIHAN-ACT). The data with 2 min time resolution were subdivided into three atmospheric layers of the upper troposphere, middle troposphere and boundary layer (from top to bottom), with mean values binned for 2.5° of latitude for each tropospheric layer. The corresponding numbers indicate the total number of data points per bin.

ers (0–6 km) the hydrogen peroxide mixing ratios during BLUESKY differed significantly from those measured previously. The mean mixing ratios for hydrogen peroxide show further pronounced reductions with values up to 72 % and 76 % lower compared to HOOVER and UTOPIHAN-ACT for both lower tropospheric layers. Mixing ratios of 0.42 ± 0.25 (0.37) ppb_v within the MT and 0.48 ± 0.17 (0.48) ppb_v in the BL were determined. During previous campaigns much higher hydrogen peroxide mixing ratios of 1.49 ± 0.71 (1.33) ppb_v during HOOVER and 1.74 ± 0.97 (1.80) ppb_v during UTOPIHAN were measured at altitudes of 2–6 km. Also, the results within the boundary layer display a significant discrepancy with the previously measured 1.59 ± 0.78 (1.48) ppb_v for HOOVER and 1.65 ± 0.16 (1.32) ppb_v during UTOPIHAN. The observed mixing ratios are only in approximately 30 % agreement with previous results.

A significant tendency towards lower mixing ratios for hydrogen peroxide during the BLUESKY project was observed, in particular at altitudes below approximately 7 km (Fig. 3a). The altitude profile does not agree very well with the described inverted C-shaped distribution trend in the literature (Klippel et al., 2011; Bozem et al., 2017). The most striking feature of the BLUESKY observations is the absence of a local maximum of H_2O_2 above the BL. Instead, the mixing ratio is rather constant in the 3–7 km range. We hypothesize that these differences between the campaigns predominately originate from differences in the meteorological rather than chemical conditions. We will show that the low observed mixing ratios of hydrogen peroxide during BLUESKY are most likely caused by enhanced wet scavenging processes due to a pronounced presence of clouds at altitudes of 3–7 km. An analysis of hourly cloud coverage at altitudes of 2–7 km based on ERA5 reanalysis generated using Copernicus Climate Change Service information (Hersbach et al., 2018; Fig. S2) for single flights (BLUESKY) shows high average values. Further, based on log book information for all campaigns, there was a pronounced presence of clouds during BLUESKY in comparison with previous airborne measurements. We have observed a high number of cloud and rain events along the flight tracks during the BLUESKY campaign compared to the mostly cloud-free measurement conditions during HOOVER and UTOPIHAN-ACT.

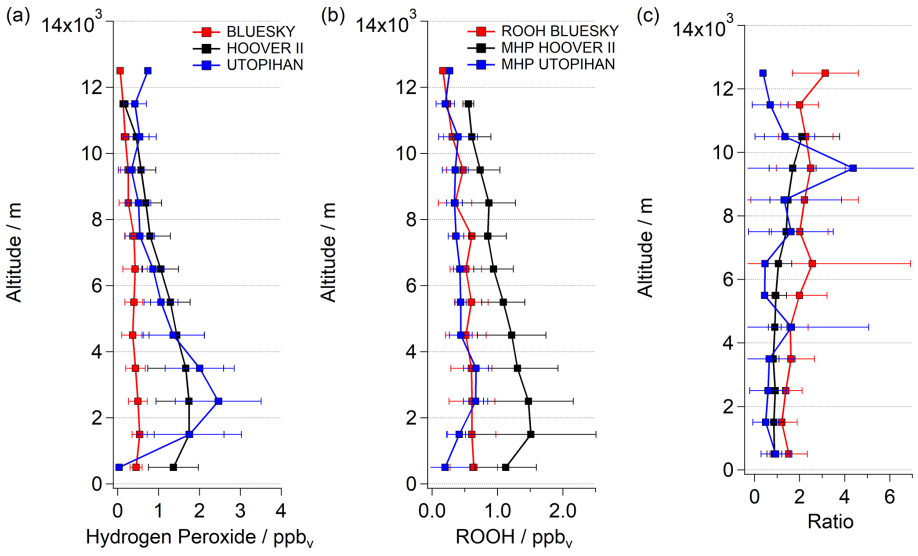

Figure 3. Comparison of vertical hydrogen peroxide profiles **(a)**, ROOH **(b)** and ROOH/H_2O_2 ratio **(c)** during BLUESKY (red) with outcomes of the earlier campaigns, HOOVER II (black) and UTOPIHAN-ACT II/III (blue). The data were plotted as mean $\pm 1\sigma$.

Generally, the presence of clouds has a marked impact on H_2O_2 but a much smaller effect on the majority of organic peroxides. ROOHs are less sensitive to wet deposition due to lower Henry's law coefficients (2.2×10^4 mol L^{-1} atm^{-1} at 298 K for MHP in contrast to 7.4×10^4 mol L^{-1} atm^{-1} at 298 K for H_2O_2). Therefore, the concentration ratio of both species can be an indicator of cloud presence (Heikes et al., 1996b; O'Sullivan et al., 1999; Snow, 2003; Snow et al., 2007; Klippel et al., 2011). The assumption of cloud processing via ratio comparison is derived from the fact that highly soluble species are transferred into the aqueous phase of clouds, wherein they are removed by reactions with other soluble species or by precipitation (Crutzen and Lawrence, 2000). Consequently, an increase in the ratio between ROOH and hydrogen peroxide of ≥ 1 can ensue as a result of deposition processes within clouds. Please note that due to the characteristics of the measurement technique, which derives the estimated ROOH mixing ratio as its tropospheric upper limit (Sect. 3.1), the vertical trend of ROOH and therefore also the ROOH/H_2O_2 ratio are expressed as qualitative comparisons. Vertical profiles of ROOH measured during the BLUESKY and UTOPIHAN-ACT projects are comparable, while HOOVER II found higher values (Fig. 3b). However, the vertical trends of peroxides during HOOVER II can be assumed to be about equal, leading to an ROOH vs. H_2O_2 ratio of approximately 1. Thus, the two previous campaigns over Europe show corresponding trends with decreasing ROOH/H_2O_2 ratios above the boundary layer, where H_2O_2 mixing ratios are at their maxima (Fig. 3c). In contrast, increasing ratios of ROOH vs. hydrogen peroxide at altitudes of 3–7 km were observed during the BLUESKY campaign. These increases during the BLUESKY campaign can be attributed to the lower mixing ratio of H_2O_2 and are indicative of more pronounced cloud scavenging.

4.2 Comparison with the EMAC model

In order to test the hypothesis that hydrogen peroxide is depleted at altitudes of 3–7 km due to cloud scavenging, a comparison of in situ data with the output of the EMAC model was performed. The analysis of the EMAC and in situ results for different latitudinal distribution subdivided into three main tropospheric air layers is presented in the Supplement (Fig. S3). The comparison between the model results and observations shows generally good agreement for the UT as well as for the majority of data in the BL. Discrepancies here at low latitudes can be seen for Mediterranean areas strongly influenced by marine air masses (Barcelona at 41°24′ N and Rome at 41°53′ N), where the model tends to overestimate the mixing ratio of hydrogen peroxide by up to a factor of 3. This is most likely related to model resolution (~ 180 km $\times$ 180 km), which makes it difficult to differentiate marine from continental air masses in coastal areas. The difference between observed and modeled data for both tropospheric regions is not significant and good agreement between the simulated and measured sources and sinks within the top and bottom tropospheric layers can be assumed (latitudinal distribution at 0–2 and 6–12 km; Fig. S3). In contrast, the model tends to overestimate H_2O_2 concentrations in the 2–6 km range. As stated above, the observed mixing ratios are generally low at 3–7 km, most likely related to the high impact of deposition processes within clouds. An analysis of the impact of emissions from anthropogenic sources on modeled H_2O_2 data shows an average difference of approximately 2.5 % between mixing ratios with and with-

out the lockdown emissions reductions within lower tropospheric layers (1–7 km; Fig. S4). Thus, emission reduction is not considered to be responsible for the strong deviation between the simulated and observed hydrogen peroxide mixing ratios (Reifenberg et al., 2022).

In order to investigate potential causes for the observed difference between observations and model simulations, we calculate the hydrogen peroxide budget based on photostationary steady-state conditions using model-simulated radical and photolysis rate data. In the free troposphere, the production rate P of hydrogen peroxide can be calculated from Eq. (2) and the photochemical loss rate L due to photolysis and reaction with OH from Eq. (3).

$$P(H_2O_2) = k_{HO_2+HO_2} \cdot [HO_2]^2 \quad (2)$$

$$L(H_2O_2) = \left(k_{H_2O_2+OH} \cdot [OH] + j(H_2O_2)\right) \cdot [H_2O_2] \quad (3)$$

Neglecting deposition and transport processes impacting the hydrogen peroxide budget, the maximum concentration of H_2O_2 can be calculated as presented in Eq. (4).

$$[H_2O_2]^{PSS} = \frac{[HO_2]^2 \cdot k_{HO_2+HO_2}}{[OH] \cdot k_{H_2O_2+OH} + j(H_2O_2)} \quad (4)$$

Vertical profiles of observed, simulated and calculated H_2O_2 under the assumption of photostationary state conditions are displayed in Fig. 4a. Additionally, a model sensitivity study in which the scavenging of H_2O_2 in clouds was omitted has been incorporated.

The comparison of all datasets shows that no significant hydrogen peroxide loss occurs within the cloud-free layers of the upper troposphere (above 10 km), where the resulting mixing ratios show a similar vertical trend (Fig. 4a). Both the sensitivity study and the PSS calculation further indicate that wet scavenging in clouds followed by rainout as the ultimate removal process forms a substantial sink for H_2O_2, in particular in the middle and lower troposphere. Please note that this sink is not always associated with in-cloud conditions along the flight paths. Due to the photochemical lifetime of H_2O_2, which is on the order of several days, local H_2O_2 mixing ratios will also depend on upwind cloud processing (Cohan et al., 1999; Hua et al., 2008). Although EMAC reproduces this cloud processing, the absolute mixing ratios are still overestimated, indicating a potential underestimation of the deposition rate in the model.

Based on $[H_2O_2]^{PSS}$ the deposition loss rate constant was calculated by comparing to $[H_2O_2]^{Obs}$ and $[H_2O_2]^{EMAC}$,

$$\left\{k_{H_2O_2+OH} \cdot [OH] + j(H_2O_2) + k_{SCAV}\right\} \cdot [H_2O_2] = P(H_2O_2) \quad (5)$$

The total modeled loss rate constant due to deposition k_{SCAV} based on PSS conditions (Eqs. 2 and 3) shows an underestimation of 2.2 compared to the observationally derived constant. The vertical profile of the simulated deposition rates is in good agreement with the observations at low altitudes (below 2 km), where dry deposition plays a key role in the removal of H_2O_2 species (Fig. 4b). At high altitudes (UT) EMAC loss rate results agree well with the observations. The majority of the loss processes take place within the MT (2–8 km). Here, EMAC underestimates the deposition impact most prominently, which corresponds to the discrepancies between observed and modeled hydroperoxide mixing ratios (Fig. 4a).

Since the loss of hydrogen peroxide in the atmosphere strongly depends on the presence of clouds, the temporal uptake and loss of the species within cloud droplets, and the permanent loss by rainout, it is important that the model correctly reproduces cloud coverage, liquid water content (LWC) and precipitation rates. In Fig. 5a, a histogram of the average total cloud coverage over all measurement days based on EMAC and ERA5 (containing modified Copernicus Climate Change Service information; Hersbach et al., 2018), respectively, indicates an underestimation of cloud coverage by EMAC in comparison with ERA5. The discrepancy is most pronounced over central Europe (47 to 55° N, 6 to 15° E) and smaller over the North Atlantic (approximately 30 to 40° N, −50 to −30° E; Fig. S5). The comparison of the average liquid water path (LWP) based on LWC of the measurement days shows a difference of approximately 2 % by EMAC in comparison to ERA5, which indicates a minor deficit in the simulated species uptake (Fig. S6). The main difference between EMAC and ERA5 arises from the comparison of the total precipitation. As shown in Fig. 5b, the model underestimates heavy rain events ($> 0.5\,mm\,s^{-1}$) in comparison with the ERA5 reanalysis model (modified Copernicus Climate Change Service information; Hersbach et al., 2018). With respect to ERA5, a difference by a factor of 2.2 was estimated for the entirety of the region compared to EMAC, which agrees well with the calculated ratio of the loss rates. Further, a less pronounced impact of scavenging on the hydrogen peroxide budget and therefore higher mixing ratios are simulated by the model.

As shown based on the difference in total precipitation between EMAC and ERA5, EMAC appears to underestimate the majority of the rainout events at the location of the flight tracks (Fig. 6). Detailed comparison of the average total precipitation between EMAC and ERA5 during the campaign can be found in the Supplement of this work (Fig. S7).

Assuming a linear dependence between ultimate removal of H_2O_2 in cloud droplets and precipitation as given by EMAC simulations, total large-scale scavenging was estimated based on precipitation given by ERA5. The prediction is based on extrapolating the linear relationship between EMAC scavenging and simulated total precipitation. The simulated scavenging by EMAC falls short by $7.6 \times 10^{13}\,molec.\,m^{-2}\,s^{-1}$ relative to the scavenging prediction based on ERA5 output (Fig. S8). The differences between hydrogen peroxide mixing ratios obtained using EMAC and the observations (Fig. 4a) estimated as the integral between the observed and simulated mixing ratios over the entire tro-

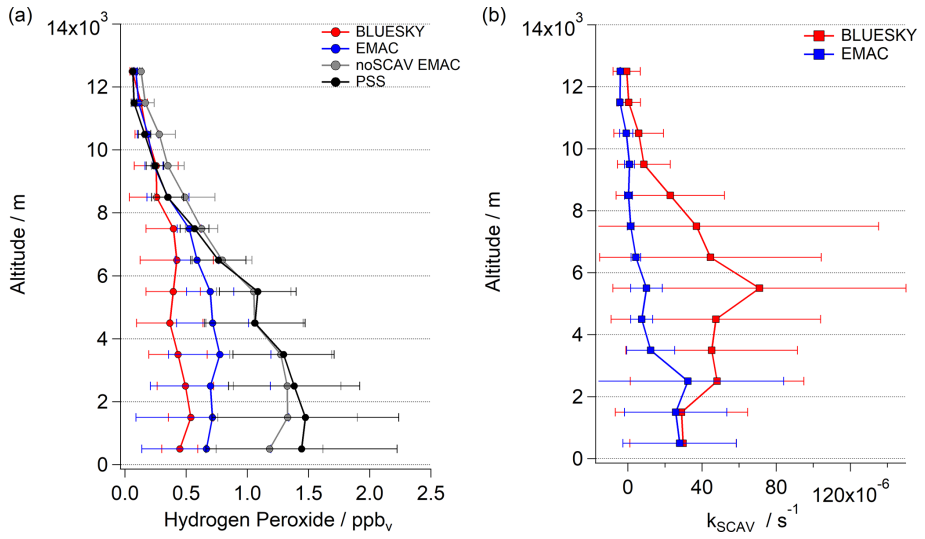

Figure 4. Vertical profiles of observed (red), simulated (blue), reduced simulated (gray) and calculated under the assumption of PSS (photostationary steady-state) conditions (black) for hydrogen peroxide **(a)** and the calculated loss rate constant k_{SCAV} by scavenging **(b)**; red lines show observed values, while blue lines show modeled H_2O_2.

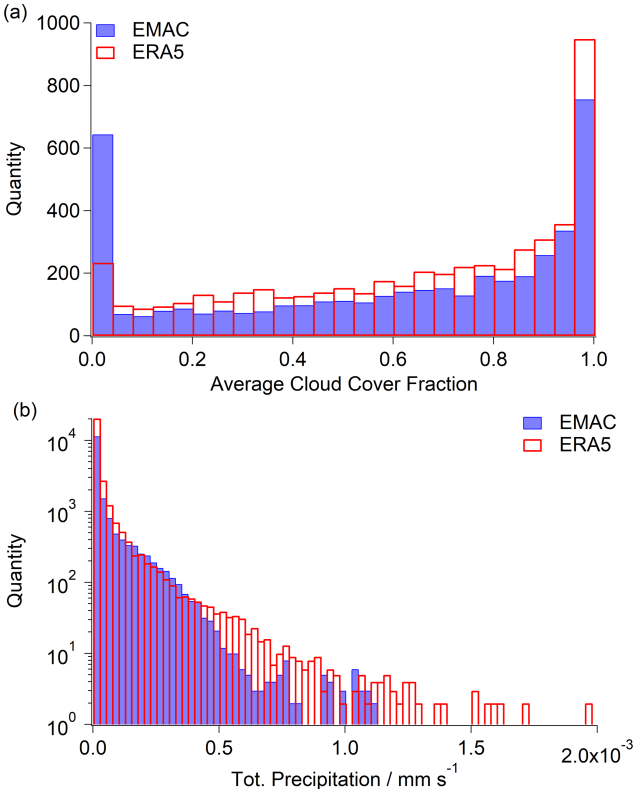

Figure 5. Histograms of average cloud cover fraction **(a)** and total precipitation **(b)** over the North Atlantic and Europe (73 to 28° N, −50 to 15° E) based on ERA5 (red; modified Copernicus Climate Change Service information; Hersbach et al., 2018) and EMAC simulation (blue).

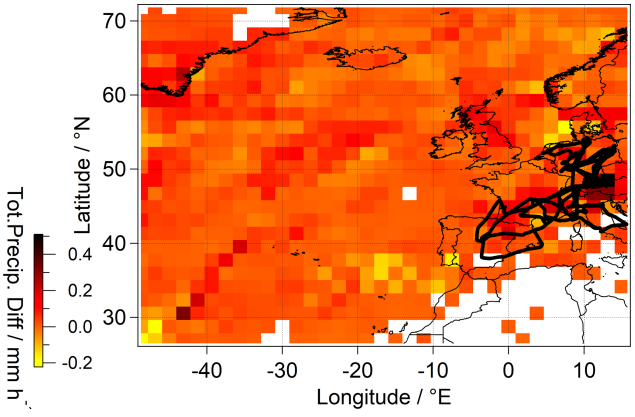

Figure 6. Average total precipitation difference between ERA5 and EMAC over Europe and the North Atlantic (73 to 28° N, −50 to 15° E; contains modified Copernicus Climate Change Service information; Hersbach et al., 2018). The North Atlantic region was included in view of the H_2O_2 lifetime in the atmosphere and the air mass origins based on backward trajectories. The performed flights are indicated in black.

posphere for the total measurement time in molec. m^{-2} s^{-1} are comparable (7.3×10^{13} molec. m^{-2} s^{-1}). This indicates that the underestimation of the rain rate by EMAC relative to ERA5 is responsible for the overestimation of H_2O_2 in the model. As indicated by the rainout discrepancy between EMAC and ERA5, higher variability in scavenging can be expected along the flight tracks (Fig. 6).

Other major causes leading to the observed discrepancy might be an overestimation of peroxide sources as well as an underestimation of its photochemical sinks. The analysis of the photolysis frequencies for both datasets showed a

discrepancy by a factor of approximately 1.5. However, the underestimation of the photolysis frequencies by the model can be partly explained by the use of additional extrapolated absorption cross sections of H_2O_2 in order to reproduce the entire photolytic activity range of the species (Hottmann et al., 2020). Calculations of hydrogen peroxide mixing ratios under PSS conditions based on simulated and observed photolysis frequencies are in good agreement (Fig. S9). Therefore, the impact of photochemical loss processes on the hydrogen peroxide budget is considered to be minor. An impact of peroxide precursor discrepancies cannot be determined due to the lack of HO_x measurement, although the study of Reifenberg et al. (2022) demonstrates good agreement between observations and model results for those species affecting H_2O_2, i.e., NO_x, O_3 and H_2O. Thus, the overestimation of hydrogen peroxide in the model is most likely due to underestimation of scavenging processes.

4.3 The fate of hydrogen peroxide below clouds

The distribution of hydrogen peroxide above, in and below clouds at Frankfurt airport (50°1′59″ N and 8°34′14″ O) was measured during BLUESKY flight no. 1 and showed untypical increases in hydrogen peroxide mixing ratios at low altitudes.

Based on NOAA HYSPLIT backward trajectory analysis (model duration of 24 h), the probed air masses originated from the North Atlantic, passing northern France, and were nearly uniformly affected by rainout during 6 h prior to the measurement time. During the measurement the aircraft passed a cloud layer at approximately 2–6 km during descending and ascending legs of the vertical profile. The descent and ascent into and out of Frankfurt took place between 09:00 and 11:00 UTC. Figure 7 displays the time series of the approach to Frankfurt. Mixing ratios of H_2O_2 from observations and EMAC are shown.

The relative humidity (RH) of 100 % (gray areas in Fig. 7) indicates the presence of clouds. Rain was mainly observed below the clouds at low altitudes (light blue areas) at slightly lower RH. ERA5 reanalysis (Fig. S11a) confirmed the presence of clouds at altitudes of 2–6 km (flight no. 1). Based on local meteorological reports, light rain started approximately 1 h prior to the vertical profile measurement and lasted approximately half an hour. The average mixing ratio of H_2O_2 over Frankfurt (Fig. 7) was $0.646 \pm 0.229\ \mathrm{ppb_v}$. Above the tops of the clouds, no significant increase in mixing ratios could be observed. An increase in observed hydrogen peroxide mixing ratios occurred after exiting the clouds during the descending part of the vertical profile track. Here, the H_2O_2 concentration exceeded $0.7\ \mathrm{ppb_v}$ and dropped again within a short time (10 min) to $0.567\ \mathrm{ppb_v}$. The maximum measured hydrogen peroxide mixing ratio was $0.8\ \mathrm{ppb_v}$. The observed hydrogen peroxide mixing ratio peak might be caused by cloud scavenging, which is strongest at the bottom, where the liquid water content is also highest. However, this assumption is not supported by the simultaneous ROOH mixing ratio observations (Fig. 7b). In contrast to hydrogen peroxide, ROOH mixing ratios display a decreasing trend below 2 km. It seems that the increase in hydrogen peroxide concentrations was caused by an additional source of this species below clouds. An analogous phenomenon was observed for measurements taken over Bordeaux (Figs. S10 and S11b).

Previous studies on the possibility of mass transfer of H_2O_2 from rainwater to the surrounding air indicate a possible release of hydrogen peroxide to the atmosphere (Hua et al., 2008; Huang and Chen, 2010; Xuan et al., 2020). Raindrops are affected by the temperature gradient between the earth's surface and the cloud base. The negative dependence of hydrogen peroxide solubility on temperature derived from the Henry's law constant means that an impact on the aqueous-gas phase equilibrium can be assumed. Moreover, the mass transfer coefficient is dependent on the surface-to-volume ratio of the raindrops and is diminished for large raindrops due to a smaller contact surface between the liquid and gas phase (Xuan et al., 2020). The size of the raindrops can be derived from the rain intensity, as shown by Kumar (1985). During the vertical profile flights light rain (drizzle) was reported, consistent with rain sum measurements (approximately $10^{-4}\ \mathrm{mm\,h^{-1}}$) and ERA5 reanalysis plots provided by the Copernicus Climate Change Service (Hersbach et al., 2018; Fig. S11). It seems that evaporation of small raindrops releases hydrogen peroxide, causing elevated hydrogen peroxide mixing ratios at low altitudes.

5 Conclusions

A comparison of hydrogen peroxide mixing ratios during the BLUESKY campaign with the previous HOOVER and UTOPIHAN-ACT campaigns shows significant differences within the middle troposphere and the boundary layer. The measurements are only in 30 % agreement with previous observations within the lower tropospheric layers. Hydrogen peroxide does not exhibit the expected local maximum at altitudes of 3–7 km. The rather constant vertical distribution of the mixing ratio is most likely related to the enhanced presence of clouds and the subsequent wet scavenging during the measurement period relative to previous airborne studies.

The measured hydrogen peroxide mixing ratios agree with those simulated by EMAC within the upper troposphere and the boundary layer. The model simulations partly reproduce the strong effect of cloud uptake and rainout loss of the species in the middle troposphere. The calculated deposition loss rates based on EMAC reveal an underestimation relative to the observations, indicating difficulties in the simulation of wet scavenging by the model. This was confirmed by the discrepancies between the rain rates and H_2O_2 scavenging values simulated by EMAC and ERA5 meteorological reanalysis data.

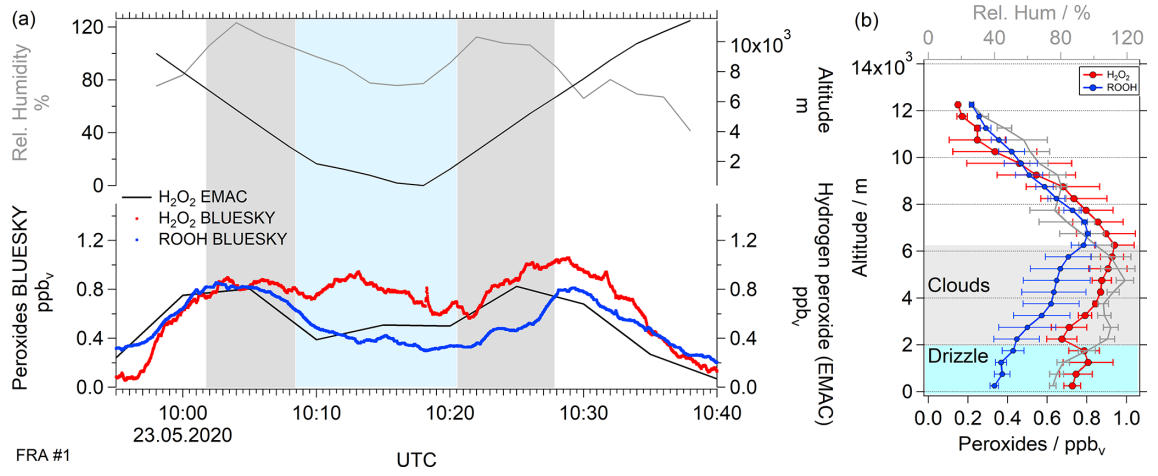

Figure 7. Temporal series of BLUESKY flight no. 1 over Frankfurt (50°1′59″ N and 8°34′14″ O; **a**) and vertical distribution **(b)** of hydrogen peroxide impacted by cloud and rain scavenging. Data were plotted for observed (red) and simulated (black) hydrogen peroxide mixing ratios as well as the observed ROOH mixing ratio (blue) in relation to altitude (top black) and relative humidity (light gray). Cloud scavenging and precipitation are highlighted in gray and light blue shading, respectively. Please note that the displayed peroxide data have a temporal resolution of 1 s in contrast to the model resolution of 5 min.

While the BLUESKY campaign was performed under lockdown conditions, with substantially reduced anthropogenic emissions, particularly of NO_x, we find that reduced H_2O_2 mixing ratios compared to the HOOVER and UTOPIHAN-ACT campaigns are not explained by chemical but rather by meteorological conditions. The importance of rain as an H_2O_2 sink, but potentially also in vertically redistributing H_2O_2, was shown in a case study based on aircraft measurements over central Germany. While precipitation scavenging removed H_2O_2 from the cloud layer, the evaporation of drizzle droplets in the boundary layer beneath locally increased H_2O_2 mixing ratios.

Data availability. The data presented in this paper are available from the contact authors under request.

Supplement. The supplement related to this article is available online at: https://doi.org/10.5194/acp-22-9483-2022-supplement.

Author contributions. JL and HF planned the campaign; ZTH, FO and BB performed the measurements; ZTH and HF designed the study; ZTH, FO, BB and BS analyzed the data; AP developed the model code and performed the simulation; ZTH wrote the paper draft with contributions of all co-authors; JL, HF, AP, BB, FO and BS reviewed and edited the paper.

Competing interests. At least one of the (co-)authors is a member of the editorial board of *Atmospheric Chemistry and Physics*. The peer-review process was guided by an independent editor, and the authors also have no other competing interests to declare.

Disclaimer. Publisher's note: Copernicus Publications remains neutral with regard to jurisdictional claims in published maps and institutional affiliations.

Special issue statement. This article is part of the special issues "BLUESKY atmospheric composition measurements by aircraft during the COVID-19 lockdown in spring 2020" and "The Modular Earth Submodel System (MESSy) (ACP/GMD inter-journal SI)". It is not associated with a conference.

Acknowledgements. The authors are very grateful to the BLUESKY team, the Forschungszentrum Jülich, Karlsruhe Institute of Technology and Deutsches Zentrum für Luft- und Raumfahrt (DLR) in Oberpfaffenhofen for their great support. Their work was essential for the BLUESKY project. Special thanks to Ovid Oktavian Krüger, Department of Multiphase Chemistry, Max Planck Institute for Chemistry, for providing the trajectories and the rain rates along the flight tracks.

Financial support. Birger Bohn was supported by the DFG priority program HALO-SPP 1294 under grant BO 1580/5-1.

The article processing charges for this open-access publication were covered by the Max Planck Society.

Review statement. This paper was edited by Robert McLaren and reviewed by two anonymous referees.

References

Anastasio, C., Faust, B. C., and Allen, J. M.: Aqueous phase photochemical formation of hydrogen peroxide in authentic cloud waters, J. Geophys. Res., 99, 8231, https://doi.org/10.1029/94JD00085, 1994.

Bohn, B. and Lohse, I.: Calibration and evaluation of CCD spectroradiometers for ground-based and airborne measurements of spectral actinic flux densities, Atmos. Meas. Tech., 10, 3151–3174, https://doi.org/10.5194/amt-10-3151-2017, 2017.

Bozem, H., Pozzer, A., Harder, H., Martinez, M., Williams, J., Lelieveld, J., and Fischer, H.: The influence of deep convection on HCHO and H2O2 in the upper troposphere over Europe, Atmos. Chem. Phys., 17, 11835–11848, https://doi.org/10.5194/acp-17-11835-2017, 2017.

Brimblecombe, P. and Dawson, G. A.: Wet removal of highly soluble gases, J. Atmos. Chem., 2, 95–107, https://doi.org/10.1007/BF00127265, 1984.

Calvert, J. G., Lazrus, A., Kok, G. L., Heikes, B. G., Walega, J. G., Lind, J., and Cantrell, C. A.: Chemical mechanisms of acid generation in the troposphere, Nature, 317, 27–35, https://doi.org/10.1038/317027a0, 1985.

Campbell, M. J., Sheppard, J. C., and Au, B. F.: Measurement of hydroxyl concentration in boundary layer air by monitoring CO oxidation, Geophys. Res. Lett., 6, 175–178, https://doi.org/10.1029/GL006i003p00175, 1979.

Cohan, D. S., Schultz, M. G., Jacob, D. J., Heikes, B. G., and Blake, D. R.: Convective injection and photochemical decay of peroxides in the tropical upper troposphere: Methyl iodide as a tracer of marine convection, J. Geophys. Res., 104, 5717–5724, https://doi.org/10.1029/98JD01963, 1999.

Colomb, A., Williams, J., Crowley, J., Gros, V., Hofmann, R., Salisbury, G., Klüpfel, T., Kormann, R., Stickler, A., Forster, C., and Lelieveld, J.: Airborne Measurements of Trace Organic Species in the Upper Troposphere Over Europe: the Impact of Deep Convection, Environ. Chem., 3, 244–259, https://doi.org/10.1071/EN06020, 2006.

Crippa, M., Guizzardi, D., Muntean, M., Schaaf, E., Dentener, F., van Aardenne, J. A., Monni, S., Doering, U., Olivier, J. G. J., Pagliari, V., and Janssens-Maenhout, G.: Gridded emissions of air pollutants for the period 1970–2012 within EDGAR v4.3.2, Earth Syst. Sci. Data, 10, 1987–2013, https://doi.org/10.5194/essd-10-1987-2018, 2018.

Crutzen, P.: A discussion of the chemistry of some minor constituents in the stratosphere and troposphere, Pure Appl. Geophys., 106–108, 1385–1399, https://doi.org/10.1007/BF00881092, 1973.

Crutzen, P. J. and Lawrence, M. G.: The Impact of Precipitation Scavenging on the Transport of Trace Gases: A 3-Dimensional Model Sensitivity Study, J. Atmos. Chem., 37, 81–112, https://doi.org/10.1023/A:1006322926426, 2000.

Crutzen, P. J., Lawrence, M. G., and Pöschl, U.: On the background photochemistry of tropospheric ozone, Tellus B, 51, 123–146, https://doi.org/10.3402/tellusb.v51i1.16264, 1999.

Damschen, D. E. and Martin, L. R.: Aqueous aerosol oxidation of nitrous acid by O_2, O_3 AND H_2O_2, Atmos. Environ., 17, 2005–2011, https://doi.org/10.1016/0004-6981(83)90357-8, 1983.

Edy, J., Cautenet, S., and Brémaud, P.: Modeling ozone and carbon monoxide redistribution by shallow convection over the Amazonian rain forest, J. Geophys. Res., 101, 28671–28681, https://doi.org/10.1029/96JD01867, 1996.

Faloona, I., Tan, D., Brune, W. H., Jaeglé, L., Jacob, D. J., Kondo, Y., Koike, M., Chatfield, R., Pueschel, R., Ferry, G., Sachse, G., Vay, S., Anderson, B., Hannon, J., and Fuelberg, H.: Observations of HO x and its relationship with NO_x in the upper troposphere during SONEX, J. Geophys. Res., 105, 3771–3783, https://doi.org/10.1029/1999JD900914, 2000.

Fels, M. and Junkermann, W.: The occurrence of organic peroxides in air at a mountain site, Geophys. Res. Lett., 21, 341–344, https://doi.org/10.1029/93GL01892, 1994.

Graedel, T. E., Mandich, M. L., and Weschler, C. J.: Kinetic model studies of atmospheric droplet chemistry: 2. Homogeneous transition metal chemistry in raindrops, J. Geophys. Res., 91, 5205, https://doi.org/10.1029/JD091iD04p05205, 1986.

Granier, C., Darras, S., Denier van der Gon, H., Doubalova, J., Elguindi, N., Galle, B., Gauss, M., Guevara, M., Jalkanen, J.-P., Kuenen, J., Liousse, C., Quack, B., Simpson, D., and Sindelarova, K.: The Copernicus Atmosphere Monitoring Service global and regional emissions (April 2019 version), Copernicus Atmosphere Monitoring Service [Research Report], https://doi.org/10.24380/d0bn-kx16, 2019.

Guevara, M., Jorba, O., Soret, A., Petetin, H., Bowdalo, D., Serradell, K., Tena, C., Denier van der Gon, H., Kuenen, J., Peuch, V.-H., and Pérez García-Pando, C.: Time-resolved emission reductions for atmospheric chemistry modelling in Europe during the COVID-19 lockdowns, Atmos. Chem. Phys., 21, 773–797, https://doi.org/10.5194/acp-21-773-2021, 2021.

Guilbault, G. G., Brignac, P. J., and Juneau, M.: New substrates for the fluorometric determination of oxidative enzymes, Anal. Chem., 40, 1256–1263, https://doi.org/10.1021/ac60264a027, 1968.

Hall, B. D. and Claiborn, C. S.: Measurements of the dry deposition of peroxides to a Canadian boreal forest, J. Geophys. Res., 102, 29343–29353, https://doi.org/10.1029/97JD01113, 1997.

Hall, B., Claiborn, C., and Baldocchi, D.: Measurement and modeling of the dry deposition of peroxides, Atmos. Environ., 33, 577–589, https://doi.org/10.1016/S1352-2310(98)00271-4, 1999.

Heikes, B., Lee, M., Jacob, D., Talbot, R., Bradshaw, J., Singh, H., Blake, D., Anderson, B., Fuelberg, H., and Thompson, A. M.: Ozone, hydroperoxides, oxides of nitrogen, and hydrocarbon budgets in the marine boundary layer over the South Atlantic, J. Geophys. Res., 101, 24221–24234, https://doi.org/10.1029/95JD03631, 1996a.

Heikes, B. G., Lee, M., Bradshaw, J., Sandholm, S., Davis, D. D., Crawford, J., Rodriguez, J., Liu, S., McKeen, S., Thornton, D., Bandy, A., Gregory, G., Talbot, R., and Blake, D.: Hydrogen peroxide and methylhydroperoxide distributions related to ozone and odd hydrogen over the North Pacific in the fall of 1991, J. Geophys. Res., 101, 1891–1905, https://doi.org/10.1029/95JD01364, 1996b.

Hersbach, H., Bell, B., Berrisford, P., Biavati, G., Horányi, A., Muñoz Sabater, J., Nicolas, J., Peubey, C., Radu, R., Rozum, I., Schepers, D., Simmons, A., Soci, C., Dee, D., and Thépaut, J.-N.: ERA5 hourly data on single levels from 1979 to present, CDS [data set], https://doi.org/10.24381/cds.adbb2d47, 2018.

Hersbach, H., Bell, B., Berrisford, P., Biavati, G., Horányi, A., Muñoz Sabater, J., Nicolas, J., Peubey, C., Radu, R., Rozum, I., Schepers, D., Simmons, A., Soci, C.,

Dee, D., and Thépaut, J-N.: ERA5 monthly averaged data on single levels from 1959 to present, CDS [data set] https://doi.org/10.24381/CDS.F17050D7, 2019.

Hoesly, R. M., Smith, S. J., Feng, L., Klimont, Z., Janssens-Maenhout, G., Pitkanen, T., Seibert, J. J., Vu, L., Andres, R. J., Bolt, R. M., Bond, T. C., Dawidowski, L., Kholod, N., Kurokawa, J.-I., Li, M., Liu, L., Lu, Z., Moura, M. C. P., O'Rourke, P. R., and Zhang, Q.: Historical (1750–2014) anthropogenic emissions of reactive gases and aerosols from the Community Emissions Data System (CEDS), Geosci. Model Dev., 11, 369–408, https://doi.org/10.5194/gmd-11-369-2018, 2018.

Hoffmann, M. R. and Edwards, J. O.: Kinetics of the oxidation of sulfite by hydrogen peroxide in acidic solution, J. Phys. Chem., 79, 2096–2098, https://doi.org/10.1021/j100587a005, 1975.

Hottmann, B., Hafermann, S., Tomsche, L., Marno, D., Martinez, M., Harder, H., Pozzer, A., Neumaier, M., Zahn, A., Bohn, B., Stratmann, G., Ziereis, H., Lelieveld, J., and Fischer, H.: Impact of the South Asian monsoon outflow on atmospheric hydroperoxides in the upper troposphere, Atmos. Chem. Phys., 20, 12655–12673, https://doi.org/10.5194/acp-20-12655-2020, 2020.

Hua, W., Chen, Z. M., Jie, C. Y., Kondo, Y., Hofzumahaus, A., Takegawa, N., Chang, C. C., Lu, K. D., Miyazaki, Y., Kita, K., Wang, H. L., Zhang, Y. H., and Hu, M.: Atmospheric hydrogen peroxide and organic hydroperoxides during PRIDE-PRD'06, China: their concentration, formation mechanism and contribution to secondary aerosols, Atmos. Chem. Phys., 8, 6755–6773, https://doi.org/10.5194/acp-8-6755-2008, 2008.

Huang, D. and Chen, Z.: Reinvestigation of the Henry's law constant for hydrogen peroxide with temperature and acidity variation, J. Environ. Sci., 22, 570–574, https://doi.org/10.1016/S1001-0742(09)60147-9, 2010.

Jackson, A. V. and Hewitt, C. N.: Hydrogen peroxide and organic hydroperoxide concentrations in air in a eucalyptus forest in central Portugal, Atmos. Environ., 30, 819–830, https://doi.org/10.1016/1352-2310(95)00348-7, 1996.

Jacob, P. and Klockow, D.: Hydrogen peroxide measurements in the marine atmosphere, J. Atmos. Chem., 15, 353–360, https://doi.org/10.1007/BF00115404, 1992.

Jaeglé, L., Jacob, D. J., Wennberg, P. O., Spivakovsky, C. M., Hanisco, T. F., Lanzendorf, E. J., Hintsa, E. J., Fahey, D. W., Keim, E. R., Proffitt, M. H., Atlas, E. L., Flocke, F., Schauffler, S., McElroy, C. T., Midwinter, C., Pfister, L., and Wilson, J. C.: Observed OH and HO_2 in the upper troposphere suggest a major source from convective injection of peroxides, Geophys. Res. Lett., 24, 3181–3184, https://doi.org/10.1029/97GL03004, 1997.

Jaeglé, L., Jacob, D. J., Brune, W. H., Faloona, I. C., Tan, D., Kondo, Y., Sachse, G. W., Anderson, B., Gregory, G. L., Vay, S., Singh, H. B., Blake, D. R., and Shetter, R.: Ozone production in the upper troposphere and the influence of aircraft during SONEX: approach of NO_x-saturated conditions, Geophys. Res. Lett., 26, 3081–3084, https://doi.org/10.1029/1999GL900451, 1999.

Jaeglé, L., Jacob, D. J., Brune, W. H., Faloona, I., Tan, D., Heikes, B. G., Kondo, Y., Sachse, G. W., Anderson, B., Gregory, G. L., Singh, H. B., Pueschel, R., Ferry, G., Blake, D. R., and Shetter, R. E.: Photochemistry of HO_x in the upper troposphere at northern midlatitudes, J. Geophys. Res., 105, 3877–3892, https://doi.org/10.1029/1999JD901016, 2000.

Jöckel, P., Sander, R., Kerkweg, A., Tost, H., and Lelieveld, J.: Technical Note: The Modular Earth Submodel System (MESSy) – a new approach towards Earth System Modeling, Atmos. Chem. Phys., 5, 433–444, https://doi.org/10.5194/acp-5-433-2005, 2005.

Jöckel, P., Tost, H., Pozzer, A., Brühl, C., Buchholz, J., Ganzeveld, L., Hoor, P., Kerkweg, A., Lawrence, M. G., Sander, R., Steil, B., Stiller, G., Tanarhte, M., Taraborrelli, D., van Aardenne, J., and Lelieveld, J.: The atmospheric chemistry general circulation model ECHAM5/MESSy1: consistent simulation of ozone from the surface to the mesosphere, Atmos. Chem. Phys., 6, 5067–5104, https://doi.org/10.5194/acp-6-5067-2006, 2006.

Jöckel, P., Kerkweg, A., Pozzer, A., Sander, R., Tost, H., Riede, H., Baumgaertner, A., Gromov, S., and Kern, B.: Development cycle 2 of the Modular Earth Submodel System (MESSy2), Geosci. Model Dev., 3, 717–752, https://doi.org/10.5194/gmd-3-717-2010, 2010.

Jöckel, P., Tost, H., Pozzer, A., Kunze, M., Kirner, O., Brenninkmeijer, C. A. M., Brinkop, S., Cai, D. S., Dyroff, C., Eckstein, J., Frank, F., Garny, H., Gottschaldt, K.-D., Graf, P., Grewe, V., Kerkweg, A., Kern, B., Matthes, S., Mertens, M., Meul, S., Neumaier, M., Nützel, M., Oberländer-Hayn, S., Ruhnke, R., Runde, T., Sander, R., Scharffe, D., and Zahn, A.: Earth System Chemistry integrated Modelling (ESCiMo) with the Modular Earth Submodel System (MESSy) version 2.51, Geosci. Model Dev., 9, 1153–1200, https://doi.org/10.5194/gmd-9-1153-2016, 2016.

Kelly, T. J., Daum, P. H., and Schwartz, S. E.: Measurements of peroxides in cloudwater and rain, J. Geophys. Res., 90, 7861–7871, https://doi.org/10.1029/JD090iD05p07861, 1985.

Kerkweg, A., Buchholz, J., Ganzeveld, L., Pozzer, A., Tost, H., and Jöckel, P.: Technical Note: An implementation of the dry removal processes DRY DEPosition and SEDImentation in the Modular Earth Submodel System (MESSy), Atmos. Chem. Phys., 6, 4617–4632, https://doi.org/10.5194/acp-6-4617-2006, 2006a.

Kerkweg, A., Sander, R., Tost, H., and Jöckel, P.: Technical note: Implementation of prescribed (OFFLEM), calculated (ONLEM), and pseudo-emissions (TNUDGE) of chemical species in the Modular Earth Submodel System (MESSy), Atmos. Chem. Phys., 6, 3603–3609, https://doi.org/10.5194/acp-6-3603-2006, 2006b.

Kleinman, L. I.: Photochemical formation of peroxides in the boundary layer, J. Geophys. Res., 91, 10889, https://doi.org/10.1029/JD091iD10p10889, 1986.

Klippel, T., Fischer, H., Bozem, H., Lawrence, M. G., Butler, T., Jöckel, P., Tost, H., Martinez, M., Harder, H., Regelin, E., Sander, R., Schiller, C. L., Stickler, A., and Lelieveld, J.: Distribution of hydrogen peroxide and formaldehyde over Central Europe during the HOOVER project, Atmos. Chem. Phys., 11, 4391–4410, https://doi.org/10.5194/acp-11-4391-2011, 2011.

Kormann, C., Bahnemann, D. W., and Hoffmann, M. R.: Photocatalytic production of hydrogen peroxides and organic peroxides in aqueous suspensions of titanium dioxide, zinc oxide, and desert sand, Environ. Sci. Technol., 22, 798–806, https://doi.org/10.1021/es00172a009, 1988.

Krautstrunk, M. and Giez, A.: The Transition From FALCON to HALO Era Airborne Atmospheric Research, in: Atmospheric Physics, edited by: Schumann, U., Springer Berlin Heidelberg, Berlin, Heidelberg, 609–624, https://doi.org/10.1007/978-3-642-30183-4_37, 2012.

Kumar, S.: An Eulerian model for scavenging of pollutants by raindrops, Atmos. Environ., 19, 769–778, https://doi.org/10.1016/0004-6981(85)90065-4, 1985.

Kunen, S. M., Lazrus, A. L., Kok, G. L., and Heikes, B. G.: Aqueous oxidation of SO_2 by hydrogen peroxide, J. Geophys. Res., 88, 3671, https://doi.org/10.1029/JC088iC06p03671, 1983.

Lazrus, A. L., Kok, G. L., Gitlin, S. N., Lind, J. A., and McLaren, S. E.: Automated fluorimetric method for hydrogen peroxide in atmospheric precipitation, Anal. Chem., 57, 917–922, https://doi.org/10.1021/ac00281a031, 1985.

Lazrus, A. L., Kok, G. L., Lind, J. A., Gitlin, S. N., Heikes, B. G., and Shelter, R. E.: Automated Fluorometric Method for Hydrogen Peroxide in Air, Anal. Chem., 58, 594–597, 1986.

Lee, M., Heikes, B. G., and O'Sullivan, D. W.: Hydrogen peroxide and organic hydroperoxide in the troposphere: a review, Atmos. Environ., 34, 3475–3494, https://doi.org/10.1016/S1352-2310(99)00432-X, 2000.

Lee, Y.-N. and Lind, J. A.: Kinetics of aqueous-phase oxidation of nitrogen(III) by hydrogen peroxide, J. Geophys. Res., 91, 2793, https://doi.org/10.1029/JD091iD02p02793, 1986.

Lelieveld, J. and Crutzen, P. J.: Influences of cloud photochemical processes on tropospheric ozone, Nature, 343, 227–233, https://doi.org/10.1038/343227a0, 1990.

Lelieveld, J. and Crutzen, P. J.: The role of clouds in tropospheric photochemistry, J. Atmos. Chem., 12, 229–267, https://doi.org/10.1007/BF00048075, 1991.

Lelieveld, J. and Crutzen, P. J.: Role of deep cloud convection in the ozone budget of the troposphere, Science, 264, 1759–1761, https://doi.org/10.1126/science.264.5166.1759, 1994.

Levy, H.: Normal atmosphere: large radical and formaldehyde concentrations predicted, Science, 173, 141–143, https://doi.org/10.1126/science.173.3992.141, 1971.

Lightfoot, P. D., Cox, R. A., Crowley, J. N., Destriau, M., Hayman, G. D., Jenkin, M. E., Moortgat, G. K., and Zabel, F.: Organic peroxy radicals: Kinetics, spectroscopy and tropospheric chemistry, Atmos. Environ. A-Gen., 26, 1805–1961, https://doi.org/10.1016/0960-1686(92)90423-I, 1992.

Logan, J. A., Prather, M. J., Wofsy, S. C., and McElroy, M. B.: Tropospheric chemistry: A global perspective, J. Geophys. Res., 86, 7210, https://doi.org/10.1029/JC086iC08p07210, 1981.

Madronich, S.: Photodissociation in the atmosphere: 1. Actinic flux and the effects of ground reflections and clouds, J. Geophys. Res., 92, 9740, https://doi.org/10.1029/JD092iD08p09740, 1987.

McArdle, J. V. and Hoffmann, M. R.: Kinetics and mechanism of the oxidation of aquated sulfur dioxide by hydrogen peroxide at low pH, J. Phys. Chem., 87, 5425–5429, https://doi.org/10.1021/j150644a024, 1983.

Olszyna, K. J., Meagher, J. F., and Bailey, E. M.: Gas-phase, cloud and rain-water measurements of hydrogen peroxide at a high-elevation site, Atmos. Environ., 22, 1699–1706, https://doi.org/10.1016/0004-6981(88)90398-8, 1988.

O'Sullivan, D. W., Heikes, B. G., Lee, M., Chang, W., Gregory, G. L., Blake, D. R., and Sachse, G. W.: Distribution of hydrogen peroxide and methylhydroperoxide over the Pacific and South Atlantic Oceans, J. Geophys. Res., 104, 5635–5646, https://doi.org/10.1029/98JD01250, 1999.

Palenik, B., Zafiriou, O. C., and Morel, F. M. M.: Hydrogen peroxide production by a marine phytoplankter1, Limnol. Oceanogr., 32, 1365–1369, https://doi.org/10.4319/lo.1987.32.6.1365, 1987.

Penkett, S. A., Jones, B. M. R., Brich, K. A., and Eggleton, A. E. J.: The importance of atmospheric ozone and hydrogen peroxide in oxidising sulphur dioxide in cloud and rainwater, Atmos. Environ., 13, 123–137, https://doi.org/10.1016/0004-6981(79)90251-8, 1979.

Perros, P. E.: Large-scale distribution of hydrogen peroxide from aircraft measurements during the TROPOZ II experiment, Atmos. Environ. A-Gen., 27, 1695–1708, https://doi.org/10.1016/0960-1686(93)90232-N, 1993.

Pilz, W. and Johann, I.: Die Bestimmung Kleinster Mengen von Wasserstoffperoxyd in Luft, Int. J. Environ. Anal. Chem., 3, 257–270, https://doi.org/10.1080/03067317408071087, 1974.

Reeves, C. E. and Penkett, S. A.: Measurements of peroxides and what they tell us, Chem. Rev., 103, 5199–5218, https://doi.org/10.1021/cr0205053, 2003.

Reifenberg, S. F., Martin, A., Kohl, M., Bacer, S., Hamryszczak, Z., Tadic, I., Röder, L., Crowley, D. J., Fischer, H., Kaiser, K., Schneider, J., Dörich, R., Crowley, J. N., Tomsche, L., Marsing, A., Voigt, C., Zahn, A., Pöhlker, C., Holanda, B. A., Krüger, O., Pöschl, U., Pöhlker, M., Jöckel, P., Dorf, M., Schumann, U., Williams, J., Bohn, B., Curtius, J., Harder, H., Schlager, H., Lelieveld, J., and Pozzer, A.: Numerical simulation of the impact of COVID-19 lockdown on tropospheric composition and aerosol radiative forcing in Europe, Atmos. Chem. Phys., 22, 10901–10917, https://doi.org/10.5194/acp-22-10901-2022, 2022.

Robbin Martin, L. and Damschen, D. E.: Aqueous oxidation of sulfur dioxide by hydrogen peroxide at low pH, Atmos. Environ., 15, 1615–1621, https://doi.org/10.1016/0004-6981(81)90146-3, 1981.

Roeckner, E., Bäuml, G., Bonaventura, L., Brokopf, R., Esch, M., Giorgetta, M., Hagemann, S., Kirchner, I., Kornblueh, L., Manzini, E., Rhodin, A., Schlese, U., Schulzweida, U., and Tompkins, A.: The atmospheric general circulation model ECHAM 5. PART I: Model description, Max-Planck-Institut für Meteorologie, https://doi.org/10.17617/2.995269, 2003.

Roeckner, E., Brokopf, R., Esch, M., Giorgetta, M., Hagemann, S., Kornblueh, L., Manzini, E., Schlese, U., and Schulzweida, U.: Sensitivity of Simulated Climate to Horizontal and Vertical Resolution in the ECHAM5 Atmosphere Model, J. Climate, 19, 3771–3791, https://doi.org/10.1175/JCLI3824.1, 2006.

Sakugawa, H., Kaplan, I. R., Tsai, W., and Cohen, Y.: Atmospheric hydrogen peroxide, Environ. Sci. Technol., 24, 1452–1462, https://doi.org/10.1021/es00080a002, 1990.

Sakugawa, H., Kaplan, I. R., and Shepard, L. S.: Measurements of H2O2, aldehydes and organic acids in Los Angeles rainwater: Their sources and deposition rates, Atmos. Environ. B-Urb., 27, 203–219, https://doi.org/10.1016/0957-1272(93)90006-R, 1993.

Sander, R., Kerkweg, A., Jöckel, P., and Lelieveld, J.: Technical note: The new comprehensive atmospheric chemistry module MECCA, Atmos. Chem. Phys., 5, 445–450, https://doi.org/10.5194/acp-5-445-2005, 2005.

Sander, R., Baumgaertner, A., Gromov, S., Harder, H., Jöckel, P., Kerkweg, A., Kubistin, D., Regelin, E., Riede, H., Sandu, A., Taraborrelli, D., Tost, H., and Xie, Z.-Q.: The atmospheric chemistry box model CAABA/MECCA-3.0, Geosci. Model Dev., 4, 373–380, https://doi.org/10.5194/gmd-4-373-2011, 2011.

Sander, R., Baumgaertner, A., Cabrera-Perez, D., Frank, F., Gromov, S., Grooß, J.-U., Harder, H., Huijnen, V., Jöckel, P., Karydis, V. A., Niemeyer, K. E., Pozzer, A., Riede, H., Schultz, M. G., Taraborrelli, D., and Tauer, S.: The community atmospheric chemistry box model CAABA/MECCA-4.0, Geosci. Model Dev., 12, 1365–1385, https://doi.org/10.5194/gmd-12-1365-2019, 2019.

Slemr, F. and Tremmel, H. G.: Hydroperoxides in the marine troposphere over the Atlantic Ocean, J. Atmos. Chem., 19, 371–404, https://doi.org/10.1007/BF00694493, 1994.

Snow, J. A.: Winter-spring evolution and variability of HO_x reservoir species, hydrogen peroxide, and methyl hydroperoxide, in the northern middle to high latitudes, J. Geophys. Res., 108, 1890, https://doi.org/10.1029/2002JD002172, 2003.

Snow, J. A., Heikes, B. G., Shen, H., O'Sullivan, D. W., Fried, A., and Walega, J.: Hydrogen peroxide, methyl hydroperoxide, and formaldehyde over North America and the North Atlantic, J. Geophys. Res., 112, 8353, https://doi.org/10.1029/2006JD007746, 2007.

Stickler, A., Fischer, H., Williams, J., Reus, M. de, Sander, R., Lawrence, M. G., Crowley, J. N., and Lelieveld, J.: Influence of summertime deep convection on formaldehyde in the middle and upper troposphere over Europe, J. Geophys. Res., 111, D14308, https://doi.org/10.1029/2005JD007001, 2006.

Tost, H., Jöckel, P., Kerkweg, A., Sander, R., and Lelieveld, J.: Technical note: A new comprehensive SCAVenging submodel for global atmospheric chemistry modelling, Atmos. Chem. Phys., 6, 565–574, https://doi.org/10.5194/acp-6-565-2006, 2006.

Valverde-Canossa, J., Wieprecht, W., Acker, K., and Moortgat, G. K.: H_2O_2 and organic peroxide measurements in an orographic cloud: The FEBUKO experiment, Atmos. Environ., 39, 4279–4290, https://doi.org/10.1016/j.atmosenv.2005.02.040, 2005.

Voigt, C., Lelieveld, J., Schlager, H., Schneider, J., Curtius, J., Meerkötter, R., Sauer, D., Bugliaro, L., Bohn, B., Crowley, J. N., Erbertseder, T., Groß, S., Hahn, V., Li, Q., Mertens, M., Pöhlker, M. L., Pozzer, A., Schumann, U., Tomsche, L., Williams, J., Zahn, A., Andreae, M., Borrmann, S., Bräuer, T., Dörich, R., Dörnbrack, A., Edtbauer, A., Ernle, L., Fischer, H., Giez, A., Granzin, M., Grewe, V., Harder, H., Heinritzi, M., Holanda, B. A., Jöckel, P., Kaiser, K., Krüger, O. O., Lucke, J., Marsing, A., Martin, A., Matthes, S., Pöhlker, C., Pöschl, U., Reifenberg, S., Ringsdorf, A., Scheibe, M., Tadic, I., Zauner-Wieczorek, M., Henke, R., and Rapp, M.: Cleaner skies during the COVID-19 lockdown, B. Am. Meteorol. Soc., https://doi.org/10.1175/BAMS-D-21-0012.1, online first, 2022.

Walker, S. J., Evans, M. J., Jackson, A. V., Steinbacher, M., Zellweger, C., and McQuaid, J. B.: Processes controlling the concentration of hydroperoxides at Jungfraujoch Observatory, Switzerland, Atmos. Chem. Phys., 6, 5525–5536, https://doi.org/10.5194/acp-6-5525-2006, 2006.

Warneck, P.: Chemical reactions in clouds, Fresen. J. Anal. Chem., 340, 585–590, https://doi.org/10.1007/BF00322434, 1991.

Warneck, P.: Chemistry of the natural atmosphere, 3rd print, International geophysics series, Vol. 41, Academic Press, San Diego, Calif., 757 pp., ISBN 0127356304, 1994.

Weinstein-Lloyd, J. B., Lee, J. H., Daum, P. H., Kleinman, L. I., Nunnermacker, L. J., Springston, S. R., and Newman, L.: Measurements of peroxides and related species during the 1995 summer intensive of the Southern Oxidants Study in Nashville, Tennessee, J. Geophys. Res., 103, 22361–22373, https://doi.org/10.1029/98JD01636, 1998.

Xuan, X., Chen, Z., Gong, Y., Shen, H., and Chen, S.: Partitioning of hydrogen peroxide in gas-liquid and gas-aerosol phases, Atmos. Chem. Phys., 20, 5513–5526, https://doi.org/10.5194/acp-20-5513-2020, 2020.

Zahn, A., Weppner, J., Widmann, H., Schlote-Holubek, K., Burger, B., Kühner, T., and Franke, H.: A fast and precise chemiluminescence ozone detector for eddy flux and airborne application, Atmos. Meas. Tech., 5, 363–375, https://doi.org/10.5194/amt-5-363-2012, 2012.

Zepp, R. G., Faust, B. C., and Hoigne, J.: Hydroxyl radical formation in aqueous reactions (pH 3–8) of iron(II) with hydrogen peroxide: the photo-Fenton reaction, Environ. Sci. Technol., 26, 313–319, https://doi.org/10.1021/es00026a011, 1992.

Zuo, Y. and Deng, Y.: Iron(II)-catalyzed photochemical decomposition of oxalic acid and generation of H_2O_2 in atmospheric liquid phases, Chemosphere, 35, 2051–2058, https://doi.org/10.1016/S0045-6535(97)00228-2, 1997.

Zuo, Y. and Hoigne, J.: Formation of hydrogen peroxide and depletion of oxalic acid in atmospheric water by photolysis of iron(III)-oxalato complexes, Environ. Sci. Technol., 26, 1014–1022, https://doi.org/10.1021/es00029a022, 1992.

Zuo, Y. and Hoigné, J.: Evidence for Photochemical Formation of H_2O_2 and Oxidation of SO_2 in Authentic Fog Water, Science, 260, 71–73, https://doi.org/10.1126/science.260.5104.71, 1993.

Supplement of Atmos. Chem. Phys., 22, 9483–9497, 2022 https://doi.org/10.5194/acp-22-9483-2022-supplement

Atmospheric Chemistry and Physics Open Access

Supplement of

Distribution of hydrogen peroxide over Europe during the BLUESKY aircraft campaign

Zaneta T. Hamryszczak et al.

Correspondence to: Zaneta T. Hamryszczak (z.hamryszczak@mpic.de) and Horst Fischer (horst.fischer@mpic.de)

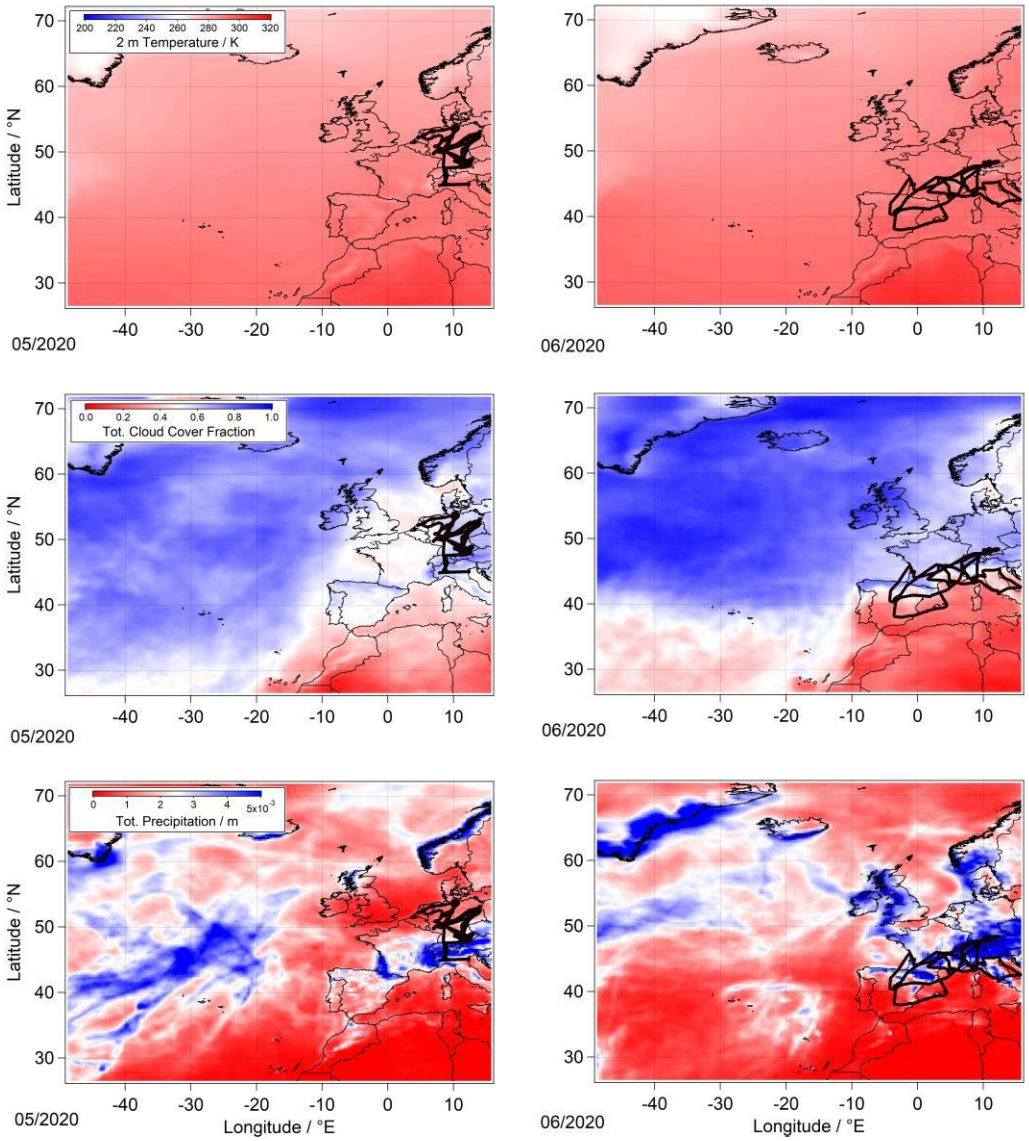

Figure S1: Average monthly 2 m temperature (top panel), total cloud cover fraction (middle panel) and total precipitation (bottom panel) during May (left row) and June (right row) derived by ERA 5 reanalysis generated using Copernicus Climate Change Service information (Hersbach et al. 2019).[1] Flight tracks of measurement flights are plotted in black.

[1] Hersbach, H., Bell, B., Berrisford, P., Biavati, G., Horányi, A., Muñoz Sabater, J., Nicolas, J., Peubey, C., Radu, R., Rozum, I., Schepers, D., Simmons, A., Soci, C., Dee, D., Thépaut, J-N. (2019): ERA5 monthly averaged data on single levels from

Table S1: General median (bottom) and mean (± 1 sigma; top) overview of hydrogen peroxide during the campaigns UTOPIHAN-ACT II/III, HOOVER II and CAFE-EU/BLUESKY (Stickler et al. 2006; Colomb et al. 2006; Klippel et al. 2011).

Campaign	**Time period**	**Latitudinal range**	**Mean (Median) Mixing Ratio / ppb_v**		
			UT	MT	BL
			6 – 14 km	2 – 6 km	0 – 2 km
UTOPIHAN-ACT	03&07/03	40°N – 65°N	0.47±0.36 (0.47)	1.74±0.97 (1.80)	1.65±0.16 (1.32)
HOOVER II	07/07	30°N – 75°N	0.67±0.43 (0.56)	1.49 ±0.71 (1.33)	1.59 ±0.78 (1.48)
BLUESKY	05– 06/20	35°N – 60°N	0.28±0.22 (0.24)	0.42±0.25 (0.37)	0.48±0.17 (0.48)

1979 to present. Copernicus Climate Change Service (C3S) Climate Data Store (CDS). (Accessed on < 04-05-2021 >), 10.24381/cds.f17050d7

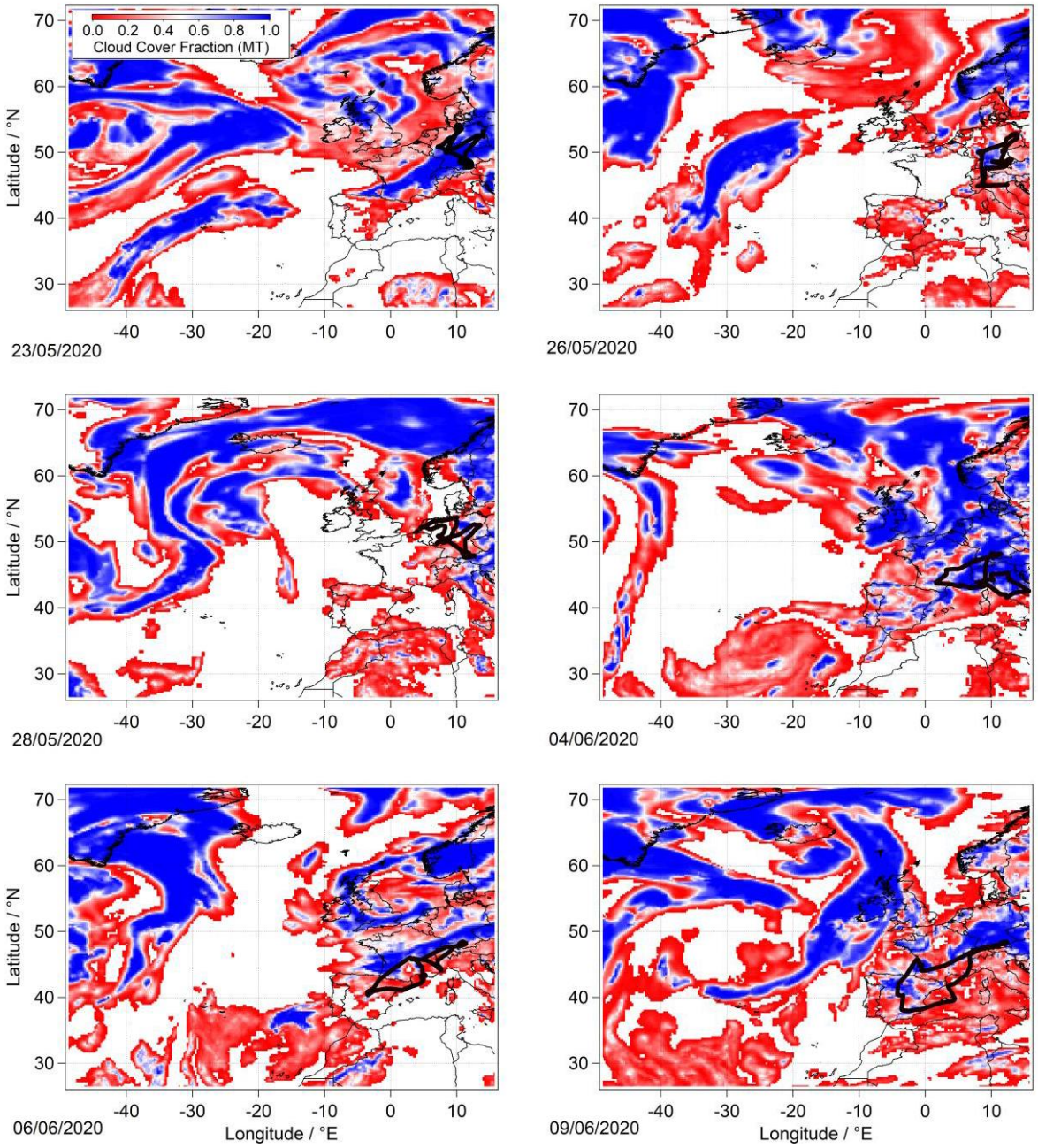

Figure S2: Hourly cloud cover fraction at middle altitudes (2 – 7 km; 12:00 UTC) during the performed flights (black tracks) in agreement with ERA5 reanalysis generated using Copernicus Climate Change Service information (Hersbach et al. 2018)[2].

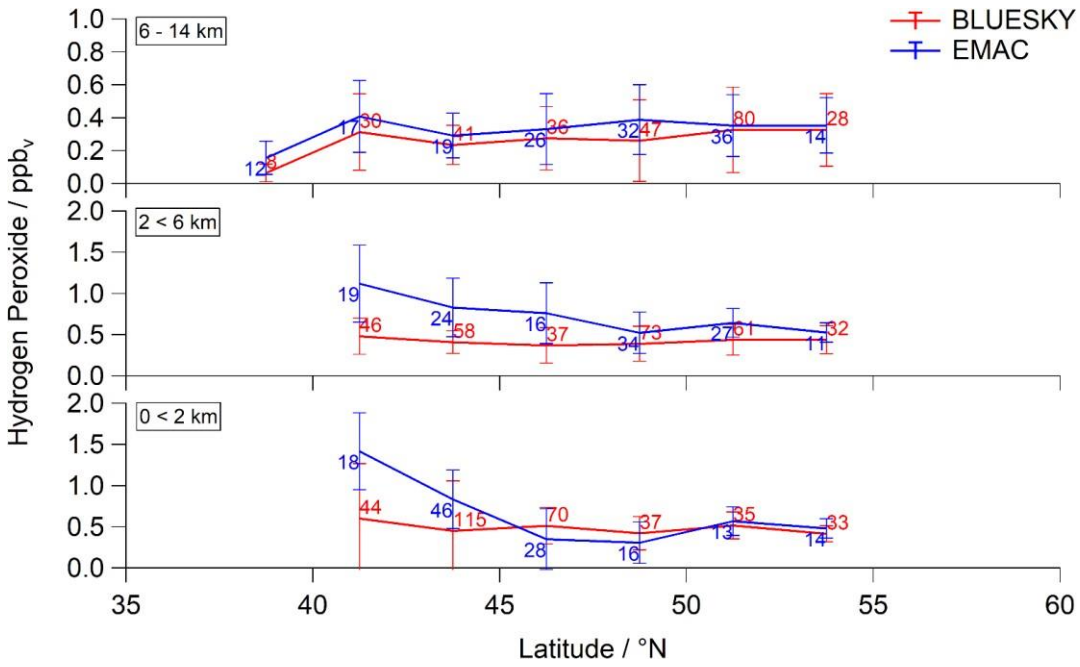

Figure S3: Latitudinal distribution of hydrogen peroxide in comparison to model EMAC (red: BLUESKY; blue: EMAC). The data was subdivided into three atmospheric layers, upper troposphere, middle troposphere and boundary layer (from top to bottom) with mean values binned for 2.5° of latitude for each tropospheric layer. The corresponding numbers indicate the total amount of data points per bin.

[2] Hersbach, H., Bell, B., Berrisford, P., Biavati, G., Horányi, A., Muñoz Sabater, J., Nicolas, J., Peubey, C., Radu, R., Rozum, I., Schepers, D., Simmons, A., Soci, C., Dee, D., Thépaut, J-N. (2018): ERA5 hourly data on single levels from 1979 to present. Copernicus Climate Change Service (C3S) Climate Data Store (CDS). (Accessed on < 04-05-2021 >), 10.24381/cds.adbb2d47

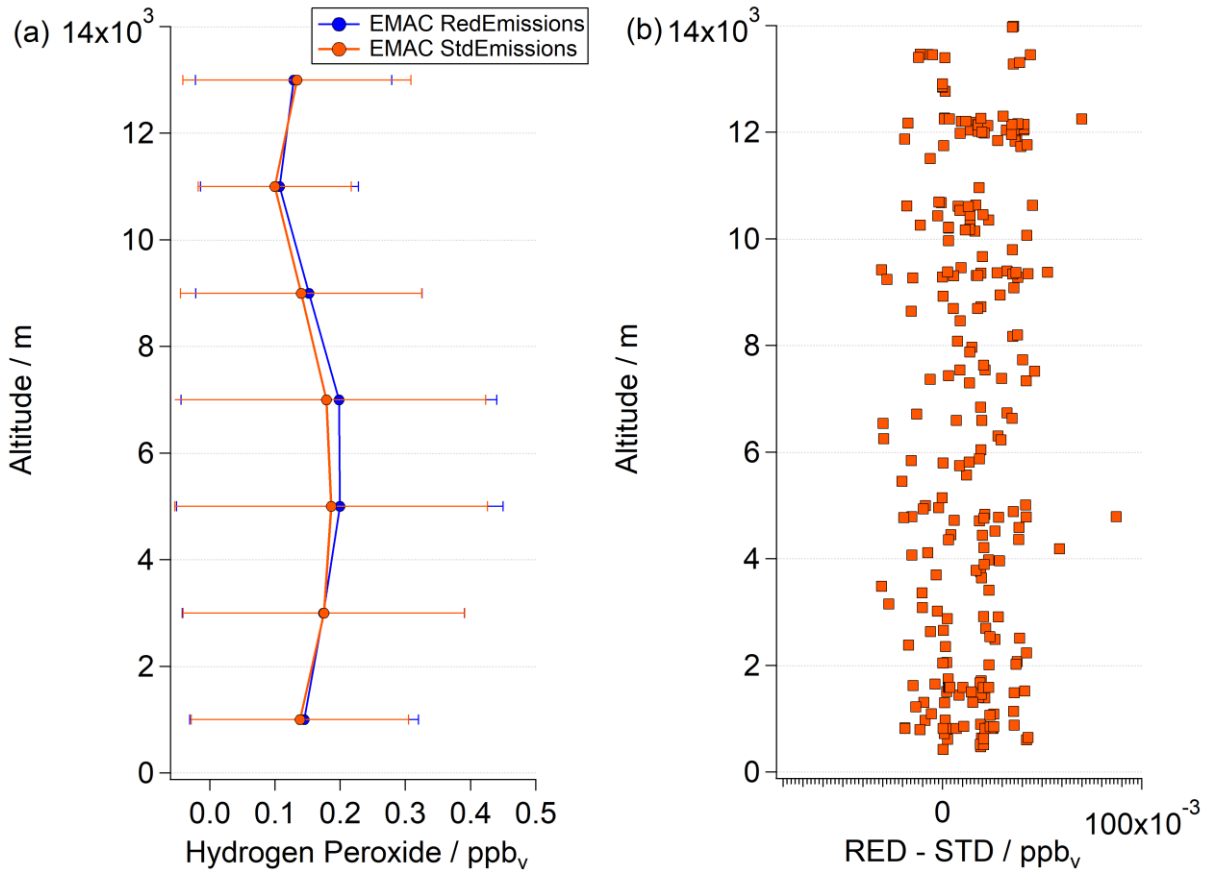

Figure S4: Vertical profiles of hydrogen peroxide with (blue) and without (orange) the CORONA lockdown emission reductions (a) and absolute difference of the modelled mixing ratios (b). In order to examine the impact of the reduced emissions on the budget of H_2O_2, the entirety of both datasets provided by EMAC was used. Please note that the data was not filtered analogously to the procedure described in Sect 3.1.

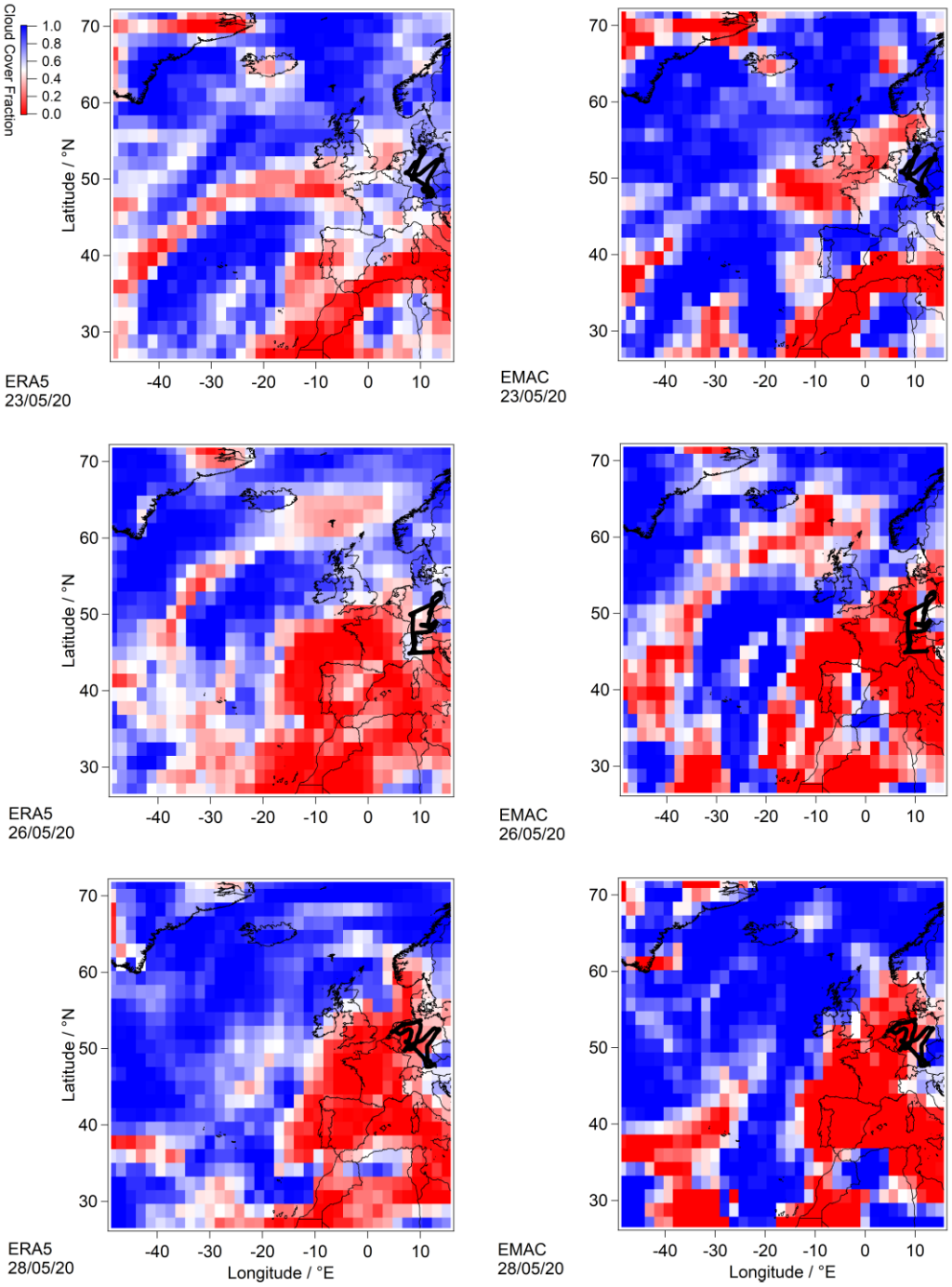
Cloud Cover Fraction
1.0
0.8
0.6
0.4
0.2
0.0
Latitude / °N
Longitude / °E
ERA5
23/05/20
EMAC
23/05/20
ERA5
26/05/20
EMAC
26/05/20
ERA5
28/05/20
EMAC
28/05/20

60

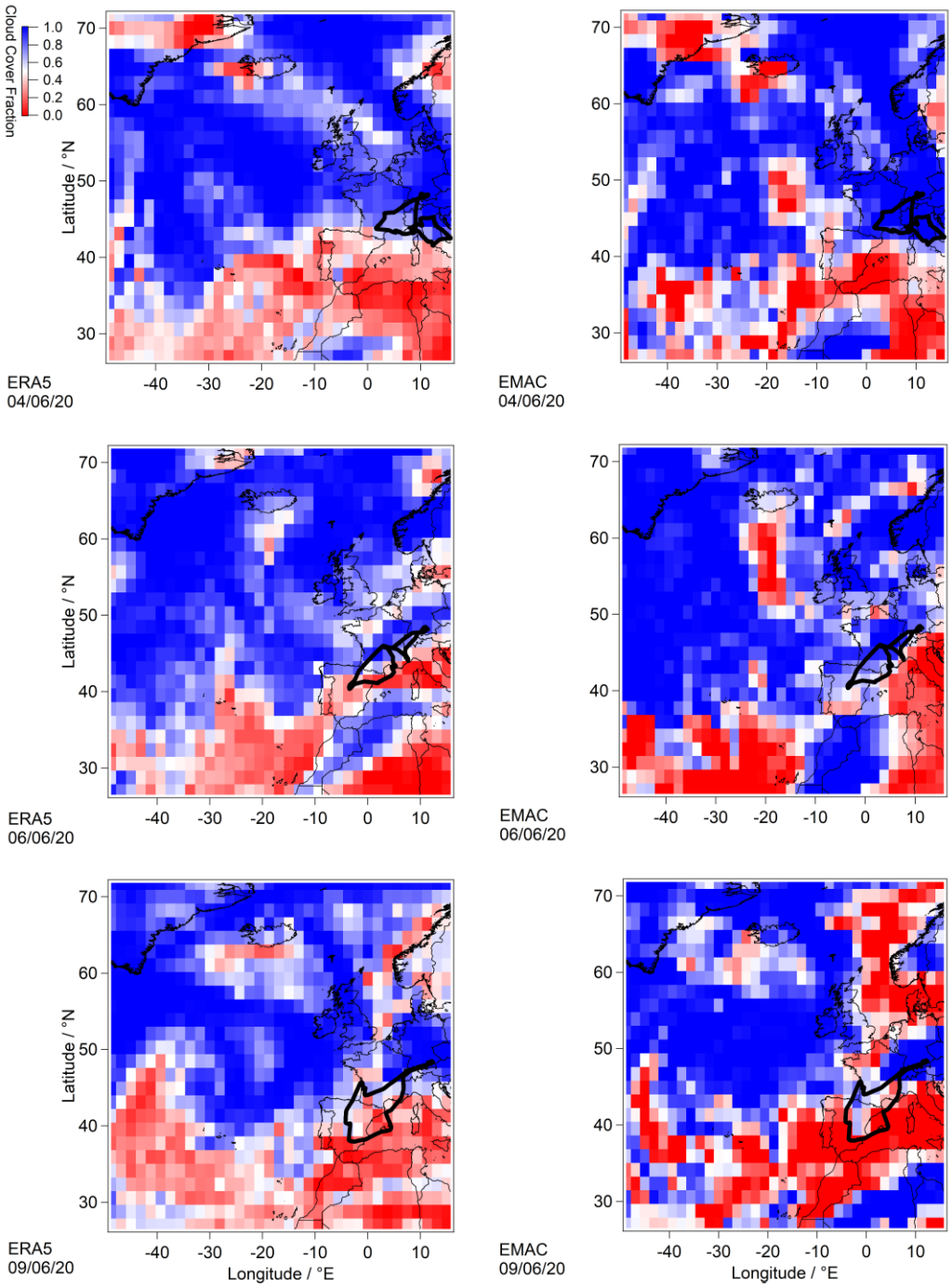

65 **Figure S5: Average total cloud coverage over Europe and North Atlantic during the measurement period (73 - 28°N, -50 – 15°E) provided by ERA5 (left panel; modified Copernicus Climate Change Service information; left panel; Hersbach et al. 2018) and EMAC (right panel).**

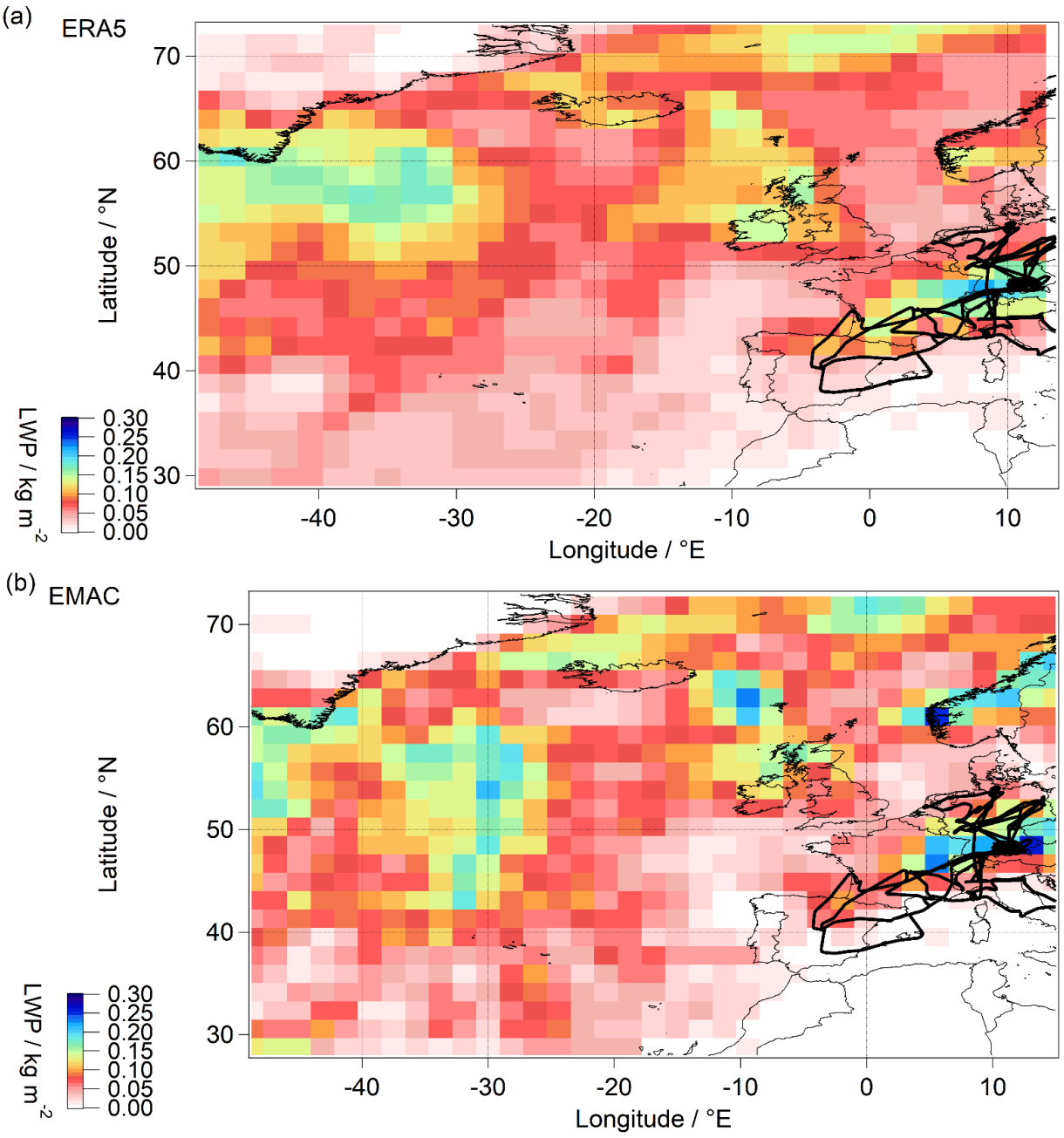

Figure S6: Average liquid water path (LWP) over Europe and the North Atlantic (73°N- 28°N, -50°E – 15°E) during the flight days of the campaign based on ERA5 (a;contains modified Copernicus Climate Change Service information; Hersbach et al. 2018) in comparison to EMAC (b).

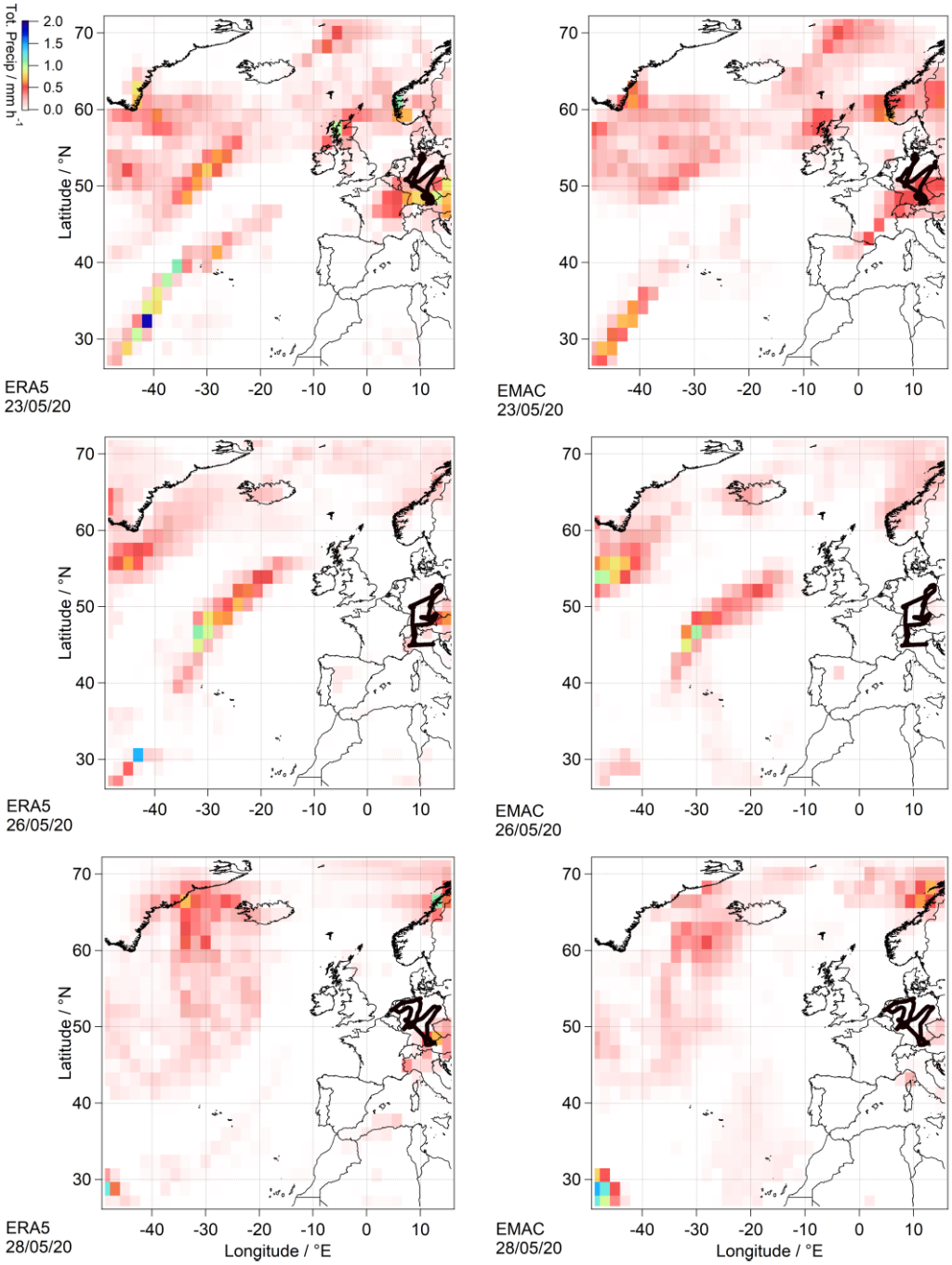
Tot. Precip / mm h-1
2.0
1.5
1.0
0.5
0.0
Latitude / °N
Longitude / °E
ERA5
23/05/20
EMAC
23/05/20
ERA5
26/05/20
EMAC
26/05/20
ERA5
28/05/20
EMAC
28/05/20

75

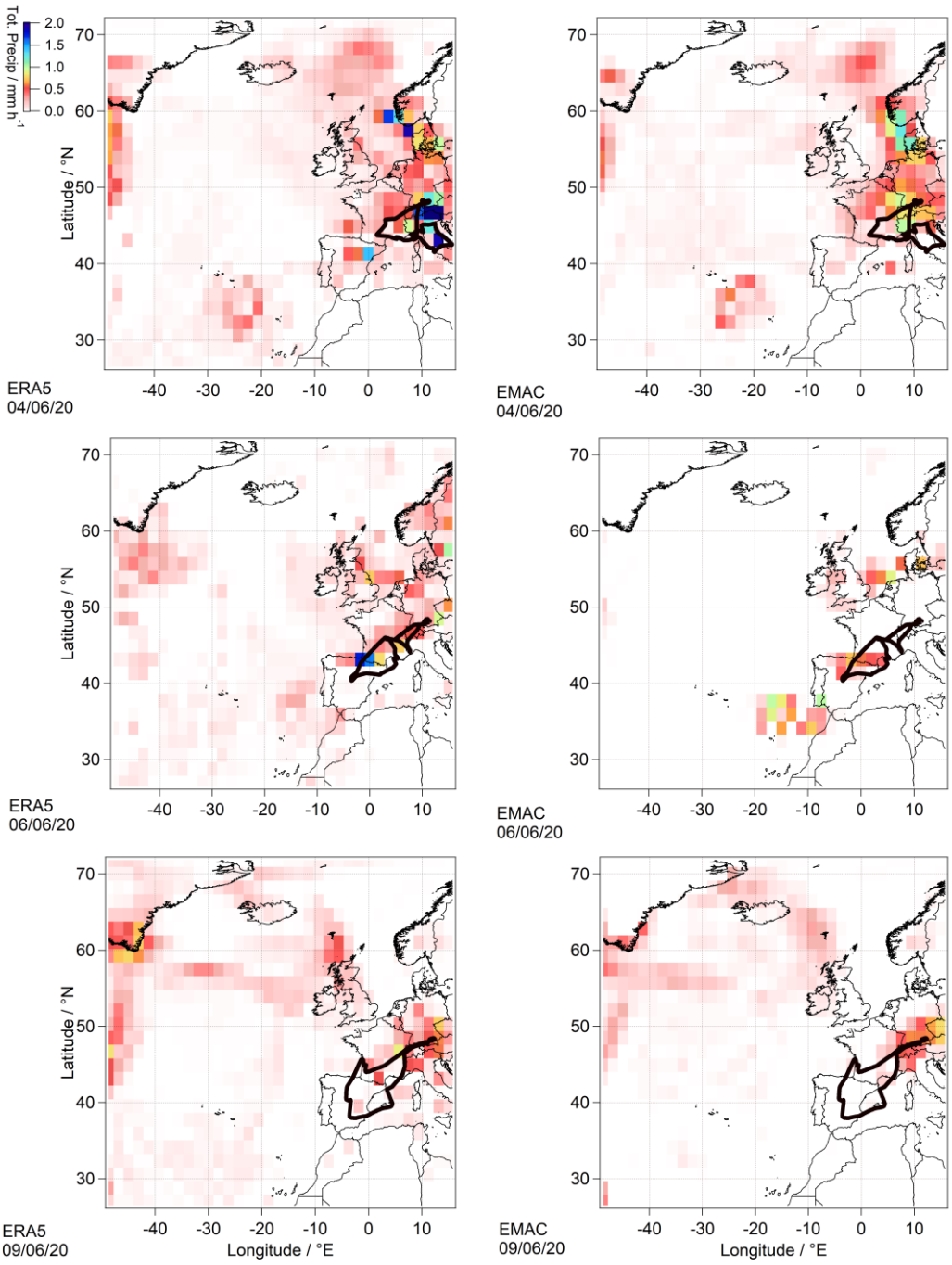

Figure S7: Average total precipitation over Europe and North Atlantic during the campaign BLUESKY (73°N- 28°N, -50°E – 15°E) provided by ERA5 (left panel; contains modified Copernicus Climate Change Service information; Hersbach et al. 2018) in comparison to EMAC (right panel).

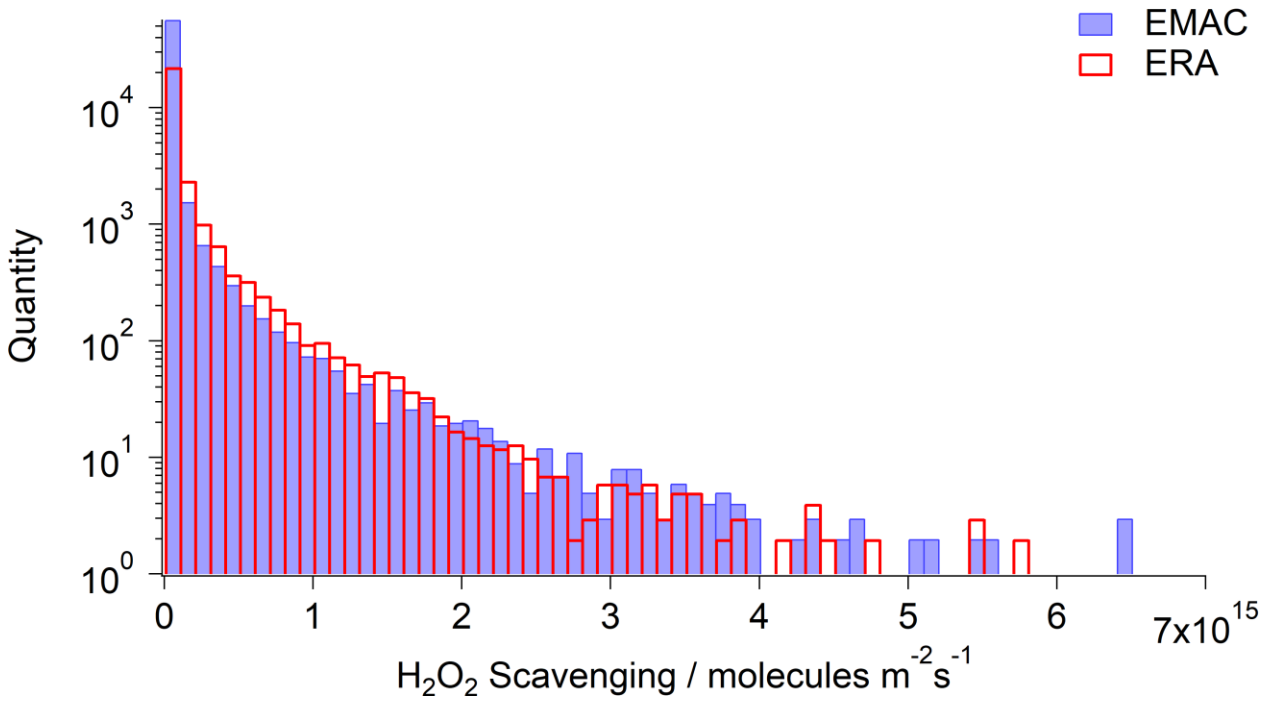

Figure S8: Histogram of the hydrogen peroxide scavenging modelled by EMAC (blue) and the predicted scavenging by ERA5 (red). The scavenging data of ERA5 were obtained by extrapolation based on linear regression between scavenging and precipitation by EMAC.

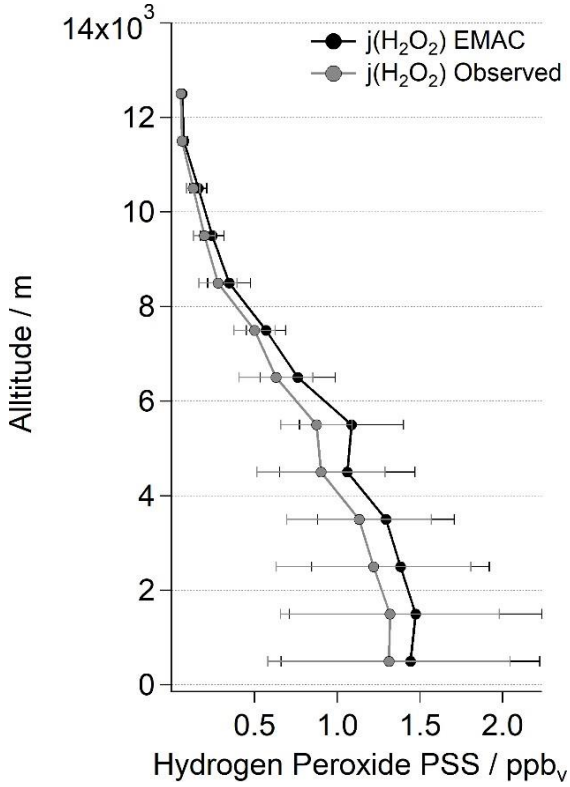

Figure S9: Vertical profiles of hydrogen peroxide mixing ratios under PSS conditions derived from observed (gray) and EMAC simulated (black) photolysis rates of H_2O_2 ($j(H_2O_2)$).

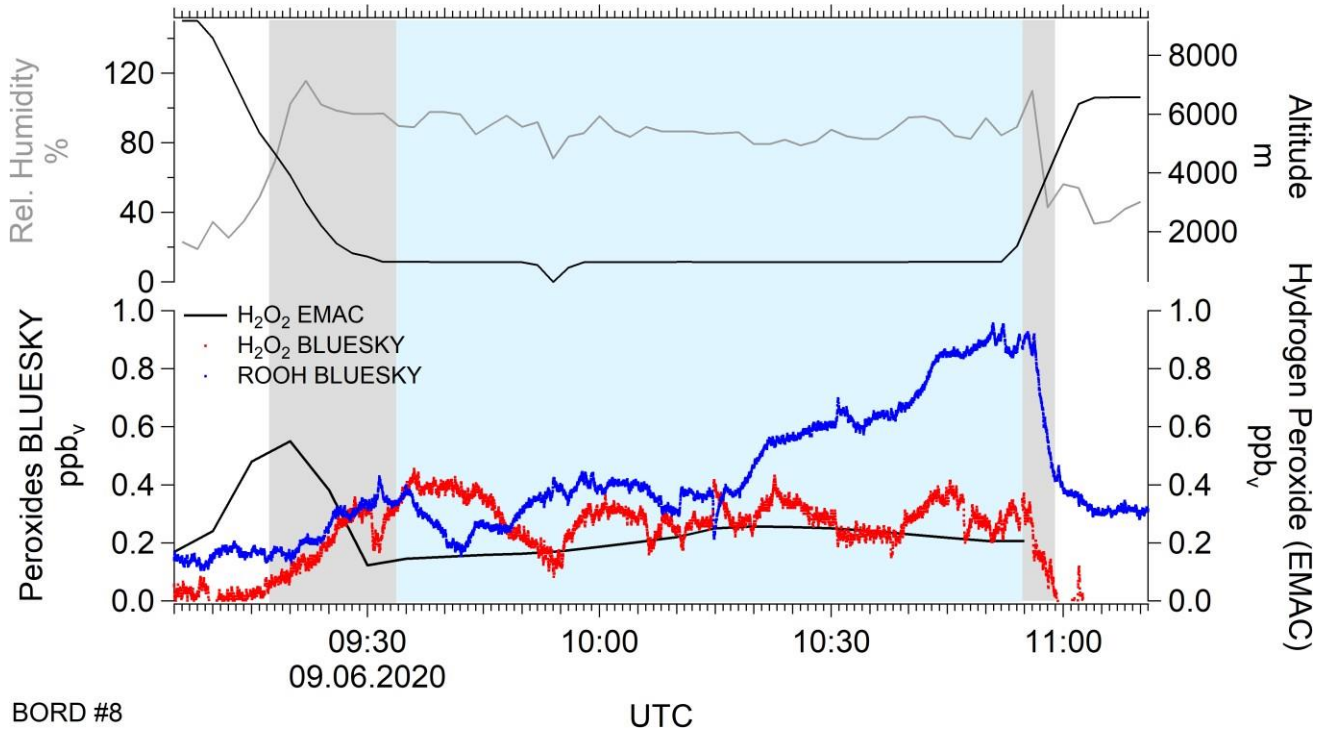

Figure S10: Temporal series of peroxide mixing ratios over the Bordeaux area on 09.06.2020 (red: observed H2O2; blue: observed ROOH; black: simulated H_2O_2, grey: relative humidity; top black: GPS altitude). Cloud scavenging and precipitation are highlighted by gray and light blue shading, respectively. Please note that the observed peroxide data displayed has 1 sec time resolution in comparison to the model resolution of 5 min.

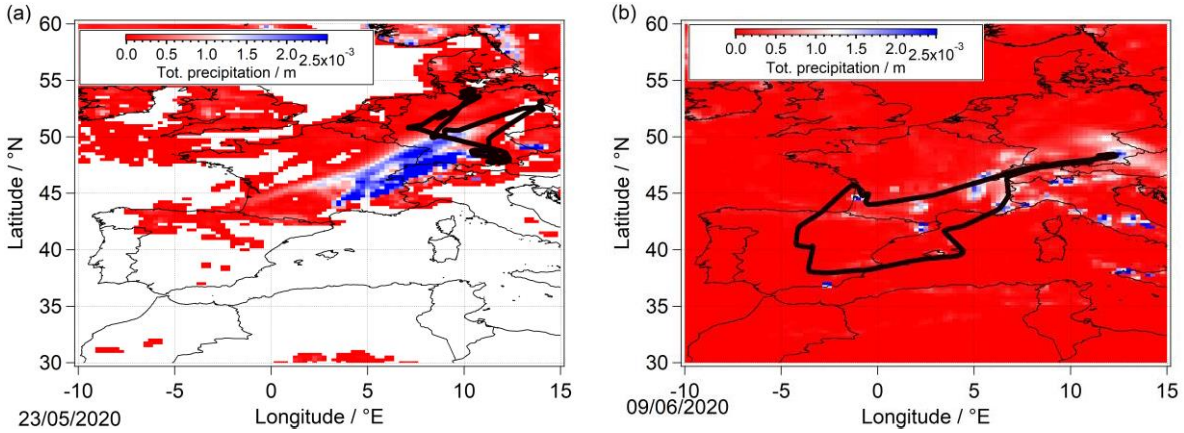

Figure S11: Hourly total precipitation at 12:00 UTC during the measurement flights performed on 23.05.2020 (a) and 09.06.2020 (b) in agreement with ERA5 reanalysis (generated using Copernicus Climate Change Service information; Hersbach et al. 2018)[3].

[3] Hersbach, H., Bell, B., Berrisford, P., Biavati, G., Horányi, A., Muñoz Sabater, J., Nicolas, J., Peubey, C., Radu, R., Rozum, I., Schepers, D., Simmons, A., Soci, C., Dee, D., Thépaut, J-N. (2018): ERA5 hourly data on single levels from 1979 to present. Copernicus Climate Change Service (C3S) Climate Data Store (CDS). (Accessed on < 04-05-2021 >), 10.24381/cds.adbb2d47

4. The CAFE-Africa airborne campaign

The section is presenting in situ measurement results of hydroperoxides during the Chemistry of the Atmosphere: The field experiment in Africa (CAFE-Africa) aircraft campaign, which was performed in August – September 2018. The trace species observations were obtained from marine and continental air masses. In the first section (Sec. 4.1.), the scientific objective of the research project and a summary of the meteorological conditions during the airborne campaign are presented. Information on the instrumentation of the research aircraft HALO significant to hydroperoxide analyses was presented in the previous Section (Sect. 3.1.). An overview of the hydroperoxide measurement results based on the determined mean ($\pm 1\sigma$) and median mixing ratios of hydrogen peroxide and the sum of organic hydroperoxides with respect to the main tropospheric layers is discussed in Sect. 4.2. Special emphasis was put on the spatial distribution of hydrogen peroxide in the upper troposphere and the impact of the Intertropical Convergence Zone (ITCZ) on the distribution of H_2O_2 in the tropics and subtropics in perspective of EMAC simulations and quasi PSS calculations (Sect. 4.3.). The analysis results are presented as a published manuscript with the title: "Hydrogen peroxide in the upper tropical troposphere over the Atlantic Ocean and western Africa during the CAFE-Africa aircraft campaign" and the corresponding Supplement.

4.1. The campaign – Objectives and meteorological conditions

Hydroperoxides were measured predominantly in the free troposphere over the Atlantic Ocean and western Africa during the CAFE-Africa campaign in August and September 2018. The airborne research project investigated the large-scale distribution of trace gases, aerosol particles, and radicals over the tropical eastern Atlantic and along the western coast of Africa. The campaign focused on the potential influence of biomass burning emissions and long-distance pollution transport on the oxidation capacity of the atmosphere and the chemical processing of trace gases and aerosols in clean versus polluted air masses. CAFE-Africa was performed from the base of operation in Sal, Cabo Verde (16.75° N, 22.95° W) with 14 measurement flights over the Atlantic Ocean and the western African coast with the HALO research aircraft. The sampled area covered a latitudinal and longitudinal range of 10° S – 50° N and 50° W – 15° E extending from the tropical Atlantic Ocean towards West Africa (over Senegal, Guinea up to the Ivory Coast) with the measurement flights focused mainly on the upper troposphere up to an altitude of 15 km. Vertical profiles of the trace species extending over the entire tropospheric column were measured predominantly in close proximity to the base of operation in Sal. Fig. 10 illustrates the GPS flight tracks. Corresponding detailed flight information on the individual flights was given by Tadic et al. (2021).

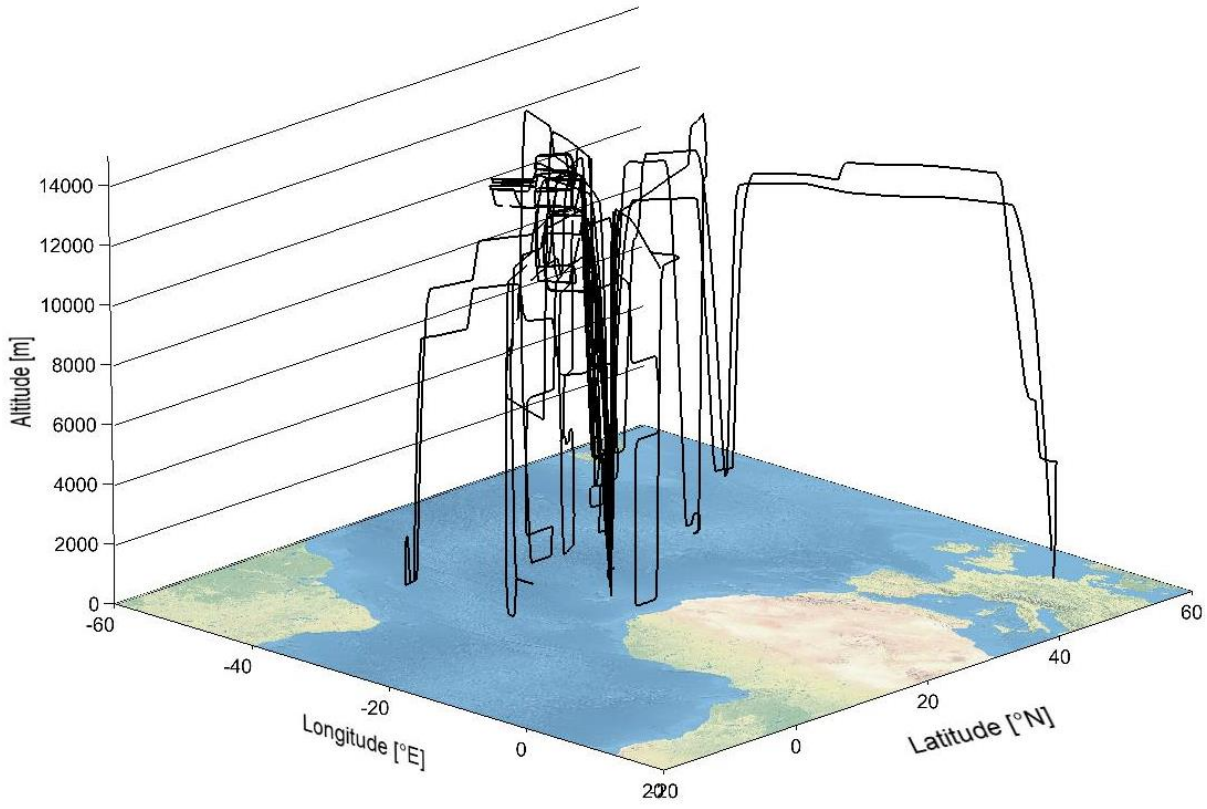

Figure 10: General overview of GPS flight tracks during the CAFE-Africa campaign (08/09 2018) based on data output by BAHAMAS instrument with 3 min temporal resolution.

An overview of the average monthly 2 m temperature, high, medium, and low cloud cover fractions, and convective and total precipitation during the measurement period derived by ERA5 reanalysis generated using Copernicus Climate Change Service information (Hersbach et al. 2019) is presented in Sect. 4.3. in the scope of the published measurement report (Supplement; Fig. S1 – S3). The corresponding GPS flight tracks of the individual flights are indicated in black. In August 2018, the monthly average 2 m temperature during the measurement period based on the defined region was 296.48 (±5.52) K with a maximum of 311.82 K over the African continent and a minimum of 278.01 K towards the North. Analogously, 295.98 (± 5.98) K, 309.27 K, and 275.86 K, respectively were reported in September 2018. Average high, medium, and low cloud coverages were 0.24 (±0.17), 0.16 (±0.12), and 0.32 (±0.23) in August and 0.29 (±0.17), 0.17 (±0.12), and 0.30 (±0.21) in September with a high cloud coverage of up to unity within the Intertropical Convergence Zone (ITCZ) over the African continent. Convective and total precipitation varied between 1.26 (±1.62) · 10^{-3} m and 2.12 (±2.86) · 10^{-3} m, respectively in August and 1.53 (±1.81) · 10^{-3} m, and 2.59 (±3.01) · 10^{-3} m, respectively in September, with maximum values of 13.55 · 10^{-3} m and 16.61 · 10^{-3} m within ITCZ. The ITCZ is the region marking the equatorial low-pressure area, where the northeast and southwest wind trades converge, hence its name.

4.2. Hydroperoxide in situ observations during CAFE-Africa – an overview

During the CAFE-Africa campaign, mean (±1σ) and median H_2O_2 and ROOH levels based on the entirety of the measurements performed during the campaign were 0.74 (±1.31) ppb_v and 0.20 ppb_v, and 0.26 (±0.23) ppb_v and 0.17 ppb_v for H_2O_2 and ROOH, respectively. Due to a lack of detailed information regarding the measured VOCs serving and the corresponding alkyl peroxyl radicals, the obtained ROOH mixing ratios were not corrected for their reduced striping and transmission efficiencies. The maximum mixing ratios of 9.43 ppb_v and 1.42 ppb_v for H_2O_2 and ROOH, respectively, were detected in the middle troposphere. The peak values are most likely due to air masses originating from the southwest of Africa affected by biomass burning emissions, as reported in the flight protocols during the corresponding measurement flights. The following table gives an overview of the determined mean (±1σ), median and maximum hydroperoxide mixing ratios with respect to the main tropospheric layers (Tab. 3). Please note that for convenience purposes, the BL height has been assumed to be at approximately 2 km. However, for the marine region over the Atlantic Ocean, the Boundary Layer Height (BLH) is expected to be far lower (~500 m).

Table 3: Overview of the H_2O_2 and ROOH mean, median, and maximum mixing ratios (ppb_v) in the boundary layer (BL), middle troposphere (MT), and the upper troposphere (UT) during CAFE-Africa airborne campaign.

	BL (0 < 2 km)	**MT (2 < 8 km)**	**UT (8 < 15 km)**
H_2O_2			
Mean (±1σ) /ppb_v	2.25 (±1.30)	2.19 (±1.86)	0.18 (±0.13)
Median /ppb_v	2.18	1.78	0.15
Maximum /ppb_v	6.97	9.42	1.21
ROOH			
Mean (±1σ) /ppb_v	0.70 (±0.18)	0.55 (±0.25)	0.15 (±0.07)
Median /ppb_v	0.67	0.51	0.14
Maximum /ppb_v	1.24	1.42	0.64

The highest mean (±1σ) and median hydroperoxide levels were detected in the boundary layer with 2.25 (±1.30) ppb_v and 2.18 ppb_v for H_2O_2 and 0.70 (±0.18) ppb_v and 0.67 ppb_v for ROOH, respectively. The levels decrease slightly towards the middle troposphere with 2.19 (±1.86) ppb_v and 1.78 ppb_v for H_2O_2 and 0.55 (±0.25) ppb_v and 0.51 ppb_v for ROOH, respectively. Please note that the majority of the research flights was performed over the Atlantic Ocean. Thus, the deviation from the expected trend of maximum hydroperoxide mixing ratios in the middle troposphere, directly above the BL might be rather due to the course subdivision of the troposphere presented for the purpose of this overview. However, the assumption of the BLH does apply to the sampled region over Africa. The lowest mixing ratios of hydroperoxides were detected, as expected in the UT, at altitudes above 8 km. Here, the mean (±1σ) and median levels were 0.18 (±0.13) ppb_v and 0.15 ppb_v for H_2O_2 and 0.15 (±0.07) ppb_v and 0.14 ppb_v

for ROOH, respectively. The measured hydroperoxide mixing ratios during the CAFE-Africa campaign are presented as latitude vs. longitude plots with mean values aggregated into a subset of 1° x 1° bins for the sampled region along the GPS flight tracks subdivided into the main tropospheric layers (BL: 0 < 2 km; MT: 2 < 8 km; UT 8 < 15 km; Fig. 11). Please note that the observed hydroperoxide levels are color-coded for each plot separately to improve the resolution of each layer.

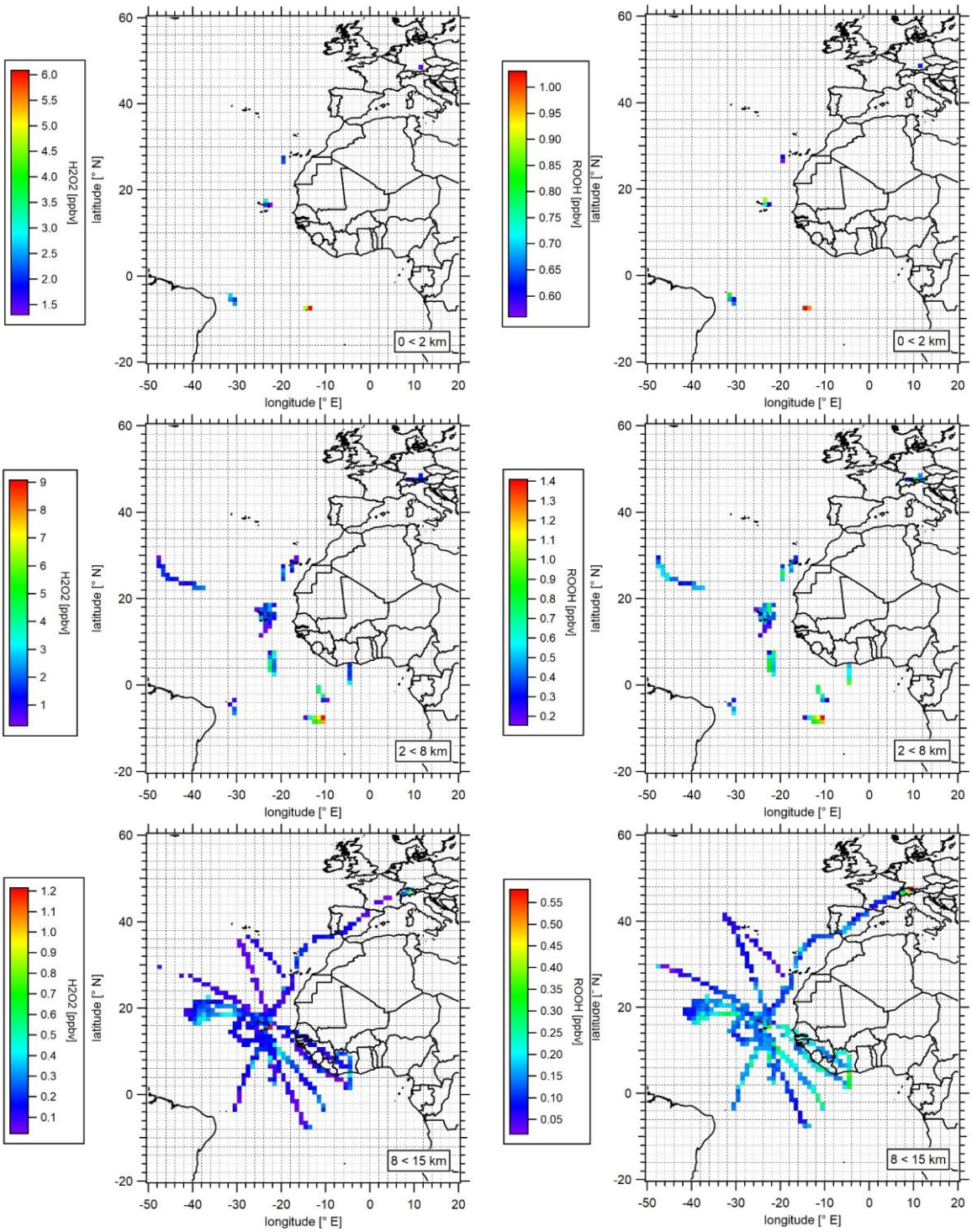

Figure 11: Spatial distribution of measured H_2O_2 (left column) and ROOH (right column) in the boundary layer (0 < 2 km; upper panel), the middle free troposphere (2 < 8 km; middle panel),

and the upper troposphere (8 < 15 km; bottom panel) during CAFE-Africa campaign performed in August – September 2018. Data were binned into a 1° x 1° subset along the GPS flight tracks.

Within the assumed boundary layer (0 < 2 km), the highest mixing ratios of up to 6.97 ppb_v and 1.24 ppb_v for H_2O_2 and ROOH, respectively were observed in the south of the sampled region. Analogously, within the middle troposphere (2 < 8 km) the levels of H_2O_2 and ROOH increase towards the South reaching levels of up to 9.42 ppb_v for H_2O_2 and 1.42 ppb_v for ROOH, respectively. However, due to the sparse measurements performed in the lower troposphere (below 8 km), no reliable statement about a potential latitudinal gradient with increasing hydroperoxide mixing ratios from the subtropics towards the tropics can be made. Additionally, according to the flight reports during the measurement period, increased hydroperoxide mixing ratios might mainly originate from air masses significantly affected by biomass burning emissions originating from the south-west of the African continent, whilst the low hydroperoxide mixing ratios in the north of the sampled region might be a result from dry deposition processes due to Saharan dust episodes during the measurement period. In the upper troposphere (> 8 km), maximum mixing ratios of 1.21 ppb_v and 0.64 ppb_v for H_2O_2 and ROOH, respectively were detected. While the ROOH levels increase from the northwest (approximately 0.05 – 0.10 ppb_v) towards the southeast (up to 0.40 ppb_v), no clear trend was observed in the spatial distribution of H_2O_2. A detailed discussion of the spatial distribution of H_2O_2 and the factors potentially influencing the budget of H_2O_2 in the upper troposphere is presented in the next section in the scope of the published manuscript with the title: "Hydrogen peroxide in the upper tropical troposphere over the Atlantic Ocean and western Africa during the CAFE-Africa aircraft campaign" (Sect. 4.3.).

4.3. Measurement results in the scope of the measurement report: "Hydrogen peroxide in the upper tropical troposphere over the Atlantic Ocean and western Africa during the CAFE-Africa aircraft campaign "

This section presents a measurement report about the H_2O_2 distribution over the Atlantic Ocean and the western coast of Africa affected by deep convection of the ITCZ. I am the first author of the manuscript, which was published in the journal *Atmospheric Chemistry and Physics* (ACP) on 30.05.23. The measurements were performed by D. Dienhart and B. Brendel. Together with D. Dienhart, I performed the data processing and data analysis. Supported by H. Fischer, I designed the study and wrote the manuscript draft with the contributions of all co-authors.

The report illustrates the spatial H_2O_2 distribution in the upper tropical troposphere at altitudes between 8 – 15 km based on in situ observations during the CAFE-Africa aircraft campaign performed in August – September 2018. In contrast to expectations based on the hydroperoxide distribution trends (as discussed in Sect. 1.4.), H_2O_2 levels in the upper troposphere display no clear latitudinal trend. Increased

hydrogen peroxide levels (up to 1 ppb_v) were observed locally in the ITCZ, over the African coast, and in the proximity of the tropical storm Florence. The observations suggest a significant influence of convective transport in the tropical and subtropical regions rather than a high dependency on photochemical processes. Based on a comparison with photostationary steady-state calculations and simulations by the EMAC model, the H_2O_2 measurements show no clear gradient with latitude in the mixing ratios of H_2O_2 in the upper troposphere. The largest discrepancies relative to PSS calculations and EMAC simulations correspond most likely with underestimated atmospheric transport and H_2O_2 cloud and precipitation scavenging in the ITCZ and towards the south of the sampled region.

Atmos. Chem. Phys., 23, 5929–5943, 2023
https://doi.org/10.5194/acp-23-5929-2023

Atmospheric Chemistry and Physics
Open Access
EGU

Measurement report: Hydrogen peroxide in the upper tropical troposphere over the Atlantic Ocean and western Africa during the CAFE-Africa aircraft campaign

Zaneta Hamryszczak[1], Dirk Dienhart[1], Bettina Brendel[1], Roland Rohloff[1], Daniel Marno[1], Monica Martinez[1], Hartwig Harder[1], Andrea Pozzer[1,4], Birger Bohn[2], Martin Zöger[3], Jos Lelieveld[1,4], and Horst Fischer[1]

[1]Atmospheric Chemistry Department, Max Planck Institute for Chemistry, 55128 Mainz, Germany
[2]Institute of Energy and Climate Research, IEK-8: Troposphere, Forschungszentrum Jülich GmbH, 52428 Jülich, Germany
[3]Flight Experiments, German Aerospace Center (DLR), 82234 Oberpfaffenhofen, Germany
[4]Climate and Atmosphere Research Center, The Cyprus Institute, Nicosia, 1645, Cyprus

Correspondence: Zaneta Hamryszczak (z.hamryszczak@mpic.de) and Horst Fischer (horst.fischer@mpic.de)

Received: 29 September 2022 – Discussion started: 18 October 2022
Revised: 1 February 2023 – Accepted: 4 May 2023 – Published: 30 May 2023

Abstract. This study focuses on the distribution of hydrogen peroxide (H_2O_2) in the upper tropical troposphere at altitudes between 8 and 15 km based on in situ observations during the Chemistry of the Atmosphere: Field Experiment in Africa (CAFE-Africa) campaign conducted in August–September 2018 over the tropical Atlantic Ocean and western Africa. The measured hydrogen peroxide mixing ratios in the upper troposphere show no clear trend in the latitudinal distribution with locally increased levels (up to 1 ppbv) within the Intertropical Convergence Zone (ITCZ), over the African coastal area, as well as during measurements performed in proximity to the tropical storm Florence (later developing into a hurricane). The observed H_2O_2 distribution suggests that mixing ratios in the upper troposphere seem to be far less dependent on latitude than assumed previously and the corresponding factors influencing the photochemical production and loss of H_2O_2. The observed levels of H_2O_2 in the upper troposphere indicate the influence of convective transport processes on the distribution of the species not only in the tropical but also in the subtropical regions. The measurements are compared to observation-based photostationary steady-state (PSS) calculations and numerical simulations by the global ECHAM/MESSy Atmospheric Chemistry (EMAC) model. North of the ITCZ, PSS calculations produce mostly lower H_2O_2 mixing ratios relative to the observations. The observed mixing ratios tend to exceed the PSS calculations by up to a factor of 2. With the exception of local events, the comparison between the calculated PSS values and the observations indicates enhanced H_2O_2 mixing ratios relative to the expectations based on PSS calculations in the north of the ITCZ. On the other hand, PSS calculations tend to overestimate the H_2O_2 mixing ratios in most of the sampled area in the south of the ITCZ by a factor of up to 3. The significant influence of convection in the ITCZ and the enhanced presence of clouds towards the Southern Hemisphere indicate contributions of atmospheric transport and cloud scavenging in the sampled region.

Simulations performed by the EMAC model also overestimate hydrogen peroxide levels particularly in the Southern Hemisphere, most likely due to underestimated cloud scavenging. EMAC simulations and PSS calculations both indicate a latitudinal gradient from the Equator towards the subtropics. In contrast, the measurements show no clear gradient with latitude in the mixing ratios of H_2O_2 in the upper troposphere with a slight decrease from the ITCZ towards the subtropics, indicating a relatively low dependency on the solar radiation intensity and the corresponding photolytic activity. The largest model deviations relative to the observations correspond with the underestimated hydrogen peroxide loss due to enhanced cloud presence, scavenging, and rainout in the ITCZ and towards the south.

Published by Copernicus Publications on behalf of the European Geosciences Union.

1 Introduction

The key role of hydrogen peroxide in the oxidative chemistry of the troposphere is well acknowledged (Lelieveld and Crutzen, 1990; Crutzen et al., 1999). On the one hand, H_2O_2 serves as a reservoir of HO_x ($OH + HO_2 = HO_x$) species, which are the most prominent oxidants controlling the self-cleansing capacity of the atmosphere (Levy, 1971; Logan et al., 1981; Kleinman, 1991). On the other hand, hydrogen peroxide can oxidize SO_2 and to a minor extent NO_2 and convert them into H_2SO_4 and HNO_3 in clouds, rain, and fog, leading to their acidification (Hoffmann and Edwards, 1975; Penkett et al., 1979; Robbin Martin and Damschen, 1981; Damschen and Martin, 1983; Calvert et al., 1985).

The most prominent pathway leading to H_2O_2 production is the self-reaction of HO_2 radicals (Reaction R4). HO_2 can be formed by many pathways. Under the upper troposphere conditions investigated in this work, HO_2 is mainly formed via reaction of carbon monoxide by OH radicals, which can be formed initially in the photolysis of ozone and the subsequent reaction of O^1D with water vapor (Reactions R1–R3). Moreover, OH can be recycled from HO_2 in reactions with NO or O_3. The budget of H_2O_2 is thus controlled by the steady-state concentration of the HO_2 radicals and the main gas-phase loss processes photolysis and reaction with OH (Reactions R5–R6).

$$O_3 \xrightarrow{h\nu\ (\lambda < 319\,\mathrm{nm})} O_2 + O(^1D), \quad \text{(R1)}$$

$$O(^1D) + H_2O \rightarrow 2OH, \quad \text{(R2)}$$

$$OH + CO + O_2 \rightarrow HO_2 + CO_2, \quad \text{(R3)}$$

$$2HO_2 \rightarrow H_2O_2 + O_2, \quad \text{(R4)}$$

$$H_2O_2 \xrightarrow{h\nu\ (\lambda < 360\,\mathrm{nm})} 2OH, \quad \text{(R5)}$$

$$H_2O_2 + OH \rightarrow HO_2 + H_2O. \quad \text{(R6)}$$

The global distribution of hydrogen peroxides is not only dependent on the chemical composition of the atmosphere but also on meteorological conditions. The amount of hydrogen peroxide is strongly dependent on the availability of water vapor and near-UV radiation (Jacob and Klockow, 1992; Perros, 1993; Slemr and Tremmel, 1994; Snow, 2003; Snow et al., 2007; Klippel et al., 2011). Towards the tropopause as well as towards the poles, the amount of water vapor generally decreases, resulting in a reduced primary production of HO_x radicals. Additionally, with increasing altitudes near-UV radiation and therefore H_2O_2 photolysis increase leading to a pronounced production of OH via H_2O_2 photolysis in R5 (Jaeglé et al., 1997, 2000; Faloona et al., 2000, 2004; Lee et al., 2000). On the other hand, the availability of hydrogen peroxide precursors is diminished with increasing latitude, due to the decreasing inclination of solar radiation and reduced amount of water vapor towards the poles. Physical loss of hydrogen peroxide occurs through deposition processes promoted by its high solubility (Walcek, 1987; Chang et al., 2004; Nguyen et al., 2015). The aqueous uptake and subsequent removal of H_2O_2 strongly depends upon the uptake by aerosols and clouds (O'Sullivan et al., 1999). In effect, based on the availability of the H_2O_2 precursors (OH and hence HO_2) and the corresponding photochemical reactions producing and removing H_2O_2 in the troposphere as well as on the discussed physical processes, the vertical distribution of H_2O_2 often follows an inverted C-shape with decreased mixing ratios within the boundary layer and the upper troposphere and a local maximum in the middle troposphere at altitudes between 2 and 5 km. Additionally, observations in the upper troposphere (UT) (> 8 km) indicate a decreasing trend approximately from the Equator towards the north and south (Daum et al., 1990; Heikes, 1992; O'Sullivan et al., 1996; Weinstein-Lloyd et al., 1998; Snow, 2003; Snow et al., 2007; Klippel et al., 2011).

In general, the global budget of hydrogen peroxide is significantly affected by anthropogenic as well as natural emissions of nitrogen oxides. In urban areas, the formation of hydrogen peroxide is diminished by the increased mixing ratios of NO_x ($NO_x = NO_2 + NO$) derived from anthropogenic sources, as the self-reaction of HO_2 to H_2O_2 is competing with the much faster reaction of HO_2 with NO (Lee et al., 2000; Reeves and Penkett, 2003). In contrast, biomass burning events lead to significant injections of additional hydrogen peroxide through primary as well as secondary chemical production (Lee et al., 1997; Rinsland et al., 2007; Snow et al., 2007; Allen et al., 2022). Finally, convection processes are considered to increase the mixing ratios of hydrogen peroxide in the upper troposphere (Jaeglé et al., 1997, 2000; Klippel et al., 2011; Bozem et al., 2017). Especially within the Intertropical Convergence Zone (ITCZ), convective processes play a key role in the transport of a large suite of trace species to higher tropospheric layers. The ITCZ is a low-pressure region, which marks the meeting zone of air masses transported from both hemispheres and constitutes the ascending branch of the Hadley circulation (Waliser and Gautier, 1993). Due to the high sea surface temperatures, strong solar radiation, and increased air humidity, this band-like area near the Equator is mainly characterized by highly dynamic weather phenomena, namely, large convective cumulonimbus clouds penetrating deep into the upper troposphere (Hastenrath and Lamb, 1977; Waliser and Gautier, 1993). Thus, convective processes are expected to contribute to increased levels of hydrogen peroxide in the upper troposphere and promote elevated HO_x levels via subsequent photochemical processes involving H_2O_2 degradation as well as HCHO production due to efficient HO_x recycling via the reaction with NO produced by lightning during the convective episodes (Jaeglé et al., 1997, 2000; Nussbaumer et al., 2021; Tadic et al., 2021).

Numerous airborne measurements of hydrogen peroxide were performed over the past decades over the Atlantic Ocean and in proximity to the ITCZ. The majority of these studies focused on the troposphere in the Northern Hemisphere, providing an overview on the vertical and latitudinal distribution of hydrogen peroxide.

In September and October 1992, as part of NASA's Global Tropospheric Experiment (GTE) program, the Transport and Atmospheric Chemistry Near the Equatorial Atlantic (TRACE A) mission took place over the Atlantic Ocean. The mean observed mixing ratio of hydrogen peroxide was approximately 0.2 ppbv in the upper troposphere (8–12 km) (Prather and Jacob, 1997; O'Sullivan et al., 1999). During the Subsonic Assessment Ozone and Nitrogen Oxide Experiment (SONEX) campaign, which took place in autumn 1997 over the North Atlantic, mean values of 0.12 ppbv (median: 0.08 ppbv) specifically in the upper troposphere were observed (Snow et al., 2007). Allen et al. (2013) presented satellite-based global distribution data of H_2O_2 in the mid-to-upper troposphere obtained by the Atmospheric Chemistry Experiment (ACE) mission and reported mean levels of 0.10–0.28 ppbv in the upper tropical troposphere (> 8 km), symmetrically decreasing towards the poles. During the Atmospheric Tomography Mission (ATom) campaigns performed in August 2016 (ATom-1), February 2017 (ATom-2), October 2017 (ATom-3), and May 2018 (ATom-4), mean values ranging between 0.09 up to 0.14 ppbv were measured over the mid-Atlantic Ocean (20° S–20° N; Allen et al., 2022; Anonymous referee, 2022). Please note that the average values within the upper troposphere cited here are based on exclusively sampling the ATom data over the tropical Atlantic above 8 km of altitude and do not necessarily match the general results over the entire sampled tropospheric column, as presented in the cited work. Further, Hottmann et al. (2020) deduced mean ($\pm 1\sigma$) and median hydrogen peroxide mixing ratios of 0.17 (± 0.09) and 0.15 ppbv, respectively, during the Oxidation Mechanism Observation (OMO) mission in summer 2015, which took place over the Arabian Peninsula, the eastern Mediterranean, and northern Indian Ocean, covering the marine ITCZ region east of the African continent.

Numerous measurements have been performed in the marine tropical troposphere. In this study, we address the budget of hydrogen peroxide specifically in the upper tropical troposphere within the equatorial Atlantic region with a main focus on the ITCZ. Our objective was to study the distribution of trace gases and radicals over the central Atlantic and the possible impact of convection in the ITCZ on the abundance of H_2O_2 in the upper troposphere.

2 CAFE-Africa campaign

The distribution of hydrogen peroxide (H_2O_2) was measured in the free troposphere over the Atlantic Ocean during the Chemistry of the Atmosphere: Field Experiment in Africa (CAFE-Africa) campaign. The major objective of the mission was to investigate the large-scale distribution of trace gases, radicals, and aerosols in the tropical eastern Atlantic and along the western coast of Africa. In particular, the influence of biomass burning emissions and long-distance pollution transport on the atmosphere's oxidation capacity and the chemical processing of trace gases and aerosols in clean and polluted air masses were studied.

The campaign took place in August and September 2018 during the West African monsoon. During this period, 14 measurement flights were made over the Atlantic Ocean and the African coast with the High Altitude and LOng-range research aircraft (HALO), operating from the international airport on Sal, Cabo Verde (16.75° N, 22.95° W). The flights focused on the upper troposphere up to an altitude of 15 km with a few vertical profiles mostly in the Northern Hemisphere. The investigated area covered a latitudinal and longitudinal range of approximately 10° S–50° N and 50° W–15° E, respectively. The majority of vertical sampling was performed in close proximity to the base of operation and covered the altitudinal range between a few tens of meters above the surface, and the maximal flown altitude (15 km). In sum, 30 takeoff and landings with ascending and descending rates of 900–1100 and 450–650 m min^{-1}, respectively were performed, giving an average descend/ascent rate of 775 m min^{-1} (with 1 point per 1550 m in vertical sampling at an instrument temporal resolution of 2 min). An overview of the corresponding flight dates and the objectives of the individual flights was presented by Tadic et al. (2021). The flight tracks color-coded by GPS flight altitudes are presented in Fig. 1.

Related to the location of the base of operations on Cabo Verde, the majority of the flights was performed in close proximity to the ITCZ, which allowed for the study of tropical trace gases and aerosol distributions in both hemispheres. During the campaign, the ITCZ roughly covered positions between approximately 5 and 15° N (Tadic et al., 2021). Information on the meteorological conditions with special emphasis on the total cloud coverage and convective precipitation located mostly within the ITCZ (5–20° N) is presented in the Supplement of this work (Figs. S1–S3).

3 Methods

3.1 Hydrogen peroxide measurements

Hydroperoxides were measured as the sum of organic hydroperoxides and hydrogen peroxide and were determined using a wet chemical system named the HYdrogen Peroxide and Higher Organic Peroxides monitor (HYPHOP; Klippel et al., 2011; Bozem et al., 2017; Hottmann et al., 2020; Hamryszczak et al., 2022) based on a previous design by Lazrus et al. (1985, 1986). The ambient air was sampled from the top of the aircraft fuselage via a trace gas inlet (TGI) with a 1/2 in. perfluoroalkoxy (PFA) liner that left

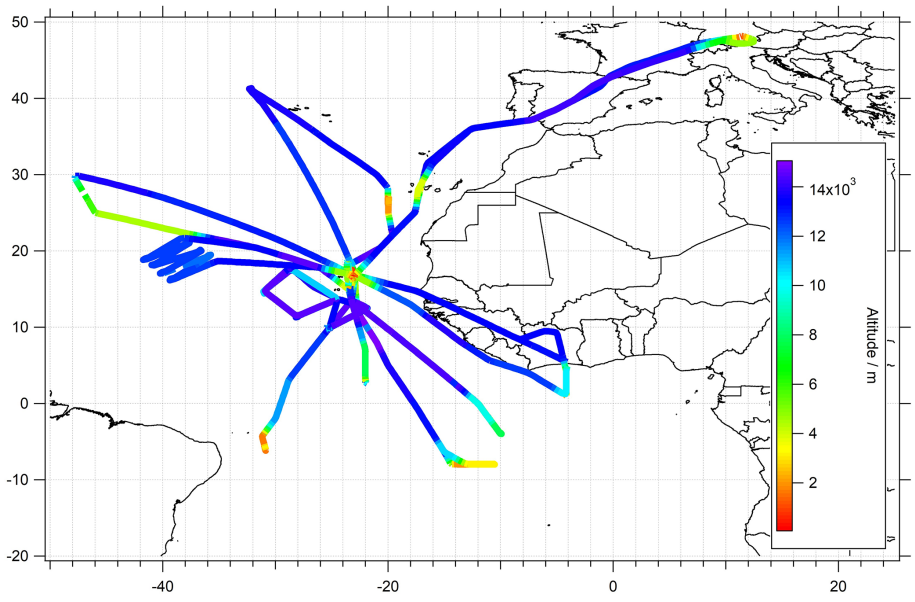

Figure 1. Flight tracks and the sampled region during the CAFE-Africa campaign color-coded by the GPS flight altitude. The majority of flights were performed from the base of operations in Sal, Cabo Verde.

the cabin again through a second exhaust line. From this bypass, a 1/4 in. PFA sampling line was connected to a Teflon-coated membrane pump (type MD 1C; Vacuubrand, Wertheim, Germany) and a pressure control unit, regulating the pump speed to a line pressure of 1000 hPa (constant pressure inlet, CPI). The CPI provides a constant inlet pressure covering external pressure variations between 1000 and 150 hPa. Following the CPI inlet, the ambient air passed through a stripping coil with a buffered sampling solution (potassium hydrogen phthalate / NaOH; pH 6; stripping efficiency of 1 for hydrogen peroxide and between 0.6 and 1 for organic peroxides; Lee et al., 2000). The hydroperoxide solution was sampled in two individual channels in response to addition of *p*-hydroxyphenyl acetic acid (POPHA) and horseradish peroxidase (HRP). The formed chemiluminescent 6,6′- dihydroxy-3,3′-biphenyldiacetic acid was detected via fluorescence spectroscopy using a Cd pen-ray lamp at 326 nm. The hydroperoxide-specific fluorescence (Guilbault et al., 1968) was detected at 400–420 nm using photomultiplier tubes for each channel separately.

Hydrogen peroxide mixing ratios are then calculated from the difference between the entirety of the measured peroxides (channel A) and the sum of organic ROOH hydroperoxides (channel B), where H_2O_2 is selectively destroyed by the addition of catalase. Further information on the mixing ratios of individual organic peroxides cannot be provided by the monitor, due to the characteristics of the measurement technique. Please note that, especially within the boundary layer and due to biomass burning, a variety of organic peroxides might contribute to the total measured signal of organic peroxide (Fels and Junkermann, 1994; Slemr and Tremmel, 1994; Valverde-Canossa et al., 2005; Hua et al., 2008; Dienhart et al., 2023).

Prior to ambient measurements, both channels are simultaneously calibrated using a liquid standard (0.98 µmol L^{-1}) produced from serial dilution of a H_2O_2 stock solution. The H_2O_2 destruction efficiency in channel B corresponding to the added catalase was determined to be 0.95–0.98 based on liquid calibrations. In-flight background measurements were performed using purified zero air, generated by a cartridge with silica gel (type IAC-502; Infiltec, Speyer, Germany) and Hopcalite (type IAC-330; Infiltec, Speyer, Germany). Using a gas-phase calibration source (low-density polyethylene (LDPE) permeation devices), the H_2O_2 transmission efficiency through the inlet ($\pm 1\sigma$) was determined regularly by measuring the difference between the addition of the standard before and after the CPI and was found to be 0.61 ± 0.06. Due to a positive ozone interference, the H_2O_2 data were further corrected by subtraction of 0.056 ppbv H_2O_2 / 100 ppbv O_3 based on a scatter plot of hydrogen peroxide vs. ozone mixing ratios in the lower stratosphere, assuming that ambient H_2O_2 above the tropopause is essentially zero. The total measurement uncertainty (TMU) of the monitor was estimated as

$$\mathrm{TMU} = \sqrt{\left((P)^2 + (\mathrm{US})^2 + (\mathrm{UOI})^2 + (\mathrm{UTE})^2\right)} \quad (1)$$

by considering the instrument's precision (P), uncertainty of the standard (US), uncertainty of the H_2O_2 transmission efficiency (UTE), and the uncertainty of the ozone interference (UOI). The determined precision with 1σ confidence interval was determined from the reproducibility of the liquid calibrations performed during the campaign to be 1.3 % at 5.46 ppbv

for hydrogen peroxide and 0.8 % at 5.64 ppbv for the organic hydroperoxides. The uncertainty of the standard was included in the instrument precision calculation. The uncertainty of the transmission efficiency was calculated to be 6 %. The total measurement uncertainty was determined to be 9 % for hydrogen peroxide and 41 % for the sum of organic hydroperoxides. The total measurement uncertainty of organic hydroperoxides is increased by 40 % due to the varying solubility of individual organic hydroperoxides in aqueous solution, which ranges between 60 % (e.g., methyl hydroperoxide) and 100 % (e.g., peroxyacetic acid). The instrumental time resolution was determined to be 122 s based on the calibration signal rise and fall time from 10 % to 90 % and 90 % to 10 %, respectively. The detection limit with a 2σ confidence was derived from the reproducibility of the in-flight background measurements as 15 pptv for hydrogen peroxide and 6 pptv for the sum of organic hydroperoxides, respectively. For the purposes of this study, hydrogen peroxide data were filtered for stratospheric influences by removing all data points with ozone mixing ratios higher than 100 ppbv.

3.2 Measurement of other relevant species

GPS altitude and coordinates, temperature, pressure, and wind speed were obtained using the BAsic HALO Measurement And Sensor System, BAHAMAS. Water vapor mixing ratios and the corresponding air humidity were measured with the Sophisticated Hygrometer for Atmospheric ResearCh (SHARC) based on a tunable diode laser (TDL) setup (Krautstrunk and Giez, 2012). HO_x radicals were measured by laser-induced fluorescence with the HydrOxyl Radical measurement Unit based on fluorescence Spectroscopy (HORUS; Marno et al., 2020). Spectrally resolved upward and downward actinic flux density was obtained with two spectroradiometers (Bohn and Lohse, 2017). A brief overview of the campaign instrumentation, measurement methods, their TMU values, and the corresponding technical references are listed in Table 1.

3.3 ECHAM/MESSy Atmospheric Chemistry (EMAC)

For the purposes of this study, the in situ observations are compared to numerical simulations from the global chemistry and climate 3-D model EMAC (ECHAM/MESSy Atmospheric Chemistry; Jöckel et al., 2010). The model numerically simulates the chemistry and dynamics of the troposphere and stratosphere using a large variety of submodels describing chemical and meteorological processes and the influences arising from anthropogenic and natural emissions from continental and marine environments (Jöckel et al., 2006). The basis of the atmospheric model is the fifth generation of the European Centre HAMburg general circulation model (ECHAM5; Roeckner et al., 2003, 2006). The communication between the various submodels is achieved by the Modular Earth Submodel System (MESSy; Jöckel et al., 2005, 2010, 2016). Atmospheric chemistry is simulated by the Module for Efficiently Calculating the Chemistry of the Atmosphere (MECCA) submodel (Sander et al., 2005, 2011, 2019), using the Mainz Organic Mechanism (MOM) and photolysis rate calculations from a radiation transfer model (Sander et al., 2014, 2019). Primary emissions and dry deposition as well as aqueous-phase chemistry in clouds and cloud scavenging are simulated by the ONLEM, OFFLEM, TNUDGE, and DRYDEP submodels (Kerkweg et al., 2006a, b), as well as the scavenging of tracers submodel (SCAV; Tost et al., 2006). Anthropogenic emissions are based on the EDGARv4.3.2 inventory (European Joint Center, JRC; Crippa et al., 2018) and are distributed vertically according to Pozzer et al. (2009). Biomass burning emissions were simulated based on the Global Fire Assimilation System (GFAS; Kaiser et al., 2012). The model has a vertical resolution of 47 vertical levels up to 0.01 hPa, a horizontal resolution of T63 (i.e., approximately $1.8° \times 1.8°$), and a time resolution of 6 min. The model was further weakly nudged towards the ECMWF ERA-Interim data (Tadic et al., 2021). This model setup has been extensively evaluated for different trace gases and aerosols (Pozzer et al., 2022). For comparison to observations, the simulation results were interpolated on the GPS flight tracks using the S4D submodel (Jöckel et al., 2010).

3.4 Simulations based on photostationary steady-state conditions

The hydrogen peroxide mixing ratios in the upper troposphere under the assumption of photostationary steady-state conditions were calculated based on measured precursors and photochemical loss processes of hydrogen peroxide (HO_2, OH, $j(H_2O_2)$) and the rate coefficient data from Atkinson et al. (2004).

In the upper troposphere, the production rate $P(H_2O_2)$ of hydrogen peroxide due to the self-reaction of HO_2 can be calculated from Eq. (2). The photochemical loss rate of hydrogen peroxide, $L(H_2O_2)$, can be derived from H_2O_2 photolysis and the reaction with OH as shown in Eq. (3). The equations are derived from the reaction pathways presented in Sect. 1 (Reactions R4–R6).

$$P(H_2O_2) = k_{HO_2+HO_2} \cdot [HO_2]^2, \quad (2)$$

$$L(H_2O_2) = \left(k_{H_2O_2+OH} \cdot [OH] + j(H_2O_2)\right) \cdot [H_2O_2]. \quad (3)$$

The calculations of the rate coefficients were based on the measured parameters along the flight tracks according to Atkinson et al., 2004 (Eqs. 4–5). Due to the water dependence of the hydrogen peroxide production rate coefficient, both expressions in Eq. (4) were further extended by the factor $1 + 1.4 \times 10^{-21}\ cm^3\ [H_2O] \exp(2200/T)$.

Table 1. Overview of observed species with corresponding measurement method, total measurement uncertainty (TMU), and references regarding the instrumentation.

Measurement	Method	TMU	References
H_2O_2	Chemiluminescence	H_2O_2: 9 %; ROOH: 41 %	Hamryszczak et al. (2022)
HO_x	Laser-induced fluorescence (LIF; additional chem. conversion for HO_2)	50 %	Marno et al. (2020)
Actinic flux density	Spectroradiometer	7 %–8 % (15 % for $j(H_2O_2)$)	Bohn and Lohse (2017)
H_2O	TDL	5 %	Krautstrunk and Giez (2012)

$$k_{HO_2+HO_2} = 2.2 \times 10^{-13} \cdot \exp^{\frac{600}{T}} \mathrm{cm^3\,s^{-1}} + 1.9 \times 10^{-33}[N_2] \cdot \exp^{\frac{980}{T}} \mathrm{cm^6\,s^{-1}}, \quad (4)$$

$$k_{H_2O_2+OH} = 2.9 \times 10^{-12} \cdot \exp^{\frac{-160}{T}} \mathrm{cm^3\,s^{-1}}. \quad (5)$$

Neglecting deposition and transport processes impacting the hydrogen peroxide budget, the mixing ratio of H_2O_2 was calculated via Eq. (6).

$$[H_2O_2]^{PSS} = \frac{[HO_2]^2 \cdot k_{HO_2+HO_2}}{[OH] \cdot k_{H_2O_2+OH} + j\,(H_2O_2)} \quad (6)$$

3.5 Data processing details

For the purpose of the present study, we used measured H_2O_2, OH, HO_2, water vapor, $j(H_2O_2)$, temperature, and pressure and compared these with the concurrent spatially interpolated EMAC simulations. To synchronize the time resolution of the simulated data with the measurement output, we calculated a mean of the measurement data with a matching temporal resolution of 6 min (equivalent to model output).

Vertical profiles of all species under investigation were calculated as 1000 m bins (means and medians) over the entire sampled atmospheric column. Profile information is restricted to 30 takeoffs and landings at Sal, while other areas are not considered due to a lack of statistically significant data.

The spatially resolved data based on measurements, photostationary steady-state (PSS) model calculations, and EMAC simulations were binned into 1° × 1° subsets over the full extension of the flight tracks in the upper troposphere (≥ 8 km).

The latitudinal distribution of the species was examined using 2.5° bins over the upper tropospheric region. Please note that due to a reduced amount of data in the lower troposphere, the analysis of spatial and latitudinal distributions was restricted to measurements performed in the upper troposphere.

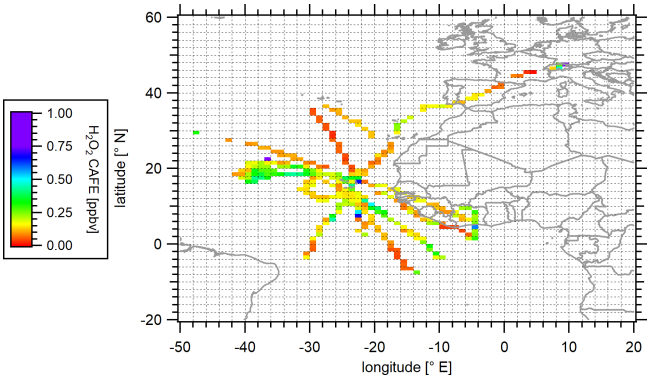

Figure 2. Spatial distribution of measured hydrogen peroxide in the upper troposphere (≥ 8 km) during the CAFE-Africa campaign. Data were binned into 1° × 1° bins over the full extension of the flight tracks.

4 Results

4.1 Observations of hydrogen peroxide during CAFE-Africa and previous airborne measurements

The observed mixing ratios of hydrogen peroxide during the CAFE-Africa campaign are presented as a latitude vs. longitude plot with mean mixing ratio values binned into a subset of 1° × 1° bins for the entirety of the upper troposphere (≥ 8 km) along the flight tracks (Fig. 2). The color scale represents the measured mixing ratio of H_2O_2.

The mean ($\pm 1\sigma$) and median mixing ratios based on all measured H_2O_2 mixing ratios during the campaign were 0.18 (±0.13) and 0.15 ppbv, respectively, with maximum hydrogen peroxide mixing ratios reaching 1.03 ppbv. Slightly higher H_2O_2 levels were observed in the ITCZ (approx. 5–20° N), where locally mixing ratios up to 0.67 ppbv over a 1° × 1° bin of merged data were observed. These maxima are most likely due to atmospheric transport of H_2O_2 into the upper troposphere. This is in accordance with previous reports about increased hydrogen peroxide mixing ratios due to biomass burning and convective activity, elevating the H_2O_2 mixing ratios in the upper troposphere (Lee et al., 1998; O'Sullivan et al., 1999; Allen et al., 2022). Locally en-

Table 2. Comparison of hydrogen peroxide mean and median mixing ratios (ppbv) in the upper troposphere during CAFE-Africa with measurements from previous campaigns (TRACE A, SONEX, OMO, ATom-1, and ATom-3; O'Sullivan et al., 1999; Snow et al., 2007; Hottmann et al., 2020; Allen et al., 2022).

	CAFE-Africa	TRACE A	SONEX	OMO	ATom-1		ATom-3	
	10° S–40° N	40° S–15° N	15–60° N	0–50° N	20–60° N	20° S–20° N	20–60° N	20° S–20° N
Mean	0.18	< 0.20	0.12	0.16	0.55	0.61	0.18	0.40
Median	0.15	0.15	0.08	0.15	0.29	0.27	0.12	0.20

hanced H_2O_2 was further observed during the measurement flight in close proximity to the tropical storm Florence on 2 September 2018 (approx. 18° N, 38.5° W). Here, the mean mixing ratios were between 0.10 and 0.43 ppbv with a maximum of up to 0.94 ppbv. Based on the high convective activity during the tropical storm, as reported by Nussbaumer et al. (2021), the H_2O_2 mixing ratios were expected to rise due to the rapid transport of air masses from the marine boundary layer (MBL) into the UT. Table 2 gives an overview of the estimated mean and median hydrogen peroxide mixing ratios measured during CAFE-Africa in relation to previous airborne measurements performed at a comparable latitudinal range.

The mean and median values during CAFE-Africa are comparable to previously reported mixing ratios during TRACE A and OMO campaigns, which covered a comparable latitude and altitude range (Table 2). Enhanced mixing ratios for CAFE-Africa relative to observations during the SONEX campaign are most likely due to differences in the examined regional range, since the latter campaign focused on the north Atlantic. Mean and median values in the Northern Hemisphere (20–40° N; Table S1) during CAFE-Africa (0.14 ± 0.11 and 0.12 ppbv, respectively) are comparable to observations during SONEX. During the ATom campaigns, slightly higher mean values were observed, although median values are comparable. This could be due to differences in the sampled altitudes, since ATom measurements were generally restricted to altitudes below 12 km.

Based on the comparison with previous studies, the observed mixing ratios of hydrogen peroxide during CAFE-Africa fit well into the general range of recent studies over the equatorial and subtropical Atlantic. The observed H_2O_2 distribution confirms further that mixing ratios of hydrogen peroxide in the upper troposphere seem to be far less dependent on latitude than those at lower altitudes. The latitudinal distribution of H_2O_2 during CAFE-Africa displays a rather small symmetrical latitudinal decrease between the inner tropics and the subtropics.

4.2 Comparison of measured hydrogen peroxide with photostationary steady-state and EMAC calculations

In order to investigate the impact of deep convection in the ITCZ on the H_2O_2 budget in the upper troposphere, a comparison of the in situ data with the output of photostationary steady-state (achieved) calculations and EMAC simulations was performed. The complementary spatial distributions of the hydrogen peroxide levels were expressed as latitude versus longitude plots of mean mixing ratios aggregated over a spatial grid of $1° \times 1°$ in the upper troposphere (≥ 8 km) (Fig. S4 in the Supplement).

The calculated PSS-H_2O_2 levels range between approximately 0.01 and 0.88 ppbv with mean ($\pm 1\sigma$) and median mixing ratios of 0.14 (± 0.16) and 0.07 ppbv, respectively, which is a factor of 1.3 lower than the observations. PSS-based H_2O_2 mixing ratios tend to be higher at the southernmost coastal area (2.5° S, 10.5° W), where the levels range between 0.40 and 0.88 ppbv, and in proximity to the tropical storm Florence at up to 0.40 ppbv (approx. 18° N, 38.5° W). Hydrogen peroxide mixing ratios simulated by EMAC vary between 0.10 and 0.75 ppbv. The mean ($\pm 1\sigma$) and median simulated mixing ratios are 0.30 (± 0.19) and 0.29 ppbv, respectively, with maximum mixing ratios up to 1.04 ppbv (3.5° S, 9.5° W; Fig. S4b), which is slightly higher than the observations. The spatial distributions of the point-by-point ratio between PSS calculations and EMAC simulations versus the observations in the upper troposphere above 8 km are presented in Fig. 3, which gives an overview of the local differences relative to the observations varying from low ratios (yellow) to high (deep blue) values. Please note that for resolution purposes the color scaling is restricted to ratios up to 4.5.

Generally, the H_2O_2 (EMAC) / H_2O_2 (measurement) ratios indicate better agreement between the simulations and the measurements in the Northern Hemisphere ($\geq 20°$ N; Fig. 3b). With decreasing latitude, the model tends to significantly overestimate hydrogen peroxide; H_2O_2 (EMAC) / H_2O_2 (measurement) ratios are increasing from approximately 2 to 4 with decreasing latitude. Locally, most likely due to underestimated cloud scavenging as will be further discussed in this work, EMAC simulates highly elevated

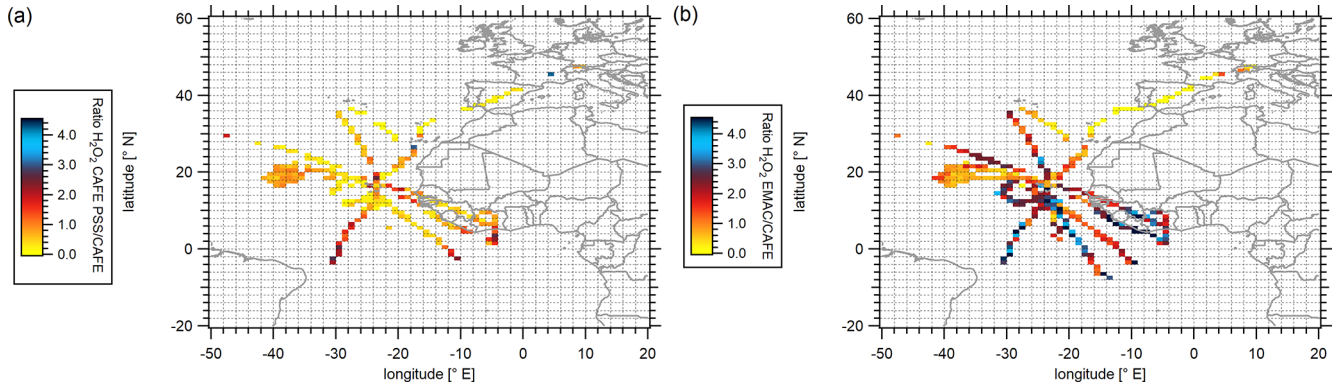

Figure 3. Spatial distribution of H_2O_2 (PSS) / H_2O_2 (measurements) ratios **(a)** and H_2O_2 (EMAC) / H_2O_2 (measurements) ratios **(b)** in the upper troposphere ($\geq$ 8 km) during the CAFE-Africa campaign. Data were binned into 1° × 1° bins over the full extension of the flight tracks.

hydrogen peroxide with a factor of up to 14 higher than the measurements (4.5° N, 9.5° W).

Good agreement between the observation-based PSS calculations and the measurements was found in proximity to the tropical storm Florence. Here, the H_2O_2 (PSS) / H_2O_2 (measurement) ratios agree between 0.83 and 1.04. Beyond the measurements taken here, the agreement with respect to the measured hydrogen peroxide levels is generally less satisfactory. Towards the southern subtropics as well as locally in the coastal area and at the base of operations in Sal (Cabo Verde), the ratios increase to 2.8, indicating an overestimation of the hydroperoxide levels relative to the observations, similar to the EMAC simulations. On the other hand, the PSS calculations tend to strongly underestimate hydrogen peroxide concentrations in the ITCZ (5–20° N) and in the northern part of the investigated region ($\geq$ 20° N) by factors of up to 10 and 12, respectively. This indicates that, since the local photostationary steady-state conditions based on observed radical levels do not account for additional sources and sinks of the H_2O_2, the observed discrepancy between the observations and local PSS are most likely related to transport and cloud scavenging. The calculated difference between production (Eq. 2) and loss (Eq. 3) of hydrogen peroxide, (P–L)H_2O_2 based on the observations is expressed as a latitude vs. longitude plot with mean mixing ratios binned into a subset of 1° × 1° bins for the entirety of the upper troposphere ($\geq$ 8 km) along the flight tracks (Fig. 4).

Generally, the majority of the sampled region is dominated by loss, especially in the ITCZ (approx. 5–20° N) and towards the north, where an H_2O_2 deficit of up to approximately -0.01 ppbv h^{-1} was determined. H_2O_2 production-dominated regions of up to 0.03 ppbv h^{-1} are observed towards the south and in the coastal area. The difference between the photochemical production and loss paths is directly linked to the deviations from the photostationary steady state and thus to the additional sources and sinks of hydrogen peroxide on a local scale. These are associated with the local

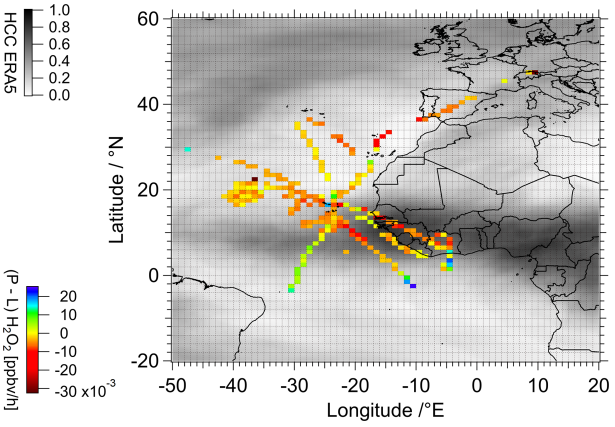

Figure 4. Color-coded spatial resolution of calculated deviation from PSS based on the difference between the observed hydrogen peroxide photochemical production and loss. The calculated data were binned into 1° × 1° bins over the full extension of the flight tracks. Shaded background is the average high cloud coverage (HCC) ($\geq$ 6 km) during the measurement period based on ERA5 reanalysis results (Hersbach et al., 2019).

meteorological conditions and transport processes. Based on ERA5 reanalysis results, especially towards the south and in the coastal area, an enhanced presence of clouds at altitudes above 6 km (gray shading in Fig. 4) and convective precipitation were observed during the measurement period (Hersbach et al., 2019). At a mean ($\pm 1\sigma$) horizontal wind speed of 14.3 ($\pm$7.3) m s^{-1} measured along the flight tracks and a species lifetime of 3–4 d, transport towards the subtropics impacts H_2O_2 levels and further justifies the difference between the local PSS calculations and the observations.

Based on the coincidence with the latitudinal range of the ITCZ, the enhanced loss in the H_2O_2 budget relative to the PSS in the upper troposphere is most likely due to convective injection of H_2O_2 from lower layers into the upper troposphere and the subsequent redistribution of the species to-

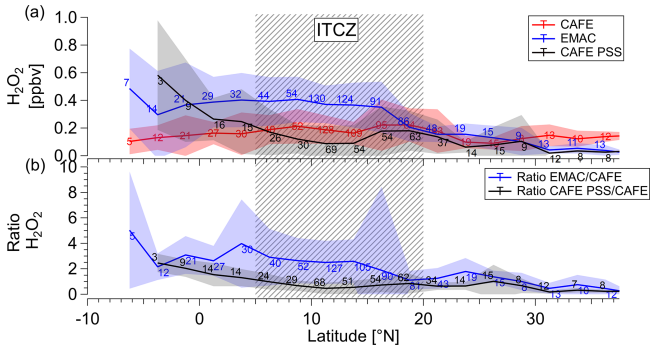

Figure 5. Latitudinal dependence of hydrogen peroxide mixing ratios (mean $\pm 1\sigma$) compared to EMAC simulations and calculations based on PSS (red: CAFE-Africa; black: PSS CAFE-Africa; blue: EMAC; **a**) and calculated ratios between the simulations and the observations and PSS-modeled calculations, and the observations, respectively **(b)**. The data with 6 min time resolution and mean values were binned for 2.5° of latitude for altitudes ≥ 8 km. The corresponding numbers indicate the total number of data points per bin. The shaded pattern marks the ITCZ region.

wards the north and south. Below, we show that, based on the comparison with EMAC simulation output, convective transport is important for the budget of hydrogen peroxide in the upper troposphere not only in the ITCZ but also in the subtropics.

As discussed above, the comparison between observations and both PSS calculations and EMAC simulations indicate large deviations at the most southern latitudes that were visited by HALO. This is clearly demonstrated in Fig. 5, which shows observations, PSS calculations, and EMAC simulations of H_2O_2 as functions of latitude in the upper troposphere (above 8 km). The mean values of each dataset with 6 min time resolution are binned into subsets of 2.5° of latitude for the investigated region from 6° S to 40° N. The lines and the complementary shading represent mean values and the supplementary standard deviations. The area of the ITCZ between 5 and 20° N is highlighted by gray shading.

Contrary to the calculations based on local photostationary steady-state conditions and the simulations by EMAC, the observations show very little latitudinal variation with mean values of approximately 0.1–0.2 ppbv. A tendency towards slightly enhanced values is observed in the ITCZ, where the mixing ratios increase up to 0.22 ppbv. However, considering the standard deviation range (up to 0.19 ppbv), the rather flat distribution in the upper troposphere indicates nearly constant hydrogen peroxide levels throughout the whole investigated tropospheric region (see also Table S1).

Both the EMAC-simulated and PSS-calculated latitudinal hydrogen peroxide distributions display decreasing trends with increasing latitudes towards the north. The highest mean values of 0.49 ($\pm$0.29) ppbv for PSS and 0.583 ($\pm$0.40) ppbv for EMAC are found in the southernmost part of the sampled region. The elevated levels of H_2O_2 in the EMAC simulations starts already in the ITCZ, while the PSS calculations only increase south of 5° N.

Overall H_2O_2 mixing ratios from the PSS calculations show a decreasing tendency from the Equator towards the subtropics. At approximately 5° N, the PSS-based mixing ratios decrease from 0.09 to 0.25 ppbv and tend to be lower than the measured levels at the northern part of the domain by a factor of up to 5. In contrast, the mixing ratios of hydrogen peroxide simulated by EMAC remain elevated from 6° S to 15° N (0.30 to 0.35 ppbv), yielding H_2O_2 (EMAC) / H_2O_2 (measurements) ratios of 2.2 to 2.5. Further north of 15° N, the H_2O_2 levels in EMAC decrease by almost half to 0.15 ppbv, resulting in H_2O_2 (EMAC) / H_2O_2 (measurements) ratios between 1.1 and 1.2 and a rather good agreement between simulations and observations. An overview of numerical values for measured means ($\pm 1\sigma$) as well as medians and PSS-calculated and EMAC-simulated hydrogen peroxide levels subdivided into three hemispheric regions – the Northern Hemisphere (20–40° N), ITCZ (5 < 20° N), and Southern Hemisphere (10° S < 5° N) – is given in Table S1 in the Supplement.

Please note that the steady-state calculations only account for photochemical production and loss of hydrogen peroxide. EMAC simulations additionally account for vertical and horizontal transport processes, as well as local losses due to cloud scavenging (Hamryszczak et al., 2022). Thus, deviations between local photostationary steady-state budget calculations and EMAC simulations can indicate the impact of convective processes in the ITCZ in the upper troposphere. This requires that the EMAC model correctly simulates precursors (HO_2) and sinks (OH, H_2O_2 photolysis) of photochemical H_2O_2 formation.

A comparison between observations and EMAC simulations for the basic species reveals that while HO_2 is adequately reproduced by EMAC the simulations tend to underestimate OH and the photolysis frequencies in particular, south of 15° N (Fig. S5b). At the same time, model results partly tend to overestimate HO_2, indicating issues with HO_2 / OH partitioning. Since the production of OH in the UT depends to an extent on the reaction of HO_2 with NO, these might be associated with the underestimation of NO by EMAC in the southern part of the domain, as shown by Tadic et al. (2021). Additionally, the measured H_2O_2 photolysis frequencies show minor discrepancies with those from the model (Fig. S5c). Due to the overestimated HO_2 mixing ratios, EMAC simulates higher levels of H_2O_2. At the same time, the lower OH mixing ratios and the underestimated H_2O_2 photolysis frequencies might cause decreased loss rates, thus leading to underestimation of the H_2O_2 loss pathways. Therefore, overestimation of the photochemical source and underestimation of the photochemical H_2O_2 sinks by EMAC explain the differences between PSS calculations and simulations at southern latitudes; however, these observations do not explain the differences relative to the observations south of the ITCZ. Also, it is highly unlikely that

a measurement error is responsible for the discrepancies, as this would have to be restricted to the most southerly latitudes.

Potential causes leading to the discrepancy between the measurement and the simulations might be an underestimation of cloud scavenging and removal of hydrogen peroxide by wet deposition processes within the ITCZ and also further south. A number of flights south of 15° N were performed in close proximity to the western shores of Africa and also even over land (Fig. 2), close to enhanced convective precipitation (Fig. S3). Based on the ERA5 reanalysis results on cloud coverage during the measurement period (Hersbach et al., 2019; Fig. S2), we hypothesize that the air masses sampled in this area were affected by cloud processing especially in the UT, causing the model discrepancies.

Since H_2O_2 in the upper atmosphere is influenced by convective transport from the lower troposphere as well as by losses to clouds and rainout, it is important that EMAC simulations and PSS calculations reproduce the levels of hydrogen peroxide in the middle troposphere and the boundary layer. In Fig. 6, averages of hydrogen peroxide mixing ratios based on in situ observations, PSS calculations, and EMAC simulations and the corresponding H_2O_2 (EMAC) / H_2O_2 (measurements) and H_2O_2 (PSS) / H_2O_2 (measurements) ratios are shown. The data are binned into subsets of 1 km of altitude with respect to the center of the bin width based on takeoff and landings in proximity to the base of operations in Sal, Cabo Verde. The lines and the shadings represent mean values and the 1σ standard deviations. Dashed lines represent median values.

In general, the observed, PSS-calculated, and EMAC-simulated vertical profiles of hydrogen peroxide follow the expected trend throughout the troposphere (Fig. 6a–b). The lowest hydrogen peroxide mixing ratios of 0.141 ppbv were measured in the upper troposphere, where the availability of the H_2O_2 precursor HO_2 is limited due to low water vapor concentrations. The highest mean values ($\pm 1\sigma$) of 2.44 ($\pm$0.78) ppbv were measured directly above the boundary layer (2–5 km) in the free troposphere. Below 2 km, the levels of observed H_2O_2 decrease to 1.7 ($\pm$1.1) ppbv, reflecting the impact of deposition processes on H_2O_2 in the boundary layer in proximity to Cabo Verde. Based on the good agreement of the observed vertical distribution with the expected trend as well as logbook reports, the presence of clouds and their subsequent scavenging is assumed to have a minor impact on the local budget of the species.

A good agreement between the measured and EMAC-simulated datasets with a H_2O_2 (EMAC) / H_2O_2 (measurement) ratio of approximately 1 was found in the lower troposphere (2–6 km; Fig. 6c). Model results tend to overestimate hydrogen peroxide in the boundary layer, which might be due to the model resolution (1.8° × 1.8°) and the corresponding restrictions in resolving small-scale variations in hydrogen peroxide deposition processes in proximity to the base of operations on the island. The vertical profiles of the observations and the model show that the differences arise mainly in the upper troposphere, with increased ratios of simulated vs. measured H_2O_2 of up to a factor 5.6 at 12 km altitude, which might indicate convective outflow in the model. Vertical profiles of observed and simulated HO_2, OH, and H_2O_2 photolysis rates are in excellent agreement (Fig. S6), indicating that the model accurately simulates photochemical processes throughout the troposphere, so the remaining differences for H_2O_2 are most likely caused by physical processes (e.g., deposition and transport).

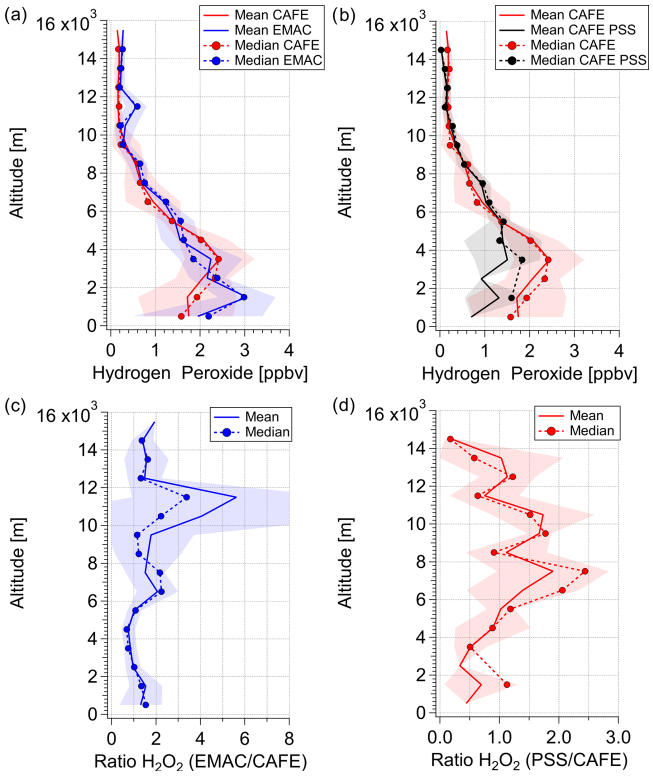

Figure 6. Vertical profiles of observed (red), simulated (blue), and calculated based on the PSS assumption (black) hydrogen peroxide means and medians **(a–b)** and vertical profiles of mean and median H_2O_2 (EMAC) / H_2O_2 (measurements) and H_2O_2 (PSS) / H_2O_2 (measurements) ratios **(c–d)**. Vertical profile estimations were calculated within 1 km means and medians over the atmospheric column based on the data obtained in the region in proximity to the base of operations in Sal, Cabo Verde (approx. 16°35′–16°51′ N; 22°52′–23° W).

The comparison of measured and PSS-calculated H_2O_2 vertical profiles indicates a missing source or an overestimated sink below altitudes of 5 km (Fig. 6b). Here, the PSS-calculated hydrogen peroxide levels fall short by about 1 ppbv at altitudes below 4 km, yielding H_2O_2 (PSS) / H_2O_2 (measured) ratios smaller than unity at these altitudes (Fig. 6d). The absolute difference between the measured and calculated mixing ratios seems to be very prominent in and directly above the boundary layer (< 5 km) and can be asso-

ciated with air masses affected by Saharan dust, which was often sampled during takeoff and landings at Sal. Heterogeneous loss of HO_2 on desert dust particles, while modest, is expected to lower the production of H_2O_2 (de Reus et al., 2005). Thus, local mixing ratios of HO_2 could be affected by heterogeneous loss, while PSS is not yet achieved (Fig. S7).

In order to investigate the extent of the potential hydrogen peroxide injection into the upper troposphere, we calculate excess hydrogen peroxide mixing ratios as the difference between the observed and the corresponding H_2O_2 based on PSS. Analogously, potential excess of H_2O_2 using model-simulated data was determined. The spatial distribution of the calculated excess H_2O_2 mixing ratios in the upper troposphere is presented in Fig. 7 as latitude vs. longitude plots of mean hydrogen peroxide levels aggregated over a spatial $1° \times 1°$ grid at altitudes above 8 km. The color scale represents the average excess mixing ratios determined for the species (in pptv).

The H_2O_2 observations exceed the calculated values based on PSS mostly in the range of 70 to 110 pptv with the exception of the values derived in the Southern Hemisphere. Highest deviations were derived in the ITCZ and reach up to 310 pptv at their maximum. The excess mixing ratios show a clear trend with the most impactful injection events in the ITCZ region (5–15° N), where convective transport is expected (Waliser and Gautier, 1993; Fontaine et al., 2011). From there, a subsequent redistribution of hydrogen peroxide towards the Northern Hemisphere and Southern Hemispheres occurs, which agrees well with the decreasing gradient towards the north and south. EMAC simulates exceeding H_2O_2 mixing ratios mostly in the range of 20 to 150 pptv, with maximum excess up to 240 pptv in the ITCZ (12.5° N, 25.5° W; Fig. 7b). EMAC reproduces the transport rates to a lower extent in the ITCZ, but local convective events such as those occurring within tropical storm Florence and above the African coast are not simulated by the model. In contrast, no significant excess of H_2O_2 was determined at 1.5° N, 4.5° W.

The calculated absolute difference between the measured and the PSS-calculated H_2O_2 in the upper troposphere displays an average excess of 44 (±120) pptv hydrogen peroxide over the entire region relative to the PSS-modeled conditions. In comparison, injections based on EMAC simulations show about 60 % lower values of 18 (±120) pptv. The mixing ratios of the H_2O_2 measurements below 4 km at Sal were in the range of 1.7–2.4 ppbv, which would contribute with up to 1.8 %–2.6 % of H_2O_2 in the outflow, assuming potential inflow below 4 km. A similar calculation based solely on EMAC data indicates a contribution of 0.6 %–0.8 % within the model (based on EMAC mixing ratios of 2.1–3.0 ppbv). Thus, although EMAC reproduces potential transport processes from the lower troposphere, the discrepancy in the transmission efficiencies indicates a smaller contribution to the simulated hydrogen peroxide levels. Consequently, the enhanced hydrogen peroxide mixing ratios cannot be justified exclusively by photochemical reactions within the upper troposphere. Additional injections from the lower troposphere via convective transport and the subsequent redistribution towards the subtropics have to be considered.

5 Conclusions

Hydrogen peroxide was measured during the CAFE-Africa campaign over the tropical Atlantic and western Africa in the upper troposphere (above 8 km). Generally, the measured levels of hydrogen peroxide in the upper troposphere fit well to the previously observed H_2O_2 at latitudes 10° S–40° N. At high altitudes, a minor symmetrical decrease from the ITCZ towards northern and southern latitudes was observed, which deviates from previously reported observations in the upper troposphere. According to previous reports, the H_2O_2 mixing ratios are expected to be elevated in the equatorial upper troposphere due to biomass burning and atmospheric transport. However, the H_2O_2 mixing ratios measured during the CAFE-Africa campaign show only very little latitudinal variation over the Atlantic with a shift of the maximum mixing ratios towards the ITCZ. The measured hydrogen peroxide mixing ratios show a rather uniform distribution with peak events in the ITCZ and over the African coast, indicating the influence of convective transport processes on the distribution of hydrogen peroxide in the upper troposphere.

Whilst the observations of hydrogen peroxide are in good general agreement with the range of previous observations performed in the upper troposphere, the measured H_2O_2 mixing ratios deviate from the PSS calculations based on OH and HO_2 measurements and the simulations performed by EMAC. The local PSS calculations significantly underestimate the H_2O_2 mixing ratios in the north of the sampled region. There, the comparison of the H_2O_2 measurements with PSS calculations reveals a large impact of vertical transport within the ITCZ and the associated redistribution in the upper troposphere on the spatial distribution of hydrogen peroxide. Further, the enhanced presence of clouds in the ITCZ and towards the Southern Hemisphere indicates significant cloud scavenging in the sampled region, justifying the deviations to the local photostationary steady-state calculations, which only account for photochemical sources and sinks of H_2O_2. The EMAC simulations of H_2O_2, HO_2, and OH agree with the observations in the lower tropospheric layers. An overestimation of model results compared with the observations of hydrogen peroxide mixing ratios due to inaccuracies in cloud scavenging was observed in the upper troposphere towards the Southern Hemisphere. Based on our calculations, the model simulates only partially the impacts of atmospheric transport on the H_2O_2 budget. In fact, the calculated excess hydrogen peroxide mixing ratios based on EMAC are lower compared to those based on the PSS calculations by approximately 60 %. The comparison between the EMAC- and PSS-calculated data versus measured hydrogen peroxide confirms that convective transport and consequent redistribution most

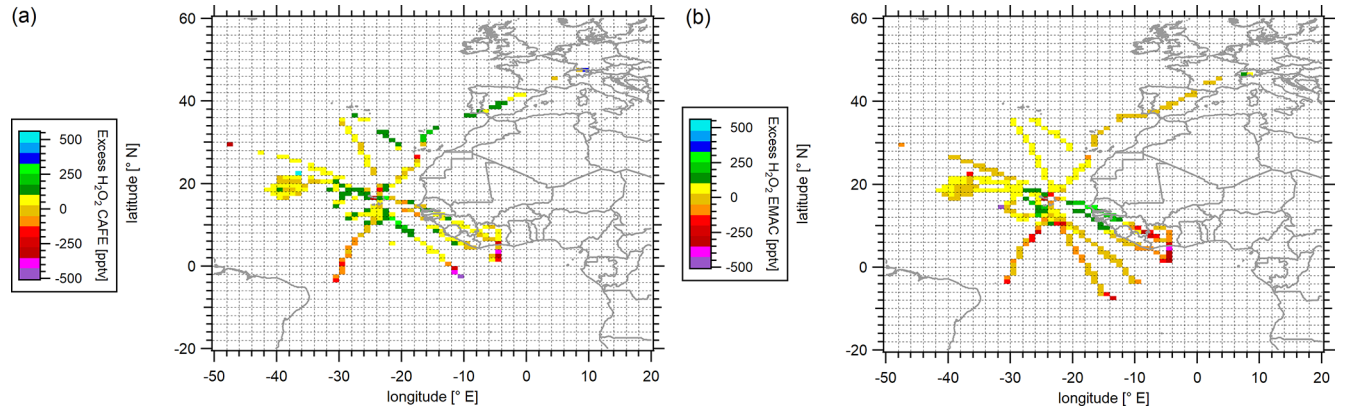

Figure 7. Color-coded spatial resolution of calculated H_2O_2 excess based on the difference between the observations and PSS-based calculations **(a)** and EMAC simulations and calculations at steady state based on the EMAC data output **(b)**. Data were binned into $1° \times 1°$ bins over the full extension of the flight tracks.

likely by northerly and southerly winds towards the subtropics has a significant impact on H_2O_2. This redistribution alters the spatial distribution of H_2O_2 towards more uniform mixing ratios in the marine tropical upper troposphere than would be expected based exclusively on photochemical production and loss processes in the UT.

Data availability. All CAFE-Africa datasets used in this study are stored at https://doi.org/10.5281/zenodo.7845890 (Hamryszczak et al., 2023).

Supplement. The supplement related to this article is available online at: https://doi.org/10.5194/acp-23-5929-2023-supplement.

Author contributions. JL and HF planned the campaign; DD, BBr, RR, DM, MM, HH, and BBo performed the measurements; ZH and HF designed the study; ZH, DD, RR, BBo, and MZ processed and analyzed the data; AP developed the model code and performed the simulation; ZH wrote the manuscript draft with contributions of all co-authors.

Competing interests. At least one of the (co-)authors is a member of the editorial board of *Atmospheric Chemistry and Physics*. The authors have no other competing interests to declare.

Disclaimer. Publisher's note: Copernicus Publications remains neutral with regard to jurisdictional claims in published maps and institutional affiliations.

Special issue statement. This article is part of the special issue "The Modular Earth Submodel System (MESSy) (ACP/GMD interjournal SI)". It is not associated with a conference.

Acknowledgements. The authors are very grateful to the CAFE-Africa team, Forschungszentrum Jülich, Karlsruhe Institute of Technology, and Deutsches Zentrum für Luft- und Raumfahrt (DLR) in Oberpfaffenhofen for their great support. Their work was essential for the project.

Financial support. The article processing charges for this open-access publication were covered by the Max Planck Society.

Review statement. This paper was edited by Gabriele Stiller and reviewed by two anonymous referees.

References

Allen, H. M., Crounse, J. D., Kim, M. J., Teng, A. P., Ray, E. A., McKain, K., Sweeney, C., and Wennberg, P. O.: H_2O_2 and CH_3OOH (MHP) in the Remote Atmosphere: 1. Global Distribution and Regional Influences, J. Geophys. Res.-Atmos., 127, e2021JD035701, https://doi.org/10.1029/2021JD035701, 2022.

Allen, N. D. C., González Abad, G., Bernath, P. F., and Boone, C. D.: Satellite observations of the global distribution of hydrogen peroxide (H_2O_2) from ACE, J. Quant. Spectrosc. Ra., 115, 66–77, https://doi.org/10.1016/j.jqsrt.2012.09.008, 2013.

Anonymous referee: Referee comment 2, https://doi.org/10.5194/acp-2022-693-RC2, 2022.

Atkinson, R., Baulch, D. L., Cox, R. A., Crowley, J. N., Hampson, R. F., Hynes, R. G., Jenkin, M. E., Rossi, M. J., and Troe, J.: Evaluated kinetic and photochemical data for atmospheric chemistry: Volume I – gas phase reactions of O_x, HO_x, NO_x and SO_x species, Atmos. Chem. Phys., 4, 1461–1738, https://doi.org/10.5194/acp-4-1461-2004, 2004.

Bohn, B. and Lohse, I.: Calibration and evaluation of CCD spectroradiometers for ground-based and airborne measurements of spectral actinic flux densities, Atmos. Meas. Tech., 10, 3151–3174, https://doi.org/10.5194/amt-10-3151-2017, 2017.

Bozem, H., Pozzer, A., Harder, H., Martinez, M., Williams, J., Lelieveld, J., and Fischer, H.: The influence of deep convection on HCHO and H_2O_2 in the upper troposphere over Europe, Atmos. Chem. Phys., 17, 11835–11848, https://doi.org/10.5194/acp-17-11835-2017, 2017.

Calvert, J. G., Lazrus, A., Kok, G. L., Heikes, B. G., Walega, J. G., Lind, J., and Cantrell, C. A.: Chemical mechanisms of acid generation in the troposphere, Nature, 317, 27–35, https://doi.org/10.1038/317027a0, 1985.

Chang, W., Lee, M., and Heikes, B. G.: One-dimensional photochemical study of $H_2O_2CH_3OOH$, and HCHO in the marine boundary layer during Pacific Exploratory Mission in the Tropics (PEM-Tropics) B, J. Geophys. Res., 109, D06307, https://doi.org/10.1029/2003jd004256, 2004.

Crippa, M., Guizzardi, D., Muntean, M., Schaaf, E., Dentener, F., van Aardenne, J. A., Monni, S., Doering, U., Olivier, J. G. J., Pagliari, V., and Janssens-Maenhout, G.: Gridded emissions of air pollutants for the period 1970–2012 within EDGAR v4.3.2, Earth Syst. Sci. Data, 10, 1987–2013, https://doi.org/10.5194/essd-10-1987-2018, 2018.

Crutzen, P. J., Lawrence, M. G., and Pöschl, U.: On the background photochemistry of tropospheric ozone, Tellus B, 51, 123–146, https://doi.org/10.3402/tellusb.v51i1.16264, 1999.

Damschen, D. E. and Martin, L. R.: Aqueous aerosol oxidation of nitrous acid by O_2, O_3 AND H_2O_2, Atmos. Environ., 17, 2005–2011, https://doi.org/10.1016/0004-6981(83)90357-8, 1983.

Daum, P. H., Kleinman, L. I., Hills, A. J., Lazrus, A. L., Leslie, A. C. D., Busness, K., and Boatman, J.: Measurement and interpretation of concentrations of H_2O_2 and related species in the upper midwest during summer, J. Geophys. Res., 95, 9857–9871, https://doi.org/10.1029/JD095iD07p09857, 1990.

de Reus, M., Fischer, H., Sander, R., Gros, V., Kormann, R., Salisbury, G., Van Dingenen, R., Williams, J., Zöllner, M., and Lelieveld, J.: Observations and model calculations of trace gas scavenging in a dense Saharan dust plume during MINATROC, Atmos. Chem. Phys., 5, 1787–1803, https://doi.org/10.5194/acp-5-1787-2005, 2005.

Dienhart, D., Brendel, B., Crowley, J. N., Eger, P. G., Harder, H., Martinez, M., Pozzer, A., Rohloff, R., Schuladen, J., Tauer, S., Walter, D., Lelieveld, J., and Fischer, H.: Formaldehyde and hydroperoxide distribution around the Arabian Peninsula – evaluation of EMAC model results with ship-based measurements, Atmos. Chem. Phys., 23, 119–142, https://doi.org/10.5194/acp-23-119-2023, 2023.

Faloona, I., Tan, D., Brune, W. H., Jaeglé, L., Jacob, D. J., Kondo, Y., Koike, M., Chatfield, R., Pueschel, R., Ferry, G., Sachse, G., Vay, S., Anderson, B., Hannon, J., and Fuelberg, H.: Observations of HO_x and its relationship with NO_x in the upper troposphere during SONEX, J. Geophys. Res., 105, 3771–3783, https://doi.org/10.1029/1999JD900914, 2000.

Faloona, I. C., Tan, D., Lesher, R. L., Hazen, N. L., Frame, C. L., Simpas, J. B., Harder, H., Martinez, M., Di Carlo, P., Ren, X., and Brune, W. H.: A Laser-induced Fluorescence Instrument for Detecting Tropospheric OH and HO_2 Characteristics and Calibration, J. Atmos. Chem., 47, 139–167, https://doi.org/10.1023/B:JOCH.0000021036.53185.0e, 2004.

Fels, M. and Junkermann, W.: The occurrence of organic peroxides in air at a mountain site, Geophys. Res. Lett., 21, 341–344, https://doi.org/10.1029/93GL01892, 1994.

Fontaine, B., Roucou, P., Gaetani, M., and Marteau, R.: Recent changes in precipitation, ITCZ convection and northern tropical circulation over North Africa (1979–2007), Int. J. Climatol., 31, 633–648, https://doi.org/10.1002/joc.2108, 2011.

Guilbault, G. G., Brignac, P. J., and Juneau, M.: New substrates for the fluorometric determination of oxidative enzymes, Anal. Chem., 40, 1256–1263, https://doi.org/10.1021/ac60264a027, 1968.

Hamryszczak, Z., Dienhart, D., Brendel, B., Rohloff, R., Marno, D., Martinez, M., Harder, H., Pozzer, A., Bohn, B., Zöger, M., Lelieveld, J., and Fischer, H.: Hydrogen peroxide in the upper tropical troposphere over the Atlantic Ocean and western Africa during the CAFE-Africa aircraft campaign (1.0), Zenodo [data set], https://doi.org/10.5281/zenodo.7845890, 2023.

Hamryszczak, Z. T., Pozzer, A., Obersteiner, F., Bohn, B., Steil, B., Lelieveld, J., and Fischer, H.: Distribution of hydrogen peroxide over Europe during the BLUESKY aircraft campaign, Atmos. Chem. Phys., 22, 9483–9497, https://doi.org/10.5194/acp-22-9483-2022, 2022.

Hastenrath, S. and Lamb, P.: Some Aspects of Circulation and Climate over the Eastern Equatorial Atlantic, Mon. Wea. Rev., 105, 1019–1023, https://doi.org/10.1175/1520-0493(1977)105<1019:SAOCAC>2.0.CO;2, 1977.

Heikes, B. G.: Formaldehyde and hydroperoxides at Mauna Loa Observatory, J. Geophys. Res., 97, 18001, https://doi.org/10.1029/92JD00268, 1992.

Hersbach, H., Bell, B., Berrisford, P., Biavati, G., Horányi, A., Muñoz Sabater, J., Nicolas, J., Peubey, C., Radu, R., Rozum, I., Schepers, D., Simmons, A., Soci, C., Dee, D., and Thépaut, J.-N.: ERA5 monthly averaged data on single levels from 1979 to present, Copernicus Climate Change Service (C3S) Climate Data Store (CDS) [data set], https://doi.org/10.24381/CDS.F17050D7, 2019.

Hoffmann, M. R. and Edwards, J. O.: Kinetics of the oxidation of sulfite by hydrogen peroxide in acidic solution, J. Phys. Chem., 79, 2096–2098, https://doi.org/10.1021/j100587a005, 1975.

Hottmann, B., Hafermann, S., Tomsche, L., Marno, D., Martinez, M., Harder, H., Pozzer, A., Neumaier, M., Zahn, A., Bohn, B., Stratmann, G., Ziereis, H., Lelieveld, J., and Fischer, H.: Impact of the South Asian monsoon outflow on atmospheric hydroperoxides in the upper troposphere, Atmos. Chem. Phys., 20, 12655–12673, https://doi.org/10.5194/acp-20-12655-2020, 2020.

Hua, W., Chen, Z. M., Jie, C. Y., Kondo, Y., Hofzumahaus, A., Takegawa, N., Chang, C. C., Lu, K. D., Miyazaki, Y., Kita, K., Wang, H. L., Zhang, Y. H., and Hu, M.: Atmospheric hydrogen peroxide and organic hydroperoxides during PRIDE-PRD'06, China: their concentration, formation mechanism and contribution to secondary aerosols, Atmos. Chem. Phys., 8, 6755–6773, https://doi.org/10.5194/acp-8-6755-2008, 2008.

Jacob, P. and Klockow, D.: Hydrogen peroxide measurements in the marine atmosphere, J. Atmos. Chem., 15, 353–360, https://doi.org/10.1007/BF00115404, 1992.

Jaeglé, L., Jacob, D. J., Wennberg, P. O., Spivakovsky, C. M., Hanisco, T. F., Lanzendorf, E. J., Hintsa, E. J., Fahey, D. W., Keim, E. R., Proffitt, M. H., Atlas, E. L., Flocke, F., Schauffler, S., McElroy, C. T., Midwinter, C., Pfister, L., and Wilson, J. C.: Observed OH and HO_2 in the upper troposphere suggest a ma-

jor source from convective injection of peroxides, Geophys. Res. Lett., 24, 3181–3184, https://doi.org/10.1029/97GL03004, 1997.

Jaeglé, L., Jacob, D. J., Brune, W. H., Faloona, I., Tan, D., Heikes, B. G., Kondo, Y., Sachse, G. W., Anderson, B., Gregory, G. L., Singh, H. B., Pueschel, R., Ferry, G., Blake, D. R., and Shetter, R. E.: Photochemistry of HO_x in the upper troposphere at northern midlatitudes, J. Geophys. Res., 105, 3877–3892, https://doi.org/10.1029/1999JD901016, 2000.

Jöckel, P., Sander, R., Kerkweg, A., Tost, H., and Lelieveld, J.: Technical Note: The Modular Earth Submodel System (MESSy) – a new approach towards Earth System Modeling, Atmos. Chem. Phys., 5, 433–444, https://doi.org/10.5194/acp-5-433-2005, 2005.

Jöckel, P., Tost, H., Pozzer, A., Brühl, C., Buchholz, J., Ganzeveld, L., Hoor, P., Kerkweg, A., Lawrence, M. G., Sander, R., Steil, B., Stiller, G., Tanarhte, M., Taraborrelli, D., van Aardenne, J., and Lelieveld, J.: The atmospheric chemistry general circulation model ECHAM5/MESSy1: consistent simulation of ozone from the surface to the mesosphere, Atmos. Chem. Phys., 6, 5067–5104, https://doi.org/10.5194/acp-6-5067-2006, 2006.

Jöckel, P., Kerkweg, A., Pozzer, A., Sander, R., Tost, H., Riede, H., Baumgaertner, A., Gromov, S., and Kern, B.: Development cycle 2 of the Modular Earth Submodel System (MESSy2), Geosci. Model Dev., 3, 717–752, https://doi.org/10.5194/gmd-3-717-2010, 2010.

Jöckel, P., Tost, H., Pozzer, A., Kunze, M., Kirner, O., Brenninkmeijer, C. A. M., Brinkop, S., Cai, D. S., Dyroff, C., Eckstein, J., Frank, F., Garny, H., Gottschaldt, K.-D., Graf, P., Grewe, V., Kerkweg, A., Kern, B., Matthes, S., Mertens, M., Meul, S., Neumaier, M., Nützel, M., Oberländer-Hayn, S., Ruhnke, R., Runde, T., Sander, R., Scharffe, D., and Zahn, A.: Earth System Chemistry integrated Modelling (ESCiMo) with the Modular Earth Submodel System (MESSy) version 2.51, Geosci. Model Dev., 9, 1153–1200, https://doi.org/10.5194/gmd-9-1153-2016, 2016.

Kaiser, J. W., Heil, A., Andreae, M. O., Benedetti, A., Chubarova, N., Jones, L., Morcrette, J.-J., Razinger, M., Schultz, M. G., Suttie, M., and van der Werf, G. R.: Biomass burning emissions estimated with a global fire assimilation system based on observed fire radiative power, Biogeosciences, 9, 527–554, https://doi.org/10.5194/bg-9-527-2012, 2012.

Kerkweg, A., Buchholz, J., Ganzeveld, L., Pozzer, A., Tost, H., and Jöckel, P.: Technical Note: An implementation of the dry removal processes DRY DEPosition and SEDImentation in the Modular Earth Submodel System (MESSy), Atmos. Chem. Phys., 6, 4617–4632, https://doi.org/10.5194/acp-6-4617-2006, 2006a.

Kerkweg, A., Sander, R., Tost, H., and Jöckel, P.: Technical note: Implementation of prescribed (OFFLEM), calculated (ONLEM), and pseudo-emissions (TNUDGE) of chemical species in the Modular Earth Submodel System (MESSy), Atmos. Chem. Phys., 6, 3603–3609, https://doi.org/10.5194/acp-6-3603-2006, 2006b.

Kleinman, L. I.: Seasonal dependence of boundary layer peroxide concentration: The low and high NO_x regimes, J. Geophys. Res., 96, 20721, https://doi.org/10.1029/91JD02040, 1991.

Klippel, T., Fischer, H., Bozem, H., Lawrence, M. G., Butler, T., Jöckel, P., Tost, H., Martinez, M., Harder, H., Regelin, E., Sander, R., Schiller, C. L., Stickler, A., and Lelieveld, J.: Distribution of hydrogen peroxide and formaldehyde over Central Europe during the HOOVER project, Atmos. Chem. Phys., 11, 4391–4410, https://doi.org/10.5194/acp-11-4391-2011, 2011.

Krautstrunk, M. and Giez, A.: The Transition From FALCON to HALO Era Airborne Atmospheric Research, in: Atmospheric physics: Background-methods-trends, edited by: Schumann, U., Springer-Verlag, Berlin, Heildelberg, 609–624, https://doi.org/10.1007/978-3-642-30183-4_37, 2012.

Lazrus, A. L., Kok, G. L., Gitlin, S. N., Lind, J. A., and McLaren, S. E.: Automated fluorimetric method for hydrogen peroxide in atmospheric precipitation, Anal. Chem., 57, 917–922, https://doi.org/10.1021/ac00281a031, 1985.

Lazrus, A. L., Kok, G. L., Lind, J. A., Gitlin, S. N., Heikes, B. G., and Shetter, R. E.: Automated fluorometric method for hydrogen peroxide in air, Anal. Chem., 58, 594–597, https://doi.org/10.1021/ac00294a024, 1986.

Lee, M., Heikes, B. G., Jacob, D. J., Sachse, G., and Anderson, B.: Hydrogen peroxide, organic hydroperoxide, and formaldehyde as primary pollutants from biomass burning, J. Geophys. Res., 102, 1301–1309, https://doi.org/10.1029/96jd01709, 1997.

Lee, M., Heikes, B. G., and Jacob, D. J.: Enhancements of hydroperoxides and formaldehyde in biomass burning impacted air and their effect on atmospheric oxidant cycles, J. Geophys. Res., 103, 13201–13212, https://doi.org/10.1029/98jd00578, 1998.

Lee, M., Heikes, B. G., and O'Sullivan, D. W.: Hydrogen peroxide and organic hydroperoxide in the troposphere: a review, Atmos. Environ., 34, 3475–3494, https://doi.org/10.1016/S1352-2310(99)00432-X, 2000.

Lelieveld, J. and Crutzen, P. J.: Influences of cloud photochemical processes on tropospheric ozone, Nature, 343, 227–233, https://doi.org/10.1038/343227a0, 1990.

Levy, H.: Normal atmosphere: large radical and formaldehyde concentrations predicted, Science, 173, 141–143, https://doi.org/10.1126/science.173.3992.141, 1971.

Logan, J. A., Prather, M. J., Wofsy, S. C., and McElroy, M. B.: Tropospheric chemistry: A global perspective, J. Geophys. Res., 86, 7210, https://doi.org/10.1029/JC086iC08p07210, 1981.

Marno, D., Ernest, C., Hens, K., Javed, U., Klimach, T., Martinez, M., Rudolf, M., Lelieveld, J., and Harder, H.: Calibration of an airborne HO_x instrument using the All Pressure Altitude-based Calibrator for HO_x Experimentation (APACHE), Atmos. Meas. Tech., 13, 2711–2731, https://doi.org/10.5194/amt-13-2711-2020, 2020.

Nguyen, T. B., Crounse, J. D., Teng, A. P., St Clair, J. M., Paulot, F., Wolfe, G. M., and Wennberg, P. O.: Rapid deposition of oxidized biogenic compounds to a temperate forest, P. Natl. Acad. Sci. USA, 112, 392–401, https://doi.org/10.1073/pnas.1418702112, 2015.

Nussbaumer, C. M., Tadic, I., Dienhart, D., Wang, N., Edtbauer, A., Ernle, L., Williams, J., Obersteiner, F., Gutiérrez-Álvarez, I., Harder, H., Lelieveld, J., and Fischer, H.: Measurement report: In situ observations of deep convection without lightning during the tropical cyclone Florence 2018, Atmos. Chem. Phys., 21, 7933–7945, https://doi.org/10.5194/acp-21-7933-2021, 2021.

O'Sullivan, D. W., Lee, M., Noone, B. C., and Heikes, B. G.: Henry's Law Constant Determinations for Hydrogen Peroxide, Methyl Hydroperoxide, Hydroxymethyl Hydroperoxide, Ethyl Hydroperoxide, and Peroxyacetic Acid, J. Phys. Chem., 100, 3241–3247, https://doi.org/10.1021/jp951168n, 1996.

O'Sullivan, D. W., Heikes, B. G., Lee, M., Chang, W., Gregory, G. L., Blake, D. R., and Sachse, G. W.: Distribution of hydrogen peroxide and methylhydroperoxide over the Pacific and South Atlantic Oceans, J. Geophys. Res., 104, 5635–5646, https://doi.org/10.1029/98JD01250, 1999.

Penkett, S. A., Jones, B. M. R., Brich, K. A., and Eggleton, A. E. J.: The importance of atmospheric ozone and hydrogen peroxide in oxidising sulphur dioxide in cloud and rainwater, Atmos. Environ., 13, 123–137, https://doi.org/10.1016/0004-6981(79)90251-8, 1979.

Perros, P. E.: Large-scale distribution of hydrogen peroxide from aircraft measurements during the TROPOZ II experiment, Atmos. Environ. A-Gen., 27, 1695–1708, https://doi.org/10.1016/0960-1686(93)90232-N, 1993.

Pozzer, A., Jöckel, P., and Van Aardenne, J.: The influence of the vertical distribution of emissions on tropospheric chemistry, Atmos. Chem. Phys., 9, 9417–9432, https://doi.org/10.5194/acp-9-9417-2009, 2009.

Pozzer, A., Reifenberg, S. F., Kumar, V., Franco, B., Kohl, M., Taraborrelli, D., Gromov, S., Ehrhart, S., Jöckel, P., Sander, R., Fall, V., Rosanka, S., Karydis, V., Akritidis, D., Emmerichs, T., Crippa, M., Guizzardi, D., Kaiser, J. W., Clarisse, L., Kiendler-Scharr, A., Tost, H., and Tsimpidi, A.: Simulation of organics in the atmosphere: evaluation of EMACv2.54 with the Mainz Organic Mechanism (MOM) coupled to the ORACLE (v1.0) submodel, Geosci. Model Dev., 15, 2673–2710, https://doi.org/10.5194/gmd-15-2673-2022, 2022.

Prather, M. J. and Jacob, D. J.: A persistent imbalance in HO_x and NO_x photochemistry of the upper troposphere driven by deep tropical convection, Geophys. Res. Lett., 24, 3189–3192, https://doi.org/10.1029/97GL03027, 1997.

Reeves, C. E. and Penkett, S. A.: Measurements of peroxides and what they tell us, Chem. Rev., 103, 5199–5218, https://doi.org/10.1021/cr0205053, 2003.

Rinsland, C. P., Coheur, P. F., Herbin, H., Clerbaux, C., Boone, C., Bernath, P., and Chiou, L. S.: Detection of elevated tropospheric hydrogen peroxide (H_2O_2) mixing ratios in atmospheric chemistry experiment (ACE) subtropical infrared solar occultation spectra, J. Quant. Spectrosc. Ra., 107, 340–348, https://doi.org/10.1016/j.jqsrt.2007.02.009, 2007.

Robbin Martin, L. and Damschen, D. E.: Aqueous oxidation of sulfur dioxide by hydrogen peroxide at low pH, Atmos. Environ., 15, 1615–1621, https://doi.org/10.1016/0004-6981(81)90146-3, 1981.

Roeckner, E., Bäuml, G., Bonaventura, L., Brokopf, R., Esch, M., Giorgetta, M., Hagemann, S., Kirchner, I., Kornblueh, L., Manzini, E., Rhodin, A., Schlese, U., Schulzweida, U., and Tompkins, A.: The atmospheric general circulation model ECHAM 5. PART I: Model description, Report, Max-Planck-Institut für Meteorologie, https://doi.org/10.17617/2.995269, 2003.

Roeckner, E., Brokopf, R., Esch, M., Giorgetta, M., Hagemann, S., Kornblueh, L., Manzini, E., Schlese, U., and Schulzweida, U.: Sensitivity of Simulated Climate to Horizontal and Vertical Resolution in the ECHAM5 Atmosphere Model, J. Climate, 19, 3771–3791, https://doi.org/10.1175/JCLI3824.1, 2006.

Sander, R., Kerkweg, A., Jöckel, P., and Lelieveld, J.: Technical note: The new comprehensive atmospheric chemistry module MECCA, Atmos. Chem. Phys., 5, 445–450, https://doi.org/10.5194/acp-5-445-2005, 2005.

Sander, R., Baumgaertner, A., Gromov, S., Harder, H., Jöckel, P., Kerkweg, A., Kubistin, D., Regelin, E., Riede, H., Sandu, A., Taraborrelli, D., Tost, H., and Xie, Z.-Q.: The atmospheric chemistry box model CAABA/MECCA-3.0, Geosci. Model Dev., 4, 373–380, https://doi.org/10.5194/gmd-4-373-2011, 2011.

Sander, R., Jöckel, P., Kirner, O., Kunert, A. T., Landgraf, J., and Pozzer, A.: The photolysis module JVAL-14, compatible with the MESSy standard, and the JVal PreProcessor (JVPP), Geosci. Model Dev., 7, 2653–2662, https://doi.org/10.5194/gmd-7-2653-2014, 2014.

Sander, R., Baumgaertner, A., Cabrera-Perez, D., Frank, F., Gromov, S., Grooß, J.-U., Harder, H., Huijnen, V., Jöckel, P., Karydis, V. A., Niemeyer, K. E., Pozzer, A., Riede, H., Schultz, M. G., Taraborrelli, D., and Tauer, S.: The community atmospheric chemistry box model CAABA/MECCA-4.0, Geosci. Model Dev., 12, 1365–1385, https://doi.org/10.5194/gmd-12-1365-2019, 2019.

Slemr, F. and Tremmel, H. G.: Hydroperoxides in the marine troposphere over the Atlantic Ocean, J. Atmos. Chem., 19, 371–404, https://doi.org/10.1007/BF00694493, 1994.

Snow, J. A.: Winter-spring evolution and variability of HO_x reservoir species, hydrogen peroxide, and methyl hydroperoxide, in the northern middle to high latitudes, J. Geophys. Res., 108, 1890, https://doi.org/10.1029/2002JD002172, 2003.

Snow, J. A., Heikes, B. G., Shen, H., O'Sullivan, D. W., Fried, A., and Walega, J.: Hydrogen peroxide, methyl hydroperoxide, and formaldehyde over North America and the North Atlantic, J. Geophys. Res., 112, 8353, https://doi.org/10.1029/2006JD007746, 2007.

Tadic, I., Nussbaumer, C. M., Bohn, B., Harder, H., Marno, D., Martinez, M., Obersteiner, F., Parchatka, U., Pozzer, A., Rohloff, R., Zöger, M., Lelieveld, J., and Fischer, H.: Central role of nitric oxide in ozone production in the upper tropical troposphere over the Atlantic Ocean and western Africa, Atmos. Chem. Phys., 21, 8195–8211, https://doi.org/10.5194/acp-21-8195-2021, 2021.

Tost, H., Jöckel, P., Kerkweg, A., Sander, R., and Lelieveld, J.: Technical note: A new comprehensive SCAVenging submodel for global atmospheric chemistry modelling, Atmos. Chem. Phys., 6, 565–574, https://doi.org/10.5194/acp-6-565-2006, 2006.

Valverde-Canossa, J., Wieprecht, W., Acker, K., and Moortgat, G. K.: H_2O_2 and organic peroxide measurements in an orographic cloud: The FEBUKO experiment, Atmos. Environ., 39, 4279–4290, https://doi.org/10.1016/j.atmosenv.2005.02.040, 2005.

Walcek, C. J.: A theoretical estimate of O_3 and H_2O_2 dry deposition over the northeast United States, Atmos. Environ., 21, 2649–2659, https://doi.org/10.1016/0004-6981(87)90196-x, 1987.

Waliser, D. E. and Gautier, C.: A Satellite-derived Climatology of the ITCZ, J. Climate, 6, 2162–2174, https://doi.org/10.1175/1520-0442(1993)006<2162:ASDCOT>2.0.CO;2, 1993.

Weinstein-Lloyd, J. B., Lee, J. H., Daum, P. H., Kleinman, L. I., Nunnermacker, L. J., Springston, S. R., and Newman, L.: Measurements of peroxides and related species during the 1995 summer intensive of the Southern Oxidants Study in Nashville, Tennessee, J. Geophys. Res., 103, 22361–22373, https://doi.org/10.1029/98JD01636, 1998.

Supplement of Atmos. Chem. Phys., 23, 5929–5943, 2023 https://doi.org/10.5194/acp-23-5929-2023-supplement

Atmospheric Chemistry and Physics Open Access

Supplement of

Measurement report: Hydrogen peroxide in the upper tropical troposphere over the Atlantic Ocean and western Africa during the CAFE-Africa aircraft campaign

Zaneta Hamryszczak et al.

Correspondence to: Zaneta Hamryszczak (z.hamryszczak@mpic.de) and Horst Fischer (horst.fischer@mpic.de)

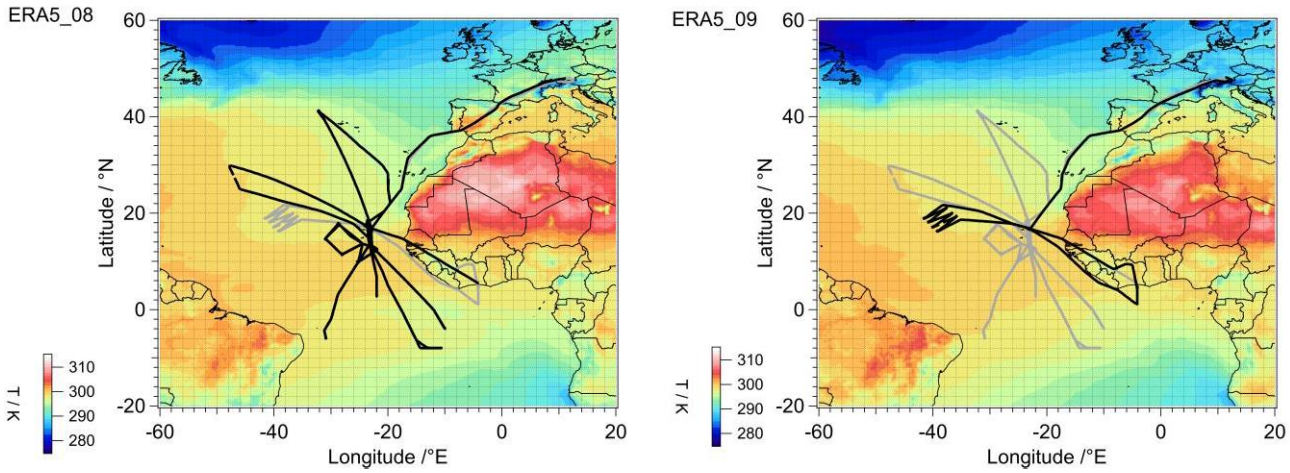

Figure S1. Average 2 m dewpoint temperature during the campaign CAFE-Africa in August (left) and September (right) 2018 based on ERA5 data output (contains modified Copernicus Climate Change Service information; Hersbach et al. 2019; Accessed on < 22-07-2022 >)[1]. The performed flights are indicated in black.

[1] **Hersbach, H., Bell, B., Berrisford, P., Biavati, G., Horányi, A., Muñoz Sabater, J., Nicolas, J., Peubey, C., Radu, R., Rozum, I., Schepers, D., Simmons, A., Soci, C., Dee, D., Thépaut, J-N. (2019): ERA5 monthly averaged data on single levels from 1959 to present. Copernicus Climate Change Service (C3S) Climate Data Store (CDS). (Accessed on < 22-07-2022 >), 10.24381/cds.f17050d7**

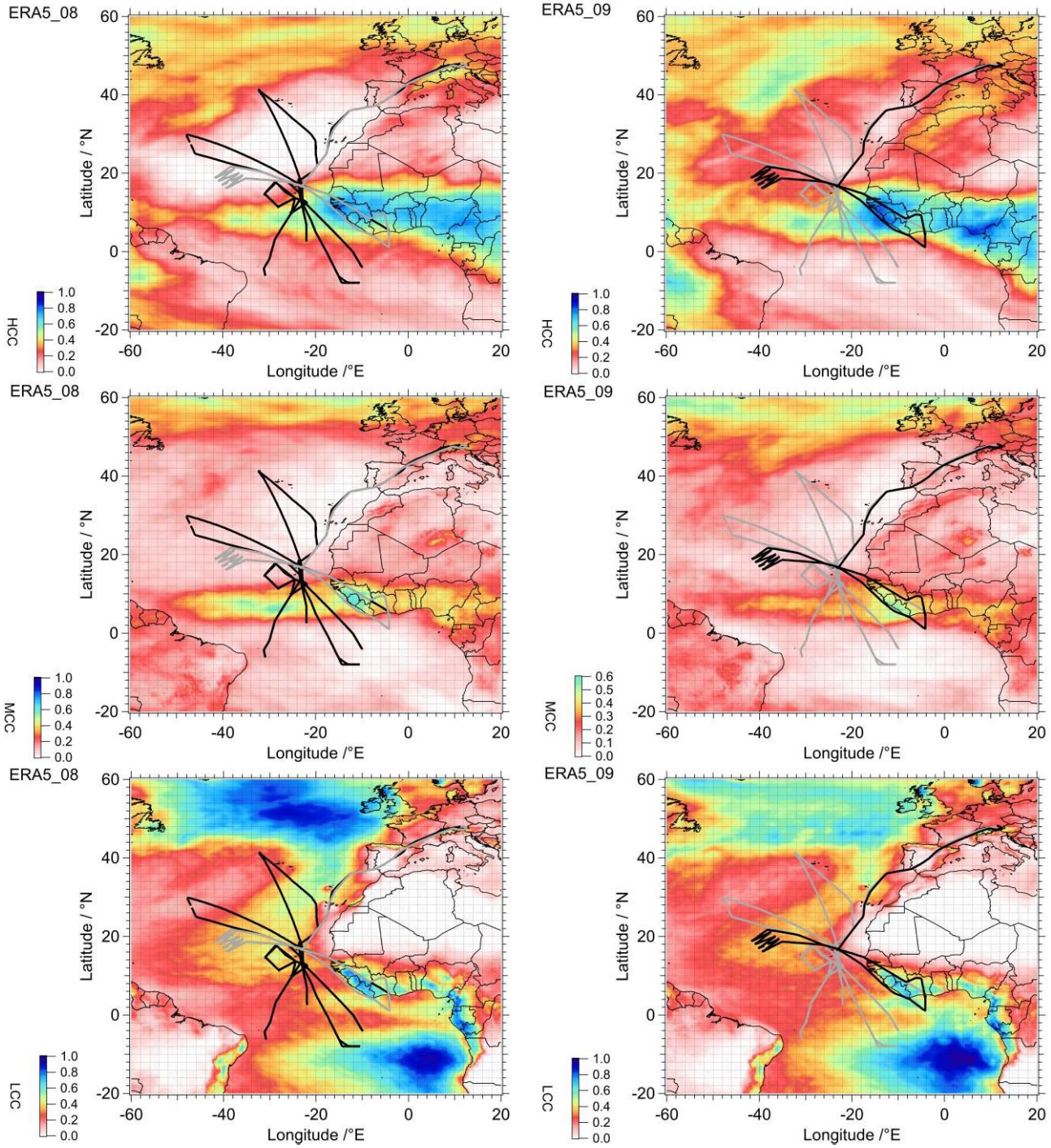

Figure S2. Average high, medium and low (top to bottom panels) cloud coverage during the campaign CAFE-Africa in August (left panel) and September (right panel) 2018 based on ERA5 data output (modified Copernicus Climate

Change Service information; Hersbach et al. 2019; Accessed on < 22-07-2022 >)[2]. The performed flights are indicated in black. Please note the approximate altitudinal range of low, medium and high cloud cover at 0–2, 2–6, >6 km, respectively.

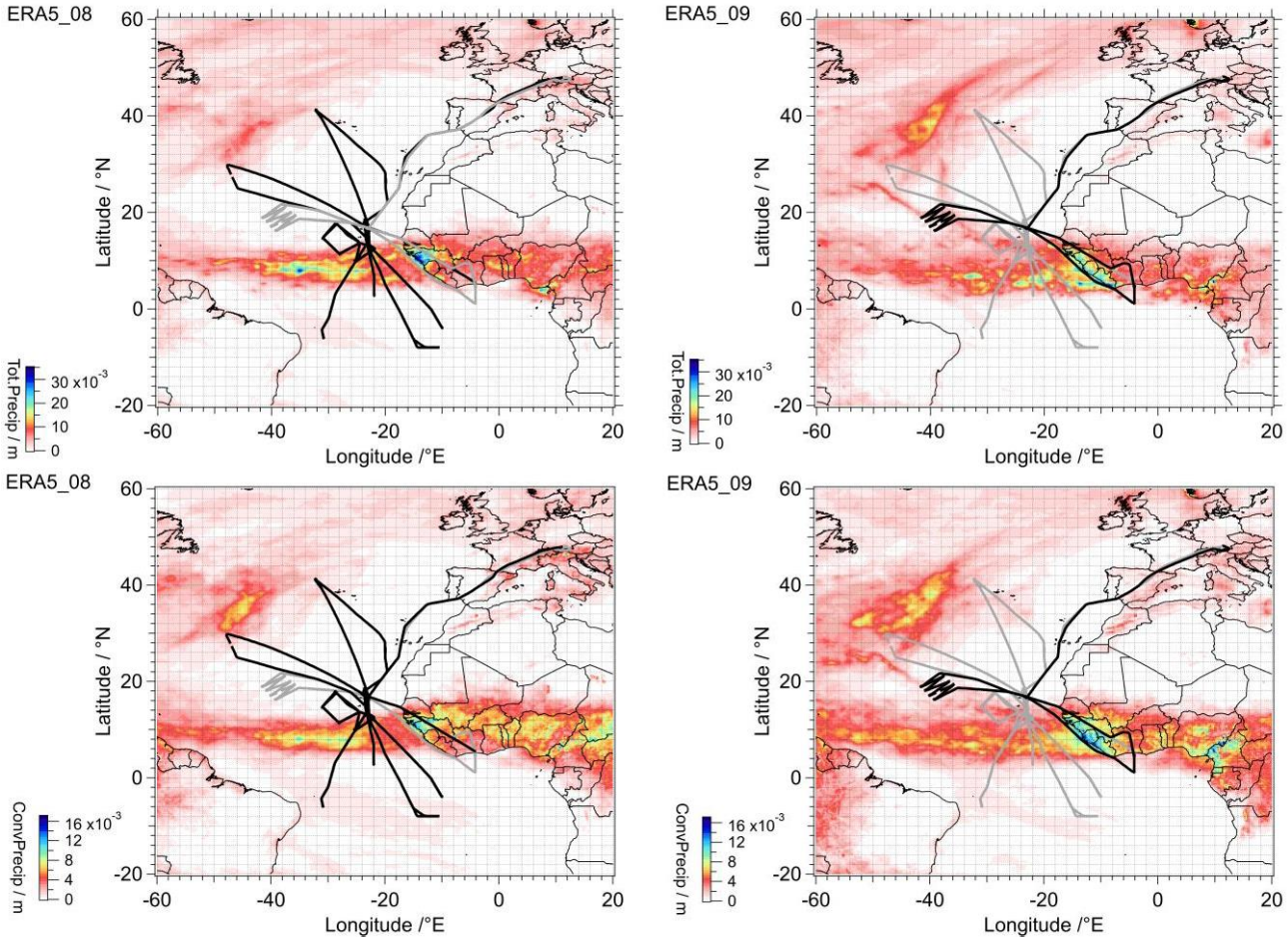

Figure S3. Average total and convective precipitation (top to bottom panels) during CAFE-Africa in August (left panel) and September (right panel) 2018 based on ERA5 datasets (contains modified Copernicus Climate Change Service information; Hersbach et al. 2019; Accessed on < 22-07-2022 >)[3]. The performed flights are indicated in black.

[2] **Hersbach, H., Bell, B., Berrisford, P., Biavati, G., Horányi, A., Muñoz Sabater, J., Nicolas, J., Peubey, C., Radu, R., Rozum, I., Schepers, D., Simmons, A., Soci, C., Dee, D., Thépaut, J-N. (2019): ERA5 monthly averaged data on single levels from 1959 to present. Copernicus Climate Change Service (C3S) Climate Data Store (CDS). (Accessed on < 22-07-2022 >), 10.24381/cds.f17050d7**

[3] **Hersbach, H., Bell, B., Berrisford, P., Biavati, G., Horányi, A., Muñoz Sabater, J., Nicolas, J., Peubey, C., Radu, R., Rozum, I., Schepers, D., Simmons, A., Soci, C., Dee, D., Thépaut, J-N. (2019): ERA5 monthly averaged data on single levels from 1959 to present. Copernicus Climate Change Service (C3S) Climate Data Store (CDS). (Accessed on < 22-07-2022 >), 10.24381/cds.f17050d7**

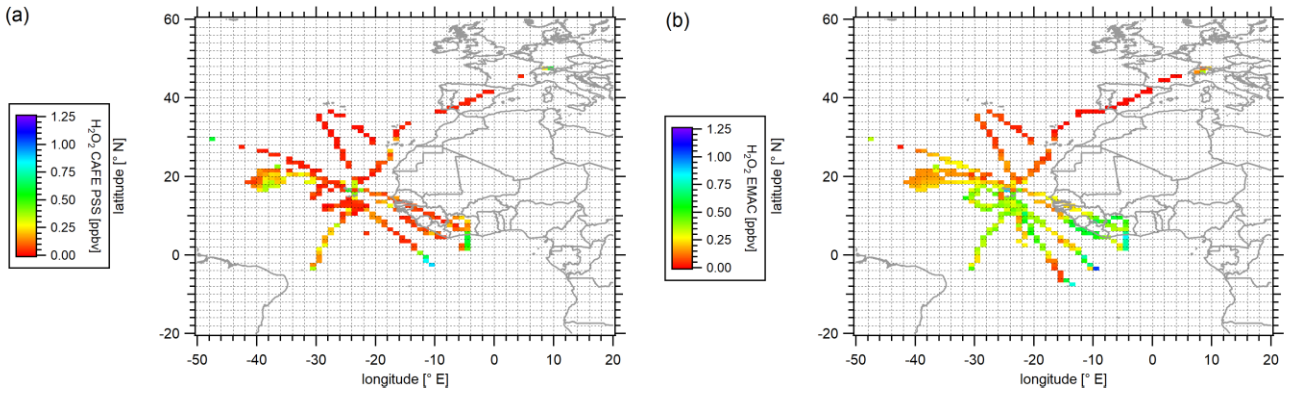

Figure S4. Spatial distribution of hydrogen peroxide modelled based on photostationary steady state conditions (a) and simulated by the model EMAC (b) in the upper troposphere (≥8 km) during CAFE-Africa campaign. Data were binned into 1°x1° bins over the full extension of the flight tracks.

Table S1. General mean (± 1 sigma) and median overview of measured, simulated and modelled based on steady state conditions hydrogen peroxide mixing ratios subdivided into northern (approx. 20 °N- 40 °N; top) hemisphere, ITCZ (approx. 5 °N < 20 °N; middle) and southern hemisphere (approx. 10 °S < 5 °N; bottom).

Northern Hemisphere

	CAFE-Africa	EMAC	CAFE PSS
Mean ± 1sigma	0.14 ±0.11	0.11 ±0.08	0.08 ±0.11
Median	0.12	0.11	0.04

Intertropical Convergence Zone

	CAFE-Africa	EMAC	CAFE PSS
Mean ± 1sigma	0.20 ±0.13	0.35 ±0.17	0.14 ±0.15
Median	0.17	0.33	0.08

Southern Hemisphere

	CAFE-Africa	EMAC	CAFE PSS
Mean ± 1sigma	0.15 ±0.12	0.38 ±0.24	0.31 ±0.25
Median	0.12	0.31	0.25

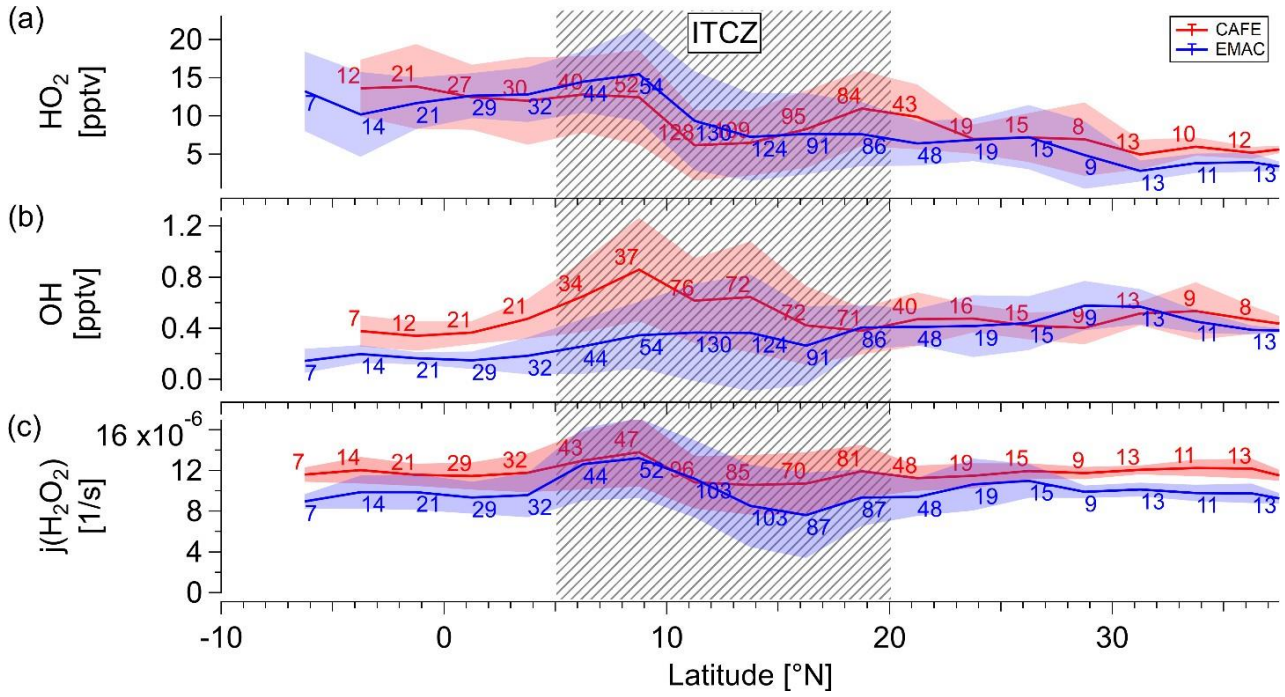

Figure S5. Latitudinal dependence of measured (red) hydroperoxyl radical levels (a), hydroxyl radical concentrations (b) and hydrogen peroxide photolysis rates (c; mean ± 1 sigma) compared to EMAC simulations (blue). The data sets with 6 min time resolution and mean values were binned for 2.5° of latitude at altitudes ≥ 8 km. The corresponding numbers indicate the total amount of data points per bin. The shaded pattern marks the ITCZ.

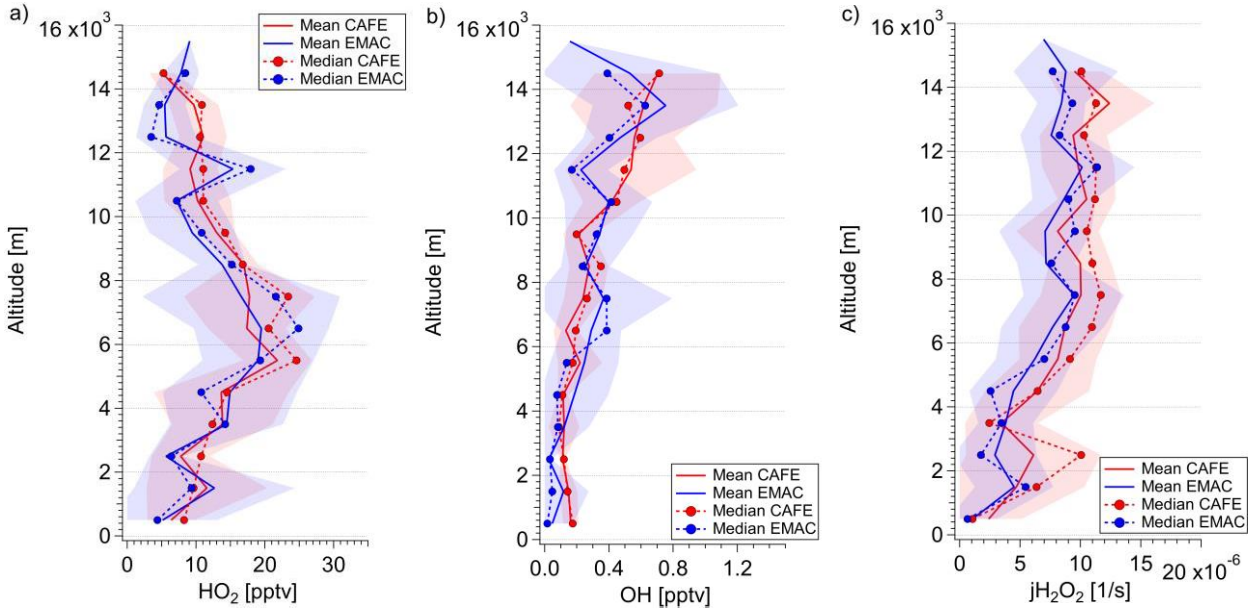

Figure S6. Vertical profiles of observed (red) and simulated (blue) hydroperoxyl radical (a), hydroxyl radical (b) and hydrogen peroxide photolysis rates (c). Vertical profile estimations were calculated within 1000 m means and medians over the entire probed atmospheric column based on data obtained within the region of the base of operation in Sal, Cape Verde (approx.16° 35' – 16° 51' N; 22° 52' - 23 °W).

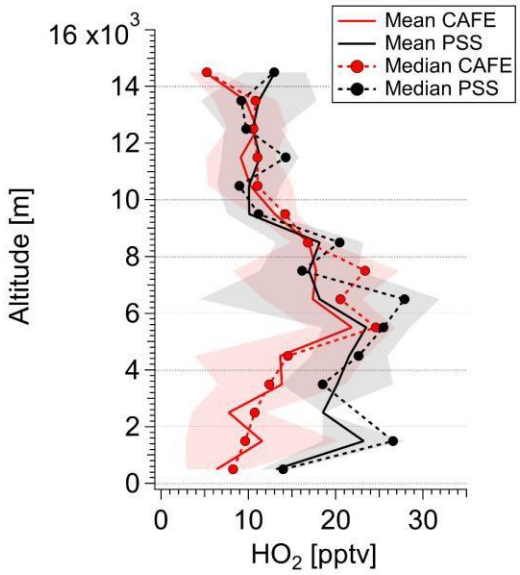

Figure S7. Vertical profile of observed (red) and PSS calculated (black) hydroperoxyl radical calculated within 1000 m means and medians over the entire probed atmospheric column based on data obtained at the base of operation. Please note that the HO_2 PSS calculations are based on assumptions made in Eq. 6 in the manuscript.

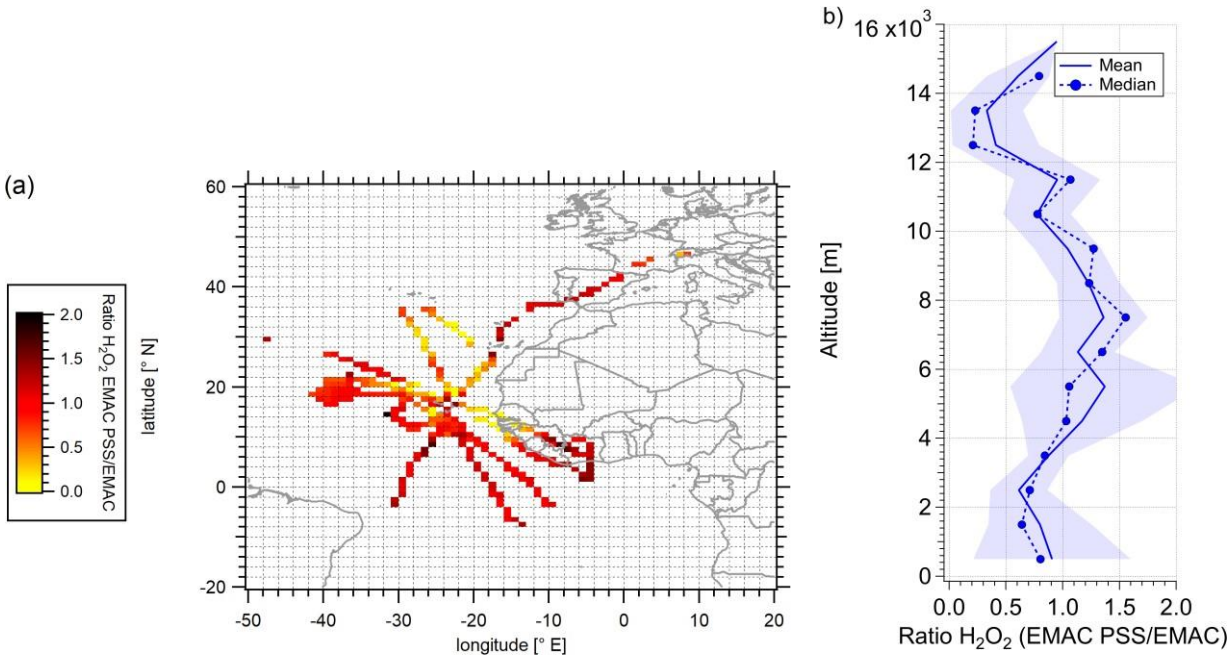

Figure S8. Spatial distribution of H2O2(PSS EMAC)/H2O2(EMAC) ratio (a) and the corresponding vertical profile (b) in the upper troposphere (≥8 km) during CAFE-Africa campaign. For the purposes of the spatial distribution analysis, data were binned into 1°x1° bins over the full extension of the flight tracks. The vertical distribution was estimated within 1000 m altitude bins over the entire probed column based on the simulated data within the region of the base of operation in Sal, Cape Verde (approx.16° 35' – 16° 51' N; 22° 52' - 23 °W).

5. The CAFE-Brazil airborne campaign

This section is dedicated to the most recent hydroperoxide measurements in the scope of the airborne campaign, Chemistry of the Atmosphere: Field Experiment in Brazil (CAFE-Brazil). The research project was performed in December 2022 – January 2023. In Sect. 5.1., the campaign objectives, the spatial resolution of the sampled region with the corresponding measurement flights, and an overview of the meteorological conditions during the measurement period is introduced. Detailed information on the instrumentation onboard the research aircraft HALO relevant to the hydroperoxide analyses in this work was presented in a previous section (Sect. 3.1.). An overview of the measured hydroperoxide mixing ratios was discussed in Sect. 2.1. as a part of the technical research article with the title: "HYPHOP: a tool for high-altitude, long-range monitoring of hydrogen peroxide and higher organic peroxides in the atmosphere", where the spatial, and vertical hydroperoxide distribution is discussed in detail. Mean ($\pm 1\sigma$) and median mixing ratios of hydrogen peroxide and the sum of organic hydroperoxides were compared with former measurement results in the region during the GABRIEL (Guyanas Atmosphere-Biosphere exchange and Radicals Intensive Experiment with the Learjet) aircraft campaign in 2005. Additionally, the observations were compared with the model simulations performed by EMAC in perspective of potential deviations and their meteorologically and photochemically driven sources (Sect. 5.2.).

5.1. The campaign – Objectives and meteorological conditions

The purpose of the CAFE-Brazil campaign conducted in December 2022 and January 2023 was to compare the large-scale distribution of atmospheric trace species in pristine versus anthropogenically influenced environments. The research project investigated the impact of convective transport on trace gases and aerosol particles and the arising interactions between the tropospheric layers under various meteorological conditions. Furthermore, atmospheric chemical exchange between the atmosphere and the biosphere and cloud formation processes over the tropical rainforest were the focus of the performed measurements. From the base of operation in Manaus (3° 6′ S, 60° 1′ W), 20 measurement flights were performed mostly over the Amazon Basin with the extension of 12° S – 4° N and 70 – 38° W covering an altitudinal range from few tens of meters above the surface to approximately 15 km. Fig. 12 illustrates the sampled region with the corresponding GPS flight tracks.

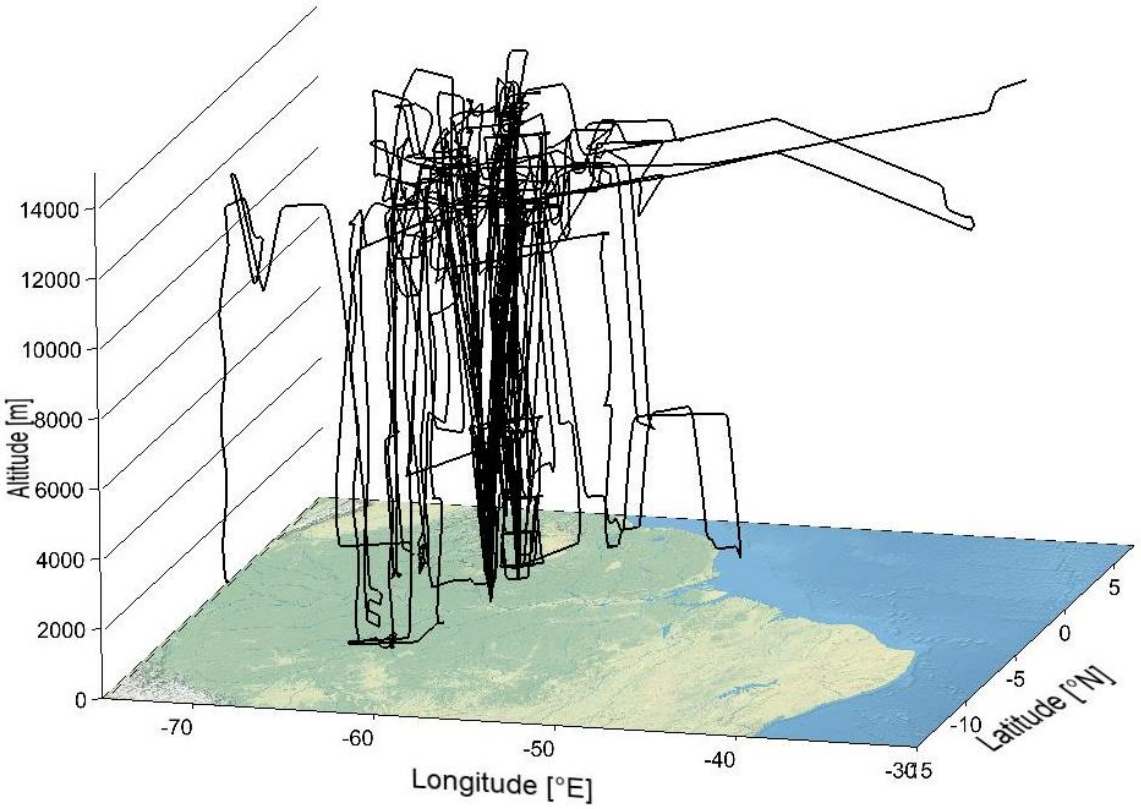

Figure 12: General overview of performed measurement flights during the CAFE-Brazil campaign (12/2022 – 01/2023) based on GPS flight tracks output by BAHAMAS instrument with 2 min temporal resolution.

Average monthly 2 m temperature, total cloud cover fractions, and total precipitation during the measurement period derived from ERA5 reanalysis generated using Copernicus Climate Change Service information (Hersbach et al., 2019) are presented in the following figure (Fig. 13). The corresponding GPS flight tracks of the individual flights are indicated in black.

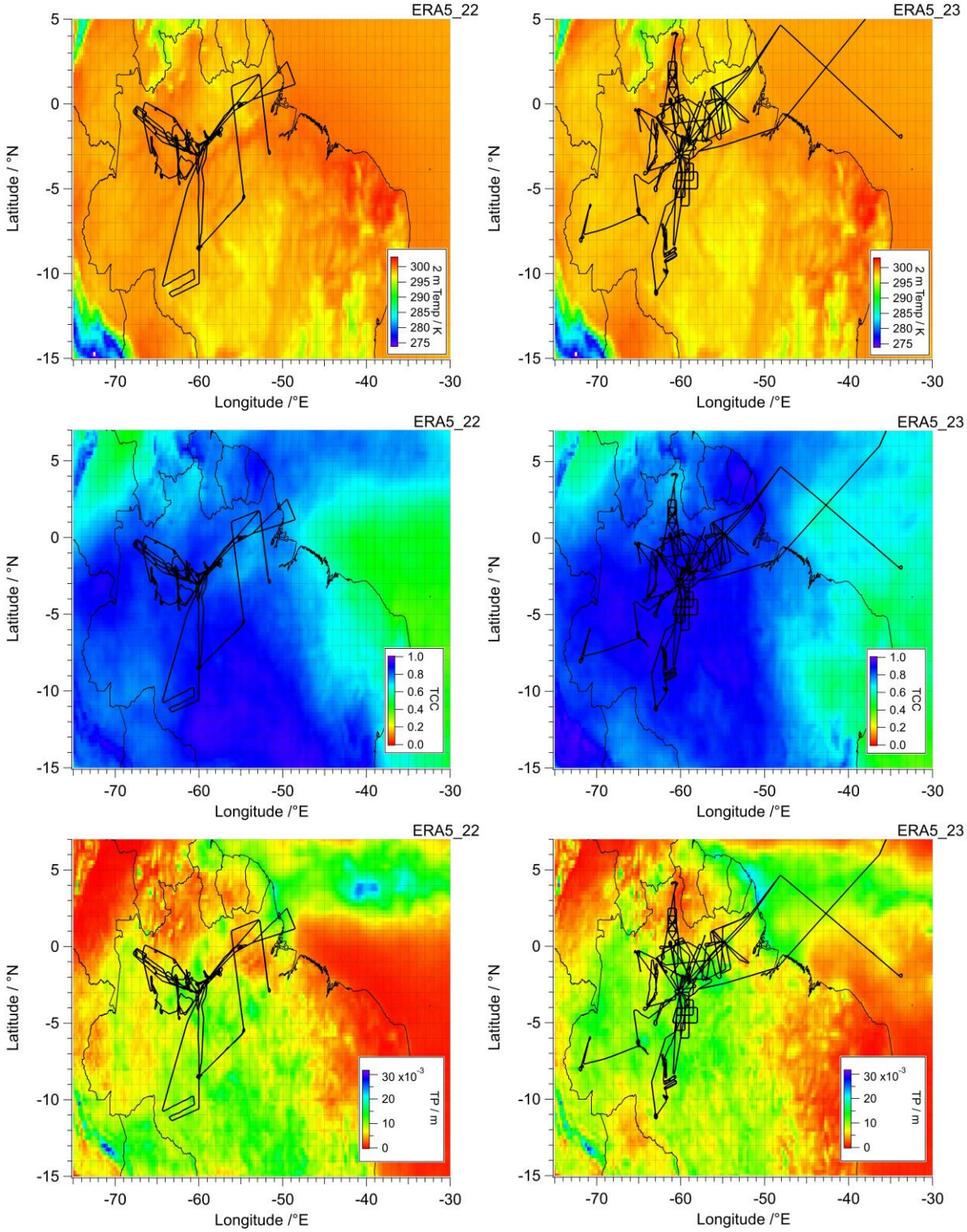

Figure 13: Average monthly 2 m temperature (2 m Temp; top panel), total cloud coverage (TCC; middle panel), total precipitation (TP; bottom panel) during December 2022 (left column) and January 2023 (right column) derived by ERA5 reanalysis generated using Copernicus Climate Change Service (Hersbach et al., 2019). GPS flight tracks of performed measurement flights are indicated in black.

During the first phase of the measurement period (December 2022), the average 2 m temperature was 298.56 (±2.47) K with a maximum of 302.32 K at the western South American coast and a minimum

of 274.78 K towards the south-west. In January 2023, during the second phase of the campaign, 298.17 (±2.42) K, 302.64 K, and 275.38 K, respectively, were reported. Maximum and minimum 2 m air temperatures were observed in comparable regions as during the first campaign phase. Average total cloud coverages were 0.73 (±0.14), and 0.75 (±0.13) in December 2022 and in January 2023, respectively, with a predominantly high proportion of high clouds (Fig. S5, top panel; Sect. 7.3.). Monthly average total and convective precipitations were reported to be 6.65 (±4.22) · 10^{-3} m and 4.56 (±2.72) · 10^{-3} m, respectively, in December and 6.98 (±3.77) · 10^{-3} m, and 5.14 (±2.64) · 10^{-3} m, respectively, in January, with maximum values of 20.18 · 10^{-3} m and 19.81 · 10^{-3} m towards the south-west of the sampled region. Based on the comparison of the total and convective precipitation (Fig. S3 in Sect. 7.3.), the majority of the reported rain episodes is assumed to originate from convective clouds. The sampled region extended through the northern part of the South Atlantic Convergence Zone (SACZ), an atmospheric system of convective clouds, precipitation, and convergent winds from the north-west towards south-east extending over Brazil towards the south-west of the Atlantic Ocean.

5.2. Hydroperoxides during the CAFE-Brazil aircraft campaign – comparison with former measurements during GABRIEL 2005 and EMAC model simulations

The vertical distribution of hydroperoxides during CAFE-Brazil follows the expected inverted C-shaped trend throughout the lower troposphere, as shown and discussed in detail in Sect. 2.1 within the scope of the technical research article: “HYPHOP: a tool for high-altitude, long-range monitoring hydrogen peroxide and higher organic peroxides in the atmosphere”. During the sampling period, the mean (±1σ) and median mixing ratios were 0.30 (±0.30) ppb_v, and 0.17 ppb_v for H_2O_2 and 0.43 (±0.36) ppb_v, and 0.28 ppb_v for ROOH, respectively. The lowest hydroperoxide levels were measured in the upper troposphere (at altitudes above 8 km) at approximately 0.10 ppb_v. The highest mean mixing ratios were measured directly above the boundary layer in the free troposphere with 0.90 ppb_v and 1.10 ppb_v for H_2O_2 and ROOH, respectively. In the boundary layer, due to deposition, the hydroperoxide levels decrease to 0.60 ppb_v and 0.70 ppb_v for H_2O_2 and ROOH, respectively. On average, ROOH are approximately by a factor of 1.3 – 1.5 higher relative to H_2O_2 in the lower troposphere reflecting the contribution of VOCs-driven ROOH precursor production at simultaneous H_2O_2 uptake by the dense vegetation. The ROOH-to-H_2O_2-ratio increases up to a factor of 5 in the upper troposphere above 8 km indicating the direct impact of convective transport.

Hydroperoxide measurement results during CAFE-Brazil campaign are put into perspective with previous measurement results during the GABRIEL (Guyanas Atmosphere-Biosphere exchange and Radicals Intensive Experiment with the Learjet) aircraft campaign performed in October 2005 in a region from 3° – 6° N and 51°– 59° W extending from the north-east of French Guayana, over the

tropical Atlantic to Guayana with the base of operation in Paramaribo-Johan Adolf Pengel Airport at Zanderij (5°45´6´´ N; 55°20´ W) in Suriname up to altitudes of 8 km. A comparison of the H_2O_2 and ROOH vertical distribution is presented in the figure below (Fig. 14; left column) as 500 m bins (means ± 1σ and medians) based on data output with a temporal resolution of 2 min over the sampled atmospheric column. Profile information derived based on the GABRIEL campaign is restricted to 6.5 km due to lack of instrumental line pressure stability above 450 hPa pressure altitude. Please note that for the purposes of the comparison, the CAFE-Brazil hydroperoxide output was purged from observation results most likely affected by anthropogenic emissions with respect to the so-called Manaus plume in close proximity to the operational base.

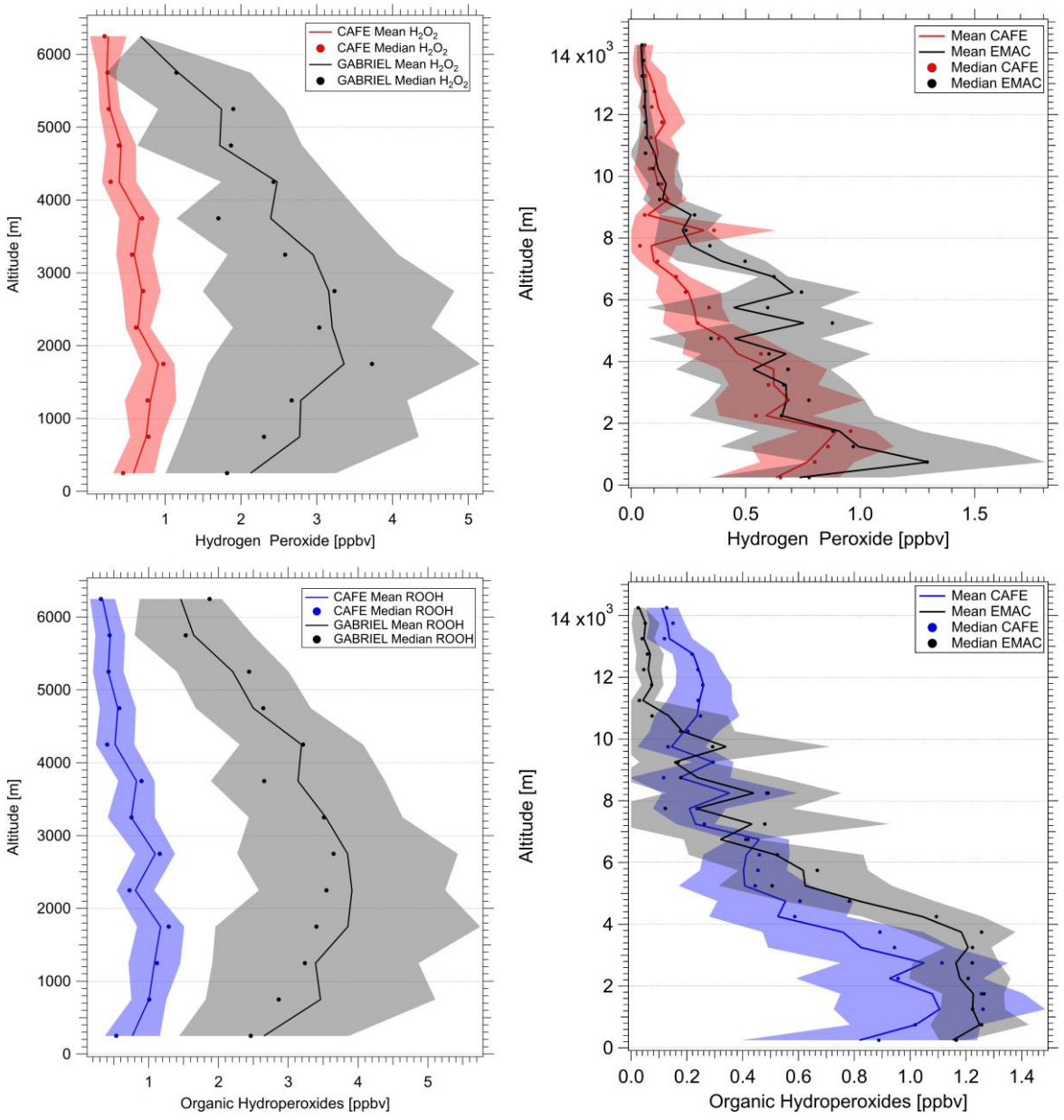

Figure 14: Comparison of H_2O_2 (top panel) and ROOH (bottom panel) vertical distribution during GABRIEL 2005 (left column) and EMAC simulations during CAFE-Brazil (right column) relative to in situ observations during CAFE-Brazil. Vertical profiles were calculated within 500

m means and medians over the entire available atmospheric column. Please note that in order to avoid any bias caused by anthropogenic emissions, measured and simulated data output in close proximity to the base of operation in Manaus during CAFE-Brazil was removed from the corresponding datasets.

An overview of the measured hydroperoxide levels during the GABRIEL campaign subdivided into the main tropospheric layers, BL and MT is presented in the table below.

Table 4: Overview of the hydroperoxide mean, median, and maximum mixing ratios (ppb_v) in the boundary layer and in the middle troposphere during the GABRIEL aircraft campaign in 2005.

	H_2O_2 - GABRIEL		**ROOH - GABRIEL**	
	0 < 2 km	**2 < 6.5 km**	**0 < 2 km**	**2 < 6.5 km**
Mean (±1σ) /ppb_v	2.53 (±1.45)	2.70 (±1.33)	3.08 (±1.52)	3.38 (±1.31)
Median /ppb_v	2.04	2.43	2.58	3.13
Maximum /ppb_v	7.40	6.76	8.74	7.86

Hydrogen peroxide and total organic hydroperoxide vertical distribution during GABRIEL in 2005 display both a distinct inverted C-shaped trend throughout the tropospheric column with a maxiumum mixing ratios of 7.40 ppb_v and 8.74 ppb_v for H_2O_2 and ROOH, respectively, directly above where the BL is assumed (at approximately 2 km) decreasing towards the free troposphere to approximate levels of 1 ppb_v (at 6 km). Within the BL the hydroperoxide levels decrease towards levels of approximately 2 ppb_v linked to deposition processes affecting the trace species at low altitudes. Due to a lack of information on hydroperoxide measurements above 6.5 km in 2005, their vertical distribution in the upper troposphere cannot be discussed. The measured H_2O_2 and ROOH mixing ratios during GABRIEL 2005 aircraft campaign are significantly higher than during CAFE-Brazil. A far more distinct inverted C-shaped gradient relative to in situ observations during CAFE-Brazil was observed. In general, the hydroperoxide levels during the GABRIEL campaign are by a factor of up to 5 higher relative to the measured levels during CAFE-Brazil. However, the ROOH-to-H_2O_2-ratios during both campaigns seem to agree well with slight deviations towards increased ROOH levels relative to measured H_2O_2 during CAFE-Brazil (Sect. 7.3.; Fig. S4). Due to ROOH mixing ratios correction regarding the instrumental stripping efficiency by a factor of 0.8 during the GABRIEL campaign, the ROOH mixing ratios are expected to be slightly higher relative to CAFE-Brazil. Nonetheless, the correction does not justify the high difference in the in situ observations relative to the most recent results. Since the trace species are sensitive to atmospheric deposition processes, it is important to compare the hydroperoxide levels during both campaigns from the perspective of their meteorological environment. Fig. 15 displays the total cloud coverage (TCC) and total precipitation (TP) during the GABRIEL campaign as monthly averages based on ERA5 reanalysis output over the sampled region.

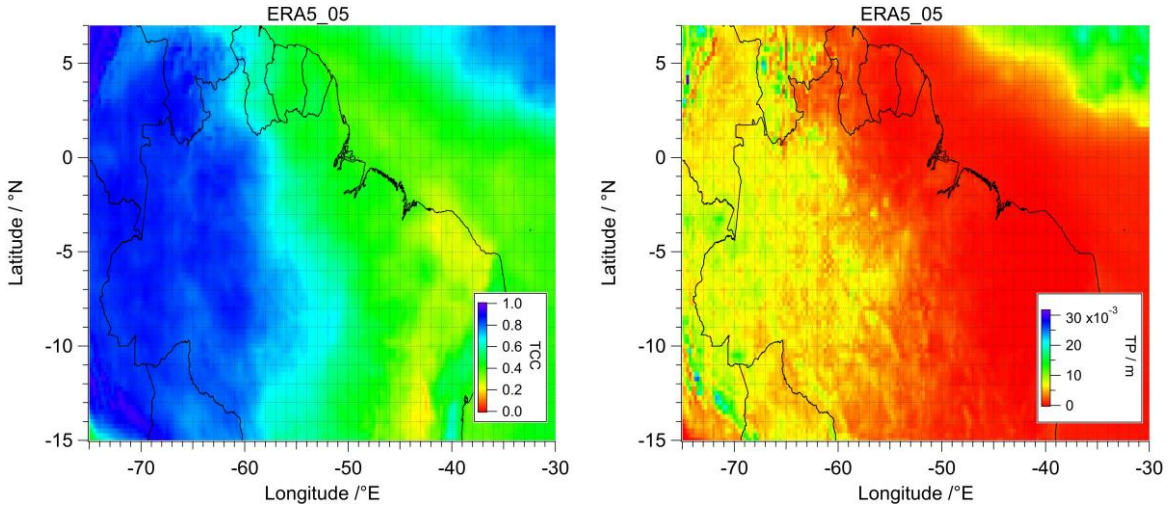

Figure 15: Average monthly total cloud coverage (TCC; left) and total precipitation (TP; right) during October 2005 derived by ERA5 reanalysis generated using Copernicus Climate Change Service (Hersbach et al., 2019). GPS flight tracks of performed measurement flights are indicated in black.

As presented in the meteorological overview based on the monthly average total cloud coverage and total precipitation by ERA5, on average about 50% lower cloud coverage and nearly no precipitation was registered during the measurement period of the GABRIEL campaign in the sampled region. The total cloud coverage varied between 0.4 and 0.6 above the French Guayanas and Guayanas (3° – 6° N; 51°– 59° W), while a cloud coverage of nearly unity with high amount high clouds (> 6 km) was observed during CAFE-Brazil campaign. Additionally, due to near no precipitation events relative to CAFE-Brazil, hydroperoxide rainout during the GABRIEL campaign can be neglected. Thus, hydroperoxide cloud and precipitation scavenging surely contribute to the observed deviations between the measurement results. However, further environmental aspects add most likely to the discrepancy of the measured hydroperoxide levels. Since ROOH are less sensitive to wet deposition processes relative to H_2O_2, the distinct shortage in ROOH during CAFE-Brazil indicates an additional photochemical or physical hydroperoxide precursor sink causing their lower availability for hydroperoxide formation during the CAFE-Brazil measurement period.

In order to investigate the impact of deposition on the hydroperoxide budget, a comparison of in situ data with the output of EMAC simulations was performed. An overview of the simulated mean, median, and maximum hydroperoxide levels is displayed below (Tab. 5).

Table 5: Overview of the simulated H_2O_2 and ROOH mean, median, and maximum mixing ratios (ppb_v) in the boundary layer (BL), the middle troposphere (MT), and the upper troposphere (UT).

	H_2O_2 - EMAC			ROOH - EMAC		
	0 < 2 km	**2 < 8 km**	**≥ 8 km**	**0 < 2 km**	**2 < 8 km**	**≥ 8 km**
Mean (±1σ) /ppb_v	1.11 (±0.51)	0.54 (±0.36)	0.08 (±0.06)	1.21 (±0.17)	0.85 (±0.38)	0.08 (±0.12)
Median /ppb_v	1.01	0.54	0.06	1.19	0.92	0.05
Max. /ppb_v	2.31	1.44	0.43	1.71	1.54	0.91

In general, the EMAC-simulated vertical profiles of hydroperoxides follow the expected trend throughout the troposphere. The lowest H_2O_2 and ROOH (determined as the sum of simulated MHP, EHP and PAA) levels of 0.08 ppb_v were simulated in the UT (at altitudes of 8 km and above). Simulated hydroperoxide mixing ratios increase to 1.11 ppb_v and 1.21 ppb_v for H_2O_2 and ROOH, respectively towards the lower troposphere with maximum H_2O_2 and ROOH levels of 2.31 ppb_v and 1.71 ppb_v at approximately 500 m. The H_2O_2 vertical distribution seems to remain nearly constant between 2 – 7 km with some variation at 5 – 6 km. A comparison of the simulated hydroperoxide vertical distribution relative to the observations during CAFE-Brazil is displayed in Fig. 14 (right column) as 500 m subsets (means ± 1σ and medians) over the sampled tropospheric column. Data output potentially affected by anthropogenic emissions in close proximity to the base of operation in Manaus was removed to avoid any biases. To synchronize the temporal resolution of the simulated data with the observations, mean values over 10 min (equivalent to the model's time resolution) were calculated.

EMAC simulations agree well with the measurements of H_2O_2, especially in the free troposphere at 2 – 5 km. The measured and simulated levels agree also in the upper troposphere, with some deviation below 12 km altitude, where EMAC tends to underestimate the H_2O_2 levels locally by a factor of up to 2. EMAC simulates the impact of convective processes on the hydroperoxide budget to an extent accounting for injections from the lower troposphere caused by deep convection (Fig. S6 in Sect. 7.3.). However, the absolute excess hydrogen peroxide amount falls short relative to the observations (Hamryszczak et al., 2023). Most striking deviations of the H_2O_2 simulations relative to the observations arise within the BL and in the free troposphere at 5 – 8 km. EMAC overestimates the H_2O_2 mixing ratios up to a factor of 1.7 in the BL. In the free troposphere, the model overestimates the H_2O_2 levels by about a factor of 4. Past research showed that EMAC tends to underestimate the impact of wet deposition due to cloud and precipitation scavenging and vegetational uptake of H_2O_2 (Klippel et al., 2011; Dienhart et al., 2023; Hamryszczak et al., 2023). In the boundary layer, the increased amount of vegetation and the corresponding H_2O_2 deposition seems to be not simulated accurately by the model. A high abundance of clouds above 6 km of altitude (high clouds; Fig. S5 in Sect. 7.3.) indicates an

increased amount of cloud processing as well as rainout of H_2O_2 in the atmosphere. EMAC simulates deposition at the surface and washout related to clouds and rain, as shown in Fig. S6 (Sect. 7.3.). A rough estimate of the simulated absolute H_2O_2 loss by deposition varies between 0.11 ppb_v in the upper troposphere (~10 km) and 2.60 ppb_v in the BL (~250 m). However, the model has some trouble predicting the intense deposition impact, which is most likely linked to its coarse resolution.

A comparison of the simulated versus observed organic hydroperoxide mixing ratios shows different results. Despite the restriction of simulated organic hydroperoxides to PAA, EHP, and MHP based on the assumption of their prominence especially in the free troposphere, the ROOH levels seem to be up to 30 – 40% higher than measured in the BL and lower free troposphere. A likely reason for the strong deviation of the ROOH simulation output relative to the observations in the lower troposphere might be (as mentioned above) the fact that the measurement output was not corrected regarding the stripping efficiency due to a lack of information on the biogenic VOCs emissions serving as potential alkyl hydroperoxyl radical source. Applying the determined factor (approximately 0.8 – 0.6, in dependence on the available VOCs composition and RO_2 formation rates), the measured levels of organic hydroperoxide are expected to rise and thus, to agree better in the BL and lower free troposphere with the simulation results. At 6 – 8 km, EMAC agrees very well with the observations. A discrepancy between simulated and observed ROOH mixing ratios arises again above 8 km in the UT. Here, EMAC tends to underestimate the ROOH levels by a factor of up to 4. As discussed in the scope of the technical research article (Sect. 2.1.), not only ROOH might be efficiently transported into the UT by convection, but also their potential precursors, such as VOCs or HOMs (Highly oxygenated Organic Molecules), which are assumed to be far less sensitive to washout processes in clouds and precipitation relative to hydroperoxides. In the upper troposphere, photolytic conversion of these trace species into organic hydroperoxide precursors, RO_2, and the subsequent production of ROOH might increase the ROOH levels additionally. Most likely the low accuracy in simulation of the convective injections and the lack of information on the highly complex ROOH production via VOCs and HOMs contribute both to the discrepancy between the simulated and observed ROOH levels in the UT. Further detailed studies considering the VOCs and HOMs influence with regard to photochemical and physical hydroperoxide sources and sinks are necessary in order to provide a better understanding of the observed discrepancies.

6. Summary and conclusions

In this thesis, hydroperoxide observation results based on three airborne research projects were presented. The measurements were conducted using a hydroperoxide measurement setup designed for operation on board the research aircraft HALO, Hydrogen Peroxide, and Higher Organic Peroxides (HYPHOP). The wet-chemical, dual-enzyme measurement method enables to perform in situ measurements up to the tropopause tracking the total amount of ambient hydroperoxides and the sum of organic hydroperoxides in two separate reactors at a measurement frequency of 1 Hz. By determining the difference between the measured hydroperoxide mixing ratios in the subsequent reactors, H_2O_2 levels in ambient air are further available. Potential chemical and physical interferences affecting the instrumental performance during airborne experiments were addressed. By the addition of sufficient reactants (formaldehyde and EDTA) and by adequate data processing removing chemical interference during the measurement process, the absolute amounts of H_2O_2 and ROOH can be easily determined. Based on the results of a test flight performed from the DLR (German Aerospace Center; Deutsche Luft- und Raumforschung) operational base in Oberpfaffenhofen (Germany), the background signal of the HYPHOP monitor suffers to a minor extent from measurement inconsistencies during rapid flight maneuvers. However, the potential impact of the noise sources, such as pressure-dependent cabin temperature fluctuations, frequent periodic roll angle changes, pitch rate changes, and temporal line pressure instabilities do not significantly affect the measurement performance of the instrument. The detected signal noise at its maximum impact was estimated to be at the instrumental detection limit or far below the expected hydroperoxide signals in the troposphere. HYPHOP sufficiently resolves the temporal and spatial variability of hydroperoxide mixing ratios in the troposphere, as was shown based on measurement results tracking highly dynamic atmospheric processes, such as deep convection, cloud scavenging, and rainout, during the most recent research project, CAFE-Brazil. Based on the measurement results during this campaign, the monitor's precision for H_2O_2 and the sum of organic hydroperoxides (ROOH) was determined to be 6.4% (at 5.7 ppb_v) and 3.6% (at 5.8 ppb_v), respectively. The instrumental limit of detection (ILD) at a measurement frequency of 1 Hz was 20 ppt_v and 19 ppt_v for H_2O_2 and ROOH, respectively. Nonetheless, the instrumental performance is subject to further optimization regarding the discussed technical noise sources. Temperature and line pressure-dependent signal drifts can be easily corrected by frequent examination of the background at different flight legs during consecutive flights. The temporal resolution of the HYPHOP monitor (currently between 60 – 120 sec) can be further optimized towards the lower value by simply reducing the transport distances of the supply tubing within the instrumental setup.

Based on the observations results during the recent years, the discussion of tropospheric hydroperoxide trends, or their lack of, was the main focus of this work. Based on the comparison of H_2O_2 mixing ratios during the BLUESKY campaign (May – June 2020) relative to previous campaigns performed over the

European continent, i. e. HOOVER II and UTOPIHAN-ACT II/III, a significant difference in the vertical and latitudinal H_2O_2 distribution was detected. The measurement results agree only to 30% in the lower troposphere (3 – 7 km). The determined average H_2O_2 and ROOH mixing ratios were 0.23 (±0.18) ppb_v, 0.42 (±0.25) ppb_v, and 0.48 (±0.17) ppb_v and 0.37 (±0.23) ppb_v, 0.57 (±0.30) ppb_v, and 0.62 (±0.36) ppb_v in the upper troposphere, middle troposphere and the boundary layer over Europe, respectively. While ROOH display the characteristic inverted C-shaped trend throughout the tropospheric column, H_2O_2 mixing ratios show a rather constant vertical distribution. Furthermore, the expected increasing trend towards decreasing latitudes was observed to an extent only for ROOH during BLUESKY. In contrast, H_2O_2 mixing ratios do not display any significant latitudinal gradient over Europe during the measurement period, which is most likely due to the enhanced cloud scavenging and the subsequent rainout. In the upper troposphere and the boundary layer, the measured H_2O_2 mixing ratios are well reproduced by the EMAC model. Additionally, the strong effect of hydrogen peroxide cloud and precipitation scavenging is partly reproduced by the simulations in the middle troposphere. However, the determined wet deposition loss rates based on the EMAC simulations fall short relative to the observations, which indicates simulation difficulties of the model regarding wet scavenging are most likely linked to its course resolution of 1.8° x 1.8°. The significantly reduced hydrogen peroxide mixing ratios relative to former observations during HOOVER II and UTOPIHAN-ACT II/III most likely do not arise due to reduced anthropogenic emissions due to COVID-19-related lockdowns, but more likely originate from significantly different meteorological environments during airborne campaigns.

Based on the hydrogen peroxide measurements performed during the CAFE-Africa campaign in August – September 2018 over the tropical Atlantic and the western coast of Africa, deep convection-related processes do not only decrease the amount of available H_2O_2 in the atmosphere but also tend to redistribute the trace species in the upper troposphere from the tropics towards the subtropics. Average H_2O_2 and ROOH mixing ratios of 0.18 (±0.13) ppb_v, 2.19 (±1.86) ppb_v, and 2.25 (±1.30) ppb_v and 0.15 (±0.07) ppb_v, 0.55 (±0.25) ppb_v, and 0.70 (±0.18) ppb_v in the upper, and middle troposphere and the boundary layer, respectively, were determined during the measurement period. The hydroperoxide measurements do not display any clear evidence of the expected latitudinal dependency of hydroperoxides in the region with decreasing levels towards the subtropics. The ROOH levels increase from the northwest (approximately 0.05 – 0.10 ppb_v) towards the southeast (up to 0.40 ppb_v) in opposition to no clear trend in the spatial distribution of H_2O_2 in the UT. However, the observed gradient might be a result of air masses significantly affected by biomass burning emissions originating from the southwest of the African continent. H_2O_2 levels show only very little latitudinal variation over the equatorial region and towards the subtropical Atlantic with a shift of maximum observed H_2O_2 mixing ratios rather towards the ITCZ (5 – 20° N). The distribution of hydrogen peroxide seems to be rather uniform with some peak events in the ITCZ, African coast (10° N; 4° W) and in close proximity to the tropical storm Florence (22° N; 36° W). The results indicate a high influence of convective transport

on the spatial distribution of the trace species. In general, the average mixing ratios of H_2O_2 agree well with previous measurements in the region. However, deviations between the H_2O_2 observations and both, observation-based PSS calculations, and EMAC simulations arise especially in the most northern and southern parts of the sampled region. Due to high vertical transport and subsequent redistribution of H_2O_2 towards the subtropics, PSS calculation fall about a factor 2 short in the North. PSS-based H_2O_2 levels are overestimated towards the South, where the pronounced presence of clouds was reported. EMAC reproduces well the H_2O_2 mixing ratios in the lower troposphere but fails to simulate cloud scavenging processes accurately in the southern part of the sampled region as well as over the African coast, which is reflecting the model's resolution-related difficulties. The EMAC model partly reproduces the impact of deep convection and atmospheric transport. Nonetheless, an underestimation of the average hydrogen peroxide excess mixing ratios by about 60% was determined. Based on these findings, convective transport and the subsequent redistribution alters the spatial H_2O_2 distribution towards more uniform mixing ratios in the marine tropical upper troposphere far more than expected based exclusively on photochemically driven processes.

Hydroperoxide measurement results based on the CAFE-Brazil airborne campaign (December 2022 – January 2023) display not only the impact of meteorological conditions on the hydroperoxide 3D-distribution in the atmosphere but further give evidence of potential secondary hydroperoxide production paths as a result of convective transport over the tropical forest. The average H_2O_2 mixing ratios of 0.74 (±0.25) ppb_v, 0.45 (±0.26) ppb_v, and 0.12 (±0.09) ppb_v were measured in the boundary layer, the middle and the upper troposphere. Accordingly, average ROOH mixing ratios of 0.83 (±0.31) ppb_v, 0.62 (±0.34) ppb_v, and 0.22 (±0.12) ppb_v were detected in the sampled region. The general region of convective outflow was determined to be 10 – 13 km above the Amazon Basin with hydroperoxide transport efficiency of up to approximately 20 – 30%. In general, ROOH levels are on average approximately by about a factor of 1.3 – 1.5 higher than H_2O_2 mixing ratios reflecting the high impact of vegetation on the production and loss of hydroperoxides in pristine regions. However, the ROOH-to-H_2O_2-ratio increases locally to a factor of up to 5 in the upper troposphere. Here, the high ROOH mixing ratios relative to H_2O_2 levels are most likely due to efficient deposition processes for H_2O_2 in the lower part of the convective clouds. ROOH mixing ratios are not as sensitively affected by wet deposition removal due to their Henry's law coefficients that are on average about two orders of magnitude lower than for hydrogen peroxide. Additionally, VOCs and HOMs efficiently injected into the UT by rapid convective transport are expected to increase the total levels of ROOH. From the perspective of previous measurements during the GABRIEL campaign, the measured hydroperoxide levels are significantly lower (up to a factor of 5), which is most likely due to contrasting meteorological conditions and the resulting higher cloud scavenging and precipitation during CAFE-Brazil. EMAC reproduces the H_2O_2 levels in the lower middle troposphere and to a considerable extent in the upper troposphere, but it tends to overestimate the levels of H_2O_2, especially in the boundary layer and in the

tropospheric regions affected by clouds. Most likely, the differences in the H_2O_2 simulations relative to the in situ observations are caused by difficulties in deposition simulations due to the limitations in the model's resolution. A comparison of ROOH simulations relative to the observations shows a good agreement within the lower troposphere. However, the model fails to reproduce the increased levels of organic hydroperoxides in the upper troposphere, which is most likely due to restrictions in the simulation of highly complex secondary VOCs and HOMs photochemistry and due to the model's resolution limitation. Detailed studies on the significance and diversity of secondary hydroperoxide production paths due to rapid natural emission redistribution are recommended in the future.

7. Supplement

7.1. Experimental

7.1.1. List of chemicals

Ethylene diamine tetra acetic acid	60-00-4	99,6%; 100 g	Sigma Aldrich
Formaldehyde	50-00-0	37%; 1 L	Carl ROTH GmbH
Potassium hydrogen phthalate	877-24-7	>99,5%; p.a.; 1 kg	Carl ROTH GmbH
Potassium permanganate	7722-64-7	0,01 M; Titrisol; 1 L	Merck KGaA
Catalase	9001-05-2	C-100, 50 mg	Sigma Aldrich
Horseradish peroxidase	9003-99-0	Type IV; 300 mg	Sigma Aldrich
Sodium	1310-73-2	1 M; 1 L	Fisher Chemical
p-Hydroxy phenylacetic acid	156-38-7	98%; 25 g	ACROS Organics
Hydrochloric acid	7647-01-0	1 M; 1 L	Merck KGaA
Sulfuric acid	7664-93-9	95 – 98%; 1 L	Merck KGaA
Titanium tetrachloride	7550-45-0	≥99,0%; 250 mL	Sigma Aldrich
Purified water		Titripack	Merck KGaA
Hydrogen peroxide	7722-84-1	30 – 33 Gew. %; 500 mL	Sigma Aldrich
Hopcalite		IAC 330; 500 g	Headline Filters Infiltec GmbH
Silica gel orange		IAC 504; 2 – 5 mm; 4 L	Headline Filters

7.1.2. Experimental procedures

Composition of the solutions used for the HYPHOP

The following list gives an overview of the solutions required for the peroxide monitor and their composition.

KHP stock solution	41 g KHP, 185 mL NaOH (1 M), 1 mL HCHO (37%), and 100 mg EDTA dissolved in 5 L purified water
Fluorescence solution	500 mg POPHA and 30 mg HRP in 2 L KHP stock solution
Stripping solution	0,5 L KHP stock solution with 4.5 L purified water
Conditioner	2 L KHP stock solution
Catalase stock solution	1 mL catalase in 99 mL KHP stock solution
Conditioner with catalase	20 mL catalase stock solution diluted with 1 L KHP stock solution
NaOH solution	50 mL NaOH (1M) in 2 L purified water

Preparation of the hydrogen peroxide stock solution and standard solutions

For the hydrogen peroxide stock solution, 1 mL of the 30 w% hydrogen peroxide solution is filled up to 1 L with purified water in a calibrated volumetric flask. The stock solution can be stored for several days if cooled and protected from light.

The H_2O_2 standard solution required for hydroperoxide monitor calibrations is prepared in two dilution steps of 1 mL each of the stock solution and the diluted stock solution is filled up to 100 mL with the stripping solution or purified water. The concentration of the prepared standard solution corresponds to 1/10,000 of the original stock solution. In order to avoid the potential decomposition of H_2O_2 in the standard solution leading to falsification of the measurement results, the standard is always freshly prepared and initiated promptly into the instrument.

Determination of hydrogen peroxide concentration in the stock solution

The absolute concentration of H_2O_2 in the stock solution is determined titrimetrically. For this purpose, 10 mL of the stock solution is mixed with 2 drops of conc. sulfuric acid (95 - 98%) and titrated against a potassium permanganate solution of known concentration (0.002 mol/L) up to the transition point (colorless to light pink). The hydrogen peroxide concentration is determined using the following equation.

$$c(H_2O) = 5 \cdot \left(\frac{c(KMnO_4) \cdot V(KMnO_4)}{2 \cdot V(H_2O_2)_{STM}}\right) \quad [A1]$$

$c(KMnO_4)$ and $V(KMnO_4)$ are the concentration and the consumed volume of the potassium permanganate solution. $V(H_2O_2)_{STM}$ is the volume of the presented stock solution. The factors appearing in the equation are due to the redox reaction taking place during the titration.

The stock solution is examined weekly for possible changes in its concentration.

Preparation of the permeation sources

The permeation source consists of a short LDPE (low-density polyethylene) tubing with a small diameter (5 – 10 cm) filled with hydrogen peroxide solution (30 w%), which was melted on both sides with a heat gun or sealed with a plastic stopper.

7.2. Supplementary tables

Table S 1: Ozone interferences determined by HYPHOP within the Fischer research group. The data from OMO (Oxidation Mechanism Observation), CAFE-Africa (Chemistry of the Atmosphere: Field Experiment in Africa), BLUESKY, and CAFE-Brazil (Chemistry of the Atmosphere: Field Experiment in Brazil) refer to those carried out within the Fischer research group measurement campaigns.

Ozone interference	Measurement conditions	Reference
150 ppt_v H_2O_2/ 100 ppb_v O_3	Laboratory	(Hafermann, 2013)
171 ppt_v H_2O_2/ 100 ppb_v O_3	Laboratory	(Hafermann, 2013)
53 ppt_v H_2O_2 / 100 ppb_v O_3	OMO	(Hottmann, 2016)
56 ppt_v H_2O_2 / 100 ppb_v O_3	CAFE-Africa	(Hamryszczak et al., 2023)
24 ppt_v H_2O_2 / 100 ppb_v O_3	Laboratory	(Christian, 2019)
16 ppt_v H_2O_2 / 100 ppb_v O_3	BLUESKY	(Hamryszczak et al., 2022)
7 ppt_v H_2O_2 / 100 ppb_v O_3	Laboratory	(Wüst, Report 2022)
10 ppt_v H_2O_2 / 100 ppb_v O_3	CAFE-Brazil	(Hamryszczak et al., 2023 submitted to AMT)

7.3. Supplementary Figures

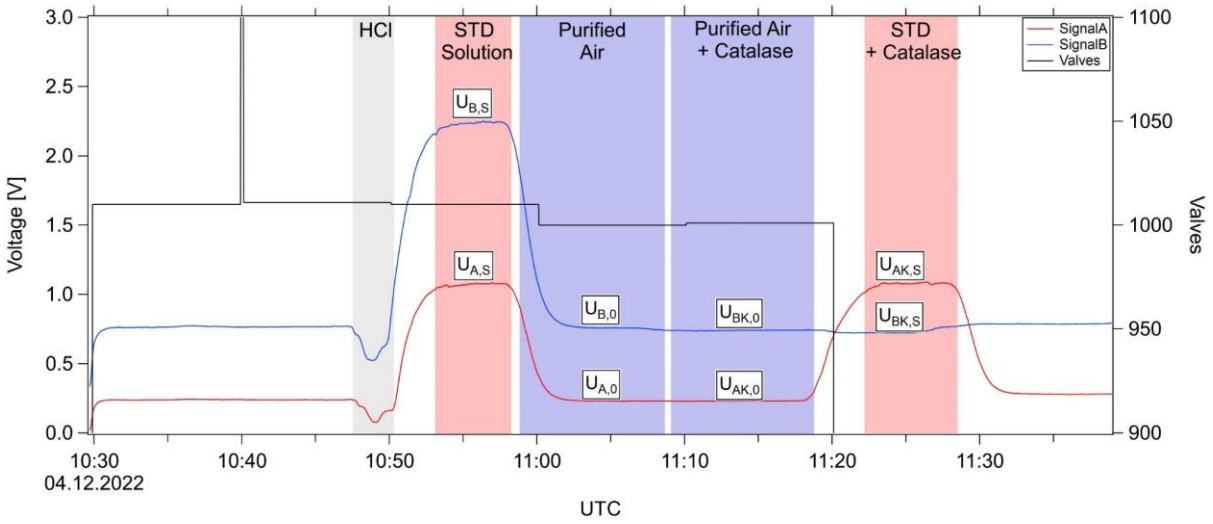

Figure S 1: Exemplary liquid calibration signals of the HYPHOP monitor and the corresponding points of the four-point-calibration-method (flushing with HCl: gray; initiation of the standard with/without catalase: red; sampling of zero air with/without catalase: blue).

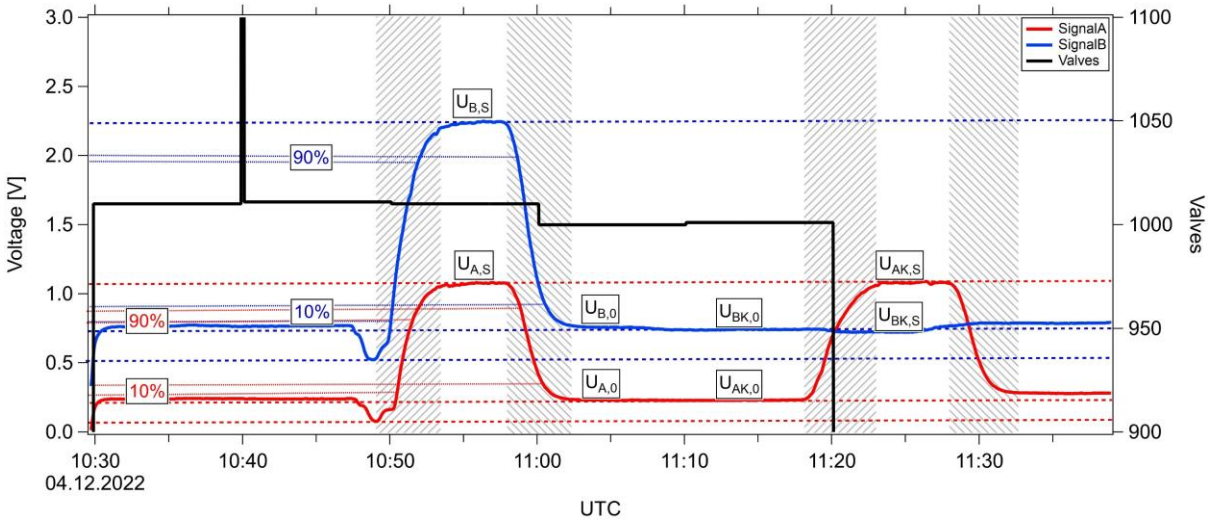

Figure S 2: Determination of the instrumental time resolution based on the 10-90 method.

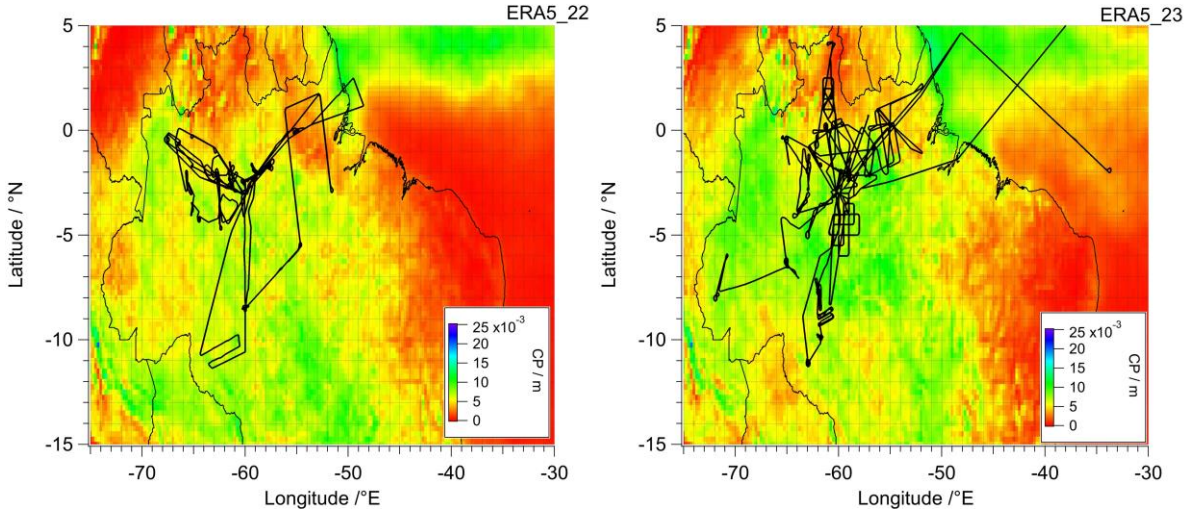

Figure S 3: Average monthly convective precipitation (CP) in December 2022 (left) and January 2023 (right) derived by ERA5 reanalysis generated using Copernicus Climate Change Service (Hersbach et al 2019). GPS flight tracks of performed measurement flights are indicated in black.

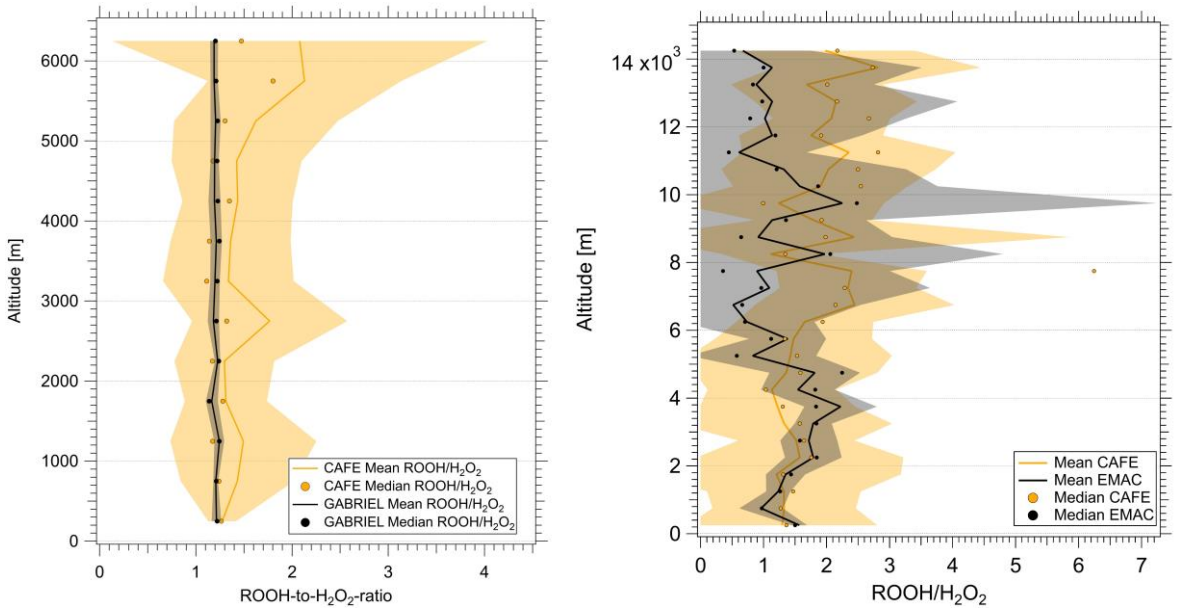

Figure S 4: Comparison of ROOH-to-H_2O_2-ratio vertical distribution during GABRIEL 2005 (left) and EMAC simulations during CAFE-Brazil (right) relative to situ observations during CAFE-Brazil. Vertical profiles were calculated within 500 m means and medians over the entire available atmospheric column. Please note that in order to avoid any bias caused by anthropogenic emissions, measured and simulated data output in close proximity to the base of operation in Manaus during CAFE-Brazil was removed from the corresponding datasets.

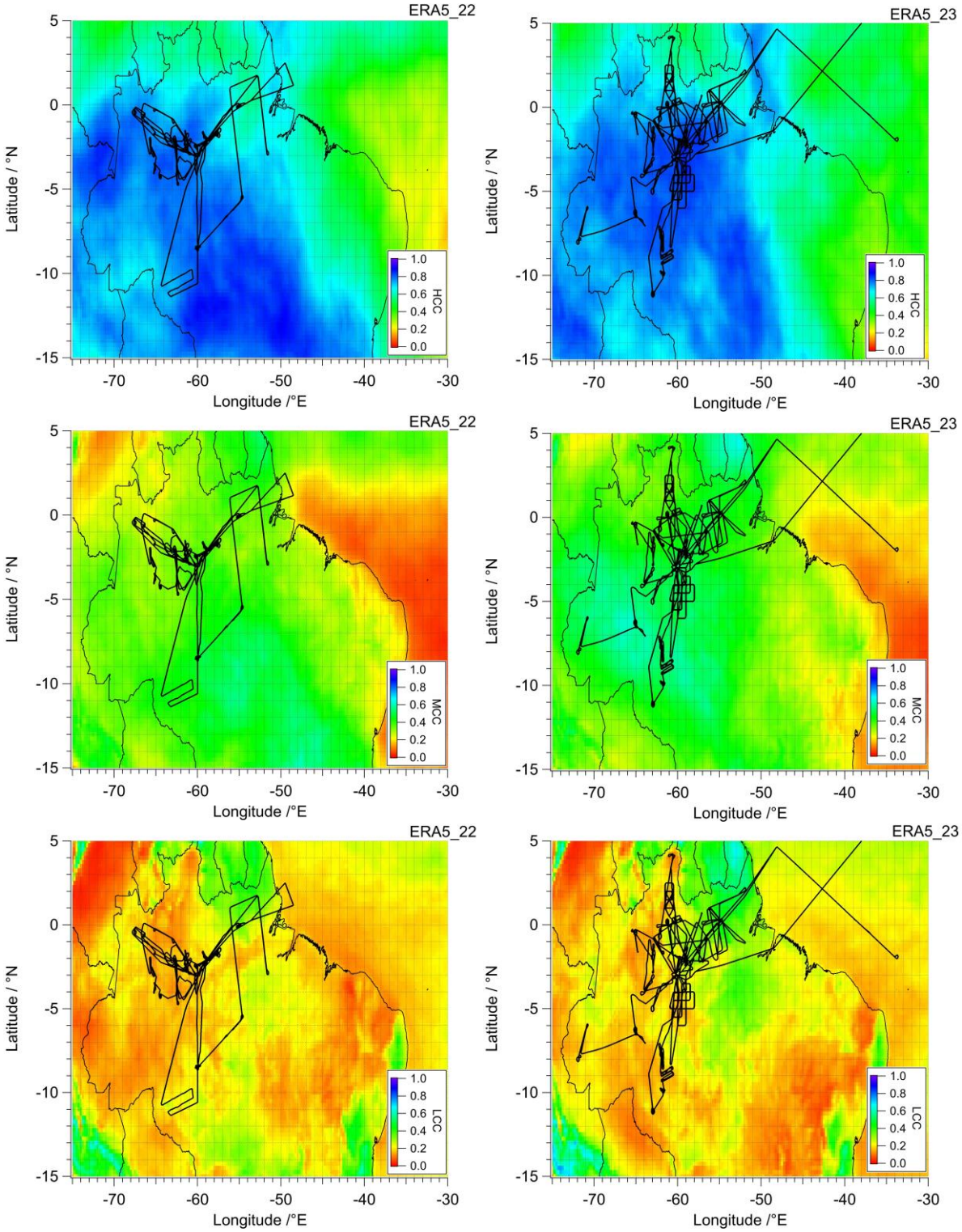

Figure S 5: Average monthly high (> 6 km; top panel), middle (2 < 6 km; middle panel), and low cloud coverage (< 2 km; bottom panel) in December 2022 (left column) and January 2023 (right column) based on ERA5 reanalysis generated using Copernicus Climate Change Service (Hersbach et al., 2019). GPS flight tracks of performed measurement flights are indicated in black.

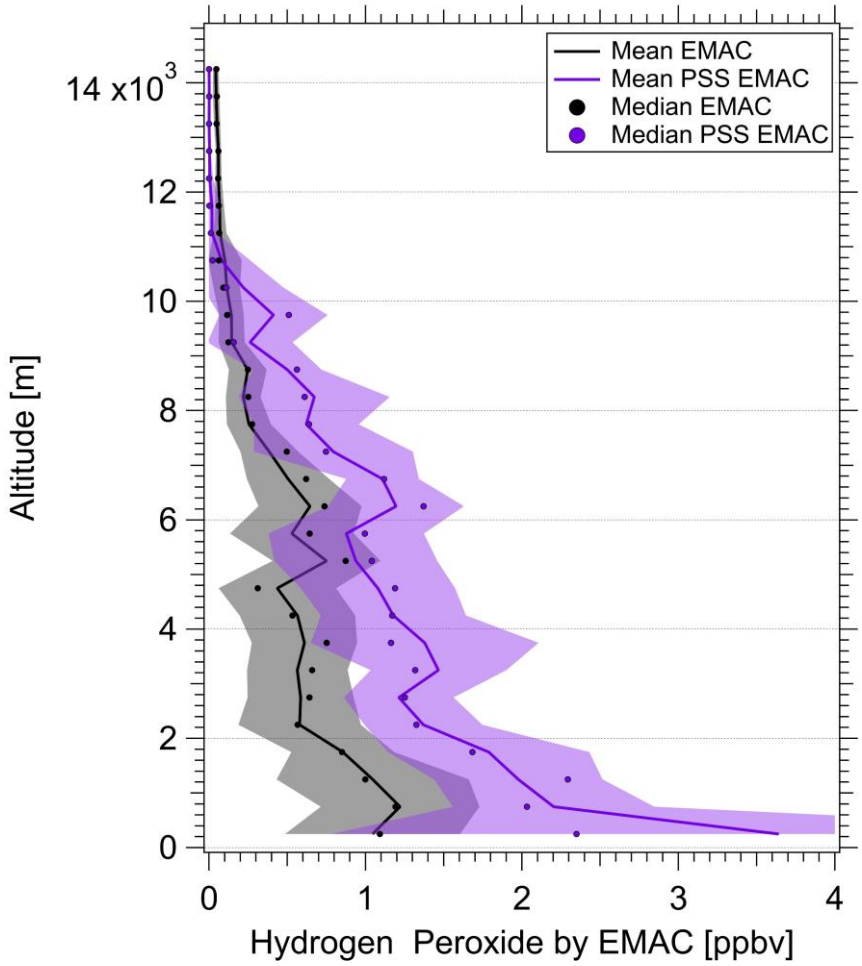

Figure S 6: Comparison of H_2O_2 vertical distribution during CAFE-Brazil based on EMAC simulations (black plot) relative to the calculated PSS-H_2O_2 based on the simulated precursors (HO_2, OH), and H_2O_2 photolysis rate. Vertical profiles were calculated within 500 m means and medians over the entire available atmospheric column.

7.4. List of Figures

7.5. List of figures included in the corresponding manuscripts

"HYPHOP; a tool for high-altitude, long-range monitoring of hydrogen peroxide and higher organic peroxides in the atmosphere"

"Distribution of hydrogen peroxide over Europe during the BLUESKY aircraft campaign"

"Hydrogen peroxide in the upper tropical troposphere over the Atlantic Ocean and western Africa during the CAFE-Africa aircraft campaign"

7.6. List of tables

7.7. List of tables included in the scientific manuscripts

"HYPHOP; a tool for high-altitude, long-range monitoring of hydrogen peroxide and higher organic peroxides in the atmosphere"

"Distribution of hydrogen peroxide over Europe during the BLUESKY aircraft campaign"

"Hydrogen peroxide in the upper tropical troposphere over the Atlantic Ocean and western Africa during the CAFE-Africa aircraft campaign"

8. References

Allen, H. M., Crounse, J. D., Kim, M. J., Teng, A. P., Ray, E. A., McKain, K., Sweeney, C., and Wennberg, P. O.: H 2 O 2 and CH 3 OOH (MHP) in the Remote Atmosphere: 1. Global Distribution and Regional Influences, J. Geophys. Res. Atmos., 127, https://doi.org/10.1029/2021JD035701, 2022a.

Allen, H. M., Bates, K. H., Crounse, J. D., Kim, M. J., Teng, A. P., Ray, E. A., and Wennberg, P. O.: H 2 O 2 and CH 3 OOH (MHP) in the Remote Atmosphere: 2. Physical and Chemical Controls, Journal of Geophysical Research: Atmospheres, 127, https://doi.org/10.1029/2021JD035702, 2022b.

Anastasio, C., Faust, B. C., and Allen, J. M.: Aqueous phase photochemical formation of hydrogen peroxide in authentic cloud waters, J. Geophys. Res., 99, 8231, https://doi.org/10.1029/94JD00085, 1994.

Atkinson, R., Baulch, D. L., Cox, R. A., Crowley, J. N., Hampson, R. F., Hynes, R. G., Jenkin, M. E., Rossi, M. J., and Troe, J.: Evaluated kinetic and photochemical data for atmospheric chemistry: Volume I - gas phase reactions of Ox, HOx, NOx and SOx species, Atmos. Chem. Phys., 4, 1461–1738, https://doi.org/10.5194/acp-4-1461-2004, 2004.

Ayers, G. P., Penkett, S. A., Gillett, R. W., Bandy, B., Galbally, I. E., Meyer, C. P., Elsworth, C. M., Bentley, S. T., and Forgan, B. W.: The annual cycle of peroxides and ozone in marine air at Cape Grim, Tasmania, J Atmos Chem, 23, 221–252, https://doi.org/10.1007/BF00055155, 1996.

Barth, M. C., Stuart, A. L., and Skamarock, W. C.: Numerical simulations of the July 10, 1996, Stratospheric-Tropospheric Experiment: Radiation, Aerosols, and Ozone (STERAO)-Deep Convection experiment storm: Redistribution of soluble tracers, J. Geophys. Res., 106, 12381–12400, https://doi.org/10.1029/2001JD900139, 2001.

Becker, K. H., Brockmann, K. J., and Bechara, J.: Production of hydrogen peroxide in forest air by reaction of ozone with terpenes, Nature, 346, 256–258, https://doi.org/10.1038/346256a0, 1990.

Bela, M. M., Barth, M. C., Toon, O. B., Fried, A., Homeyer, C. R., Morrison, H., Cummings, K. A., Li, Y., Pickering, K. E., Allen, D. J., Yang, Q., Wennberg, P. O., Crounse, J. D., St. Clair, J. M., Teng, A. P., O'Sullivan, D., Huey, L. G., Chen, D., Liu, X., Blake, D. R., Blake, N. J., Apel, E. C., Hornbrook, R. S., Flocke, F., Campos, T., and Diskin, G.: Wet scavenging of soluble gases in DC3 deep convective storms using WRF-Chem simulations and aircraft observations, J. Geophys. Res. Atmos., 121, 4233–4257, https://doi.org/10.1002/2015JD024623, 2016.

Bohn, B. and Lohse, I.: Calibration and evaluation of CCD spectroradiometers for ground-based and airborne measurements of spectral actinic flux densities, Atmos. Meas. Tech., 10, 3151–3174, https://doi.org/10.5194/amt-10-3151-2017, 2017.

Bozem, H., Pozzer, A., Harder, H., Martinez, M., Williams, J., Lelieveld, J., and Fischer, H.: The influence of deep convection on HCHO and H 2 O 2 in the upper troposphere over Europe, Atmos. Chem. Phys., 17, 11835–11848, https://doi.org/10.5194/acp-17-11835-2017, 2017.

Brimblecombe, P. and Dawson, G. A.: Wet removal of highly soluble gases, J Atmos Chem, 2, 95–107, https://doi.org/10.1007/BF00127265, 1984.

Bufalini, J. J., Lancaster, H. T., Namie, G. R., and Gay, B. W.: Hydrogen peroxide formation from the photooxidation of formaldehyde and its presence in rainwater, Journal of Environmental Science

and Health Part A: Environmental Science and Engineering, 14, 135–141, https://doi.org/10.1080/10934527909374867, 1979.

Calvert, J. G., Lazrus, A., Kok, G. L., Heikes, B. G., Walega, J. G., Lind, J., and Cantrell, C. A.: Chemical mechanisms of acid generation in the troposphere, Nature, 317, 27–35, https://doi.org/10.1038/317027a0, 1985.

Calvert, J. G. and Madronich, S.: Theoretical study of the initial products of the atmospheric oxidation of hydrocarbons, J. Geophys. Res., 92, 2211, https://doi.org/10.1029/JD092iD02p02211, 1987.

Campbell, M. J., Sheppard, J. C., and Au, B. F.: Measurement of hydroxyl concentration in boundary layer air by monitoring CO oxidation, Geophys. Res. Lett., 6, 175–178, https://doi.org/10.1029/GL006i003p00175, 1979.

Chang, W., Lee, M., and Heikes, B. G.: One-dimensional photochemical study of H 2 O 2 CH 3 OOH, and HCHO in the marine boundary layer during Pacific Exploratory Mission in the Tropics (PEM-Tropics) B, J. Geophys. Res., 109, n/a-n/a, https://doi.org/10.1029/2003jd004256, 2004.

Chatfield, R. B. and Crutzen, P. J.: Sulfur dioxide in remote oceanic air: Cloud transport of reactive precursors, J. Geophys. Res., 89, 7111, https://doi.org/10.1029/JD089iD05p07111, 1984.

Christian, N.: Charakterisierung des Peroxidmonitors HYPHOP im Hinblick auf flugzeuggetragene Messungen, Bachelorarbeit, Johannes Gutenberg-Universität, Mainz, 2019.

Cohan, D. S., Schultz, M. G., Jacob, D. J., Heikes, B. G., and Blake, D. R.: Convective injection and photochemical decay of peroxides in the tropical upper troposphere: Methyl iodide as a tracer of marine convection, J. Geophys. Res., 104, 5717–5724, https://doi.org/10.1029/98JD01963, 1999.

Colomb, A., Williams, J., Crowley, J., Gros, V., Hofmann, R., Salisbury, G., Klüpfel, T., Kormann, R., Stickler, A., Forster, C., and Lelieveld, J.: Airborne Measurements of Trace Organic Species in the Upper Troposphere Over Europe: the Impact of Deep Convection, Environ. Chem., 3, 244, https://doi.org/10.1071/EN06020, 2006.

Crippa, M., Guizzardi, D., Muntean, M., Schaaf, E., Dentener, F., van Aardenne, J. A., Monni, S., Doering, U., Olivier, J. G. J., Pagliari, V., and Janssens-Maenhout, G.: Gridded Emissions of Air Pollutants for the period 1970–2012 within EDGAR v4.3.2, 2018.

Crounse, J. D., McKinney, K. A., Kwan, A. J., and Wennberg, P. O.: Measurement of gas-phase hydroperoxides by chemical ionization mass spectrometry, Anal. Chem., 78, 6726–6732, https://doi.org/10.1021/ac0604235, 2006.

Crutzen, P.: A discussion of the chemistry of some minor constituents in the stratosphere and troposphere, PAGEOPH, 106-108, 1385–1399, https://doi.org/10.1007/BF00881092, 1973.

Crutzen, P. J., Lawrence, M. G., and Pöschl, U.: On the background photochemistry of tropospheric ozone, Tellus B: Chemical and Physical Meteorology, 51, 123–146, https://doi.org/10.3402/tellusb.v51i1.16264, 1999.

Crutzen, P. J. and Lawrence, M. G.: The Impact of Precipitation Scavenging on the Transport of Trace Gases: A 3-Dimensional Model Sensitivity Study, J Atmos Chem, 37, 81–112, https://doi.org/10.1023/A:1006322926426, 2000.

Czader, B. H., Rappenglück, B., Percell, P., Byun, D. W., Ngan, F., and Kim, S.: Modeling nitrous acid and its impact on ozone and hydroxyl radical during the Texas Air Quality Study 2006, Atmos. Chem. Phys. Discuss., 12, 5851–5880, https://doi.org/10.5194/acpd-12-5851-2012, 2012.

Damschen, D. E. and Martin, L.R.: Aqueous aerosol oxidation of nitrous acid by O2, O3 AND H2O2, Atmospheric Environment (1967), 17, 2005–2011, https://doi.org/10.1016/0004-6981(83)90357-8, 1983.

Daum, P. H., Kleinman, L. I., Hills, A. J., Lazrus, A. L., Leslie, A. C. D., Busness, K., and Boatman, J.: Measurement and interpretation of concentrations of H 2 O 2 and related species in the upper midwest during summer, J. Geophys. Res., 95, 9857–9871, https://doi.org/10.1029/JD095iD07p09857, 1990.

Dienhart, D., Brendel, B., Crowley, J. N., Eger, P. G., Harder, H., Martinez, M., Pozzer, A., Rohloff, R., Schuladen, J., Tauer, S., Walter, D., Lelieveld, J., and Fischer, H.: Formaldehyde and hydroperoxide distribution around the Arabian Peninsula – evaluation of EMAC model results with ship-based measurements, Atmos. Chem. Phys., 23, 119–142, https://doi.org/10.5194/acp-23-119-2023, 2023.

Edy, J., Cautenet, S., and Brémaud, P.: Modeling ozone and carbon monoxide redistribution by shallow convection over the Amazonian rain forest, J. Geophys. Res., 101, 28671–28681, https://doi.org/10.1029/96JD01867, 1996.

Ether: IUPAC Task Group on Atmospheric Chemical Kinetic Data Evaluation, http://iupac.pole-ether.fr/, last access: 15 April 2020, 2017.

Faloona, I., Tan, D., Brune, W. H., Jaeglé, L., Jacob, D. J., Kondo, Y., Koike, M., Chatfield, R., Pueschel, R., Ferry, G., Sachse, G., Vay, S., Anderson, B., Hannon, J., and Fuelberg, H.: Observations of HO x and its relationship with NO x in the upper troposphere during SONEX, J. Geophys. Res., 105, 3771–3783, https://doi.org/10.1029/1999JD900914, 2000.

Faloona, I. C., Tan, D., Lesher, R. L., Hazen, N. L., Frame, C. L., Simpas, J. B., Harder, H., Martinez, M., Di Carlo, P., Ren, X., and Brune, W. H.: A Laser-induced Fluorescence Instrument for Detecting Tropospheric OH and HO 2 Characteristics and Calibration, J Atmos Chem, 47, 139–167, https://doi.org/10.1023/B:JOCH.0000021036.53185.0e, 2004.

Fels, M. and Junkermann, W.: The occurrence of organic peroxides in air at a mountain site, Geophys. Res. Lett., 21, 341–344, https://doi.org/10.1029/93GL01892, 1994.

Fischer, H., Pozzer, A., Schmitt, T., Jöckel, P., Klippel, T., Taraborrelli, D., and Lelieveld, J.: Hydrogen peroxide in the marine boundary layer over the South Atlantic during the OOMPH cruise in March 2007, Atmos. Chem. Phys., 15, 6971–6980, https://doi.org/10.5194/acp-15-6971-2015, 2015.

Fischer, H., Axinte, R., Bozem, H., Crowley, J. N., Ernest, C., Gilge, S., Hafermann, S., Harder, H., Hens, K., Königstedt, R., Kubistin, D., Mallik, C., Martinez, M., Novelli, A., Parchatka, U., Plass-Dülmer, C., Pozzer, A., Regelin, E., Reiffs, A., Schmidt, T., Schuladen, J., and Lelieveld, J.: Diurnal variability, photochemical production and loss processes of hydrogen peroxide in the boundary layer over Europe, 2018.

Fischer, H., Axinte, R., Bozem, H., Crowley, J. N., Ernest, C., Gilge, S., Hafermann, S., Harder, H., Hens, K., Janssen, R. H. H., Königstedt, R., Kubistin, D., Mallik, C., Martinez, M., Novelli, A., Parchatka, U., Plass-Dülmer, C., Pozzer, A., Regelin, E., Reiffs, A., Schmidt, T., Schuladen, J., and Lelieveld, J.: Diurnal variability, photochemical production and loss processes of hydrogen peroxide in the boundary layer over Europe, Atmos. Chem. Phys., 19, 11953–11968, https://doi.org/10.5194/acp-19-11953-2019, 2019.

Fontaine, B., Roucou, P., Gaetani, M., and Marteau, R.: Recent changes in precipitation, ITCZ convection and northern tropical circulation over North Africa (1979-2007), Int. J. Climatol., 31, 633–648, https://doi.org/10.1002/joc.2108, 2011.

Gäb, S., Hellpointner, E., Turner, W. V., and Korte, F.: Hydroxymethyl hydroperoxide and bis(hydroxymethyl) peroxide from gas-phase ozonolysis of naturally occurring alkenes, Nature, 316, 535–536, https://doi.org/10.1038/316535a0, 1985.

Gold, V.: The IUPAC Compendium of Chemical Terminology, International Union of Pure and Applied Chemistry (IUPAC), Research Triangle Park, NC, 2019.

Graedel, T. E. and Goldberg, K. I.: Kinetic studies of raindrop chemistry: 1. Inorganic and organic processes, J. Geophys. Res., 88, 10865, https://doi.org/10.1029/JC088iC15p10865, 1983.

Graedel, T. E., Mandich, M. L., and Weschler, C. J.: Kinetic model studies of atmospheric droplet chemistry: 2. Homogeneous transition metal chemistry in raindrops, J. Geophys. Res., 91, 5205, https://doi.org/10.1029/JD091iD04p05205, 1986.

Granier, C., Darras, S., Denier van der Gon, H., Doubalova, J., Elguindi, N., Galle, B., Gauss, M., Guevara, M., Jalkanen, J.-P., Kuenen, J., Liousse, C., Quack, B., Simpson, D., and Sindelarova, K.: The Copernicus Atmosphere Monitoring Service global and regional emissions (April 2019 version), 2019.

Guevara, M., Jorba, O., Soret, A., Petetin, H., Bowdalo, D., Serradell, K., Tena, C., van der Denier Gon, H., Kuenen, J., Peuch, V.-H., and Pérez García-Pando, C.: Time-resolved emission reductions for atmospheric chemistry modelling in Europe during the COVID-19 lockdowns, Atmos. Chem. Phys., 21, 773–797, https://doi.org/10.5194/acp-21-773-2021, 2021.

Guilbault, G. G., Brignac, P. J., and Juneau, M.: New substrates for the fluorometric determination of oxidative enzymes, Anal. Chem., 40, 1256–1263, https://doi.org/10.1021/ac60264a027, 1968.

Gunz, D. W. and Hoffmann, M. R.: Atmospheric chemistry of peroxides: a review, Atmospheric Environment. Part A. General Topics, 24, 1601–1633, https://doi.org/10.1016/0960-1686(90)90496-A, 1990.

Hafermann, S.: Testmessungen mit dem HALO Peroxidmonitor HyPHoP, Diplomarbeit, Johannes Gutenberg-Universität, Mainz, 2013.

Hafermann, S.: Entwicklung und Anwendung von Messinstrumenten für spezifische Hydroperoxid-Messungen in der Troposphäre, Dissertation, Johannes Gutenberg-Universität, Mainz, 2016.

Hall, B. D. and Claiborn, C. S.: Measurements of the dry deposition of peroxides to a Canadian boreal forest, J. Geophys. Res., 102, 29343–29353, https://doi.org/10.1029/97JD01113, 1997.

Hall, B., Claiborn, C., and Baldocchi, D.: Measurement and modeling of the dry deposition of peroxides, Atmospheric Environment, 33, 577–589, https://doi.org/10.1016/S1352-2310(98)00271-4, available at: https://www.sciencedirect.com/science/article/pii/S1352231098002714, 1999.

Hamryszczak, Z. T., Pozzer, A., Obersteiner, F., Bohn, B., Steil, B., Lelieveld, J., and Fischer, H.: Distribution of hydrogen peroxide over Europe during the BLUESKY aircraft campaign, Atmos. Chem. Phys., 22, 9483–9497, https://doi.org/10.5194/acp-22-9483-2022, 2022.

Hamryszczak, Z., Dienhart, D., Brendel, B., Rohloff, R., Marno, D., Martinez, M., Harder, H., Pozzer, A., Bohn, B., Zöger, M., Lelieveld, J., and Fischer, H.: Measurement report: Hydrogen peroxide in the upper tropical troposphere over the Atlantic Ocean and western Africa during the CAFE-Africa aircraft campaign, Atmos. Chem. Phys., 23, 5929–5943, https://doi.org/10.5194/acp-23-5929-2023, 2023.

Harteck, P.: Chemie und Photochemie in der Erdatmosphäre, Angew. Chem., 63, 1–7, https://doi.org/10.1002/ange.19510630102, 1951.

Hastenrath, S. and Lamb, P.: Some Aspects of Circulation and Climate over the Eastern Equatorial Atlantic, Mon. Wea. Rev., 105, 1019–1023, https://doi.org/10.1175/1520-0493(1977)105<1019:SAOCAC>2.0.CO;2, 1977.

Heikes, B. G., Lazrus, A. L., Kok, G. L., Kunen, S. M., Gandrud, B. W., Gitlin, S. N., and Sperry, P. D.: Evidence for aqueous phase hydrogen peroxide synthesis in the troposphere, J. Geophys. Res., 87, 3045, https://doi.org/10.1029/JC087iC04p03045, 1982.

Heikes, B. G.: Aqueous h2o2 production from o3 in glass impingers, Atmospheric Environment (1967), 18, 1433–1445, https://doi.org/10.1016/0004-6981(84)90050-7, 1984.

Heikes, B. G., Kok, G. L., Walega, J. G., and Lazrus, A. L.: H 2 O 2 O 3 and SO 2 measurements in the lower troposphere over the eastern United States during fall, J. Geophys. Res., 92, 915, https://doi.org/10.1029/JD092iD01p00915, 1987.

Heikes, B. G.: Formaldehyde and hydroperoxides at Mauna Loa Observatory, J. Geophys. Res., 97, 18001, https://doi.org/10.1029/92JD00268, 1992.

Heikes, B. G., Lee, M., Bradshaw, J., Sandholm, S., Davis, D. D., Crawford, J., Rodriguez, J., Liu, S., McKeen, S., Thornton, D., Bandy, A., Gregory, G., Talbot, R., and Blake, D.: Hydrogen peroxide and methylhydroperoxide distributions related to ozone and odd hydrogen over the North Pacific in the fall of 1991, J. Geophys. Res., 101, 1891–1905, https://doi.org/10.1029/95JD01364, 1996a.

Heikes, B., Lee, M., Jacob, D., Talbot, R., Bradshaw, J., Singh, H., Blake, D., Anderson, B., Fuelberg, H., and Thompson, A. M.: Ozone, hydroperoxides, oxides of nitrogen, and hydrocarbon budgets in the marine boundary layer over the South Atlantic, J. Geophys. Res., 101, 24221–24234, https://doi.org/10.1029/95JD03631, 1996b.

Hellpointner, E. and Gäb, S.: Detection of methyl, hydroxymethyl and hydroxyethyl hydroperoxides in air and precipitation, Nature, 337, 631–634, https://doi.org/10.1038/337631a0, 1989.

Hersbach, H., Bell, B., Berrisford, P., Biavati, G., Horányi, A., Muñoz Sabater, J., Nicolas, J., Peubey, C., Radu, R., Rozum, I., Schepers, D., Simmons, A., Soci, C., Dee, D., Thépaut, J-N.: ERA5 hourly data on single levels from 1979 to present, https://doi.org/10.24381/cds.adbb2d47, last access: 4 May 2021, 2018.

Hersbach, H., Bell, B., Berrisford, P., Biavati, G., Horányi, A., Muñoz Sabater, J., Nicolas, J., Peubey, C., Radu, R., Rozum, I., Schepers, D., Simmons, A., Soci, C., Dee, D., Thépaut, J-N.: ERA5 monthly averaged data on single levels from 1979 to present, https://doi.org/10.24381/CDS.F17050D7, last access: 22-07-22, 2019.

Hewitt, C. N. and Kok, G. L.: Formation and occurrence of organic hydroperoxides in the troposphere: Laboratory and field observations, J Atmos Chem, 12, 181–194, https://doi.org/10.1007/BF00115779, 1991.

Hoesly, R. M., Smith, S. J., Feng, L., Klimont, Z., Janssens-Maenhout, G., Pitkanen, T., Seibert, J. J., Vu, L., Andres, R. J., Bolt, R. M., Bond, T. C., Dawidowski, L., Kholod, N., Kurokawa, J.-i., Li, M., Liu, L., Lu, Z., Moura, M. C. P., O'Rourke, P. R., and Zhang, Q.: Historical (1750–2014) anthropogenic emissions of reactive gases and aerosols from the Community Emissions Data System (CEDS), Geosci. Model Dev., 11, 369–408, https://doi.org/10.5194/gmd-11-369-2018, 2018.

Hoffmann, M. R. and Edwards, J. O.: Kinetics of the oxidation of sulfite by hydrogen peroxide in acidic solution, J. Phys. Chem., 79, 2096–2098, https://doi.org/10.1021/j100587a005, 1975.

Holton, J. R., Haynes, P. H., McIntyre, M. E., Douglass, A. R., Rood, R. B., and Pfister, L.: Stratosphere-troposphere exchange, Rev. Geophys., 33, 403, https://doi.org/10.1029/95RG02097, 1995.

Hottmann, B.: Der Peroxid-Monitor HYPHOP: Charakterisierung und Anwendung bei OMO-Asia, Diplomarbeit, Johannes Gutenberg-Universität, Mainz, 2016.

Hottmann, B., Hafermann, S., Tomsche, L., Marno, D., Martinez, M., Harder, H., Pozzer, A., Neumaier, M., Zahn, A., Bohn, B., Stratmann, G., Ziereis, H., Lelieveld, J., and Fischer, H.: Impact of the South Asian monsoon outflow on atmospheric hydroperoxides in the upper troposphere, Atmos. Chem. Phys., 20, 12655–12673, https://doi.org/10.5194/acp-20-12655-2020, 2020.

Hua, W., Chen, Z. M., Jie, C. Y., Kondo, Y., Hofzumahaus, A., Takegawa, N., Chang, C. C., Lu, K. D., Miyazaki, Y., Kita, K., Wang, H. L., Zhang, Y. H., and Hu, M.: Atmospheric hydrogen peroxide and organic hydroperoxides during PRIDE-PRD'06, China: their concentration, formation mechanism and contribution to secondary aerosols, Atmos. Chem. Phys., 8, 6755–6773, https://doi.org/10.5194/acp-8-6755-2008, 2008.

Huang, D. and Chen, Z.: Reinvestigation of the Henry's law constant for hydrogen peroxide with temperature and acidity variation, Journal of Environmental Sciences, 22, 570–574, https://doi.org/10.1016/S1001-0742(09)60147-9, 2010.

Jackson, A. V. and Hewitt, C. N.: Hydrogen peroxide and organic hydroperoxide concentrations in air in a eucalyptus forest in central Portugal, Atmospheric Environment, 30, 819–830, https://doi.org/10.1016/1352-2310(95)00348-7, available at: https://www.sciencedirect.com/science/article/pii/1352231095003487, 1996.

Jackson, A. V. and Hewitt, C. N.: Atmosphere Hydrogen Peroxide and Organic Hydroperoxides: A Review, Critical Reviews in Environmental Science and Technology, 29, 175–228, https://doi.org/10.1080/10643389991259209, 1999.

Jacob, P., Tavares, T. M., Rocha, V. C., and Klockow, D.: Atmospheric H2O2 field measurements in a tropical environment: Bahia, Brazil, Atmospheric Environment. Part A. General Topics, 24, 377–382, https://doi.org/10.1016/0960-1686(90)90117-6, available at: http://www.sciencedirect.com/science/article/pii/0960168690901176, 1990.

Jacob, P. and Klockow, D.: Hydrogen peroxide measurements in the marine atmosphere, J Atmos Chem, 15, 353–360, https://doi.org/10.1007/BF00115404, 1992.

Jaeglé, L., Jacob, D. J., Wennberg, P. O., Spivakovsky, C. M., Hanisco, T. F., Lanzendorf, E. J., Hintsa, E. J., Fahey, D. W., Keim, E. R., Proffitt, M. H., Atlas, E. L., Flocke, F., Schauffler, S., McElroy, C. T., Midwinter, C., Pfister, L., and Wilson, J. C.: Observed OH and HO 2 in the upper troposphere suggest a major source from convective injection of peroxides, Geophys. Res. Lett., 24, 3181–3184, https://doi.org/10.1029/97GL03004, 1997.

Jaeglé, L., Jacob, D. J., Brune, W. H., Faloona, I. C., Tan, D., Kondo, Y., Sachse, G. W., Anderson, B., Gregory, G. L., Vay, S., Singh, H. B., Blake, D. R., and Shetter, R.: Ozone production in the upper troposphere and the influence of aircraft during SONEX: approach of NOx-saturated conditions, Geophysical Research Letters, 26, 3081–3084, https://doi.org/10.1029/1999GL900451, available at: https://agupubs.onlinelibrary.wiley.com/doi/pdf/10.1029/1999GL900451, 1999.

Jaeglé, L., Jacob, D. J., Brune, W. H., Faloona, I., Tan, D., Heikes, B. G., Kondo, Y., Sachse, G. W., Anderson, B., Gregory, G. L., Singh, H. B., Pueschel, R., Ferry, G., Blake, D. R., and Shetter, R.

E.: Photochemistry of HO x in the upper troposphere at northern midlatitudes, J. Geophys. Res., 105, 3877–3892, https://doi.org/10.1029/1999JD901016, 2000.

Jöckel, P., Sander, R., Kerkweg, A., Tost, H., and Lelieveld, J.: Technical Note: The Modular Earth Submodel System (MESSy) - a new approach towards Earth System Modeling, Atmos. Chem. Phys., 5, 433–444, https://doi.org/10.5194/acp-5-433-2005, 2005.

Jöckel, P., Tost, H., Pozzer, A., Brühl, C., Buchholz, J., Ganzeveld, L., Hoor, P., Kerkweg, A., Lawrence, M. G., Sander, R., Steil, B., Stiller, G., Tanarhte, M., Taraborrelli, D., van Aardenne, J., and Lelieveld, J.: The atmospheric chemistry general circulation model ECHAM5/MESSy1: consistent simulation of ozone from the surface to the mesosphere, Atmos. Chem. Phys., 6, 5067–5104, https://doi.org/10.5194/acp-6-5067-2006, 2006.

Jöckel, P., Kerkweg, A., Pozzer, A., Sander, R., Tost, H., Riede, H., Baumgaertner, A., Gromov, S., and Kern, B.: Development cycle 2 of the Modular Earth Submodel System (MESSy2), Geosci. Model Dev., 3, 717–752, https://doi.org/10.5194/gmd-3-717-2010, 2010.

Jöckel, P., Tost, H., Pozzer, A., Kunze, M., Kirner, O., Brenninkmeijer, C. A. M., Brinkop, S., Cai, D. S., Dyroff, C., Eckstein, J., Frank, F., Garny, H., Gottschaldt, K.-D., Graf, P., Grewe, V., Kerkweg, A., Kern, B., Matthes, S., Mertens, M., Meul, S., Neumaier, M., Nützel, M., Oberländer-Hayn, S., Ruhnke, R., Runde, T., Sander, R., Scharffe, D., and Zahn, A.: Earth System Chemistry integrated Modelling (ESCiMo) with the Modular Earth Submodel System (MESSy) version 2.51, Geosci. Model Dev., 9, 1153–1200, https://doi.org/10.5194/gmd-9-1153-2016, 2016.

Kaiser, J. W., Heil, A., Andreae, M. O., Benedetti, A., Chubarova, N., Jones, L., Morcrette, J.-J., Razinger, M., Schultz, M. G., Suttie, M., and van der Werf, G. R.: Biomass burning emissions estimated with a global fire assimilation system based on observed fire radiative power, Biogeosciences, 9, 527–554, https://doi.org/10.5194/bg-9-527-2012, 2012.

Kelly, T. J., Stedman, D. H., and Kok, G. L.: Measurements of H 2 O 2 and HNO 3 in rural air, Geophys. Res. Lett., 6, 375–378, https://doi.org/10.1029/GL006i005p00375, 1979.

Kelly, T. J., Daum, P. H., and Schwartz, S. E.: Measurements of peroxides in cloudwater and rain, J. Geophys. Res., 90, 7861–7871, https://doi.org/10.1029/JD090iD05p07861, 1985.

Kerkweg, A., Buchholz, J., Ganzeveld, L., Pozzer, A., Tost, H., and Jöckel, P.: Technical Note: An implementation of the dry removal processes DRY DEPosition and SEDImentation in the Modular Earth Submodel System (MESSy), Atmos. Chem. Phys., 6, 4617–4632, https://doi.org/10.5194/acp-6-4617-2006, 2006a.

Kerkweg, A., Sander, R., Tost, H., and Jöckel, P.: Technical note: Implementation of prescribed (OFFLEM), calculated (ONLEM), and pseudo-emissions (TNUDGE) of chemical species in the Modular Earth Submodel System (MESSy), Atmos. Chem. Phys., 6, 3603–3609, https://doi.org/10.5194/acp-6-3603-2006, 2006b.

Kleinman, L. I.: Photochemical formation of peroxides in the boundary layer, J. Geophys. Res., 91, 10889, https://doi.org/10.1029/JD091iD10p10889, 1986.

Kleinman, L. I.: Seasonal dependence of boundary layer peroxide concentration: The low and high NO x regimes, J. Geophys. Res., 96, 20721, https://doi.org/10.1029/91JD02040, 1991.

Klippel, T., Fischer, H., Bozem, H., Lawrence, M. G., Butler, T., Jöckel, P., Tost, H., Martinez, M., Harder, H., Regelin, E., Sander, R., Schiller, C. L., Stickler, A., and Lelieveld, J.: Distribution of hydrogen peroxide and formaldehyde over Central Europe during the HOOVER project, Atmos. Chem. Phys., 11, 4391–4410, https://doi.org/10.5194/acp-11-4391-2011, 2011.

Kok, G. L., Holler, T. P., Lopez, M. B., Nachtrieb, H. A., and Yuan, M.: Chemiluminescent method for determination of hydrogen peroxide in the ambient atmosphere, Environ. Sci. Technol., 12, 1072–1076, https://doi.org/10.1021/es60145a010, 1978.

Kormann, C., Bahnemann, D. W., and Hoffmann, M. R.: Photocatalytic production of hydrogen peroxides and organic peroxides in aqueous suspensions of titanium dioxide, zinc oxide, and desert sand, Environ. Sci. Technol., 22, 798–806, https://doi.org/10.1021/es00172a009, 1988.

Kraus, H.: Die Atmosphäre der Erde: Eine Einführung in die Meteorologie, 3. erweiterte und aktualisierte Auflage, Springer Berlin Heidelberg, Berlin, Heidelberg, 1 online resource, 2004.

Krautstrunk, M. and Giez, A.: The Transition From FALCON to HALO Era Airborne Atmospheric Research, in: Atmospheric Physics, edited by: Schumann, U., Springer Berlin Heidelberg, Berlin, Heidelberg, 609–624, https://doi.org/10.1007/978-3-642-30183-4_37, 2012.

Kumar, S.: An Eulerian model for scavenging of pollutants by raindrops, Atmospheric Environment (1967), 19, 769–778, https://doi.org/10.1016/0004-6981(85)90065-4, 1985.

Kunen, S. M., LAZRUS, A. L., KOK, G. L., and HEIKES, B. G.: Aqueous oxidation of SO 2 by hydrogen peroxide, J. Geophys. Res., 88, 3671, https://doi.org/10.1029/JC088iC06p03671, 1983.

Lazrus, A. L., Kok, G. L., Gitlin, S. N., Lind, J. A., and McLaren, S. E.: Automated fluorimetric method for hydrogen peroxide in atmospheric precipitation, Anal. Chem., 57, 917–922, https://doi.org/10.1021/ac00281a031, 1985.

Lazrus, A. L., G. L. Kok, J. A. Lind, S. N. Gitlin, B. G. Heikes, and R. E. Shelter: Automated Fluorometric Method for Hydrogen Peroxide in Air, Anal. Chem., 58, 594–597, 1986.

Lee, J. H., Tang, I. N., Weinstein-Lloyd, J. B., and Halper, E. B.: Improved nonenzymatic method for the determination of gas-phase peroxides, Environmental Science and Technology; (United States), 28:6, https://doi.org/10.1021/es00055a032, 1994.

Lee, M.: Hydrogen Peroxide, Methyl Hydroperoxide, and Formaldehyde in Air Impacted by Biomass Burning, Ph.D. Thesis, 1995.

Lee, M., Heikes, B. G., Jacob, D. J., Sachse, G., and Anderson, B.: Hydrogen peroxide, organic hydroperoxide, and formaldehyde as primary pollutants from biomass burning, J. Geophys. Res., 102, 1301–1309, https://doi.org/10.1029/96jd01709, 1997.

Lee, M., Heikes, B. G., and Jacob, D. J.: Enhancements of hydroperoxides and formaldehyde in biomass burning impacted air and their effect on atmospheric oxidant cycles, J. Geophys. Res., 103, 13201–13212, https://doi.org/10.1029/98JD00578, 1998.

Lee, M., Heikes, B. G., and O'Sullivan, D. W.: Hydrogen peroxide and organic hydroperoxide in the troposphere: a review, Atmospheric Environment, 34, 3475–3494, https://doi.org/10.1016/S1352-2310(99)00432-X, available at: http://www.sciencedirect.com/science/article/pii/S135223109900432X, 2000.

Lee, Y.-N. and Lind, J. A.: Kinetics of aqueous-phase oxidation of nitrogen(III) by hydrogen peroxide, J. Geophys. Res., 91, 2793, https://doi.org/10.1029/JD091iD02p02793, 1986.

Lelieveld, J. and Crutzen, P. J.: Influences of cloud photochemical processes on tropospheric ozone, Nature, 343, 227–233, https://doi.org/10.1038/343227a0, 1990.

Lelieveld, J. and Crutzen, P. J.: The role of clouds in tropospheric photochemistry, J Atmos Chem, 12, 229–267, https://doi.org/10.1007/BF00048075, 1991.

Lelieveld, J. and Crutzen, P. J.: Role of deep cloud convection in the ozone budget of the troposphere, Science (New York, N.Y.), 264, 1759–1761, https://doi.org/10.1126/science.264.5166.1759, 1994.

Levy, H.: Normal atmosphere: large radical and formaldehyde concentrations predicted, Science (New York, N.Y.), 173, 141–143, https://doi.org/10.1126/science.173.3992.141, 1971.

Lightfoot, P.D., Cox, R.A., Crowley, J.N., Destriau, M., Hayman, G.D., Jenkin, M.E., Moortgat, G.K., and Zabel, F.: Organic peroxy radicals: Kinetics, spectroscopy and tropospheric chemistry, Atmospheric Environment. Part A. General Topics, 26, 1805–1961, https://doi.org/10.1016/0960-1686(92)90423-I, available at: https://www.sciencedirect.com/science/article/pii/096016869290423I, 1992.

Lind, J. A. and Kok, G. L.: Henry's law determinations for aqueous solutions of hydrogen peroxide, methylhydroperoxide, and peroxyacetic acid, J. Geophys. Res., 91, 7889–7895, https://doi.org/10.1029/JD091iD07p07889, 1986.

Lind, J. A., Lazrus, A. L., and Kok, G. L.: Aqueous phase oxidation of sulfur(IV) by hydrogen peroxide, methylhydroperoxide, and peroxyacetic acid, J. Geophys. Res., 92, 4171, https://doi.org/10.1029/JD092iD04p04171, 1987.

Logan, J. A., Prather, M. J., Wofsy, S. C., and McElroy, M. B.: Tropospheric chemistry: A global perspective, J. Geophys. Res., 86, 7210, https://doi.org/10.1029/JC086iC08p07210, 1981.

Mackay, G. I., Mayne, L. K., and Schiff, H. I.: Measurements of H 2 O 2 and HCHO by Tunable Diode Laser Absorption Spectroscopy During the 1986 Carbonaceous Species Methods Comparison Study in Glendora, California, Aerosol Science and Technology, 12, 56–63, https://doi.org/10.1080/02786829008959325, 1990.

Madronich, S.: Photodissociation in the atmosphere: 1. Actinic flux and the effects of ground reflections and clouds, J. Geophys. Res., 92, 9740, https://doi.org/10.1029/JD092iD08p09740, 1987.

Mari, C., Saüt, C., Jacob, D. J., Staudt, A., Avery, M. A., Brune, W. H., Faloona, I., Heikes, B. G., Sachse, G. W., Sandholm, S. T., Singh, H. B., and Tan, D.: On the relative role of convection, chemistry, and transport over the South Pacific Convergence Zone during PEM-Tropics B: A case study, J. Geophys. Res., 108, https://doi.org/10.1029/2001JD001466, 2003.

Marno, D., Ernest, C., Hens, K., Javed, U., Klimach, T., Martinez, M., Rudolf, M., Lelieveld, J., and Harder, H.: Calibration of an airborne HOx instrument using the All Pressure Altitude-based Calibrator for HOx Experimentation (APACHE), Atmos. Meas. Tech., 13, 2711–2731, https://doi.org/10.5194/amt-13-2711-2020, 2020.

McArdle, J. V. and Hoffmann, M. R.: Kinetics and mechanism of the oxidation of aquated sulfur dioxide by hydrogen peroxide at low pH, J. Phys. Chem., 87, 5425–5429, https://doi.org/10.1021/j150644a024, 1983.

Molina, M. J. and Rowland, F. S.: Predicted present stratospheric abundances of chlorine species from photodissociation of carbon tetrachloride, Geophys. Res. Lett., 1, 309–312, https://doi.org/10.1029/GL001i007p00309, 1974.

Möller, D.: Chemistry of the climate system, Second edition, De Gruyter, Berlin, 1 volume, 2017.

Nguyen, T. B., Crounse, J. D., Teng, A. P., St Clair, J. M., Paulot, F., Wolfe, G. M., and Wennberg, P. O.: Rapid deposition of oxidized biogenic compounds to a temperate forest, Proceedings of the National Academy of Sciences of the United States of America, 112, E392-401, https://doi.org/10.1073/pnas.1418702112, 2015.

Nunnermacker, L. J., Weinstein-Lloyd, J. B., Hillery, B., Giebel, B., Kleinman, L. I., Springston, S. R., Daum, P. H., Gaffney, J., Marley, N., and Huey, G.: Aircraft and ground-based measurements of hydroperoxides during the 2006 MILAGRO field campaign, Atmos. Chem. Phys., 8, 7619–7636, https://doi.org/10.5194/acp-8-7619-2008, 2008.

Nussbaumer, C. M., Tadic, I., Dienhart, D., Wang, N., Edtbauer, A., Ernle, L., Williams, J., Obersteiner, F., Gutiérrez-Álvarez, I., Harder, H., Lelieveld, J., and Fischer, H.: Measurement report: In situ observations of deep convection without lightning during the tropical cyclone Florence 2018, Atmos. Chem. Phys., 21, 7933–7945, https://doi.org/10.5194/acp-21-7933-2021, 2021.

Olszyna, K. J., Meagher, J. F., and Bailey, E. M.: Gas-phase, cloud and rain-water measurements of hydrogen peroxide at a high-elevation site, Atmospheric Environment (1967), 22, 1699–1706, https://doi.org/10.1016/0004-6981(88)90398-8, available at: http://www.sciencedirect.com/science/article/pii/0004698188903988, 1988.

O'Sullivan, D. W., Lee, M., Noone, B. C., and Heikes, B. G.: Henry's Law Constant Determinations for Hydrogen Peroxide, Methyl Hydroperoxide, Hydroxymethyl Hydroperoxide, Ethyl Hydroperoxide, and Peroxyacetic Acid, J. Phys. Chem., 100, 3241–3247, https://doi.org/10.1021/jp951168n, 1996.

O'Sullivan, D. W., Heikes, B. G., Lee, M., Chang, W., Gregory, G. L., Blake, D. R., and Sachse, G. W.: Distribution of hydrogen peroxide and methylhydroperoxide over the Pacific and South Atlantic Oceans, J. Geophys. Res., 104, 5635–5646, https://doi.org/10.1029/98JD01250, 1999.

Palenik, B., Zafiriou, O. C., and Morel, F. M. M.: Hydrogen peroxide production by a marine phytoplankter1, Limnol. Oceanogr., 32, 1365–1369, https://doi.org/10.4319/lo.1987.32.6.1365, 1987.

Penkett, S. A., Jones, B.M.R., Brich, K. A., and Eggleton, A.E.J.: The importance of atmospheric ozone and hydrogen peroxide in oxidising sulphur dioxide in cloud and rainwater, Atmospheric Environment (1967), 13, 123–137, https://doi.org/10.1016/0004-6981(79)90251-8, available at: http://www.sciencedirect.com/science/article/pii/0004698179902518, 1979.

Perros, P.E.: Large-scale distribution of hydrogen peroxide from aircraft measurements during the TROPOZ II experiment, Atmospheric Environment. Part A. General Topics, 27, 1695–1708, https://doi.org/10.1016/0960-1686(93)90232-N, available at: https://www.sciencedirect.com/science/article/pii/096016869390232N, 1993.

Pilz, W. and Johann, I.: Die Bestimmung Kleinster Mengen von Wasserstoffperoxyd in Luft, International journal of environmental analytical chemistry, 3, 257–270, https://doi.org/10.1080/03067317408071087, 1974.

Pozzer, A., Jöckel, P., and van Aardenne, J.: The influence of the vertical distribution of emissions on tropospheric chemistry, Atmos. Chem. Phys., 9, 9417–9432, https://doi.org/10.5194/acp-9-9417-2009, 2009.

Pozzer, A., Reifenberg, S. F., Kumar, V., Franco, B., Kohl, M., Taraborrelli, D., Gromov, S., Ehrhart, S., Jöckel, P., Sander, R., Fall, V., Rosanka, S., Karydis, V., Akritidis, D., Emmerichs, T., Crippa, M., Guizzardi, D., Kaiser, J. W., Clarisse, L., Kiendler-Scharr, A., Tost, H., and Tsimpidi, A.: Simulation of organics in the atmosphere: evaluation of EMACv2.54 with the Mainz Organic Mechanism (MOM) coupled to the ORACLE (v1.0) submodel, Geosci. Model Dev., 15, 2673–2710, https://doi.org/10.5194/gmd-15-2673-2022, 2022.

Prather, M. J. and Jacob, D. J.: A persistent imbalance in HO x and NO x photochemistry of the upper troposphere driven by deep tropical convection, Geophys. Res. Lett., 24, 3189–3192, https://doi.org/10.1029/97GL03027, 1997.

Reeves, C. E. and Penkett, S. A.: Measurements of peroxides and what they tell us, Chemical reviews, 103, 5199–5218, https://doi.org/10.1021/cr0205053, 2003.

Reifenberg, S. F., Martin, A., Kohl, M., Hamryszczak, Z., Tadic, I., Röder, L., Crowley, D. J., Fischer, H., Kaiser, K., Schneider, J., Dörich, R., Crowley, J. N., Tomsche, L., Marsing, A., Voigt, C., Zahn, A., Pöhlker, C., Holanda, B., Krüger, O. O., Pöschl, U., Pöhlker, M., Jöckel, P., Dorf, M., Schumann, U., Williams, J., Curtius, J., Harder, H., Schlager, H., Lelieveld, J., and Pozzer, A.: Impact of reduced emissions on direct and indirect aerosol radiative forcing during COVID–19 lockdown in Europe, 2021.

Reus, M. de, Fischer, H., Sander, R., Gros, V., Kormann, R., Salisbury, G., van Dingenen, R., Williams, J., Zöllner, M., and Lelieveld, J.: Observations and model calculations of trace gas scavenging in a dense Saharan dust plume during MINATROC, Atmos. Chem. Phys., 5, 1787–1803, https://doi.org/10.5194/acp-5-1787-2005, 2005.

Rinsland, C. P., Coheur, P. F., Herbin, H., Clerbaux, C., Boone, C., Bernath, P., and Chiou, L. S.: Detection of elevated tropospheric hydrogen peroxide (H2O2) mixing ratios in atmospheric chemistry experiment (ACE) subtropical infrared solar occultation spectra, Journal of Quantitative Spectroscopy and Radiative Transfer, 107, 340–348, https://doi.org/10.1016/j.jqsrt.2007.02.009, 2007.

Robbin Martin, L. and Damschen, D. E.: Aqueous oxidation of sulfur dioxide by hydrogen peroxide at low pH, Atmospheric Environment (1967), 15, 1615–1621, https://doi.org/10.1016/0004-6981(81)90146-3, 1981.

Roeckner, E., Bäuml, G., Bonaventura, L., Brokopf, R., Esch, M., Giorgetta, M., Hagemann, S., Kirchner, I., Kornblueh, L., Manzini, E., Rhodin, A., Schlese, U., Schulzweida, U., and Tompkins, A.: The atmospheric general circulation model ECHAM 5. PART I: Model description, 2003.

Roeckner, E., Brokopf, R., Esch, M., Giorgetta, M., Hagemann, S., Kornblueh, L., Manzini, E., Schlese, U., and Schulzweida, U.: Sensitivity of Simulated Climate to Horizontal and Vertical Resolution in the ECHAM5 Atmosphere Model, Journal of Climate, 19, 3771–3791, https://doi.org/10.1175/JCLI3824.1, 2006.

Römer, F. G., Viljeer, J. W., van den Beld, L., Slangewal, H. J., Veldkamp, A. A., Kema, N. V., and Reunders, H.F.R.: The chemical composition of cloud and rainwater. Results of preliminary measurements from an aircraft, Atmospheric Environment (1967), 19, 1847–1858, https://doi.org/10.1016/0004-6981(85)90010-1, 1985.

Sakugawa, H., Kaplan, I. R., Tsai, W., and Cohen, Y.: Atmospheric hydrogen peroxide, Environ. Sci. Technol., 24, 1452–1462, https://doi.org/10.1021/es00080a002, 1990.

Sakugawa, H., Kaplan, I. R., and Shepard, L. S.: Measurements of H2O2, aldehydes and organic acids in Los Angeles rainwater: Their sources and deposition rates, Atmospheric Environment. Part B. Urban Atmosphere, 27, 203–219, https://doi.org/10.1016/0957-1272(93)90006-R, 1993.

Sander, R., Kerkweg, A., Jöckel, P., and Lelieveld, J.: Technical note: The new comprehensive atmospheric chemistry module MECCA, Atmos. Chem. Phys., 5, 445–450, https://doi.org/10.5194/acp-5-445-2005, 2005.

Sander, R., Baumgaertner, A., Gromov, S., Harder, H., Jöckel, P., Kerkweg, A., Kubistin, D., Regelin, E., Riede, H., Sandu, A., Taraborrelli, D., Tost, H., and Xie, Z.-Q.: The atmospheric chemistry box model CAABA/MECCA-3.0gmdd, 2011.

Sander, R., Jöckel, P., Kirner, O., Kunert, A. T., Landgraf, J., and Pozzer, A.: The photolysis module JVAL-14, compatible with the MESSy standard, and the JVal PreProcessor (JVPP), Geosci. Model Dev., 7, 2653–2662, https://doi.org/10.5194/gmd-7-2653-2014, 2014.

Sander, R., Baumgaertner, A., Cabrera-Perez, D., Frank, F., Gromov, S., Grooß, J.-U., Harder, H., Huijnen, V., Jöckel, P., Karydis, V. A., Niemeyer, K. E., Pozzer, A., Riede, H., Schultz, M. G., Taraborrelli, D., and Tauer, S.: The community atmospheric chemistry box model CAABA/MECCA-4.0, Geosci. Model Dev., 12, 1365–1385, https://doi.org/10.5194/gmd-12-1365-2019, 2019.

Schöne, E.: Ueber das atmosphärische Wasserstoffhyperoxyd, Ber. Dtsch. Chem. Ges., 7, 1693–1708, https://doi.org/10.1002/cber.187400702232, 1874.

Schöne, E.: Zur Frage über das Vorkommen des Wasserstoffhyperoxyds in der atmosphärischen Luft und den atmosphärischen Niederschlägen, Ber. Dtsch. Chem. Ges., 26, 3011–3027, https://doi.org/10.1002/cber.189302603136, 1893.

Schöne, E.: Ueber den Nachweis des Wasserstoffhyperoxyds in der atmosphärischen Luft und den atmosphärischen Niederschlägen, Fresenius, Zeitschrift f. anal. Chemie, 33, 137–184, https://doi.org/10.1007/BF01335790, 1894.

Seinfeld, J. H. and Pandis, S. N.: Atmospheric chemistry and physics: From air pollution to climate change, 2. ed., Wiley, Hoboken, NJ, 1203 pp., 2006.

Slemr, F., Harris, G. W., Hastie, D. R., Mackay, G. I., and Schiff, H. I.: Measurement of gas phase hydrogen peroxide in air by tunable diode laser absorption spectroscopy, Journal of Geophysical Research: Atmospheres, 91, 5371–5378, https://doi.org/10.1029/JD091iD05p05371, available at: https://onlinelibrary.wiley.com/doi/pdf/10.1029/JD091iD05p05371, 1986.

Slemr, F. and Tremmel, H. G.: Hydroperoxides in the marine troposphere over the Atlantic Ocean, J Atmos Chem, 19, 371–404, https://doi.org/10.1007/BF00694493, 1994.

Snow, J. A.: Winter-spring evolution and variability of HO x reservoir species, hydrogen peroxide, and methyl hydroperoxide, in the northern middle to high latitudes, J. Geophys. Res., 108, 1890, https://doi.org/10.1029/2002JD002172, 2003.

Snow, J. A., Heikes, B. G., Shen, H., O'Sullivan, D. W., Fried, A., and Walega, J.: Hydrogen peroxide, methyl hydroperoxide, and formaldehyde over North America and the North Atlantic, J. Geophys. Res., 112, https://doi.org/10.1029/2006JD007746, 2007.

St Clair, J. M., McCabe, D. C., Crounse, J. D., Steiner, U., and Wennberg, P. O.: Chemical ionization tandem mass spectrometer for the in situ measurement of methyl hydrogen peroxide, The Review of scientific instruments, 81, 94102, https://doi.org/10.1063/1.3480552, 2010.

Staehelin, J. and Hoigne, J.: Decomposition of ozone in water: rate of initiation by hydroxide ions and hydrogen peroxide, Environ. Sci. Technol., 16, 676–681, https://doi.org/10.1021/es00104a009, 1982.

Stickler, A., Fischer, H., Bozem, H., Gurk, C., Schiller, C., Martinez-Harder, M., Kubistin, D., Harder, H., Williams, J., Eerdekens, G., Yassaa, N., Ganzeveld, L., Sander, R., and Lelieveld, J.: Chemistry, transport and dry deposition of trace gases in the boundary layer over the tropical Atlantic Ocean and the Guyanas during the GABRIEL field campaign, Atmos. Chem. Phys., 7, 3933–3956, https://doi.org/10.5194/acp-7-3933-2007, 2007.

Studies on the formation of H2O2 in the ozonolysis of alkenes, Atmospheric Environment. Part A. General Topics, 27, 57–61, https://doi.org/10.1016/0960-1686(93)90070-F, 1993.

Tadic, I., Nussbaumer, C. M., Bohn, B., Harder, H., Marno, D., Martinez, M., Obersteiner, F., Parchatka, U., Pozzer, A., Rohloff, R., Zöger, M., Lelieveld, J., and Fischer, H.: Central role of nitric oxide in ozone production in the upper tropical troposphere over the Atlantic Ocean and western Africa, Atmos. Chem. Phys., 21, 8195–8211, https://doi.org/10.5194/acp-21-8195-2021, 2021.

Tomsche, L., Pozzer, A., Ojha, N., Parchatka, U., Lelieveld, J., and Fischer, H.: Upper tropospheric CH4 and CO affected by the South Asian summer monsoon during the Oxidation Mechanism Observations mission, Atmos. Chem. Phys., 19, 1915–1939, https://doi.org/10.5194/acp-19-1915-2019, 2019.

Tost, H., Jöckel, P., Kerkweg, A., Sander, R., and Lelieveld, J.: Technical note: A new comprehensive SCAVenging submodel for global atmospheric chemistry modelling, Atmos. Chem. Phys., 6, 565–574, https://doi.org/10.5194/acp-6-565-2006, 2006.

Urey, H., Dawsey, L., Rice, F. O.: The absorption spectrum and decomposition of hydrogen peroxide by light, J. Am. Chem. Soc., 51 (5), 1371–1383, https://doi.org/10.1021/ja01380a011, 1929.

Valverde-Canossa, J., Wieprecht, W., Acker, K., and Moortgat, G. K.: H2O2 and organic peroxide measurements in an orographic cloud: The FEBUKO experiment, Atmospheric Environment, 39, 4279–4290, https://doi.org/10.1016/j.atmosenv.2005.02.040, 2005.

Villena, G., Wiesen, P., Cantrell, C. A., Flocke, F., Fried, A., Hall, S. R., Hornbrook, R. S., Knapp, D., Kosciuch, E., Mauldin, R. L., McGrath, J. A., Montzka, D., Richter, D., Ullmann, K., Walega, J., Weibring, P., Weinheimer, A., Staebler, R. M., Liao, J., Huey, L. G., and Kleffmann, J.: Nitrous acid (HONO) during polar spring in Barrow, Alaska: A net source of OH radicals?, J. Geophys. Res., 116, L02809, https://doi.org/10.1029/2011JD016643, 2011.

Voigt, C., Lelieveld, J., Schlager, H., Schneider, J., Curtius, J., Meerkötter, R., Sauer, D., Bugliaro, L., Bohn, B., Crowley, J. N., Erbertseder, T., Groβ, S., Hahn, V., Li, Q., Mertens, M., Pöhlker, M. L., Pozzer, A., Schumann, U., Tomsche, L., Williams, J., Zahn, A., Andreae, M., Borrmann, S., Bräuer, T., Dörich, R., Dörnbrack, A., Edtbauer, A., Ernle, L., Fischer, H., Giez, A., Granzin, M., Grewe, V., Harder, H., Heinritzi, M., Holanda, B. A., Jöckel, P., Kaiser, K., Krüger, O. O., Lucke, J., Marsing, A., Martin, A., Matthes, S., Pöhlker, C., Pöschl, U., Reifenberg, S., Ringsdorf, A., Scheibe, M., Tadic, I., Zauner-Wieczorek, M., Henke, R., and Rapp, M.: Cleaner skies during the COVID-19 lockdown, Bulletin of the American Meteorological Society, https://doi.org/10.1175/BAMS-D-21-0012.1, 2022.

Walcek, C. J.: A theoretical estimate of O3 and H2O2 dry deposition over the northeast United States, Atmospheric Environment (1967), 21, 2649–2659, https://doi.org/10.1016/0004-6981(87)90196-x, 1987.

Waliser, D. E. and Gautier, C.: A Satellite-derived Climatology of the ITCZ, J. Climate, 6, 2162–2174, https://doi.org/10.1175/1520-0442(1993)006<2162:ASDCOT>2.0.CO;2, 1993.

Walker, S. J., Evans, M. J., Jackson, A. V., Steinbacher, M., Zellweger, C., and McQuaid, J. B.: Processes controlling the concentration of hydroperoxides at Jungfraujoch Observatory, Switzerland, Atmos. Chem. Phys., 6, 5525–5536, https://doi.org/10.5194/acp-6-5525-2006, 2006.

Warneck, P.: Chemistry of the natural atmosphere, International geophysics series, 41, Acad. Press, San Diego, 757 pp., 1988.

Warneck, P.: Chemical reactions in clouds, Fresenius J Anal Chem, 340, 585–590, https://doi.org/10.1007/BF00322434, 1991.

Weinstein-Lloyd, J. and Schwartz, S. E.: Low-intensity radiolysis study of free-radical reactions in cloudwater: hydrogen peroxide production and destruction, Environ. Sci. Technol., 25, 791–800, https://doi.org/10.1021/es00016a027, 1991.

Weinstein-Lloyd, J. B., Lee, J. H., Daum, P. H., Kleinman, L. I., Nunnermacker, L. J., Springston, S. R., and Newman, L.: Measurements of peroxides and related species during the 1995 summer intensive of the Southern Oxidants Study in Nashville, Tennessee, J. Geophys. Res., 103, 22361–22373, https://doi.org/10.1029/98JD01636, 1998.

Wennberg, P. O., Hanisco, T. F., Jaegle, L., Jacob, D. J., Hintsa, E. J., Lanzendorf, E. J., Anderson, J. G., Gao, R., Keim, E. R., Donnelly, S. G., Negro, L. A.D., Fahey, D. W., McKeen, S. A., Salawitch, R. J., Webster, C. R., May, R. D., Herman, R. L., Proffitt, M. H., Margitan, J. J., Atlas, E. L., Schauffler, S. M., Flocke, F., McElroy, C. T., and Bui, T. P.: Hydrogen radicals, nitrogen radicals, and the production of O3 in the upper troposphere, Science (New York, N.Y.), 279, 49–53, https://doi.org/10.1126/science.279.5347.49, 1998.

Wennberg, P. O., Bates, K. H., Crounse, J. D., Dodson, L. G., McVay, R. C., Mertens, L. A., Nguyen, T. B., Praske, E., Schwantes, R. H., Smarte, M. D., St Clair, J. M., Teng, A. P., Zhang, X., and Seinfeld, J. H.: Gas-Phase Reactions of Isoprene and Its Major Oxidation Products, Chemical reviews, 118, 3337–3390, https://doi.org/10.1021/acs.chemrev.7b00439, 2018.

Weschler, C. J., Mandich, M. L., and Graedel, T. E.: Speciation, photosensitivity, and reactions of transition metal ions in atmospheric droplets, J. Geophys. Res., 91, 5189, https://doi.org/10.1029/JD091iD04p05189, 1986.

Xuan, X., Chen, Z., Gong, Y., Shen, H., and Chen, S.: Partitioning of hydrogen peroxide in gas-liquid and gas-aerosol phases, Atmos. Chem. Phys., 20, 5513–5526, https://doi.org/10.5194/acp-20-5513-2020, 2020.

Zahn, A., Weppner, J., Widmann, H., Schlote-Holubek, K., Burger, B., Kühner, T., and Franke, H.: A fast and precise chemiluminescence ozone detector for eddy flux and airborne application, Atmos. Meas. Tech., 5, 363–375, https://doi.org/10.5194/amt-5-363-2012, 2012.

Zepp, R. G., Faust, B. C., and Hoigne, J.: Hydroxyl radical formation in aqueous reactions (pH 3-8) of iron(II) with hydrogen peroxide: the photo-Fenton reaction, Environ. Sci. Technol., 26, 313–319, https://doi.org/10.1021/es00026a011, 1992.

Zhou, X. and Lee, Y. N.: Aqueous solubility and reaction kinetics of hydroxymethyl hydroperoxide, J. Phys. Chem., 96, 265–272, https://doi.org/10.1021/j100180a051, 1992.

Zuo, Y. and Hoigne, J.: Formation of hydrogen peroxide and depletion of oxalic acid in atmospheric water by photolysis of iron(III)-oxalato complexes, Environ. Sci. Technol., 26, 1014–1022, https://doi.org/10.1021/es00029a022, 1992.

Zuo, Y. and Hoigné, J.: Evidence for Photochemical Formation of H2O2 and Oxidation of SO2 in Authentic Fog Water, Science (New York, N.Y.), 260, 71–73, https://doi.org/10.1126/science.260.5104.71, 1993.

Zuo, Y. and Deng, Y.: Iron(II)-catalyzed photochemical decomposition of oxalic acid and generation of H2O2 in atmospheric liquid phases, Chemosphere, 35, 2051–2058, https://doi.org/10.1016/S0045-6535(97)00228-2, available at: http://www.sciencedirect.com/science/article/pii/S0045653597002282, 1997.